Some Studies on the Fabrication and Optimization of Cu_xN based Optoelectronic Sensors and Devices

THESIS SUBMITTED FOR THE DEGREE OF DOCTOR OF PHILOSOPHY (ENGINEERING)

of

JADAVPUR UNIVERSITY

By

Mr. Avijit Paul

(Ph.D. INDEX NUMBER: D-7/ISLM/63/21)

School of Energy Studies

Jadavpur University

Kolkata-700032

INDIA

Nov, 2025

INDEX NO: - D-7/ISLM/63/21

1. **Title of the Thesis:**
   "Some Studies on the Fabrication and Optimization of Cu_xN based Optoelectronic Sensors and Devices"

2. **Name, Designation, and Institution of the Supervisor**
   Prof. (Dr.) Ratan Mandal
   Professor and Director, School of Energy Studies,
   Jadavpur University,
   Kolkata-700032,
   India

3. **List of Journals:**

   Published:

   a) **Avijit Paul,** Mainak Ghosh, Indranil Dutta, Ratan Mandal; A novel method for fabricating semiconducting monocrystalline copper nitride nanowires for optoelectronic applications, was published in **Journal of Crystal Growth 617 (2023) 127307, Elsevier.**

   b) **Avijit Paul,** Mainak Ghosh, Tanay Chattopadhyay, Ratan Mandal; Investigation on Optoelectronic response of crystalline copper nitride (Cu_xN) thin film semiconducting material, was published in **Journal of Materials Science: Materials in Electronics (2025), 36:87, Springer.**

   c) **Avijit Paul,** Ratan Mandal; Scope and possibilities of copper based semiconducting materials in optoelectronic applications - A review, was published in **Invertis Journal of Renewable Energy (2017) Vol.7 No.2 pp. 106-112.**

   Communicated (Under review process):

   d) Mainak Ghosh, **Avijit Paul**, Anandamoy Mukhopadhyay, Ratan Mandal; Synthesis of tin chalcogenide based nanostructured thin film by SILAR method for photovoltaic applications, has been communicated in **Applied Solar Energy, Springer, June, 2025**.

4. **List of Book Chapters**
   Published:

   a) **Avijit Paul,** Ratan Mandal; Advances in nanostructure thin film materials for solar cell applications, was published in **Comprehensive Materials Processing (2024), 2nd Edition, Vol 4, pp. 136-150, Elsevier.**

b) Ratan Mandal, Mainak Ghosh, **Avijit Paul**; Electroless Nickel Coating on Magnesium Substrates: Fabrication method and Applications, was published in **Comprehensive Materials Processing (2024), 2nd Edition, Vol 4, pp.547-564, Elsevier.**

c) Mainak Ghosh, **Avijit Paul,** Ratan Mandal; Thin film Fabrication for Wearable Electronics: Journey so far, was published in **Comprehensive Materials Processing (2024), 2nd Edition, Vol 4, pp.39-60, Elsevier.**

d) **Ratan Mandal, Mainak Ghosh, Avijit Paul;** Synthesis methods, fabrication & performance evaluation techniques of super capacitor-based electrode materials, has been published in Supercapacitors: Fundamentals, Advances and Future Applications, **Royal Society of Chemistry (2025), Volume 3, Print ISSN: 2752-7441, DOI: https://doi.norg / 10.1039/9781837676774.**

5. List of Presentation in International Conferences:

a) **IEEE Conference: Avijit Paul**, Ratan Mandal; Some Studies on the contact properties of $Cd_{1-x}Zn_xTe$ Thin Film for Application in Optoelectronics Devices, was published in the International Conference on 21stCentury Energy Needs-Materials, Systems and Applications to be held on Nov 17-19,2016 at **School of Energy Science & Engineering, Indian Institute of Technology (IIT), Kharagpur, WB, India.**

b) **Avijit Paul,** Indranil Dutta, Ratan Mandal; Analytical Study of the Efficiency of CdS/Cu_xS Based Thin Film Solar Cells using MATLAB Platform, was published in the International Conference on Renewable Energy and Sustainable Technologies (ICREST) to be held on July 04-06, 2024 at **Department of Applied Science & Humanities, Faculty of Engineering & Technology, Jamia Millia Islamia, New Delhi, India.**

STATEMENT OF ORIGINALITY

I, Avijit Paul (Index Number: D-7/ISLM/63/21) registered on 10th January 2022, do hereby declare that this thesis entitled **"Some Studies on the Fabrication and Optimization of Cu_xN based Optoelectronic Sensors and Devices"**, contains literature survey and original research work conducted by the undersigned candidate for a PhD degree.

All information in this thesis has been obtained and presented in accordance with existing academic rules and ethical conduct. I declare that, as required by these rules and conduct, I have fully cited and referred all materials and results that are not original to this work.

I also declare that I have checked this thesis as per the "Policy on Anti Plagiarism, Jadavpur University, 2019", and the level of similarity as checked by iThenticate software is 7%.

Signature of Candidate: Avijit Paul

Date: 06/11/2025

Certified by

Supervisor:

6/11/2025

Prof. (Dr.) Ratan Mandal

Professor and Director,

School of Energy Studies

Jadavpur University

Director
School of Energy Studies
Jadavpur University
Kolkata - 700032

CERTIFICATE FROM THE SUPERVISOR

This is to certify that the thesis entitled **"Some Studies on the Fabrication and Optimization of Cu_xN based Optoelectronic Sensors and Devices"**, submitted by Mr. Avijit Paul (Index Number: D-7/ISLM/63/21), who registered his name on 10th January, 2022, for the award of Ph.D. (Engineering) degree of Jadavpur University, is absolutely based upon his work under the supervision of Prof.(Dr.) Ratan Mandal, Professor and Director, School of Energy Studies, and that neither his thesis nor any part of the thesis has been submitted for any degree/diploma or any other academic award anywhere before.

6.11.2025

Prof. (Dr.) Ratan Mandal

Director
School of Energy Studies
Jadavpur University
Kolkata - 700032

ACKNOWLEDGEMENT

The present thesis entitled **"Some Studies on the Fabrication and Optimization of Cu_xN based Optoelectronic Sensors and Devices"**, is submitted for the degree of Doctor of Philosophy (Engineering) at the Faculty of Interdisciplinary Studies, Law and Management, Jadavpur University, Kolkata. The research work presented here was carried out under the supervision of Prof. (Dr.) Ratan Mandal, Professor and Director, School of Energy Studies, Jadavpur University between the period of 2022 to 2025.

To the best of my knowledge, this work is original except where acknowledgment and references are made to previous work. Neither this nor any substantially similar thesis has been or is been submitted for any other degree, diploma, or other qualification at any other university.

While working on a Ph.D. is a lonely endeavor, it is not possible without the support of others. As I mentioned, my Ph.D. work was supervised by Prof. Ratan Mandal, whose continuous help, encouragement, advice, guidance, and unparalleled in-depth knowledge of the present subject make it possible to complete this Ph.D. work. I express my deepest gratitude to my guide and philosopher Prof. (Dr.) Ratan Mandal.

I would like to thank Prof. Biswajit Ghosh, Vice-Chancellor, Neotia University, and ex-professor, School of Energy Studies, Jadavpur University, who advised and encouraged me on different ways to approach a research problem and possible methods and solutions. I would also like to thank Prof. Tushar Jash, ex-professor, School of Energy Studies, Jadavpur University for his valuable suggestions regarding the thesis. I would like to thank my co-researcher Mr. Mainak Ghosh for his help and support regarding this work. I would also remember Dr. Subrata Das, post-doctoral researcher, School of Energy Studies, Jadavpur University, for his valuable advice and encouragement regarding this research work. I also like to thank my wife, Mrs. Arpita Paul, for her unwavering mental support over these years, without which I could not have completed this thesis.

Last but not the least, I would like to remember my parents, all my teachers, research scholars, seniors, juniors, friends, and all other well-wishers for their endless gracious, encouragement, and support. I express my sincere thanks to all of them again.

Avijit Paul

Mr. Avijit Paul

Dedicated

To

My Parents and Guides

&

Wife

&

My beloved Daughter

LIST OF CONTENTS

LIST OF TABLES

LIST OF FIGURES

NOMENCLATURES

λ	Wavelength (nm)
Θ	Bragg angle (deg.)
ß	Full-width-at-half maximum (FWHM) (deg.)
D	Crystallite Size (nm.)
ρ	Dislocation Density(m^{-2})
ε	Micro-strain
t	Thickness(nm)
E_g	Bandgap (eV)
hv	Photon Energy (eV)
ΔT	Temperature Difference (˚C)
α	Temperature co-efficient of resistance
R_{light}	Resistance at light intensities(Ω)
R_{dark}	Resistance at dark condition (Ω)
$n(\lambda)$	Real Refractive Index
$k(\lambda)$	Extinction Coefficient
$a(\lambda)$	Absorption Coefficient
r	Reflectance
A	Absorbance (a.u)
R_p	Recombination prefactor($m^{-6}.s^{-1}$)
V_{OC}	Open circuit voltage (volt)
J_{SC}	Short circuit current density (mA/cm^2)
V_m	Maximum voltage (volt)
J_m	Maximum current density (mA/cm^2)

P_m	Maximum cell power (mW/cm^2)
FF	Fill factor
η	Power conversion efficiency (%)

ABBREVIATIONS

EDX	Energy Dispersive X-Ray
LDR	Light Dependent Resistor
Oghma-Nano	Organic and Hybrid Material Nano simulation software
OFET	Organic Field Effect Transistors
OLED	Organic Light-emitting Diodes
SEM	Scanning Electron Microscope
UV-Vis-NIR	Ultraviolet-Visible-Near Infrared
XRD	X-ray diffraction

PREFACE

The thesis deals with the fabrication and optimization of semiconducting copper nitride nanostructure for the applications of optoelectronic sensors and devices. Thin film semiconductor plays a crucial role in the field of optoelectronics now-a-days. There are several promising thin film compound semiconducting materials such as gallium arsenide (GaAs), cadmium telluride (CdTe), gallium nitride (GaN), cadmium sulphide (CdS) etc. have widely used in optoelectronic devices applications. Thin film devices require less material as well as occupy less space and thus making it less expensive. Thin film devices can be developed via several physical as well as chemical deposition techniques. The most common physical deposition techniques are like thermal deposition, sputtering, molecular beam epitaxy, pulsed laser deposition, etc., and chemical deposition methods are like chemical bath deposition, spray pyrolysis, SILAR, sol-gel, etc. The fabrication of thin film nanostructure plays an important role in device performance due to its high specific surface area, higher electrical conductivity as well as mobility, enhanced mechanical strength and improved stability as well as efficiency. In this present study nanostructure copper nitride thin film has been developed for LDR and solar cell applications. Copper nitride is a less thermally stable material, and thus it is very difficult to fabricate it with high-temperature synthetic methods. It has been observed that copper nitride had mostly been developed by physical deposition techniques, but the suitable chemical composition of the material is not always obtained for providing optimum optoelectronic properties for device applications. Thus, in this present work fabrication and optimization of the material has been performed by utilizing a simple and low-cost spray deposition process which requires a low temperature arrangement. The obtained optimized film has been performed satisfactory as a LDR application. The photoconductive study has been executed by tuning the thickness of the optimized film, and the optimum film thickness has been used for solar cell applications. The performance evaluation of the solar cell device has been accomplished by implementing copper nitride as absorber and window layers in combination with various inorganic semiconductors. The best photovoltaic combination has been explored from here to determine its feasibility as a solar cell application. The obtain results have compatible with the experimental results of other conventional thin film solar cell devices. The detailed study has been presented in the volume of seven chapters. The outline of the entire work has been organized into the following major parts:

- Introduction, aims and objectives of the work
- Literature survey, research gap and scope of the work
- Comprehensive idea about various physical as well as chemical deposition processes and characterization techniques (structural, optical etc.) regarding thin film semiconductor.
- Fabrication and optimization of nanostructure Cu_xN by a simple and low-cost spray deposition method for photoresistor or LDR application.
- Investigation of optoelectronic response (photoconductive and photovoltaic) of the optimized Cu_xN film for solar cell applications.
- Conclusion and future work

There are some unsolved issues regarding the fabrication and optimization of copper nitride-based thin film that has not been completed due to the stipulated period of time. It is expected that future researchers will complete the remaining part of this research work to fulfill these unsolved issues.

A more in-depth sub-sections can be achieved from the abstract and the table of contents within this framework. The author is thankful to his guide Prof. (Dr.) Ratan Mandal, Professor and Director, School of Energy Studies, and also to all those who have associated directly or indirectly to helped me to carry out this entire thesis work. Finally, I would like to thank my family members whose love and support were a source of inspiration during this research period.

Avijit Paul

Mr. Avijit Paul

Abstract

In the 21st century we come across electronic gadgets across every sphere of life. The word ‘electronics’ originated from electron. Electronics is a branch of engineering dealing with the theory, working and use of devices operating on the basis of electrons travelling through gas or a semiconductor material. The electrical conductivity of semiconductors lies in between conductors and insulators. Semiconducting materials play a crucial role in the electronic industry for the development of many electronic devices. There are many semiconducting materials such as silicon, germanium, gallium arsenide, cadmium sulphide, etc., that are widely used today. On the other hand, thin film is a thin layer of material whose thickness varies from nanometer to several micrometer. Thin film semiconducting materials play an important role in the development of optoelectronic devices such as solar cells, LEDs, LASERs, sensors, etc. Thin-film semiconductors can be fabricated via various physical and chemical deposition techniques. The most common physical deposition methods are like thermal deposition, sputtering, molecular beam epitaxy, pulsed laser deposition, etc., and chemical deposition processes are like chemical bath deposition, spray pyrolysis, SILAR, sol-gel, etc. The fabrication of nanostructure materials has explored various advantages over bulk materials. Nanomaterials have exhibited a high specific surface area, higher electrical conductivity as well as mobility, enhanced mechanical strength and improved stability as well as efficiency. There are several nanostructures, like nanocomposites, nanorods, nanowires, quantum dots, etc., in the field of nanofabrication. Therefore, nanofabrication is more suitable for the purpose of optoelectronic device fabrication for improved efficiency as well as reducing cost.

There are lots of promising thin film semiconducting nanostructure materials like copper sulphide, gallium nitride, cadmium sulphide, gallium arsenide, titanium di-oxide, etc. used in optoelectronic device applications. Copper nitride is one of the promising semiconducting materials which can be used in optoelectronic sensors and device applications. There are some difficulties regarding the fabrication of thin film copper nitride semiconducting material. Copper nitride is a less thermally stable material, and thus it is very difficult to fabricate it with high-temperature synthetic methods. It has been observed that copper nitride had mainly been prepared by physical deposition techniques, but the suitable chemical composition of the material is not always consistent for maintaining optimum semiconducting properties to be used in optoelectronic device applications. Thus, the development of this material by a simple and low-cost method which requires a low temperature arrangement has been attempted in this present work. The fabrication of the thin film has been performed here by a chemical spray deposition process. The optimization of the film has been executed by varying doping of the material. Then the obtained optimized film has been tested for LDR application. The photoconductive study has been performed by varying the thickness of the optimally prepared film, and optimum film thickness has been used for solar cell applications. The modelling of the solar cell has been executed by implementing copper nitride as absorber and window layers in combination with various inorganic semiconductors. The best photovoltaic combination has been explored from here to determine its feasibility as a solar cell application. The details of the entire research work

have been conducted in the context of this thesis and coherently presented in several chapters to organize the total thesis.

The aims and objectives of this present research work have been presented in **Chapter 1**. The detailed literature review has been performed here regarding properties and different nanofabrication methods of various promising semiconducting materials used in optoelectronic device applications. The effectiveness of nanofabrication techniques in optoelectronic devices has been discussed in this context. The objectives of the entire thesis have been inferred in this section. The formation of nanostructure copper nitride semiconducting thin film by utilizing a simple and low-cost deposition method for the application in light dependent resistor (LDR) and solar cell applications has been discussed in this chapter.

Chapter 2 begins with a comprehensive review of earlier works related to properties and various nanofabrication methods of copper nitride (Cu_xN) material. The gap of the research and corresponding possible solutions has been discussed in this chapter. Copper nitride is very difficult to fabricate at high temperature synthetic methods due to low thermal stability of the material. In earlier this material mostly developed by physical deposition methods but the suitable compositional ratio of the material is not always obtained for providing optimum optoelectronic properties for device applications. Thus, fabrication of the Cu_xN nanostructure has been performed here by spray deposition process. The optimization of the film has been performed by varying doping of the material. The performance of the optimized sample has been tested for LDR application. The photoconductive and photovoltaic performances have been accomplished. At first, photoconductive performance has been executed by varying optimally developed film thickness, and optimum film thickness has been used for solar cell applications. The analysis of a solar cell device has been performed by using Cu_xN as absorber and window layers in combination with various inorganic semiconductors to evaluate photovoltaic performances. Finally, conclusion has made regarding the suitability of copper nitride material as an LDR and solar cell application.

Various physical and chemical deposition processes and different characterization techniques like structural and optical, regarding the thin film semiconductor have been presented in **Chapter 3**. The detailed operating principle of fabrication and characterization techniques, has contributed a comprehensive idea about the convenient possibility regarding this being used in this present work.

Chapter 4 presents the fabrication and optimization of semiconducting copper nitride (Cu_xN) nanostructure for photoresistor or LDR application. Here Cu_xN nanowires have been fabricated by a simple and low-cost spray deposition process. The optimization of the chemical composition of the material has been performed by varying the doping of the film. The doping has varied by varying the molarity of the precursor solution. The Cu_xN film has been optimized by fabricating it with varying molarities such as 0.2(M), 0.4(M), 0.6(M), 0.8(M) and 1.0(M) respectively. The structural, optical analysis has been performed to cultivate crystallinity, surface morphology, compositional ratio, and band gap of both the as-prepared and annealed samples. It has been observed that annealing has improved overall

structural as well as optical parameters. The electrical analysis of the optimized 0.6(M) Cu_xN annealed sample has been executed to determine its acceptability for light-dependent resistor (LDR) applications. LDR gain has been determined to evaluate the performance of the photoresistor, and it is found that the copper nitride sample has provided satisfactory performance as a photoresistor.

A modern computational analysis has been performed to investigate the optoelectronic responses of the fabricated optimized 0.6(M) Cu_xN annealed sample, which has been studied in **Chapter 5**. The experimental data of the optical spectroscopy has been provided as input to Oghma-Nano software (8.1.020) for carrying out numerical simulations. It is assumed that this technique can produce the outputs which are compatible with real-time data. Here the photoconductive and photovoltaic performance analyses of the fabricated optimized 0.6(M)Cu_xN annealed sample have been studied. At first photoconductive performances have been analyzed by variation of film thickness, and then optimized thickness has been used for solar cell applications. The photovoltaic performances have been observed by considering Cu_xN as absorber and window layers, respectively. Here Cu_xN as an absorber layer and CdS and ZnO as window layers have been simulated, and photovoltaic performance has been obtained. Then Cu_xN as a window layer and PbSe and InAs as absorber layers have been simulated, and photovoltaic performance has been observed. The best photovoltaic characteristics and parameters have been observed for Cu_xN as an absorber layer and CdS as a window layer. The obtained results are compatible with the experimental results of other conventional CdS-based solar cells like CdS-Cu_2S, CdS-PbS, CdS-CdTe etc. This process can be adopted in places lagging suitable infrastructure for solar cell fabrication.

The summary and concluding remarks of the entire work have been presented in **Chapter 6**. It has been started from the aims and objectives of the work to the optoelectronic performance analysis of the copper nitride (Cu_xN) thin film semiconducting material.

Although significant research work related to the fabrication and optimization of copper nitride-based optoelectronic sensors and devices has been presented in this present thesis, still many aspects are not covered due to specific period of time. Thus, all of the unsolved and uncovered parts of this work are presented in **Chapter 7**. Therefore, it is expected that future researchers will provide possible solutions regarding these unsolved issues for successful exploration regarding this research topic.

Chapter 1

Introduction

1.1 Introduction

Semiconductors have changed the world drastically in ways that could not have been imagined before them. The term “semiconducting” was used for the first time by Alessandro Volta in 1782. Semiconductor materials are the building blocks of the entire electronics and computer industry. Small, lightweight, high-speed, and low-power consumption devices would not be possible without integrated circuits, which consist of semiconductor materials. Modern electronic components like diodes, transistors, various processors, solar cells, light-emitting diodes (LEDs), etc., are developed using semiconductor materials. Silicon is the most important and abundant semiconductor material in the earth's crust. Thin film semiconductors allow easy incorporation by changing the properties of materials and reducing the size. The study on semiconducting thin films is rapidly growing due to their constructive applications in wireless communication, solar cells, semiconductor devices, integrated circuits, magneto-optic memories, light-emitting diodes, multifunctional protective coatings, liquid crystal displays, and so on. Nowadays, semiconductor nanoparticles have shown unique properties due to their large surface area or quantum size effect. Thus, nanoparticle semiconductors play a major role in several new technologies [1, 2, 3]. The properties and fabrication methods of various promising nanostructured based semiconductors have been studied for application in optoelectronic devices.

1.2 Thin Film Semiconducting Materials and it’s applications

The term thin film refers to a thin layer of material whose thickness varies from a fraction of a nanometre to several micrometres. There are various thin film materials, such as silicon, gallium arsenide, germanium, cadmium sulphide, cadmium telluride, titanium dioxide, etc., which are widely used today. Thin films find a wide range of applications, such as magnetic recording media, electronic semiconductor devices, LEDs, optical coatings, hard coatings for tribological purposes, and for both energy generation (e.g., thin-film solar cells) and storage (thin-film batteries) [4]. Fabrication of thin films can be achieved via two routes: physical deposition method and chemical deposition method. Thermal deposition, molecular beam epitaxy, pulsed laser deposition (i.e., laser beam evaporation), electron beam evaporation, arc evaporation, sputtering, etc., are some commonly used physical methods. Electrochemical deposition (ECD), chemical bath deposition (CBD), spray pyrolysis technique, sol-gel technique, the Successive Ionic Layer Adsorption Reaction (SILAR) method, etc., are some commonly used chemical methods. The nanostructured thin film devices have shown optimum efficiency compared to bulk due to their improved stability. Thin film technology has directly or indirectly introduced many new areas of research in solid state physics and chemistry which are based on phenomena uniquely characteristic of the thickness, geometry, and structure of the film [5].

1.3 Background of Nanotechnology

The particles having size in the range of 1 to 100 nm are called nanoparticles, and the applications regarding these nanosized particles are termed as nanotechnology. Nanotechnology is used in various fields like chemistry, biology, physics, materials science, and engineering. The concept of nanotechnology was first discussed by Richard Feynman in 1959, and Norio Taniguchi used the term nanotechnology in 1974 for the first time. By using nanotechnology, unique products that are stronger, lighter, cheaper, durable, and precise can be created. Apart from these, nanomaterials have made computers smaller and much faster. Nanomaterials can be classified into four categories according to their confinements: zero-dimensional (0D), one-dimensional (1D), two-dimensional (2D), and three-dimensional (3D). Zero-dimensional (0D) materials are sized at the nanoscale level in all three dimensions, and in this system, all electrons are fully confined, for example, quantum dots. On the other hand, one-dimensional (1D) structured materials are nanoscale, having two dimensions, and here electrons are confined within two dimensions, indicating electrons cannot move freely. Two-dimensional (2D) materials are sized in the nanoscale in one dimension, and here electrons are confined within one dimension, indicating electrons cannot move freely within the associated dimension. Three-dimensional (3D) nanomaterials are also known as bulk nanomaterials, and these materials are not confined to the nanoscale level in all dimensions. Nanomaterials have several advantages as compared to bulk materials. Nanomaterials have a high specific surface area, and thus they can store more energy in comparison to bulk materials. It has also been observed that the electrical conductivity of nanotubes is very high due to electron confinement in a particular direction, resulting in an increase in mobility with a corresponding decrease in scattering. Mechanical strength and toughness of nanostructures are higher than that of bulk structures [6]. On the other hand, nanostructures exhibit excellent magnetic properties and are suitable for application in magnetic storage devices. The influence of nanotechnology has been introduced in the field of optoelectronic device application, considering its various advantages. Nanostructure-based devices will provide better stability as well as higher efficiency as compared to bulk-structured ones. There are four types of nanostructures, like: (i) Nanocomposites (ii) Quantum wells (iii) Nanowires and nanotubes (iv) Nanoparticles and quantum dots (QDs) are most popular in the field of nanofabrication. Nanowires and nanotubes especially have tremendous potential for applications in optoelectronic devices in the future. Semiconductor QDs are generally composed of atoms from groups II and VI or III and V of the periodic table. The nanoscale size of QDs leads to the quantum-confinement effect, which results in interesting optical and electronic properties. The first milestone application of QDs as luminescence labels in bioimaging. Quantum dots have become very renowned among the types mentioned above due to their tunable band gap over a wide range of energy levels by varying the nanoparticle dot's size, which acts as a photovoltaic absorber material. Nowadays, rapid advances in nanotechnology and nanoscience have provided a variety of nanoscale materials with highly controlled and unique optical, electrical, magnetic, or catalytic properties. The diversity in composition (inorganic or organic, metals or semiconductors), shape (particles, rods, wires, tubes, cubes, triangles), and the readiness for surface functionalisation (physical, chemical, or biological) have enabled the fabrication of various functional nanoscale devices [7, 8].

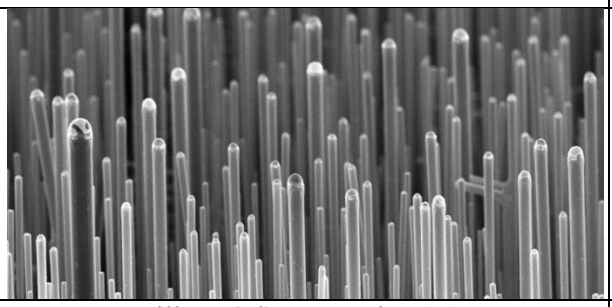	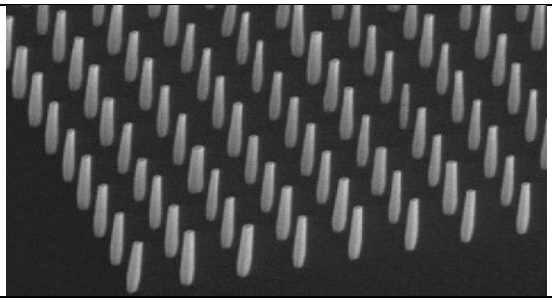
Silicon(Si) Nanowires[9]	GaliumNitride(GaN) Nanowires[10]
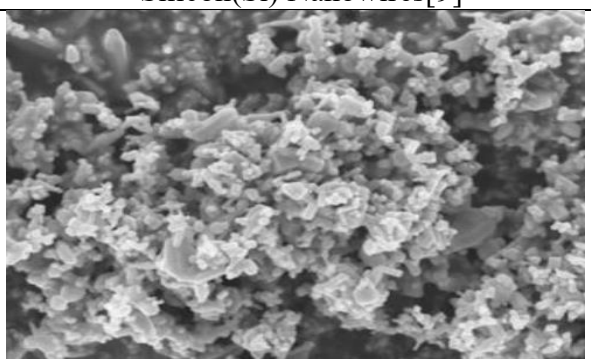	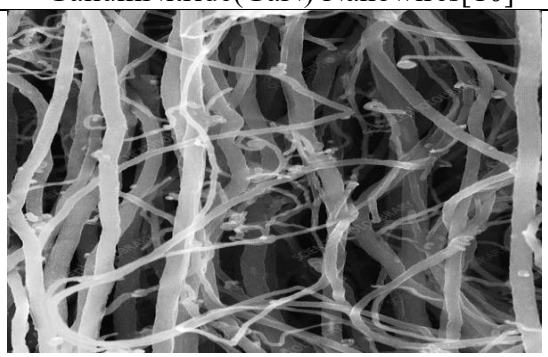
Zinc Oxide (ZnO) Nanoparticles[11]	Carbon(C) Nanotubes [12]
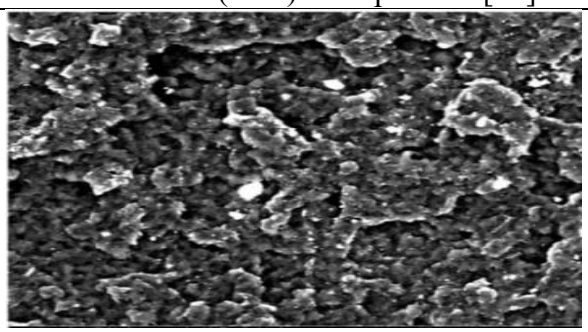	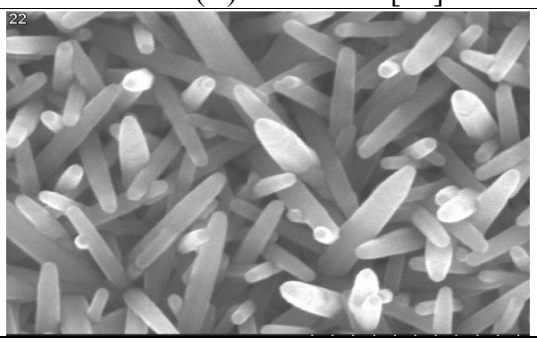
Zinc Oxide (ZnO) Nanocomposite [13]	Zinc Oxide (ZnO) Nanorods [14]
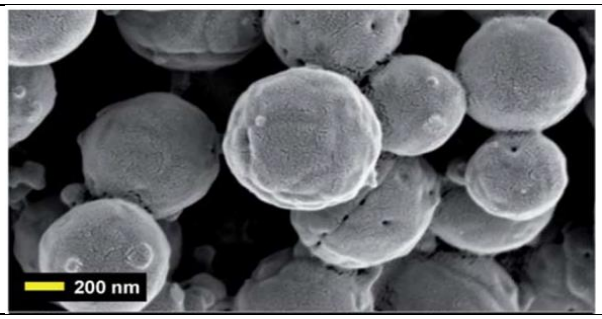	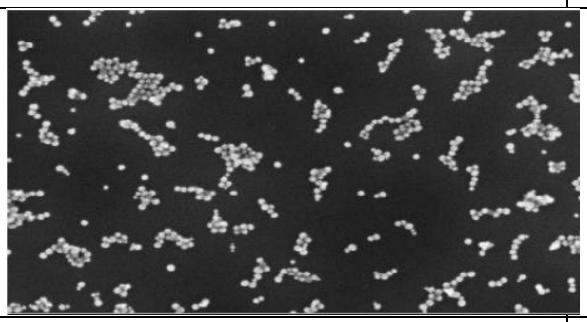
Carbon Quantum Dots [15]	Silica Nanofluid [16]

Fig 1.1: SEM images of different types of Nano-Structured formation

Therefore, nanotechnology will be used more and more in the purpose of optoelectronic device fabrication in the future for increasing the efficiency as well as manufacturing cost. Fig.1.1 shows the formation of different types of nanostructures such as nanowires, nanorods, nanotubes, nanocomposites etc.

1.4. Studies on different nanostructure semiconducting materials

Presently, some of the promising materials generally used for the optoelectronic device applications and their nanofabrication process are considered for detailed study in the following text.

1.4.1 Copper Sulphide ($Cu_{2-x}S$)

$Cu_{2-x}S$ (Copper Sulphide) is a promising p-type semiconducting material for solar cell applications. This material is cheap, abundant, and non-toxic in nature. It is best suited as an absorber layer in PV conversion structure. Several fabrication methodologies adopted by different researchers are discussed as follows:

The work reported here is about $Cu_{2-x}S$, which has been deposited by using a two-step hydrothermal method. In this process, in the first step, copper chloride, thiourea powder, and ethanol were used to form a slurry. The colour of the slurry was yellow-green. Thereafter, this slurry was placed in an autoclave maintained at a temperature of 160^0C for 6 hrs. Then it was cooled to room temperature. After that, there were observed dark precipitates, which were washed with distilled water as well as ethanol, respectively. In the second step, the film was prepared by adding the obtained nanoparticle to the other slurry, which was made by the same chemical component as well as maintained the same reaction condition [17].

$Cu_{1.75}S$ nanocrystal was synthesised by a hot-injection chemical reaction process. Here Cu (copper) precursor solution was made by using copper chloride and DEG (diethylene glycol), and S (sulphur) precursor solution was prepared by introducing TAA (thioacetamide) and PVP (polyvinylpyrrolidone). The sulphur precursor was kept in a three-necked flask that maintained a nitrogen stream. Then EDA (ethylenediamine) was added into the flask where a temperature of 120° was maintained. Thereafter, Cu (copper) precursor solution and hydrazine hydrate were added into hot sulphur solution, and then it was cooled using a water bath. At last, the final product was achieved by using high-speed centrifugation [18].

Copper sulphide has been deposited here by the alternating current electrodeposition method. The two brass meshes are used as electrodes here. The electrolyte solution contained copper sulphate, ethylenediaminetetraacetic acid disodium salt, and thioacetamide. Finally, after getting super hydrophilic surfaces, brass meshes were annealed at 300°C temperature [19].

Cu_2S nanoparticles were fabricated here via the wet chemical method. Here, at first, a chemical mixture was prepared by using copper chloride and thioglycerol. Thereafter, sodium sulphide was added dropwise into the solution, and it was kept at room temperature by maintaining continuous stirring for 4 hours. The precipitate was spread in water after 24 hours and stirred for 2 hours [20].

Cu_2S nanoparticle was deposited here by a facile solvothermal process. In this method, at first, a copper nitrate trihydrate-based solution was prepared, and after ammonia solution was

added dropwise to the mixture, it was stirred for 10 mins until a clear and indigo-blue cuprammonium solution was obtained. Then DDT (1-dodecanethiol) was added into it and placed in an autoclave where 200°C temperature was maintained. Finally, it was cooled down to room temperature [21].

Cu_2S and Cu_2O composites have been deposited here by a facile chemical bath deposition method. Then an aqueous solution was prepared by using copper sulphate and sodium thiosulphate, where the bath pH was maintained at about 5. Then the substrate was placed into the solution, which was maintained at a temperature of 50^0C, and waited for 30 min after precipitation began. Finally, the substrate was dipped into PDMS (dihydroxy polydimethylsiloxane) solution for 2 hours [22].

Here copper sulphide was deposited by the CBD (chemical bath deposition) process. The precursor solution was prepared by mixing copper salt and triethanolamine using a magnetic stirrer for 3 min. Then NH_4Cl buffer solution was added into it, and here pH was maintained at10.4. At last, thiourea was added into the solution, and the substrate was placed into it and maintained at a temperature of 50^0C for 7 hours [23].

Cu_xS was fabricated here by the modified spray pyrolysis technique. The aqueous solution was prepared by using copper acetate and thiourea. Then the substrate was kept on a hot plate maintained at a temperature of 285^0C and the solution was sprayed over it using a sprayer. This is a very convenient as well as low-cost deposition process [24].

Here copper sulphide has been deposited by the automatic spray pyrolysis method. The precursor solution was prepared by using copper chloride and thiourea, which were mixed in a solution of water, ethanol, and glycerol (water: ethanol: glycerol = 7:2:1). There was maintained temperature in the range of 275-325^0C and kept air pressure at 1.2 bar [25].

Copper sulphide thin film has been fabricated here by a wet chemistry process. The precursor solution was prepared by using polyvinyl pyrrolidone (PVP), sodium sulphide nonahydrate, and copper nitrate hydrate. Then the solution was stirred (450-500 rpm) at room temperature. After obtaining the precipitate, it was centrifuged and washed with DI water as well as ethanol. Finally, it was annealed at 100°C for 2 to 3 hours [26].

Cu_xS was fabricated here by a one-step hydrothermal approach. Here, the first solution was prepared using copper nitrate trihydrate and ammonium fluoride. Then thiourea was added into the solution and stirred. The mixed solution was kept in an autoclave maintained at a temperature of 120^0C for 6 hours. At last, the final product was collected after filtering [27].

Cu_xS nanotube was synthesised by using a facile solution reaction-based method. At first, rod-like copper tin hydroxide was achieved from an aqueous solution-based method and then converted it into CuS nanotubes by adding sodium sulphide-based aqueous solution at room temperature. At last, the obtained black product was washed and vacuum annealed at 40°C temperature [28].

In this work, copper sulphide was formed by the potentiostatic deposition method. Here Cu (copper) film was formed by the electrodeposition process. The electrolyte solution was prepared using copper sulphate and sulphuric acid. Here, solution pH of 1.35 was maintained. Thereafter, Cu_2S counter electrodes were prepared by keeping as-prepared Cu film in a polysulphide solution for 60 s [29].

Here, copper sulphide nanowall has been formed by a one-step anodization process. In this anodization system, sodium sulphide electrolyte solution is used as an anode and graphite as a cathode. Then clean Cu (copper) foil was immersed in it to form CuS nanowall. This method is very useful to form 3D copper sulphide nanowall [30].

Cu_xS was synthesised here using the microwave hydrothermal method. At first, a mixture solution was prepared using copper nitrate, polyvinylpyrrolidone (PVP), and thioacetamide. Then it was stirred for 30 mins and placed in an autoclave maintained at 100-200^{0}C temperature. Then the precipitate was separated from the solution, and the soluble salt was removed. Finally, it was introduced in a microwave hydrothermal synthesis process maintained at 300 W of microwave power [31].

Copper sulphide nanoballs were fabricated in this work by the soft chemistry method. The bath was prepared by using cupric nitrate hydrate, barium hydroxide, triethanolamine, and thiourea. Here bath temperature was maintained at 54^{0}C for 30 min. It was finally washed and dried [32].

Copper sulphide (CuS)-based thin film has been prepared here by the thermal co-evaporation method. The substrate was kept in an evaporation chamber. The chamber maintained a constant temperature of 450^{0}C during deposition [33].

In this work, a facile chemical conversion method has been implemented to fabricate copper sulphide nanotubes. Here Cu (copper) nanowire was formed by electrodeposition using a galvanostat. Here, a platinum-coated titanium stripe has been utilized as a counter electrode whereas Ag/AgCl has been considered as a reference electrode. The electrolyte has been prepared using copper sulphate and sulphuric acid. Then the sulphur precursor solution was prepared using thiourea, and as-prepared Cu nanowire was kept in it by maintaining the temperature at 90°C to form Cu_xS nanostructures [34].

Here copper sulphide nanomaterial was deposited by surfactant-free solvothermal technique. At first a green solution was prepared using copper nitrate trihydrate and ethylene glycol. Thereafter thiourea was added into it and stirred. Then the mixed solution was placed in an autoclave maintained at 150^{0}C temperature. Finally, it was washed and dried in a vacuum environment [35].

Copper sulphide (CuS)-based film has been prepared by the chemical vapour deposition (aerosol-assisted) method. Here, at first, a copper (II) complex was prepared using copper nitrate trihydrate and potassium isobutylxanthate. The deposition was performed using a single-source precursor with toluene and carrier gas argon. Then the substrate was kept in the furnace, and deposition was performed [36].

Copper sulphide has been formed here by the metal-organic fabrication method. At first, a precursor solution was prepared using 3,5-dimethylpyridine (Lutidine) and toluene. After thioacetic acid and copper salt were added into it. Then a bluish-green compound was separated by filtration and dried in air. Then a saturated solution was achieved by dissolving it in methanol. Then a few drops of solution were taken on the substrate, and at last it was pyrolyzed at 350°C in a furnace under an argon atmosphere [37].

In this work, the physical vapour deposition (PVD) method has been used for the formation of nano-structured Cu_xS. At first, Cu (copper) was fabricated on a substrate by maintained

vacuum pressure. Then S (sulphur) was deposited using sulphur powder by evaporation using an electron beam gun. This method is useful to form stable nanostructure [38].

In this work, a copper sulphide-based film was formed using the PLD (pulsed laser deposition) method. The copper and sulphur were the main sources of material. Here, substrate temperature 250^0C, pulse duration 10 ns, and frequency 3 Hz were maintained [39].

Cu_xS was deposited using atomic layer deposition (ALD) on bare silicon substrates. Here the reaction chamber contained high-purity argon gas. The precursor was kept at 60°C for about 1 hour. The fabrication process was controlled by introducing bis(dimethylamino-2-methyl-2-butoxy) copper (II) and hydrogen sulphide gas [40].

There is huge application potential for stable copper sulphide materials, and the stability can be ensured by forming nanostructures of the material. It is used as a suitable absorber material for solar PV applications. It also acts as a suitable candidate for cathode material in field emission applications.

1.4.2 Tin Sulphide

SnS (Tin Sulphide) is an earth abundant, non-toxic, and cheap material. It is an n-type semiconducting material with a high optical absorption coefficient ($> 10^4$ cm^{-1}) as well as high charge carrier mobility (18.3-230 cm^2/V. s).

Tin Sulphide (SnS) film has been deposited here by a two-step process like DC magnetron sputtering as well as sulphurisation using a vacuum tube furnace. At first tin (Sn) was deposited using DC magnetron sputtering. This deposition was carried out under argon atmosphere with maintained pressure of 5mTorr and power of 1500 watts. Then sulphurisation has been performed in a vacuum furnace by introducing a hydrogen sulphide and argon gas mixture and maintaining the temperature at 300-450°C for 2 hours [41].

SnS film was fabricated here using the CBD (chemical bath deposition) method. The precursor solution was prepared by using tin chloride and thioacetamide. Then it was kept in a temperature control system where deposition of SnS was proceeded with initially at temperature 17°C for 3 hours, and after it was maintained at temperature 8°C for 21 hours [42].

Here SnS film was fabricated using the CSS (close-spaced vacuum sublimation) method. Here the distance of 17 mm was maintained in between the evaporator and substrate. The chamber pressure was maintained at $5x10^{-3}$Pa, and evaporator temperature was fixed at 948 K. The deposition was carried out for 4 mins to form a suitable tin sulphide film [43].

Here, the SnS film was prepared by the CBD (chemical bath deposition) method. Here EDTA (Ethylenen diamine tetraacetic acid) is used as the complexing agent. Here the precursor solution was prepared using tin chloride dehydrate, acetone, EDTA, and sodium thiosulphate. The solution pH was maintained at 10.5 using NH_3 solution. The bath temperature was maintained at 45^0C for suitable deposition [44].

Tin Sulphide was formed by the CBD (chemical bath deposition) technique. The bath solution was prepared using stannous chloride, thioacetamide, and tartaric acid. Here tartaric

acid is used as the complexing agent. The deposition was carried out under different concentrations of complexing agent. The constant bath temperature of 70^0C for 50 mins was maintained during deposition of the SnS film [45].

Here copper-doped tin sulphide was developed by the spin-coating process. At first, a solution was prepared using tin chloride dihydride, thiourea, methanol, and 2-methoxy ethanol. Then the solution was sprayed on the substrate kept over a hot plate maintained at a temperature of 200^0C. The speed of the spin coater was maintained at 3000 rpm to achieve a properly deposited film [46].

SnS film was developed here by a simple bath process. This bath process was performed by mechanochemically prepared precursor solution. The solution was prepared using triethanolamine, tin chloride metal salt, thioacetamide, and ammonia. The bath temperature of 40 to 50^0C was maintained during the deposition of the tin sulphide film [47].

Tin sulphide was formed here by the wet chemical synthesis method. In this method, tin chloride and sodium sulphide were used as source materials of tin and sulphur, respectively. Here ethylene glycol was used as a solvent for this deposition. The deposition was performed to maintain temperature at 80^0C. At last, to achieve film, it was washed as well as centrifuged, and dried it at room temperature [48].

Tin sulphide (SnS) thin film was formed here using the radio frequency sputtering technique. Here argon was used as an inert gas whose flow rate of 30 sccm was maintained. The 100-watt RF power, considering working pressures of 6, 10, 30, and 50 mTorr, was set during deposition of the film [49].

SnS thin film was fabricated here by the SILAR method. The aqueous solutions were prepared here using TEA (triethanolamine), tin nitrate, and sodium sulphide. The reaction was conducted for 30 cycles considering different molar concentrations like 0.05, 0.10, 0.15, 0.20, and 0.25 (M) of tin nitrate and sodium sulphide. The cycles were performed for all concentrations to get deposited films of tin sulphide [50].

Tin sulphide was formed here using the chemical spray pyrolysis method. In this process, a solution was prepared here using tin chloride and thiourea. Thereafter, this as-prepared solution was sprayed on the substrate, which maintained temperature at 200^0C. Then it was vacuum annealed at 450°C for 1 hour to achieve suitable deposition of the film [51].

SnS film was developed here by the thermal evaporation process. In this process, high-purity SnS powder was used as source material. The distance between the source and substrate was 17 cm, and the temperature of the substrate, 250°C, was maintained here. The rate of evaporation was set at about $10A^{\circ}s^{-1}$ to form deposited film [52].

Tin sulphide can be used for the applications in PV solar cells, optoelectronic devices, etc.

1.4.3 Copper Zinc Tin Sulphide (CZTS)

CZTS (Copper Zinc Tin Sulphide) is a non-toxic and abundant element. It also has the highest absorption coefficient in the visible region.

Here CZTS (Copper Zinc Tin Sulphide) has been prepared on glass substrate by a dibenzyl dithiocarbamate-based solution process. The materials like carbon disulphide, dibenzylamine, benzene, tin chloride pentahydrate, zinc chloride, copper chloride, trichloromethane, methanol, and sodium hydroxide were required to form CZTS. In this method, at first NaDTC (Na dibenzyldithiocarbamate) was prepared, and it was synthesised using dibenzylamine, sodium hydroxide, carbon disulphide, and d-benzene. After it was reacted with metal salt like zinc chloride and washed as well as filtered, the product was dissolved in trichloromethane to remove contamination. Then the formed ZnDTC (Zn dibenzyldithiocarbamate) solution was dropped on a glass substrate. Then the coated substrate was annealed at a temperature of 350^0C under nitrogen for 30 mins to achieve the desired deposited film [53].

In this method, CZTS has been developed using metal salts and dodecanethiol (DDT). This synthesis was carried out in a nitrogen atmosphere. The solution was prepared using copper acetate, zinc acetate, tin iodide, and oleylamine. Then the as-prepared solution was heated at a temperature of 150^0C, and DDT was added into it. After the prepared solution was kept at a temperature of 250^0C for 60 min to get the desired film [54].

CZTS film was synthesised on molybdenum substrate through a solvothermal route. Here at first a homogeneous mixture was prepared using copper acetate hydrate, zinc acetate, tin chloride, thiourea, and ethylene glycol. Then it was kept in an autoclave, including a substrate maintained at a temperature of 180^0C for 12 hours. At last, the as-deposited film was annealed in a nitrogen environment at a maintained temperature of 300°C for 30 min [55].

CZTS film was formed here by a nebuliser-assisted spray pyrolysis technique. The solution was prepared with copper chloride, zinc chloride, tin chloride, and thiourea. Then the as-prepared solution was mixed with a nebuliser to achieve fine aerosols. Thereafter it was sprayed on a substrate maintained in air (carrier gas) pressure of 0.2 Pa for the time of 20 mins to get the desired deposited sample [56].

The formation of the CZTS film has been done by the spray technique. Here the solution was prepared using cuprous chloride, zinc chloride, stannous chloride, and thiourea. In this process, nitrogen was used as a carrier gas, and solution flow rate was maintained at 1 ml/min. The deposition was performed at temperatures of 200^0C to 450^0C to achieve the desired film [57].

Here, CZTS film has formed using ball milling as well as thermal evaporation techniques. At first, copper, zinc, sulphur, and tin powders were taken as source materials. Here, a ball and powder ratio of 2:1 was maintained, and powders were milled by stainless steel balls having a speed of 2750 rpm. After the synthesis of CZTS, the thermal evaporation was performed at room temperature and at 673 K to deposit it on the substrate [58].

CZTS (Copper Zinc Tin Sulphide) was fabricated using the electron beam evaporation technique. Here CZTS powder was prepared using copper nitrate, zinc nitrate, tin sulphate hexahydrate, and sodium sulphide. The solution was prepared by mixing it with ethylene glycol at room temperature. After it was irradiated via microwave oven operated at 350 watts for 5 mins. Thereafter it was washed as well as centrifuged to get the final product. Then deposition was performed on clean glass substrate at the rate of 0.5 nm/s to achieve the desired film [59].

CZTS film has been developed here using the pulsed laser deposition method. The fabrication was done at room temperature. In this process, pulsed laser energy density of 2.5 J/cm², a repetition rate of 10 Hz, and a time of deposition of 22 mins were maintained. The as-prepared was annealed under nitrogen and hydrogen sulphide atmosphere at a temperature of 575°C for 10 min to get a suitable deposited film [60].

In this work, a light sintering technique has been used for CZTS fabrication. In this work, Cu (acac)$_2$ Zn(acetylacetonate), and Sn(acetylacetonate) were used as raw materials. The solution prepared by these materials was taken in a heating flask under nitrogen, maintaining a temperature at 230^0C. Then oleylamine was added into it. The reaction was taken over for 1 hour at 230^0C.The final nanocrystal was prepared by dissolving it in butylamine and coating it on the substrate. At last, it was dried, and light sintering was introduced to achieve the desired film [61].

CZTS has been formed here by the spray pyrolysis method. Here, using the method, cupric chloride, zinc acetate, stannic chloride, and thiourea were used as source materials for copper, zinc, tin, and sulphur, respectively. The solution was sprayed on the substrate by keeping it on a hot plate to get the deposited sample [62].

Here the SILAR method has been introduced to develop CZTS film. The cationic bath consists of copper sulphate, tin sulphate, and zinc sulphate, as well as an anionic bath containing sodium sulphide. Here in this reaction, 40 cycles were set, considering adsorption and reaction time of 30 s. Finally, the precursor film was kept under nitrogen and hydrogen sulphide atmosphere at 575°C temperature to get the desired deposited film [63].

It is used for the fabrication of low-cost solar cells.

1.4.4 Copper Oxide (CuO)

CuO (copper sulphide) is cheap and nontoxic. It is easy to fabricate and has better electrochemical stability.

Here CuO (Copper Oxide) was fabricated by the wet-chemical method. The precursor solution was prepared using copper nitrate trihydrate, sodium hydroxide, and DI water. Then the as-prepared solution was kept in a Teflon flask maintained at a temperature of 770^0C. After it was centrifuged (speed 6000 rpm) and washed to achieve deposited copper oxide film [64].

CuO was fabricated here by the pulsed laser deposition technique. At first, CuO target material was prepared using the solid-state reaction method. At the time of deposition, the target-to-substrate distance was 3.5 cm, the pulse repetition rate was 5 Hz, the laser fluence was 2–3 J cm^{-2}, and the deposition temperature was 200°C was maintained to get a CuO sample [65].

Co:CuO (CuO-doped cobalt) has been fabricated here using the R.F. sputtering method. There was taken a pure metallic copper target partially filled with pure cobalt. Here, RF power is 150 watts, the target-to-substrate rate distance is 7 cm, and an inert gas argon (pressure 0.7 Pa) and oxygen (pressure 0.3 Pa) mixture were maintained to fabricate CuO-doped cobalt film [66].

Copper oxide film has been formed here by the direct current magnetron sputtering method. The DC power supply kept constant power of 100 watts during deposition. The argon gas flow rate was 2.5 sccm, and the oxygen gas flow rate of 5.5 sccm was maintained here. The time of deposition was about 60 min to get a suitable deposited film [67].

Here CuO thin film was developed using the spray pyrolysis process. The precursor solution was prepared using copper chloride dehydrate, potassium hydroxide, and DI water. After it was sprayed over where the substrate maintained a temperature of 300-450°C. The rate of spray was kept at 3 mL/min during deposition to achieve a suitable CuO film. This process is very easy and less expensive [68].

Copper oxide thin films can be used in solar cells, sensors, and optoelectronic devices. CuO-based nanomaterials have also been used in electrochemical applications.

1.4.5 Zinc Oxide (ZnO)

ZnO is a nontoxic, wide band gap semiconductor. The main characteristics of ZnO are large electric field sustain capability as well as providing higher breakdown voltages.

Here aluminium-doped ZnO was fabricated using the sol-gel method (modified). At first, two different solutions were prepared in different beakers. In beaker I, ethanol alcohol, zinc acetate dehydrated, and aluminium nitrate were added to get the various molar concentrations of aluminium. On the other hand, beaker II consists of sodium hydroxide, ethanol alcohol, and DI water. Thereafter, these two beakers were added in one by dropping the maintained temperature to 60^0C for 60 mins to achieve the desired deposited film [69].

ZnO was synthesised here by the electrodeposition method. This fabrication system consists of three electrodes: graphite as anode, clean substrate as cathode, and saturated calomel as a reference electrode. The bath was prepared here using zinc chloride and potassium chloride. There was a maintained bath temperature of 333K to 363K, a deposition on time of 5 to 30 min, and a current density of 0.25 to 1.5 mA cm^{-2} during the deposition of the ZnO film [70].

ZnO was formed here on FTO substrate by a hydrothermal process. At first, a precursor solution was prepared using zinc nitrate hexahydrate, hexamethylenetetramine, and DI water. Then hydrothermal treatment of the substrate has been performed using titanium tetrachloride by maintaining the temperature at 70^0C for 30 min. Finally, it was annealed at 150^0°C for 30 min to achieve the desired sample [71].

Here ZnO nanowires were developed on a gallium- and aluminium-cooped ZnO (GAZO) thin film seed layer. The GAZO seed layer was formed by the RF magnetron sputtering method using high-purity gallium, aluminium, and zinc oxide targets. Here, RF power was 150 watts, working pressure was 1.2×10^{-2} mbar, and the flow rate of argon at 12 sccm was maintained during deposition. After this GAZO substrate was dissolved in an aqueous solution prepared using zinc nitrate hexahydrate and hexamethylenetetramine. Here deposition temperature 60^0-90^0C was maintained for 2 to 8 hours to achieve the desired sample [72].

Here ZnO thin film was formed using the M-SILAR (modified successive ionic layer adsorption and reaction) method. The film has developed using zinc-ammonia as cationic and diluted hydrogen peroxide as an anionic source of precursor solution. There were maintained deposition cycles for 50, 100, 150, and 200 times repeatedly to achieve the desired [73].

In this method, ZnO powder has been developed first using hydrothermal synthesis, and then it was sprayed on the FTO substrate to achieve the desired film. At first, an aqueous solution was prepared by taking zinc nitrate hexahydrate with diethylamine under maintained temperature at 80^0C for 8 hours. Thereafter the precipitate of zinc oxide was sprayed over the substrate and annealed it at 450^0C for 1 hour to get the desired film [74].

Here ZnO thin film was fabricated using the CBD (chemical bath deposition) method. The bath was prepared using zinc nitrate, ammonium hydroxide, and DI water. Here, bath temperature of 80°C for 10 hours was maintained during deposition [75].

ZnO film has been developed here by the spin coating method. Here the solution was prepared by hydrolysis synthesis of zinc acetate, methanol, and potassium hydroxide. At first, zinc acetate was mixed with methanol under suitable stirring by maintaining the temperature at 60^0C. Then potassium hydroxide was added into it by maintaining the same temperature for 2 hours and finally coating it over the substrate [76].

ZnO was formed here by the MWAPPJ (microwave-excited atmospheric pressure plasma jet) method. The precursor solution was prepared using 2-methoxyethanol and acetylacetone. Then it was coated on a substrate using irradiation by MWAPPJ. In this method, He (helium) gas was used in a reactor where microwave frequency 2.45 GHz was maintained. Here, during plasma irradiation, input power of 50 watts for 60s was maintained to achieve the desired sample [77].

In this work, ZnO nanoparticle was developed using a low-temperature precipitation method. At first, the solution was prepared using zinc acetate, DI water, and aqueous NaOH under continuous stirring for 30 min. Then the as-prepared solution was kept at a temperature of 80°C for 2 hours. Then there was added cobalt acetate dehydrate to developed cobalt-doped ZnO powder. Thereafter it was kept in isopropanol and stirred with a magnetic stirrer to form a solution for deposition. Then it was spin-coated on the substrate by maintaining a rotation speed of 3000 rpm for 30 s. Finally annealed it at 250^0C for 30 min to get a suitable deposited sample [78].

ZnO has been formed here by the electrodeposition method. In this system, soda lime glass has been considered as a working electrode, whereas platinum wire was utilized as a counter electrode. Here saturated calomel has been considered for the application of the reference electrode. Here, an aqueous solution was prepared using zinc acetate dehydrate, magnesium acetate tetrahydrate, and hexamine. The bath temperature was maintained at 90^0C during deposition of the ZnO film [79].

In this study, AZO (Aluminium Zinc Oxide) film has been deposited from the power target using the RF magnetron sputtering method. At first this mixture powder was prepared using aluminium oxide and zinc oxide, and after it was merged with acetone. Then it was sintered at 700^0C, and target material was prepared for deposition. Here, RF power density 2.19 watt/cm^2, substrate temperature 400^0C were maintained during deposition of the film [80].

Here aluminium-doped ZnO has been developed using the spin-coating technique. Here, at first, a precursor solution was prepared using isopropyl alcohol, zonyl surfactant, and DI water. Then polyvinyl alcohol was added into it to improve its mechanical adhesion. Finally, this solution was spin coated on the substrate by maintained roating speed 3000 rpm to achieve desired film [81].

ZnO film has formed here by the SILAR (successive ionic layer adsorption and reaction) method. Here, zinc nitrate as the source of Zn^{2+} and hydrazine hydrate as OH^- ions were used for the deposition of the film. This two-precursor solution was prepared in different beakers by maintaining a temperature of 75^0C. Thereafter, the substrate was dissolved successively in these solutions to achieve the desired deposited film [82].

ZnO is a suitable candidate for applications in photocatalysis, piezoelectric materials, gas sensing, etc.

1.4.6 Titanium dioxide (TiO_2)

TiO_2 (titanium dioxide) semiconductor nanomaterial and functionalized carbon nanotubes were used for the preparation of solar cells. It is a wide bandgap semiconductor, and it has better photo corrosion resistance as well as good thermal stability.

TiO_2 was developed here using a refluxing method. Here, at first, a titanium glycolate precursor has been produced using tetrabutoxytitanium and ethylene glycol using a magnetic stirrer maintained at a bath temperature of 60^0C. Then it was added with acetone and DI water under continuous stirring for 1.5 hours to form titanium glycolate. Thereafter, this prepared titanium glycolate was added with water and sonicated for 5 mins. After it was kept in a water bath at a maintained temperature of 95^0C for 1 hour under continuous stirring to get the desired deposited film [83].

TiO_2(titanium dioxide) has been developed here by the solvothermal method. Here titanium isopropoxide was taken as a precursor and toluene as a solvent. Thereafter the mixture was kept in an autoclave maintained at a temperature of 180 to 240^0C for 4 to 24 hours. Finally, the sample was taken and dried in a vacuum at 60°C for 3 hours [84].

TiO_2 was formed here using the hydrothermal method. Here at first, the solution was prepared using hydrochloric acid and DI water. Then the precursor solution was made by adding TBOT (tetrabutyltitanate) into it. After this mixture solution was kept in an autoclave for hydrothermal synthesis, it was maintained at a temperature of 150^0C for 4 hours to achieve the desired film [85].

TiO_2 film has been deposited here by atomic layer deposition (ALD) technique. Here titanium dioxide film has been grown on Ti wire by using DI water with nitrogen as the carrier gas inside a reactor. This fabrication was performed by applying successive pulses of titanium tetrachloride (TDA) into the reactor by maintaining a temperature of 300^0C [86].

Here, a zinc oxide (ZnO)-doped TiO_2 film was developed by the refluxing method. At first, a solution was prepared using titanium isopropoxide, isopropyl alcohol, and DI water and kept at 450^0C for 2 hours for the formation of TiO_2 nanoparticles. Then there was formed another solution using zinc acetate dihydrate and DI water. Then the film was dissolved into it and NaOH was added dropwise to it for the formation of ZnO-doped titanium dioxide. Finally, it was refluxed by maintaining the temperature at 97^0C for 3 hours to get the desired sample [87].

TiO_2 has applied for the development of dye-sensitised solar cells. It can also be used for applications in photocatalysis, nano-paint, antibacterial agents, etc.

1.4.7 Cadmium Sulfide (CdS)

CdS is very toxic material, and it degrades with time. The band gap of the semiconducting n-type CdS material is 2.45 eV.

CdS has been developed here by a chemical synthesis method. At first, an aqueous solution was prepared using ammonium hydroxide and cadmium sulphide, where the pH of the solution was maintained at 11. Thereafter thiourea was added into this as-prepared solution. Then the substrate was dissolved into this mixed solution by maintaining a temperature of 90^0C for 10 min to achieve the desired deposited film [88].

Cadmium sulphide has been formed here by the solvothermal microwave irradiation method. At first, a solution was prepared using cadmium acetate dihydrate, thiourea, and ethylene glycol. After it was taken under continuous stirring for 1 hour. It was maintained at a temperature of 50^0C to form a homogeneous solution. Then this mixture was kept in a microwave oven where frequency was maintained at 2.45 GHz. There was performed 50% power cycle until precipitate was achieved. Finally, it was washed as well as centrifuged at 60^0C for 6 hours to get the deposited sample [89].

CdS-doped S has been formed here by the MA-CBD (microwave-assisted chemical bath deposition) method. Here the aqueous solution was prepared using cadmium nitrate, thiourea, and ammonium acetate. Here the as-prepared solution pH has been obtained as 10 by introducing ammonia into it. Then the substrate was dissolved into it and kept at a microwave oven by maintained temperature of 75^0C for 45 mins. At last, it was washed to get the desired film [90].

CdS has shown excellent properties for applications in optoelectronic devices like LDRs, solar cells, etc.

1.4.8 Cadmium telluride (CdTe)

CdTe is a semiconductor belonging to the II-VI group and exhibits a high melting point of 1041^0C as well as being insoluble in water.

CdTe has formed here over Ni substrate using the electrochemical deposition technique. Here, Ni substrate, pure graphite plate, and silver/silver chloride/potassium chloride acted as the working electrode, counter electrode, and reference electrode, respectively. The bath was prepared using cadmium sulphate and sodium tellurite. The pH of the bath was maintained using H_2SO_4. Finally, the film was annealed at 300^0C for half an hour under an N_2 environment to achieve the desired deposited sample [91].

CdTe was developed here using the spray pyrolysis method. At first, a, a solution was prepared using cadmium chloride monohydrate (with added triethanolamine) and tellurium dioxide (with added hydrazine hydrate). Then the solution was made up using deuterium-depleted water and ammonia by maintaining a 4:1 ratio. The pH of the solution was maintained at 11.5 here. The substrate temperature of 300^0C and solution flow rate of 5 ml/min were maintained here during deposition [92].

Here CdTe was formed using the sublimation method. This fabrication system consists of a rotating vapour source attached to a graphite container. Here CdTe power is used as a source material and kept in a container by maintaining a temperature of 700^0C. The container rotated at a speed of 40 rpm to maintain uniform deposition of the material over the substrate [93].

CdTe has a large absorption coefficient and can be used for photovoltaic applications. It can be developed in a low-cost fabrication process.

1.4.9 Copper indium diselenide (CIS)

CISe is a ternary compound having a high absorption coefficient and better thermal stability.

CISe was formed here using the electrochemical potentiostatic deposition technique. In this system, saturated calomel and platinum foil acted as the reference electrode and counter electrode, respectively. Here an aqueous solution was prepared using copper sulphate, indium sulphate, citric acid, and selenium selenide. The pH of the solution was maintained at 2.1 here. The deposition was carried out under an applied potential of 600 mV for a saturated calomel electrode to get the desired deposited sample [94].

Here CISe was developed on the surface of CdS (cadmium sulphide) by the chemical ion exchange method at room temperature. At first, CdS was formed on ITO substrates by the CBD (chemical bath deposition) process. Cadmium chloride, thiourea, and triethanolamine were used for the formation of CdS by maintaining the temperature at 80°C. Thereafter, CISe precursor solution was prepared using copper sulphate, indium trichloride, and sodium seleno-sulphate. This solution was prepared by mixing each material with a fixed volumetric proportion. Then the as-prepared ITO/CdS substrate was immersed in it to achieve the CISe/CdS/CdS thin film device [95].

CISe can be used for the applications in low-cost solar cell devices, nonlinear optics, and light-emitting diodes.

1.4.10 Gallium Nitride (GaN)

Gallium nitride (GaN) is a group III-nitride semiconductor that has high electron mobility, high thermal conductivity, and a high optical absorption coefficient. It is a wide-band semiconductor with an optical band gap of 3.4 eV.

Gallium Nitride **(**GaN) has been deposited here on patterned silicon (Si) substrate by using nano-imprinting as well as the pulse laser deposition (PLD) method. This imprint was created by using three basic steps. At first, imprinting was performed by utilizing a mould to produce a thickness diversity in the resin area of the silicon substrate. The next one was to pull out the mould and finally, the pattern was moved by utilizing anisotropic etching to take out the resin. Then the achieved patterned Si substrate was immersed in the solution of sulfuric acid and hydrogen peroxide at a ratio of 1:1, and thereafter, the hydrogen fluoride solution was continuously used to wash the resin on the substrate. Thereafter, initially, a thick aluminium nitride layer was developed to grow GaN on Si substrates. It was performed using the PLD method, where pressure of 5×10^{-10} Torr and temperature of 750^0 C were maintained. After GaN was deposited by maintained the temperature in between 650 to 800^0 C. Here, a nitrogen

source was created by using an RF radical generator, which was operated at a power of 300 watts under a $1x10^{-5}$ Torr nitrogen atmosphere [96].

Here, Indium Gallium Nitride (InGaN) and Gallium Nitride (GaN)-based multi-quantum wells (MQWs) were developed using the metal organic chemical vapour deposition (MOCVD) technique. At first, a GaN nanowire template was formed by using a two-step etching process. Here, Si-doped GaN on sapphire was utilized for the development of the template. The silicon nitride layer (200 nm) was formed by PECVD, or plasma-enhanced chemical vapour deposition method. Thereafter, a circular hole pattern (400 nm in diameter) was introduced here by using lithography and the lift-off process. Then, at first, ICP-RIE, or inductively coupled plasma reactive ion etching, was performed. Wet etching was done by utilizing a KOH solution. Thereafter, the MQW structure was formed by the MOCVD process, where an 1130^0 C temperature for 840 s and 100 Torr pressure were maintained. Here, hydrogen was used as a carrier gas. On the other hand, trimethylgallium and ammonia were utilized as Gr III and Gr V precursors, respectively. The MQWs structure consists of a GaN buffer, an InGaN quantum well, and a GaN protection layer [97].

In this present study, gallium nitride-based nanostructures have been grown on sapphire substrates by molecular beam epitaxy, or MBE. In the MBE method, 350-watt microwave power was used to generate nitrogen particles, and a 0.5 sccm flow rate was maintained. The surface of the template was cleaned by using organic solvent and a hydrogen fluoride solution for a duration of 6 minutes. Thereafter, it was further thermally cleaned in the chamber by maintaining a temperature of 800^0 C for a duration of 5 minutes under a nitrogen atmosphere. The growth rate was maintained at 120 nm/h to achieve the desired sample [98].

Here, the GaN nanostructure was developed on a sapphire substrate by using electron beam lithography and the reactive ion etching technique. At first, the substrate was cleaned in acetone with an ultrasonic bath. After it was rinsed in methanol as well as isopropanol, Then the sample was annealed at 85^0 C and dried in N_2 gas atmosphere. Here, polymethylmethacrylate (PMMA) was used as an electron-sensitive resist layer. In the chamber, the electron beam was maintained at 50 kV. Here, the diameter of the beam was set at 16 nm. The NiCr alloy metal was deposited by a thermal evaporation process with a thickness of 30 nm for the purpose of etching a mask. The reactive ion etching method was used, where pressure of 15 mTorr, temperature of 50^0 C, N_2 variation (0 – 75%), flow rate of 40 sccm were maintained for the purpose of deposition [99].

In this study, Gallium Nitride (GaN) / Indium Gallium Nitride (InGaN)-based nano-pyramid photoanode was developed using selective area growth, or the SAG method. At first, a GaN layer was formed on the sapphire substrate by the Metal Organic Chemical Vapour Deposition, or MOCVD, technique. The undoped GaN buffer layer as well as the n-type doped GaN or Si-doped layer were developed at temperature of 1060^0 C. The silicon di-oxide layer was developed on GaN by using Plasma-Enhanced Chemical Vapour Deposition or PECVD process. Then the membrane of anodized aluminium Oxide or AAO, was formed on SiO_2 layer. This membrane was supported by a holder that was made of polymethyl methacrylate. The AAO was transferred to the SiO_2 layer by dissolving the holder in acetone.

Finally, a GaN/InGaN-based photoanode was grown subsequently by the MOCVD process [100].

The ultra-thin Gallium Nitride (GaN) nanostructure has been fabricated here on Si substrate by the plasma-assisted molecular beam epitaxy method. At first, gallium droplets were formed by using a nucleated gallium wet layer. Thereafter, it was exposed to the active species of nitrogen ions. The substrate temperature of 770^0 C and the pressure of the gallium beam of 6.5 x 10^{-7} torr for 120 min were maintained here to achieve the GaN nanostructure film [101].

In the present study, the GaN/pSi heterojunction nanostructure was formed by using pulse laser deposition, or the PLD method. At first, the pSi substrate was developed by utilizing the photo-electrochemical etching technique. This etching process was performed using a 100-watt power laser assistant diode. The etching solution was made by utilizing hydrofluoric acid and ethanol. Then the GaN target material was prepared by using gallium nitride powder. Here, 1000mJ of laser energy and 7 ns of pulse duration were maintained during the deposition process. The vacuum pressure of the system 10^{-2} mbar was implemented to achieve the desired deposited film [102].

Here, Gallium Nitride (GaN) nanobelt was prepared by an electrochemical lift-off process. The epitaxial growth of n or p GaN has been implemented using the Metal Organic CVD or MOCVD technique. At first, a GaN buffer layer with a thickness of 500 nm was formed. Here, n-GaN was developed by maintaining a silicon doping concentration of 5 x 10^{18} cm^{-3}. Then the structure of the middle sacrificial layer (SL) (n^{++}- GaN/n^{+}-GaN/n^{++}-GaN) was introduced here. Next, the patterned photoresist (PR) was developed by implementing UV lithography as well as spin coating methods. After drying, etching was performed by inductively coupled plasma, or ICP. A gas mixer of chlorine and boron chloride was used for this etching process. The uniform GaN strip was obtained here after the removal of PR with acetone. Then the conductive silver layer was formed on it and placed in an oxalic acid solution. Thereafter, it was placed in a two-electrode cell at room temperature, where GaN and platinum sheets acted as anodes and cathodes, respectively, for performing the electrochemical etching. Here, a 13-volt DC power supply was maintained. Finally, the GaN nanobelt was achieved by extracting the SL during the etching and transferring it onto a silicon substrate [103].

In the present study, nano-porous (NP) and nano-column (NC)-based gallium nitride films were fabricated on sapphire substrates by using laser molecular beam epitaxy, or the LMBE method. The NC, or nanocolumn, was obtained by developing a low-temperature gallium nitride buffer layer on bare sapphire substrate. On the other hand, nanoporous was grown by developing a low-temperature gallium nitride buffer layer on a nitridated sapphire substrate. The growth of a low-temperature buffer layer was performed by maintaining a temperature of 500^0 C for a duration of 20 minutes. Here, the laser repetition rate and energy density were maintained at 5 Hz and 5 Jcm^{-2} respectively. The nitridation was performed using an R.F. nitrogen plasma cell, where R.F. power was 250 watts and N_2 flow rate was 0.4 sccm during the fabrication process [104].

Here, a tower-like gallium nitride (GaN) nanostructure film was fabricated by using chemical vapour deposition, or CVD method. Here, gallium oxide was taken as a source of gallium (Ga) and kept in a quartz boat. After that, it was transferred to a horizontal tube furnace under the CVD system. The aluminum oxide/Si substrate was coated with a thin Au layer and tilted in the chamber. Here, the argon flow rate was maintained at 100 sccm at a temperature of 800^0 C. Thereafter, argon was replaced by ammonia, and the flow rate was maintained at 300 sccm at a temperature of 1080^0 C. Then it was kept at 1050^0 C for a duration of 60 minutes. Finally, the ammonia flow was stopped and cooled down to room temperature to achieve the desired sample [105].

The formation of gallium nitride (GaN) nanowires as well as nanorods has been cultivated here by using catalyst-assisted chemical vapour deposition, or CVD. The film was grown on a silicon substrate where Au or gold acted as a catalyst. The substrate was washed using isopropyl alcohol as well as acetone before the start of deposition. After Au wire was deposited on the substrate by using the e-beam evaporation technique, the base pressure of 1 x 10^{-9} Torr and beam current of 5 nA were maintained. Then it was placed in a horizontal tube furnace by maintaining a distance of 10 mm from gallium metal. The base pressure of the furnace was set at 10^{-3} mbar, and the deposition has been performed at 800^0 C. The ammonia flow rate was maintained at 150 to 200 sccm during deposition for a duration of 120 min. Here, nitrogen was used as a carrier gas whose flow rate was kept at 500 sccm for the growth of the desired sample [106].

It is a suitable candidate for applications in opto-electronic devices such as light-emitting diodes, or LEDs, UV detectors etc.

1.5 Usefulness of Nanomaterials in Optoelectronic devices

Nanomaterials have created a promising path in future optoelectronic device applications. There are several advantages of nanomaterials in improving device performances. Nanostructures like nanowires, nanorods, nanotubes, and quantum dots have been introduced for optoelectronic device applications since they provide low-cost as well as high-efficiency devices. Nanomaterials can act as good-quality absorber materials for optoelectronic applications as they usually maintain an optimum optical bandgap that lies between 1.1 and 1.5 eV. Thus, more luminous intensity and corresponding charge carrier generation capacity, improving the photoelectric conversion efficiency of the device. Apart from this, fabrication of nanostructures has increased the mobility as well as decreased the scattering, and thus it can improve the overall conductivity of the device. Nanowire can provide a direct path for charge transport to the contacts as well as enhance light harvesting capacity. Apart from this, nanomaterial-based devices have shown excellent magnetic properties, which make them suitable candidates as magnetic storage device applications. The nano quantum dot technology can provide a tunable bandgap over a wide range of energy levels, which makes it possible to introduce quantum dot solar cells. On the other hand, mechanical strength and toughness have increased in nanostructure-based devices [107,108]. Thus, it can be said that nanostructure-based semiconductors have to increase the overall stability as well as the efficiency of the device.

Here some of the promising nanomaterials and their applications have been introduced. These thin film nanomaterials have shown promising results for the fabrication of optoelectronic devices. Copper Sulphide ($Cu_{2-x}S$) is one of the promising nanomaterials that has shown suitable optical bandgap in the range of 1.65 eV to 1.85 eV, and its average particle size of 12 to 100 nm was observed. $Cu_{2-x}S$ based nanostructures can also be obtained in a simple, low-cost method. Tin Sulphide (SnS) is another promising nanomaterial whose bandgap was varied from 1.1 to 1.88 eV, and an average crystalline size of 8 to 100 nm was obtained. The obtained result of Copper Zinc Tin Sulphide (CZTS) indicated that closely packed granular crystallites have been uniformly arranged on the surface of the substrate with an average grain size of 25–100 nm. It exhibited an optical band gap in the range of 1.3 to 1.74 eV. Copper oxide (CuO) can be produced as nanorods with a breadth in the range of 5-8 nm, and a bandgap was obtained in the range of 1.48 to 1.68 eV. The obtained result indicated that zinc oxide (ZnO) nanorods having diameters in the range of 100–120 nm showed hydrophobic nature, and it also exhibited flower-like morphology having crystalline size 33 nm. It is a wide bandgap semiconductor, and the highest optical transparency (92%) was obtained. Titanium dioxide (TiO_2) based nanorods exhibited good thermal stability and photo corrosion resistance. It has a wide optical bandgap, and nanoparticle size lies within the 100 nm range. Cadmium sulphide (CdS) exhibited a cauliflower-like nanostructure that was constructed by numerous nanopetals, and the edge thickness of the nanopetal was about 70 nm. CdS has shown an optical bandgap of 2.42 eV at room temperature. Cadmium telluride (CdTe) exhibited a band gap of 1.5 eV, and it formed a cubic crystal structure having a grain size of about 12 nm. Copper indium diselenide (CISe) has formed tetragonal crystal geometry with average crystalline size varying to 32 nm, and the optical bandgap of 1.25 eV was obtained. It can be used for high-efficiency, low-cost solar cells [17-95]. Therefore, the different nanomaterials mentioned here have exhibited excellent nanostructure as well as have shown suitable characteristics for application in optoelectronic devices.

1.6 Aims and Objectives of the present work

The aim of the present work is to develop semiconducting copper nitride (Cu_xN) nanostructures by using a simple and low-cost fabrication method for photo-sensors or photo-resistors as well as optoelectronic devices such as solar cell applications. A photodetector is a kind of light sensor that can convert incident light to electrical signals. Photodetectors can operate in photoconductive as well as photovoltaic mode. In photovoltaic mode, incident photons are converted into electrical energy, and solar cells can operate based on this principle. On the other hand, the resistivity of the semiconductor devices has decreased when photons are incident on them, which is known as the photoconductive mode, and light-dependent resistors (LDRs), can operate based on this principle. Photodetectors have been used in various applications, like in optoelectronic circuits, radiation detectors, space communication, military surveillance, etc. Nanostructures have an important role in the field of light sensors or photodetectors, transistors, diodes, and solar cells due to their high specific surface area as well as high electron conductivity. Here in this study, nanostructure-based semiconducting thin films have been introduced for application in optoelectronic sensors and devices.

Light Dependent Resistor (LDR), is a kind of photoresistor that is basically made of a cadmium sulphide (CdS)-based semiconductor, and it is sensitive to the visible spectrum of light. CdS is very toxic and degrades with time. On the other hand, copper is widely available as well as non-toxic, and nitride-based semiconductors such as GaN (gallium nitride), AlN (aluminium nitride), InN (indium nitride) and their alloys have shown potential applications in optoelectronic devices, but these are expensive compared to other traditional materials. So, one such promising material combining the attributes of nitride and copper-based materials is copper nitride (Cu_xN). Thus, the present research work has been trying to focus on developing semiconducting copper nitride (Cu_xN) material for the photoresistor or LDR and optoelectronic device such as solar cell applications. Here in this present work, at first, semiconducting-grade copper nitride nanostructures have been developed by introducing a simple and low-cost chemical deposition method to investigate its capability as a photoresistor or LDR application. Thereafter, the feasibility of the nanostructure Cu_xN film has been tested for solar cell applications. The modelling of a solar cell devices by using Cu_xN as an absorber as well as window layers in combination with various inorganic semiconductors has been cultivated in this present study.

Thus, here at first, author trying to focus on the development of a semiconducting copper nitride nanostructure by a simple as well as low-cost chemical deposition technique, and then the analysis of photoresistor performances has been explored by determining LDR gain. Thereafter, photoconductive and photovoltaic studies of the fabricated as-prepared film have been executed to establish it as an application in solar cell devices. Finally, the conclusion has made the suitability of Cu_xN film as photoresistor or LDR and solar cell applications.

To develop the low-cost semiconducting grade copper nitride (Cu_xN) film for the application in optoelectronic sensors or photoresistors and devices, the objectives of the thesis are as follows:

- The detailed literature review of various properties, different nanofabrication methods and applications regarding Cu_xN based thin films.

- The development of nanostructured Cu_xN semiconducting film by introducing a simple and low-cost chemical deposition method.

- To find the applicability of semiconducting copper nitride material as a light-dependent resistor (LDR) applications.

- The photoconductive and photovoltaic study of the as-prepared copper nitride (Cu_xN) film has been executed.

- The photoconductive study of the Cu_xN film has been performed by variations of film thickness and determining optimum thickness for solar cell device applications.

- The modelling of a solar cell by using Cu_xN as absorber and window layers in combination with various inorganic semiconductors has been investigated in photovoltaic studies.

- Finally, the conclusion has been drawn based on the feasibility of Cu_xN based film as light dependent resistor (LDR) and solar cell applications.

1.7 Conclusion

Thin film nanostructure semiconducting material plays a very crucial role in the performances of optoelectronic devices. In this present context, a detailed study regarding properties and nanofabrication methods of various promising semiconducting materials used in optoelectronic applications has been explored. It was found that copper nitride is a propitious semiconducting material that can be used in optoelectronic devices. Thus, the objective of this present research work is to develop a semiconducting-grade copper nitride nanostructure by utilizing a simple as well as low-cost fabrication technique and establishing its applicability as a photoresistor and solar cell application. The detailed literature review of semiconducting copper nitride material to find the gap of the knowledge and also the scope of the present research work has been discussed in Chapter 2 in this context.

References:

1. R. Shwetharani, H.R. Chandan, M. Sakar, G. R. Balakrishna, K. R. Reddy, A. V. Raghu, Photocatalytic semiconductor thin films for hydrogen production and environmental applications, International Journal of Hydrogen Energy 45(36) (2020) pp.18289-18308.

2. Md. A. Rahman, A Review on Semiconductors Including Applications and Temperature Effects in Semiconductors, American Scientific Research Journal for Engineering, Technology, and Sciences 7(1) (2014) pp.50-70.

3. M. K. Sahu, Semiconductor Nanoparticles Theory and Applications, International Journal of Applied Engineering Research 14(2) (2019) pp. 491-494.

4.. O. Sancakoglu, Technological Background and Properties of Thin Film Semiconductors, Surface Science (2020), DOI: 10.5772/intechopen.91751.

5. H. Frey, H. R. Khan, Handbook of Thin-Film Technology, Springer (2015), ISBN 978-3-642-05429-7, DOI: 10.1007/978-3-642-05430-3.

6. S. Bashir, J. Liu, Nanomaterials and Their Application, Advanced Nanomaterials and Their Applications in Renewable Energy (2015), Elsevier, ISBN: 978-0-12-801528-5.

7. J. Jortner, C. N. R. Rao, Nanostructured advanced materials. Perspectives and directions Pure Appl. Chem. 74(9) (2002) pp.1491–1506.

8. Y. Wang, Z. Tang, N. A. Kotov, Bio application of nano semiconductors, Material Today 8(5) (2005) Supplement 1, pp. 20-31.

9. First Nano, website: https://www.firstnano.com/portfolio-item/silicon-nanowires-sem-10-k-x/.

10.Uniform Nanowire Arrays for Science and Manufacturing, website: https://www.nist.gov.

11. S. K. Fatah, Synthesis and Characterization of Zinc Oxide Nano powders Prepared by Precipitation Method, Diyala Journal for Pure Science 14(3) (2018).

12. Science Photo Library, website: https://www.sciencephoto.com/media/874489/view/carbon-nanotubes-sem.

13. A. I Abou-Kandil, A. Awad, E. Mwafy, Polymer nano composites part 2: Optimization of zinc oxide/high-density polyethylene nanocomposite for ultraviolet radiation shielding, Journal of Thermoplastic Composite Materials (2014), pp.1-16, DOI:10.1177/0892705714551242.

14. O. Bogdan, A. Orlav, G. Pashkevich, V. Ulianova, Y. Yakimenko, A. Zazerin, Optimal parameters determination for nanostructure-enhanced surface acoustic waves sensor,37th ISSE International Spring Seminar in Electronics Technology (ISSE 2014).

15. N. Ngafwan, H. Rasyid, E. Salaamabood, W. Kamal, S. Ghazi Al-Shawi, D. Bokov, A. Turki Jalil, Study on novel fluorescent carbon nanomaterials in food analysis, Food Science and Technology (Campinas) 42(1) (2021) pp.1-6.

16. J. Eapen, R. Rusconi, R. Piazza, S. Yip, The Classical Nature of Thermal Conduction in Nanofluids, Journal of Heat Transfer 132 (10) (102402) (2010), DOI: 10.1115/1.4001304.

17. C. Song, H. Yin, N. Zhang, S. Li, B. Zhao, K. Yu, Two-step synthesis of novel Cu_2S nanoflowers for field emission application, Materials Letters 137 (2014) pp.56–58.

18. X. Zheng, Z. Jin, H. Liu, Y. Wang, X. Wang, H. Du, Single-phase and well-dispersed $Cu_{1.75}S$ nanocrystals by ambient pressure diethylene glycol solution synthesis, Applied Surface Science 266 (2013) pp. 39– 45.

19. L. Niu, Z. Kang, A facile approach for the fabrication of 3D flower-like Cu_2S nanostructures on brass mesh with temperature-induced wetting transition for efficient oil-water separation, Applied Surface Science 422 (2017) pp.456–468.

20. H. Kumarakuru, M. J. Coombes, J. H. Neethling, J. E. Westraadt, Fabrication of Cu_2S nanoneedles by self-assembly of nanoparticles via simple wet chemical route, Journal of Alloys and Compounds 589 (2014) pp. 67–75.

21. Q. Cao, R. Chea, N. Chen, Scalable synthesis of Cu_2S double-superlattice nanoparticle systems with enhanced UV/visible-light-driven photocatalytic activity**,** Applied Catalysis B: Environmental 162 (2015) pp.187–195.

22. P. Pi, K. Hou, C. Zhou, G. Li, X. Wen, S. Xu, J. Cheng, S. Wang, Superhydrophobic $Cu_2S@Cu_2O$ film on copper surface fabricated by a facile chemical bath deposition method and its application in oil-water separation, Applied Surface Science 396 (2017) pp.566–573.

23. O. Erken, M. Gunes, F. Kirmizigul, C. Gumus, Investigation of properties the copper sulfide thin films prepared from different copper salts, optic- International Journal for Light and Electron Optics 168 (2018) pp.884-891.

24. J. Tirado, D. Ramirez, R. Betancur, F. Jaramillo, Low-cost semi-transparent copper sulfide electrode for indium-tin-oxide-free perovskite solar cells, Thin Solid Films 662 (2018) pp.90-96.

25. L. Isac, I. Popovici, A. Enesca, A. Duta, Copper sulfide (Cu_xS) thin films as possible p-type absorbers in 3D solar cells, Energy Procedia 2 (2010) pp.71–78.

26. M. S.G. Hamed, G. T. Mola, Copper sulphide as a mechanism to improve energy harvesting in thin film solar cells, Journal of Alloys and Compounds 802 (2019) pp.252-258.

27. Q. L. Huang, H. Chen, Y. C. Zhang, Chang Le Wu, CuS nanostructures prepared by a hydrothermal method, Journal of Alloys and Compounds 509 (2011) pp.6382–6387.

28. J. Huang, Y. Wang, C. Gu, M. Zhai, Large scale synthesis of uniform CuS nanotubes by a sacrificial templating method and their application as an efficient photocatalyst, Materials Letters 99 (2013) pp.31-34.

29. X. Meng, M. Sun, Y. Hu, M. Yin, Z. L. Yu, N. Yu, Haibo Li, Ting Shu, Mesoporous nanoflakes Cu_2S counter electrode prepared from three-dimensional ordered macroporous Cu film for quantum dot-sensitized solar cell, Journal of Alloys and Compounds 735 (2018) pp.2142-2147.

30. R. M. He, J. B. Chen, B. J. Qi, C. W. Wang, Enhanced field emission properties of the copper sulfide nanowalls with optimized 3-D morphology, Physica E: Low-dimensional Systems and Nanostructures 103 (2018) pp.227-233.

31. X. Yan, E. Michael, S. Komarnenic, J. R. Brownsond, Z. F. Yan, Microwave- and conventional-hydrothermal synthesis of CuS, SnS and ZnS: Optical properties, Ceramics International 39 (2013) pp.4757–4763.

32. A.K. Romero-Jaime, D. Vargas-Hernandez, M.C. Acosta-Enríquez, J.C. Tanori-Cordova, J. Valenzuela-Badilla, S.J. Castillo, Novel route for simplified and efficient synthesis of spiky-like copper sulfide nanoballs by soft chemistry method and their basic physicochemical characterizations, Materials Science in Semiconductor Processing 107 (2020) 104830.

33. A. Bollero, S. Fernández, K. Zuzek Rozman, Z. Samardzija, M. Grossberg, Preparation and quality assessment of CuS thin films encapsulated in glass, Thin Solid Films 520 (2012) pp.4184-4189.

34. Y. Lee, Selective transformation of Cu nanowires to Cu_2S or CuS nanostructures and the roles of the Kirkendall effect and anion exchange reaction, Materials Chemistry and Physics 180 (2016) pp.104-113.

35. F. Li, J. Wu, Q. Qin, Z. Li, X. Huang, Controllable synthesis, optical and photocatalytic properties of CuS nanomaterials with hierarchical structures, Powder Technology 198 (2010) pp.267-274.

36. M.D. Khan, M.A. Malik, J. Akhtar, S. Mlowe, N. Revaprasadu, Phase pure deposition of flower-like thin films by aerosol assisted chemical vapor deposition and solvent mediated structural transformation in copper sulfide nanostructures, Thin Solid Films 638 (2017) pp.338–344.

37. S. K. Maji, N. Mukherjee, A. K. Dutta, D. N. Srivastava, P. Paul, B. Karmakar, A. Mondal, B. Adhikary, Deposition of nanocrystalline CuS thin film from a single precursor: Structural, optical and electrical properties, Materials Chemistry and Physics 130 (2011) pp.392–397.

38. R. Mandal, G. Basu, B. Ghosh, Studies on the developing of Nano-Structured Cu_2S film for photovoltaic application, Materials Today: Proceedings 5 (2018) pp.23099–23106.

39. I. S. Najm, S. M. Kadhim, A. Abdulkhaleq Alwahib, Investigation the CuS thin film prepared by pulsed laser deposition, Materials Today: Proceedings 42 (2021) pp.2609-2615.

40. R. E. Agbenyeke, S. H. Han, B. K. Park, T. M. Chung, Y. K. Lee, C. G. Kim, J. H. Han, Simultaneous etching of underlying metal oxide and sulfide thin films during Cu_2S atomic layer deposition, Applied Surface Science 524 (2020) 146452.

41. M. Leach, K.T. Ramakrishna Reddy, M.V. Reddy, J.K. Tan, D.Y. Jang, R.W. Miles, Tin Sulphide Thin Films Synthesized using a Two Step Process, Energy Procedia 15 (2012) pp.371 – 378.

42. V. E. González-Flores, R. N. Mohan, R. Ballinas-Morales, M.T.S. Nair, P.K. Nair, Thin film solar cells of chemically deposited SnS of cubic and orthorhombic structures, Thin Solid Films 672 (2019) pp.62–65.

43. A. Voznyi, V. Kosyak, A. Opanasyuk, N. Tirkusova, L. Grase, A. Medvids, G. Mezinskis, Structural and electrical properties of SnS_2 thin films, Materials Chemistry and Physics 173 (2016) pp.52-61.

44. U.Chalapathi, B. Poornaprakash, S. H. Park, Growth and properties of cubic SnS films prepared by chemical bath deposition using EDTA as the complexing agent, Journal of Alloys and Compounds 689 (2016) pp.938-944.

45. S. Gedi, V. R. M. Reddy, T. R. R. Kotte, Y. Park, W. K. Kim, Effect of $C_4H_6O_6$ concentration on the properties of SnS thin films for solar cell applications, Applied Surface Science 465 (2019) pp.802–815.

46. P. R. Bommireddy, C. S. Musalikunta, C. Uppala, S.H. Park, Influence of Cu doping on physical properties of sol-gel processed SnS thin films, Materials Science in Semiconductor Processing 71 (2017) pp.139–144.

47. A. Kothari, K. Dave, Solution-based deposition of SnS nanostructures from mechanochemically prepared precursor bath, Materials Letters 236 (2019) pp.299–302.

48. S. Sohila, M. Rajalakshmi, C. Muthamizhchelvan, S. Kalavathi, Chanchal Ghosh, R. Divakar, C.N. Venkiteswaran, N.G. Muralidharan, A.K. Arora, E. Mohandas, Synthesis and characterization of SnS nanosheets through simple chemical route, Materials Letters 65 (2011) pp.1148–1150.

49. V. K. Arepalli, Y. Shin, J. Kim, Photovoltaic behavior of the room temperature grown RF-Sputtered SnS thin films, Optical Materials 88 (2019) pp.594–600.

50. P. Mani, K. Manikandan, J. Joseph Prince, Influence of molar concentration on triethanolamine (TEA) added tin sulfide (SnS) thin films by SILAR method, J Mater Sci: Mater Electron 27 (2016) pp.9255–9264.

51. S. Polivtseva, A. Katerski, E. Kärber, I. Oja Acik, A. Mere, V. Mikli, M. Krunks, Post-deposition thermal treatment of sprayed SnS films, Thin Solid Films 633 (2017) pp.179–184.

52. B. Ghosh, R. Bhattacharjee, P. Banerjee, S. Das, Structural and optoelectronic properties of vacuum evaporated SnS thin films annealed in argon ambient, Applied Surface Science 257 (2011) pp.3670–3676.

53.M. Edler, T. Rath, A. Schenk, A. Fischereder, W. Haas, M. Edler, B. Chernev, B. Kunert, F. Hofer, R. Resel, G. Trimmel, Copper zinc tin sulfide layers prepared from solution processable metal dithiocarbamate precursors, Materials Chemistry and Physics 136 (2012) pp.582-588.

54. A. Pateter, W. Haas, B. Chernev, B. Kunert, R. Resel, F. Hofer, G. Trimmel, T. Rath, Investigation on the formation of copper zinc tin sulphide nanoparticles from metal salts and dodecanethiol, Materials Chemistry and Physics (149-150) (2015) pp.94-98.

55. J. M. Chiua, T. C. Chouc, D. P. Wong, Y. R. Lina, C.A. Shenb, S. Hy, B. J. Hwang, Y. Tai, H. L. Wu, L. C. Chen, K. H. Chen, A synergistic “cascade” effect in copper zinc tin sulfide nanowalls for highly stable and efficient lithium-ion storage, Nano Energy 44 (2018) pp.438–446.

56. K.V. Gunavathya, K. Tamilarasana, C. Rangasamia, A.M.S. Arulanantham, Solution processed copper zinc tin sulfide thin films for thermoelectric device applications, Ceramics International 46 (2020) pp.28342–28354.

57. S. K. Swami, N. Chaturvedi, A. Kumar, V. Dutta, Effect of deposition temperature on the structural and electrical properties of spray deposited kesterite (Cu_2ZnSnS_4) films, Solar Energy 122 (2015) pp.508–516.

58. T.S. Shyju, S. Anandhi, R. Suriakarthick, R. Gopalakrishnan, P. Kuppusami, Mechanosynthesis, deposition and characterization of CZTS and CZTSe materials for solar cell applications, Journal of Solid-State Chemistry 227 (2015) pp.165–177.

59. M.E. Azim-Araghi, N. Safaie, Structural, optical and electrical properties of Cu_2ZnSnS_4 thin film deposited by electron beam evaporation method, Optik - International Journal for Light and Electron Optics 258 (2022) 168936.

60. G.L. Agawane, S.A. Vanalakar, A.S. Kamble, A.V. Moholkar, J.H. Kim, Fabrication of $Cu_2(Zn_xMg_{1-x})SnS_4$ thin films by pulsed laser deposition technique for solar cell applications, Materials Science in Semiconductor Processing 76 (2018) pp.50-54.

61. M. Singh, K. Suganuma, Light energy induced sintering of Cu_2ZnSnS_4 nanocrystal-based film for solar cell, Nano-Structure & Nano-Objects 19 (2019) 100369.

62. M. Souli, C. Nefzi, Z. Seboui, A. Mejri, R. Vidu, N. Kamoun-Turki, Improved structural properties, morphological and optical behaviors of sprayed Cu_2ZnSnS_4 thin films induced by high gamma radiations for solar cells, Materials Science in Semiconductor Processing 83 (2018) pp.50–57.

63. M.P. Suryawanshi, S. W. Shin, U.V. Ghorpade, K.V. Gurav, C.W. Hong, P.S. Patil, A.V. Moholkar, J. H. Kim, Improved solar cell performance of Cu_2ZnSnS_4 (CZTS) thin films prepared by sulfurizing stacked precursor thin films via SILAR method, Journal of Alloys and Compounds 671 (2016) pp.509-516.

64. Y. Chang, H. C. Zeng, Manipulative Synthesis of Multipod Frameworks for Self-Organization and Self-Amplification of Cu_2O Microcrystals, Crystal Growth & Design 4(2) (2004) pp.273-278.

65. R. Bhardwaj, R. Barman, D. Kaur, Improved photovoltaic effect in $CuO/Zn_{1-x}Mg_xO$ heterojunction solar cell by pulsed laser deposition, Materials Letters 185 (2016) pp.230-234.

66. H. El Aakib, J.F. Pierson, L. Atourki, L. Nkhaili, A. El Kissani, A. Narjis, A. Outzourhit, Preparation and characterization of nanocomposite of Co:CuO by radio-frequency sputtering for solar selective absorber application, Thin Solid Films 709 (2020) 138199.

67. D. Prasanth, K.P. Sibin, H. C. Barshilia, Optical properties of sputter deposited nanocrystalline CuO thin films, Thin Solid Films 673 (2019) pp.78–85.

68. S.K. Shinde, S.M. Mohite, A.A. Kadam, H.M. Yadav, G.S. Ghodake, K.Y. Rajpure, D.S. Lee, D. Y. Kim, Effect of deposition parameters on spray pyrolysis synthesized CuO nanoparticle thin films for higher supercapacitor performance, Journal of Electroanalytical Chemistry 850 (2019) 113433.

69.H.E. Sanchez, D. Esparza, T. Lopez-Luke, J. Castañeda Contreras, V.F. Marañon-Ruiz, I. Zarazúa, R.A. Rodriguez, Effect of Al^{3+} doping concentration and film thickness of ZnO nanoparticles over the TiO_2 photoelectrode in CdS quantum dots sensitized solar cells, Solar Energy 197 (2020) pp.154–162.

70. S.B. Patil, A.K. Singh, Electrodeposited vertically aligned ZnO nanorods thin films on steel substrate for CdS quantum dots sensitized solar cell, Electrochimica Acta 56 (2011) pp.5693–5701.

71. K. Chen, W. Tang, Y. Chen, R. Yuan, Y. Lv, W. Shan, W. H. Zhang, A facile solution processed ZnO@ZnS core–shell nanorods arrays for high-efficiency perovskite solar cells with boosted stability, Journal of Energy Chemistry 61(2021) pp.553–560.

72. E. Muchuweni, T.S. Sathiaraj, H. Nyakotyo, Hydrothermal synthesis of ZnO nanowires on rf sputtered Ga and Al co-doped ZnO thin films for solar cell application, Journal of Alloys and Compounds 721 (2017) pp.45-54.

73. M.A. Gaikwad, M.P. Suryawanshi, P.S. Maldar, T.D. Dongale, A.V. Moholkar, Nanostructured zinc oxide photoelectrodes by green routes M-SILAR and electrodeposition for dye sensitized solar cell, Optical Materials 78 (2018) pp.325-334.

74. S. Kushwaha, L. Bahadur, Studies of structural and morphological characteristics of flower-like ZnO thin film and its application as photovoltaic material, Optik 124 (2013), pp.5696-5701.

75. D. Sinha, D. De, D. Goswami, A. Mondal, A. Ayaz, ZnO and TiO_2 Nanostructured Dye sensitized Solar Photovoltaic Cell, Materials Today: Proceedings 11 (2019) pp.782–788.

76. S. Venkataprasad Bhat, S.R.C. Vivekchand, A. Govindaraj, C.N.R.Rao, Photoluminescence and photo conducting properties of ZnO nanoparticles, Solid State Communications 149 (2009) pp.510–514.

77. Md. Shahiduzzaman, R. Yamada, T. Chikamatsu, T. Ono, Y. Tanaka, Y. Uesugi, M. Karakawa, T. Kuwabara, K. Takahashi, T. Ishijima, T. Taima, Thin film deposition method for ZnO nanosheets using low-temperature microwave-excited atmospheric pressure plasma jet, Thin solid Films 674 (2019) pp.58-63.

78. A. Kaphle, P. Hari, Enhancement in power conversion efficiency of silicon solar cells with cobalt doped ZnO nanoparticle thin film layers, Thin Solid Films 657 (2018) pp.76–87.

79. M. Wang, J. Yi, S. Yang, Z. Cao, X. Huang, Y. Li, H. Li, J. Zhong, Electrodeposition of Mg doped ZnO thin film for the window layer of CIGS solar cell, Applied Surface Science 382 (2016) pp.217-224.

80. Sathish, H. Shaik, K. N. Kumar, R. I. Jafri, A. Reddy G V, S. A. Sattar, ZnO: Al thin films from $(Al_2O_3)_x(ZnO)_{(1-x)}$ powder targets by magnetron sputtering, Ceramics International 47(2021) pp.14997-15004.

81. R. Liu, M. Tan, X. Zhang, L. Xua, J. Chen, Y. Chen, X. Tang, L. Wan, Solution-processed composite electrodes composed of silver nanowires and aluminum-doped zinc oxide nanoparticles for thin-film solar cells applications, Solar Energy Materials and Solar Cells 174 (2018) pp.584–592.

82. M. A. Desai, V. Sharma, M. Prasad, S. Jadkar, G. D. Saratale, S. D. Sartale, Seed-layer-free deposition of well-oriented ZnO nanorods thin films by SILAR and their photoelectrochemical studies, International journal of hydrogen energy 45 (2020) pp.5783-5792.

83. G. Cheng, M. S. Akhtar, O. B. Yang, F. J. Stadler, Structure modification of anatase TiO_2 nanomaterials-based photoanodes for efficient dye-sensitized solar cells, Electrochimica Acta 113 (2013) pp.527– 535.

84. A. R. Rao, V. Dutta, Low-temperature synthesis of TiO_2 nanoparticles and preparation of TiO_2 thin films by spray deposition, Solar Energy Materials & Solar Cells 91 (2007) pp.1075–1080.

85. X. Du, L. Zhao, X. He, H. Chen, W. Li, W. Fang, TiO_2 hierarchical pores/nanorod arrays composite film as photoanode for quantum dot-sensitized solar cells, Journal of Energy Chemistry 30 (2019) pp.1–7.

86. W. Song, H. Wang, G. Liu, M. Peng, D. Zou, Improving the photovoltaic performance and flexibility of fiber-shaped dye-sensitized solar cells with atomic layer deposition, Nano Energy 19 (2016) pp.1–7.

87. S.S. Kanmani, K. Ramachandran, Synthesis and characterization of TiO_2/ZnOcore/shell nanomaterials for solar cell applications, Renewable Energy 43(2012) pp.149-156.

88.S.A. Vanalakar, M.P. Suryawanshi, S.S. Mali, A.V. Moholkar, J.Y. Kim, P.S. Patil, J.H. Kim, Simplistic surface-active agents mediated morphological tweaking of CdS thin films for photoelectrochemical solar cell performance, Current Applied Physics 14 (2014), pp.1669-1676.

89. P. Gowdhaman, V.N. Praveen, R. S. Sudar Saravanan, P. Venkateswari, H. M. Pandya, Facile synthesis of undoped and Sn doped CdS nanoparticles for dye-sensitized solar cell applications, Optical Materials 120 (2021) 111465.

90. H. Abdulelah, B. Ali, M.A. Mahdi, J.J. Hassan, H.F. Al-Taay, P. Jennings, Fabrication and characterization of nanowalls CdS/dye sensitized solar cells, Physica E 90 (2017) pp.104-108.

91. J. Wang, S. Liu, X. Meng, G. Zhu, M. Shi, L. Liu, J. Zhang, W. Yang, W. Fu, H. Yang, Vertically aligned CdTe nanorods array for novel three-dimensional heterojunction solar cells on Ni substrates, Electrochimica Acta 258 (2017) pp.858-865.

92. S.S. Shaikh, Md. Shkir, E.U. Masumdar, Exploration of the spray deposited Cadmium Telluride thin films for optoelectronic devices, Physica B 580 (2020) 411831.

93. L.G. Daza, V. Canche-Caballero, E. Chan y Díaz, R. Castro-Rodríguez, A. Iribarren, Tuning optical properties of CdTe films with nanocolumnar morphology grown using OAD for improving light absorption in thin-film solar cells, Superlattices and Microstructures 111(2017) pp.1126-1136.

94. A.E.-H.B. Kashyout, E.-Z. Ahmed, T. Meaz, M. Nabil, M. Amer, (One-step) electrochemical deposition and characterization of $CuInSe_2$ thin films, Alexandria Engineering Journal 53 (2014) pp.731–736.

95. R. A. Joshi, V. S. Taur, R. Sharma, Effect of annealing on conversion efficiency of nanostructured CdS/$CuInSe_2$ heterojunction thin film solar cell prepared by chemical ion exchange route at room temperature, Materials Research Bulletin 47 (2012) pp.2206–2211.

96. F.Y. Shih, A. Kobayashi, S. Inoue, J. Ohta, H. Fujioka, Fabrication of densely packed arrays of GaN nanostructures on nano-imprinted substrates, Journal of Crystal Growth 319 (2011) pp.102–105.

97. M. A. Kulkarni, H. Ryu, H. J. Choi, A. Abdullah, H. Thaalbi, F. Tariq, S. H. Lee, H. Lim, S.W. Ryu, Large scale fabrication of GaN nanorods template and characterization of

MOCVD grown InGaN/GaN quantum wells on {1010} plane of GaN nanorods, Optical Materials 145 (2023) 114488.

98. T. Oikawa, F. Ishikawa, T. Sato, T. Hashizume, H. Hasegawa, Study on ECR dry etching and selective MBE growth of AlGaN/GaN for fabrication of quantum nanostructures on GaN (0 0 0 1) substrates, Applied Surface Science 244 (2005) pp.84–87.

99. B. Rong, R. Cheung, W. Gao and M. Kamp, Fabrication of Nanostructures in GaN, Microelectronic Engineering 53 (2000) pp.419-422.

100.X. Xi, Z. Liu, L. Zhao, H. Cao, T. Li, K. Liu, K. Su, C. Wang, Z. Suo, Y. Li, J. Guo, The fabrication of GaN/InGaN nano-pyramids photoanode and its enhanced water splitting performance, Journal of Alloys and Compounds 971 (2024) 172720.

101. L. Goswami, R. Pandey, G. Gupta, Ultra-thin GaN nanostructures based self-powered ultraviolet photodetector via non-homogeneous Au-GaN interfaces, Optical Materials 102 (2020) 109820.

102. M. A. Fakhri, Md. J. A. Razzaq, H. D. Jabbar, E. T. Salim, F. H. Alsultany, U. Hashim, Fabrication of UV photodetector based on GaN/ Psi heterojunction using pulse laser deposition method: Effect of different laser wavelengths, Optical Materials 137 (2023) 113593.

103. S. Liu, Q. Wang, Y. Xie, Y. Yang, H. Wang, J. Dong, C. He, L. He, Z. Chen, S. Li, K. Zhang, X. Wang, Fabrication of freestanding GaN nanobelts with enhanced ultraviolet photo response performance, Applied Surface Science 614 (2023) 156168.

104. V. Aggarwal, C. Ramesh, P. Tyagi, S. Gautam, A. Sharma, S. Husale, M. S. Kumar, S.S. Kushvaha, Controlled epitaxial growth of GaN nanostructures on sapphire (11–20) using laser molecular beam epitaxy for photodetector applications, Materials Science in Semiconductor Processing 125 (2021) 105631.

105. T. Wang, F. Cao, X. Ji, Q. Zhang, Study on tower-like GaN nanostructure: Growth, optical and fast UV sensing properties, Superlattices and Microstructures 134 (2019) 106233.

106. K. Upadhyaya, N. Ayachit, S.M. Shivaprasad, Stress induced modification of electronic band structure and enhanced optical emission in 1-D GaN nanostructures, Solid State Sciences 105 (2020) 106242.

107. H. Movia, N. E. Gorji, F. Sohrabi, A. Hosseinpour, H. Babaei, Application of nanostructure materials in solar cells, 2nd International Conference on Nuclear and Renewable Energy Resources (NURER 2010).

108. J. Singh, Electronics and Optoelectronic Properties of Semiconductor Structure, Cambridge University Press (2003), ISBN 9780511805745, DOI: https:// doi.org/ 10.1017/ CBO9780511805-745.

Chapter 2

Review of earlier work on copper nitride semiconducting material

2.1. Introduction

Transition metal nitrides constitute an attractive class of materials with several technological applications. Copper nitride is one such compound in this class. Accordingly, it has potential applications in the catalytic, electrochemical, optical data storage, and electronics industries [1,2]. Copper nitride (Cu_3N) has attracted attention due to its interesting crystal structure, i.e., a simple cubic compound with an anti-ReO_3 type structure. It is non-toxic and band gap of the semiconducting Cu_3N, experimental values lie within the range of 1.2–1.9 eV which is suitable for the application in optoelectronic devices [3, 4]. This encourages further research on copper nitrides in the field of electronics. Here an attempt has been made to fabricate copper nitride nano semiconducting material as an application in optoelectronic devices.

2.2 Properties of copper nitride (Cu_xN) material

Copper nitride appears as a simple cubic compound which has anti-ReO_3 type structure. Here copper ions are placed at the centre of the cubic edges whereas nitrogen ions are located at the corners of the primary unit cell. This pattern of open as well as low density crystal structure of copper nitride make it suitable candidate for intercalation and the structure is appropriate for the placing of metal atoms into the interstitial body under certain conditions. Thus, the modification of the chemical interaction occurred between nitrogen and copper atoms, and it influenced the electronic structure of the material [5]. The Cubic, anti-ReO_3 type crystal structure of copper nitride is shown in figure 2.1.

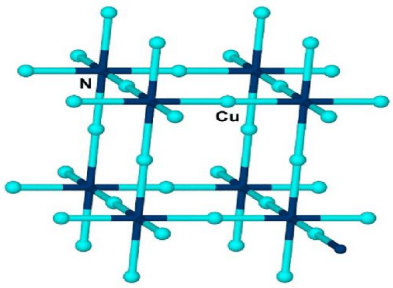

Fig. 2.1: Crystal structure of copper nitride, Cu_3N

Cu_xN has been easily thermally decomposed (i.e., its decomposition temperature is 350°C) and converted into pure metal as well as nitrogen. But copper nitride exhibits excellent properties such as nontoxicity, low cost and greater stability at room temperature. Cu_xN based thin films have notable attention as a semiconducting material due to its unique structure as well as physicochemical characteristics. It has outstanding electron emission features make it comparable to the field emission materials. Thus, researchers have special attention for their optical as well as thermal properties. Cu_xN becoming an exploration as a hotspot regarding the area of semiconducting as well as energy material. Copper nitride based semiconducting material has suitable applications in the field of optical data storage, magnetic tunnel

junctions, opto-electronic devices, high-speed integrated circuits and microscopic metal links etc. [6].

2.3 Different nano-fabrication methods regarding copper nitride based semi-conductor

Nanomaterials play a very important role in the performances regarding optoelectronic devices. On the other hand, semiconducting copper nitride is one of the promising materials for the application in devices. Here various nanofabrication techniques of copper nitride thin films are considered for detailed study in the following text.

Copper nitride has been deposited here by the ALD (atomic layer deposition) process. It was formed using bis(1-dimethylamino-2-methyl-2-butoxy) copper (II) and the reactant kept in a hot-wall tube reactor. Here ammonia was used as the reactant, and argon was used as a purging gas. The precursor and reactant were controlled by pulse time at fixed pulse pressures [7].

Here, a radio-frequency plasma source was used for the formation of copper nitride film. This deposition was performed by using an ion-pumped ultra-high vacuum chamber. It consists of a scanning tunnelling microscope and low-energy electron diffraction (LEED) optics. Here copper was taken as a substrate, and nitride formation was performed using atomic nitrogen obtained from an RF plasma source where applied power was maintained at 60 watts [8].

Copper nitride film was deposited here by the R.F. reactive sputtering method. Here high-purity nitrogen gas was used as inert gas, which was controlled by a mass flow controller. A copper film was fixed with cathode-maintained power using an R.F generator of frequency 13.56 MHz. The 100-watt power was provided to the cathode, and the target-to-substrate distance of 50 mm was maintained [9].

Copper nitride was developed on Si (silicon) substrate by the reactive magnetron sputtering method. Here, copper film was used as a substrate, and a gas mixer of argon and nitrogen was introduced as an inert gas. The substrate temperature was 60°C, and the R.F power of 150 watts was maintained here. The sputtering was performed for 30 mins to achieve a suitable deposition [10].

Copper nitride film was deposited here by the reactive radio frequency magnetron sputtering method. Here, a pure copper disc was used as a substrate. The mixer of argon and nitrogen was used as working gas for this fabrication. The substrate temperature was maintained from room temperature to 573 K, and discharge power from 50 to 300 watts was maintained here. Finally, the deposited sample was annealed in an argon environment for 40 mins, maintaining a temperature range from 473 to 573 K [11].

CuxN film has been formed by the high-power impulse magnetron sputtering method. Here, a high-purity copper target (6 mm thickness) was used for fabrication. The reactive gas has been produced by a mixture of nitrogen and argon. There was a maintained total gas flow rate

of 30 sccm and a working pressure of 3.33 Pa into the chamber to form semiconducting copper nitride [12].

Cu_xN was fabricated here using the magnetron pulse sputtering method. A 50m diameter copper target has been chosen for the purpose of fabrication. The silicon film was used as a substrate, and a target-to-substrate distance of 100 mm has been maintained. The deposition process was carried out under nitrogen environments maintained at a constant pressure of 1 Pa for 60 mins [13].

Copper nitride (Cu_xN) and silver-doped copper nitride (Ag-Cu_xN) has been formed here by the reactive magnetron co-sputtering method. It consists of two magnetron systems maintained at a distance of 120 mm. There was 0.3amp constant current to the copper target and 0.1 amp to the silver target. Here, an argon flow rate of 40 sccm as well as a nitrogen flow rate of 30 sccm was maintained during deposition. The deposition has been performed at 50°C for 20 mins [14].

Copper nitride has been formed here by the DC triode sputtering method. Here copper is used as target material. Cu_xN was fabricated under an $Ar+N_2$ (argon + nitrogen) atmosphere at room temperature and maintained a cathode voltage of –1 kV. The total working pressure ($Ar+N_2$) was set at 8 x 10^{-1} Pa, and a ratio of 0.9 was maintained. Finally, the sample was annealed at a temperature in between 100 to 300°C for 30 min and cooled down for 90 min before exposing them to environmental conditions [15].

Here Cu_3N has been fabricated by the direct nitriding synthesis method. The conversion of transition metal copper to semiconducting copper nitride has been formed using the catalytic NH_3 (ammonia) oxidation reaction method. At first, Cu (copper) has been deposited on glass substrate by the electron beam evaporation process. Then the as-prepared film was kept in a furnace consisting of a silicon carbide susceptor under an $NH_3$and NH_3/O_2 environment. The film was annealed in the furnace at a maintained temperature of 200–800^{0}C for 30 min [16].

Copper nitride was produced here through the low-energy intense pulsed light irradiation method. Here, at first, a solution was prepared using copper acetate monohydrate and urea. The solution was kept in a three-neck flask under a nitrogen atmosphere. Thereafter it was heated at a temperature of 90^{0}C for 60 min by microwave irradiation. At last, copper nitride has been achieved after the suspension was washed as well as centrifuged [17].

Cu_xN film was synthesised by using a three-step process. Here at first, copper hydroxide has been developed on copper foil. The copper hydroxide solution was prepared using sodium hydroxide and ammonium persulfate at room temperature. Then the film was kept at the centre of the furnace, and urea was introduced into it. At last, the furnace was heated at a temperature of 350^{0}C for 2 hours under an argon atmosphere to get a copper nitride film [18].

Cu_xN was prepared here by gas–solid (ammonolysis) technique. Here Copper trifluoroacetate was used for the preparation of copper nitride, and ammonolysis was done in a furnace. Here NH_3 gas is used as the nitriding agent. There was a maintained temperature of 300^{0}C for 240 min. At last, to get Cu_xN film, a post-ammonolysis technique was used to remove adsorbed ammonia [19].

The different nanofabrication methods regarding the copper nitride-based thin film provide a cumulative idea about the development of nanostructure semiconducting Cu_xN film, which can be used for applications in optoelectronic devices.

2.4 Problem identification and gap of the knowledge

After investigating all the relevant studies of properties, applications, and various nanofabrication techniques regarding semiconducting copper nitride (Cu_xN) thin film, the gap of the research work is identified and addressed, as stated in this section.

Many semiconductor devices like solar PV cells, LDR (Light Dependent Resistor), and gas sensors have been fabricated using silicon (Si), cadmium sulphide (CdS), and copper sulphide (CuS), respectively. CdS can provide LDR with high gain because the dark resistance of this semiconducting material is very high at about several mega-ohms and falls to about certain ohms when fully illuminated. But cadmium and its compounds are highly toxic and carcinogenic in nature. Apart from this, CdS has been degraded with time. Thus, there should be chosen such alternative material as an application in LDR, which will be non-toxic, stable in nature, and can provide a low cost as well as an easy fabrication process. On the other hand, copper is a material that is widely available, non-toxic and an essential nutrient for the human body. It has already been proved that generally nitride-based materials like GaN (gallium nitride), AlN (aluminium nitride), InN (indium nitride) and their alloys have been found to be useful in various optoelectronic applications, but these are expensive material compared to other traditional compound semiconductors. Thus, combining the attributes of both copper and nitride, a propitious material such as Cu_xN (copper nitride) has been considered here to establish its applicability in optoelectronic applications. In the present research work, copper nitride (Cu_xN) has been introduced as a light dependent resistor (LDR) and solar cell applications.

Cu_xN is a transition metal nitride that is less thermally stable. It has been easily decomposed at higher temperature. Copper nitride had previously been prepared mainly by physical deposition methods such as sputtering, molecular beam epitaxy, ALD, pulse laser deposition, etc., while fabricating the same by high-temperature synthetic methods, it was very difficult due to the low thermal stability of the material. It was also proved that films prepared by the physical methods are not always consistent with suitable compositional ratio of the material (i.e, it may be either copper-rich or nitrogen-rich or stoichiometric in nature) for providing optimum semiconducting properties in optoelectronic sensor and device applications. It can say that electronic properties vary with the chemical composition of the material, and it may change the material characteristics, which affect the optoelectronic device performances [20, 21, 22].

For successful optoelectronic applications, thrust is required to be given on the fabrication techniques of the compound for having it in appropriate compositional ratio. Therefore, the possible solutions and scope of the present work are discussed in the next section of this chapter.

2.5 Possible Solutions

In the present work, an attempt will be made to develop semiconducting copper nitride (Cu_xN) nanostructures for photoresistor and solar cell device applications. It can be inferred from the previous study that the fabrication of copper nitride-based film by high-temperature synthetic techniques is a very tedious job, and it has also been observed that sometimes the electronic properties of Cu_xN have been changed with varying chemical compositions while the fabrication of the material has been performed by the physical methods. Thus, it may be difficult to achieve optimum optoelectronic properties for device application. In the present volume some works have been carried out on the fabrication of nano-structured Cu_xN film using a simple and low-cost chemical deposition technique to explore their possible applications.

Thus, the author proposed the following solutions to mitigate the identified problems regarding semiconducting grade copper nitride (Cu_xN) thin film:

- Here, a semiconducting Cu_xN nanostructure can be developed by introducing a simple and low-cost spray deposition method that maintains a low-temperature arrangement. The optimization of the compositional ratio of the material can be performed by varying the doping of the film. Then the obtained optimized film can be used as a LDR and in solar cell applications. The photoresistor performances have to be analyzed by determining LDR gain. Thereafter, photoconductive studies of the optimally prepared film can be accomplished by variation of film thickness, and optimum film thickness can be achieved for use in solar cell applications. Finally, the modelling of a solar cell device by using Cu_xN as an absorber and window layers in combination with various inorganic semiconductors have executed and concluded the acceptability of the Cu_xN as a photoresistor and solar cell device application.

- Another approach may be taken for the formation of semiconducting Cu_xN nanostructures by utilizing modern computational techniques in combination with physical deposition processes. At first, optimization of the chemical composition of the material in which the film has exhibited suitable optoelectronic properties for device application can be performed by using a comprehensive simulation process. Thereafter, the obtained optimized composition of the material can be deposited on the substrate by utilizing one of the physical methods, such as molecular beam epitaxy. Then determine LDR gain to obtain the performance of the film as a photoresistor. The photoconductive studies of the optimally prepared film can be executed by varying the thickness of the film. Then the obtained optimized film thickness can be used in solar cell applications. The performance evaluation of a solar cell device can be executed by using Cu_xN as absorber and window layers in combination with various inorganic semiconductors and finally conclude the suitability of copper nitride as a photoresistor as well as solar cell applications.

2.6 Scope of the work

The present research work deals with the fabrication and optimization of semiconducting-grade copper nitride (Cu_xN) for optoelectronic sensor and device applications. A detailed literature survey has been performed on the properties and nanofabrication methods of various promising semiconducting materials, including copper nitride used in optoelectronic device applications. The problems and gap of the knowledge have been identified. The scope of this research work has been accomplished by solving the identified problems using rigorous simulation as well as experimental work. The work lies in overcoming the problem regarding the fabrication of copper nitride semiconducting nanostructures with suitable compositions by which it can be applicable for use in optoelectronic sensor and device applications. All the research work has been organised coherently in the form of a thesis from chapters 1-7.

The motivation for the present research work, along with the concept of nanotechnology, a detailed literature review regarding properties and nanofabrication methods of various promising semiconducting materials used in optoelectronic applications, the usefulness of nanomaterials in optoelectronic devices, and the aim and objectives of the present research work, have been presented in Chapter 1.

Chapter 2 describes a review regarding properties and various nanofabrication methods of copper nitride (Cu_xN) semiconducting material. According to the review, problem identification as well as the gap of the knowledge has been illustrated here. After there have been inferred possible solutions regarding the identified problems. Finally, the scope of the research work is presented here.

The working principle of various physical as well as chemical deposition methods and different characterisation techniques, such as structural and optical, regarding thin film semiconductors has been illustrated in Chapter 3. The accumulative details of the fabrication and characterization process provide a comprehensive idea to determine the suitable possibility to be applicable in the present research work.

Chapter 4 represents the work on the fabrication and optimization of semiconducting grade copper nitride (Cu_xN) in the application of photoresistor. The fabrication of a semiconducting copper nitride nanostructure has been performed by using a simple and low-cost spray deposition method. The optimization of the compositional ratio of Cu_xN has been carried out by varying the doping of the film. The structural and optical analyses have been executed to determine crystallinity, surface morphology, structural parameters, compositional ratio, and optical band gap of the as-prepared as well as annealed samples. Thereafter, electrical analysis has been performed to establish the suitability of the optimized Cu_xN film as a semiconductor and use it as a light-dependent resistor (LDR)application. The photoresistor performance has been evaluated by determining LDR gain. Thus, the fabrication of the Cu_xN nanostructure with a suitable compositional ratio by which it can be applicable as a photoresistor or LDR has been established in this chapter.

Chapter 5 initiates with the optoelectronic performance analysis of the optimized Cu_xN film as a solar cell device. A modern computational technique has been implemented here to

determine the optoelectronic response of copper nitride (Cu_xN) semiconducting material as a photovoltaic device. In this study, the experimental data of optical spectroscopy of the fabricated optimized Cu_xN film has been provided as input to the Oghma-Nano software (8.1.020) for carrying out numerical simulations. The photoconductive analysis of the optimized Cu_xN film by the variations of film thickness at different light intensities has been evaluated here. Thereafter, optimum film thickness has been achieved for use in solar cell applications. The feasibility of the Cu_xN film in photovoltaic applications was probed by modelling a solar cell device by using it as an absorber and window layers in combination with various inorganic semiconductors that have been studied. The best photovoltaic characteristics and parameters have been evaluated for the Cu_xN based solar cell, and the results have been compared with the experimental results of other conventional inorganic thin film solar cell materials. Here, providing experimental data as input to the simulation software should produce output as compatible with the practical one. This technique can be adopted in places lagging necessary laboratory infrastructure for device fabrication.

Analyzing the comprehensive literature review, the unsolved issues regarding copper nitride-based semiconducting material have been determined. The aspects of the identified problem and corresponding possible solutions have been accomplished in the subsequent chapters in this thesis. Chapter 6 summarizes the above issues as well as provides an overall conclusion of this entire research work.

Chapter 7 describes the avenues of the future work. There are alternative ways that have been explored for solving the mentioned problems regarding the development of copper nitride grade semiconducting thin film for optoelectronic applications. Apart from this, the extension of this present research work by further optimizing thin film deposition parameters for more precise results, have also been described in the future work section of this present thesis.

2.7 Conclusion

This thesis is organized on the basis of present research work, which has been started with the aim and objective, gap of the knowledge, scope, and significance of the work. The gap of the knowledge is produced by surveying the preceding research work. It is found out that copper nitride cannot be formed by high temperature synthetic methods, and during the development of physical methods, it always does not maintain a suitable compositional ratio of the material for the applications in optoelectronic devices. This mentioned issue has been accomplished here by adopting a suitable chemical deposition process that can optimize the compositional ratio of the semiconducting copper nitride material. In this present study, the author has endorsed a simple and low-cost spray deposition method for the formation of semiconducting-grade copper nitride thin film and optimize it for applications in optoelectronic photoresistor and solar cell devices. The entire research work has been carried out by implementing both experimental and simulation-based work. Thus, the familiarization of various deposition processes and different characterization techniques, like structural, optical, etc., is necessary for carrying out the entire research work, and it has been studied in Chapter 3 in the present thesis.

References:

1. S.T. Oyama, The Chemistry of Transition Metal Carbides and Nitrides (1996), Springer, pp. 1–27, DOI: 10.1007/978-94-009-1565-7_1.

2. T. Maruyama, T. Morishita, Copper nitride and tin nitride thin films for write-once optical recording media, Applied Physics Letter 69 (1996) pp.890-891.

3. R. Cremer, M. Witthaut, D. Neuschutz, C. Trappe, M. Laurenzis, O. Winkler, H. Kurz, Deposition and Characterization of Metastable Cu_3N Layers for Applications in Optical Data Storage, Mikrochim. Acta 133 (2000) pp.299-302.

4. S. Terada, H. Tanaka, K. Kubota, Heteroepitaxial growth of Cu_3N thin films, Journal of Crystal Growth 94 (1989) pp.567-568.

5. A. Scigała, E. Szłyk, L. Dobrzanska, D. H. Gregory, R. Szczesny, From binary to multinary copper-based nitrides – Unlocking the potential of new applications, Coordination Chemistry Reviews 436 (2021) 213791.

6. A. Jiang, M. Qi, J. Xiao, Preparation, structure, properties, and application of copper nitride (Cu_3N) thin films: A review, Journal of Materials Science and Technology 34(9) (2018) pp.1467-1473.

7. J. M. Park, K. Jin, B. Han, M. J. Kim, J. Jung, J. J. Kim, W. J. Lee, Atomic layer deposition of copper nitride film and its application to copper seed layer for electrodeposition, Thin Solid Films 556 (2014) pp.434–439.

8. D. Écija, J. M. Gallego, R. Miranda, The adsorption of atomic N and the growth of copper nitrides on Cu (1 0 0), Surface Science 603 (2009) pp.2283–2289.

9. S. Ghosh, F. Singh, D. Choudhary, D.K. Avasthi, V. Ganesan, P. Shah, A. Gupta, Effect of substrate temperature on the physical properties of copper nitride films by r.f reactive sputtering, Surface and Coatings Technology (142-144) (2001) pp.1034-1039.

10. Y. Du, A.L. Ji, L.B. Ma, Y.Q. Wang, Z.X. Cao, Electrical conductivity and photo reflectance of nanocrystalline copper nitride thin films deposited at low temperature, Journal of Crystal Growth 280 (2005) pp.490–494.

11. J. Xiao, Y. Li, A. Jiang, Structure, Optical Property and Thermal Stability of Copper Nitride Films Prepared by Reactive Radio Frequency Magnetron Sputtering, J. Mater. Sci. Technol. 27(5) (2011) pp.403-407.

12. S. Sakalleya, A. Saravanan, W. C. Cheng, S. C. Chen, H. Sun, C. L. Hsu, B. R. Huang, High power impulse magnetron sputtering growth processes for copper nitride thin film and its highly enhanced UV - visible photodetection properties, Journal of Alloys and Compounds 896 (2022) 162924.

13. K. Nowakowska - Langier, L. Skowronski, R. Chodun, S. Okrasa, G. W. Strzelecki, M. Wilczopolska, B. Wicher, R. Mirowski, K. Zdunek, Influence of generation control of the magnetron plasma on structure and properties of copper nitride layers, Thin Solid Films 694 (2020) 137731.

14. J.F. Pierson, D. Horwat, Addition of silver in copper nitride films deposited by reactive magnetron sputtering, Scripta Materialia 58 (2008) pp.568–570.

15. R. Gonzalez-Arrabal, N. Gordillo, M. S. Martin-Gonzalez, R. Ruiz-Bustos, F. Agulló-López, Thermal stability of copper nitride thin films: The role of nitrogen migration, Journal of Applied Physics 107 (2010) 103513.

16. K. Matsuzaki, K. Harada, Y. Kumagai, S. Koshiya, K. Kimoto, S. Ueda, M. Sasase, A. Maeda, T. Susaki, M. Kitano, F. Oba, H. Hosono, High-Mobility p-Type and n-Type Copper Nitride Semiconductors by Direct Nitriding Synthesis and In Silico Doping Design, Advance Materials 30(31) (2018) 1801968.

17. T. Nakamura, H. J. Cheong, M. Takamura, M. Yoshida, S. Uemura, Suitability of Copper Nitride as a Wiring Ink Sintered by Low-Energy Intense Pulsed Light Irradiation, Nanomaterials 8(8) (2018) 617.

18. S. Q. Liu, M. R. Gao, S. Liu, J. L. Luo, Hierarchically assembling cobalt/nickel carbonate hydroxide on copper nitride nanowires for highly efficient water splitting, Applied Catalysis B: Environmental 292 (2021) 120148.

19. R. Szczesny, E. Szłyk, M. A. Wisniewski, T. K. A. Hoang, D. H. Gregory, Facile preparation of copper nitride powders and nanostructured films, J. Mater. Chem. C 4 (2016) pp.5031-5037.

20. J. Choi, E.G. Gillan, Solvothermal Synthesis of Nanocrystalline Copper Nitride from an Energetically Unstable Copper Azide Precursor, Inorg. Chem. 44 (21) (2005) pp.7385–7393.

21. C.M. Caskey, R.M. Richards, D.S. Ginley, A. Zakutayev, Thin film synthesis and properties of copper nitride, a metastable semiconductor, Mater. Horizons.1 (4) (2014) pp.424–430.

22. X. Xu, N. Yuan, J. Qiu, J. Ding, Formation of conductive copper lines by femtosecond laser irradiation of copper nitride film on plastic substrates, Mater. Res. Bull. 65 (2015) pp.68–72.

Chapter 3

Fabrication and Characterization Methodologies of thin film Semiconductor

3.1 Introduction

Thin film is a thin layer of material which extends infinitely along any two directions but is restricted along the third direction and its thickness varies from a fraction of a nanometer to few micrometers. A thin film is said to be formed when a material is grown on a solid substrate by controlled condensation of atomic, molecular or ionic species by physical deposition techniques or by ultra-chemical reactions. Physical deposition methods cover the techniques of thermal growth of solid films involving vaporization or sputtering of materials from a source while the chemical deposition methods result in formation of thin films on solid substrate by reaction of chemical constituents. Bulk materials (i.e. materials having thickness of several microns or more) have fixed physical and chemical properties. Hence their applications are also limited. However, when material thickness reduces beyond a certain limit mechanical, electrical and optical properties begin to change quite drastically attributing unique properties to thin films rendering them useful for designing of devices for a wide range of applications. Thin film devices occupy less space and require less material thus making them less expensive [1]. Mechanical properties of thin films are highly dependent upon particle size. Thin films during fabrication develop stresses which give rise to dislocations which in turn significantly affect their mechanical properties such as hardness and yield strength. These parameters increase with more dislocations and smaller particle size. Thin film strengthening occurs with movement of dislocations as a function of applied stress. These dislocations may interact with other microstructural defects like point defects, extended defects, voids etc. which may further abet in film strengthening [2]. The reduction in particle size of films increases mean free path of charge carriers as they undergo less scattering as compared to bulk structures [3]. However thin film microstructures contain several structural defects such as voids, dangling bonds and grain boundaries which act as potential energy barrier for charge carriers, thus trapping them and reducing carrier conductivity [4]. The optical response of a thin film material with different refractive index deposited on a glass substrate is different from that of a bulk structure. When a beam of visible light is incident on such a thin film-glass interface more reflections and transmissions occur at specific angles compared to that of a bulk structure-glass interface. As a result, extinction coefficient of absorbing thin film layer also increases which in turn modifies the optical coefficients [5]. During thin film deposition several chemical reactions occur depending upon deposition parameters like substrate temperature, rate of deposition, pressure etc. The deposition may lead to formation of amorphous, polycrystalline or epitaxial thin films. Amorphous thin films are structures formed due to deviation of bond length and bond angle from a perfect crystal lattice [6]. Growth of amorphous films mainly occur at low substrate temperatures when adsorbed atoms reach thermal equilibrium with the substrate and their mobility remaining low. High deposition rate also induces amorphous growth as it prevents adsorbed atoms to diffuse into more energetic sites. Amorphous films may also be formed due to incorporation of gases like oxygen, nitrogen etc. [7]. Polycrystalline thin films consist of several micro/nano crystallites oriented in different directions separated by grain boundaries. Polycrystalline film formation depends upon mainly two parameters- deposition rate and deposition temperature. At a temperature higher than that inducing amorphous growth, adsorbed atoms are not in thermal equilibrium with substrate and they undergo

diffusion to form crystallites which finally coalesce to give rise to a polycrystalline layer**.** Epitaxial thin films are nearly perfect crystalline lattice structures deposited on a solid substrate having crystal orientation perfectly aligned with that of surface of substrate. Epitaxial film growth occurs at high substrate temperatures i.e. above a certain temperature called 'epitaxial temperature' for promoting nucleation of crystallites formed by adsorbed atom diffusion resulting in formation of solid thin films with a preferential orientation [8].

Thin films are used in several fields in optical applications like reflective/ anti-reflective coatings, optical waveguides, optical memory discs etc.; magnetic applications like magnetic memory discs etc.; electrical applications like conductors, insulators, semiconductors, piezoelectric devices etc.; thermal applications like heat sinks, barrier layers etc.; chemical applications like diffusion resistant coating, corrosion resistant coating, liquid/gas sensor etc.; mechanical applications like tribological (wear resistant) coating, microelectromechanical sensors (MEMS) etc. Thin films can also be explored for development of various Opto-electronic sensors and devices. The working principle of various fabrication and characterization techniques regarding thin film semiconductors have been explored in this context.

3.2 Fabrication Methodologies of thin film semiconductor

Thin film fabrication or deposition plays an important role in the semiconductor manufacturing industry. It is a critical process in the development of optoelectronic-based devices at the nanoscale level due to the requirement of precise control of material during deposition. There are various physical and chemical deposition techniques available for the development of thin-film semiconducting optoelectronic devices.

3.2.1 Physical Deposition Techniques

The physical deposition technique is a coating method to produce a thin film solid that involves a physical process such as high-temperature vacuum evaporation or plasma sputter bombardment rather than involving a chemical reaction at the surface of the sample. The details of the different process are given in the text below.

3.2.1.1 Vacuum Evaporation

Vacuum evaporation is a technique in which the desired materials are heated in a high vacuum space until they transform into a vapour form and are coated over the thin film substrate. The vacuum coating unit basically consists of two parts, where in the first part the chamber is vacuumed and in the second part the evaporation of the material is executed. In this unit the substrate is placed on the upper side of the chamber, whereas source material is placed below the substrate position by maintaining a distance in the range of 40 to 50 cm. The chamber is evacuated up to 10^{-6} mbar by using two pumps, such as a rotary and diffusion pump. If liquid nitrogen is used, then the chamber can be evacuated up to 10^{-11} mbar. There are two evaporation technologies, like electron-beam and resistive evaporation, that have been used to evaporate the materials on the substrate. This method consists of vaporising a solid material by heating it at high temperature and then recondensing it on the substrate for

the formation of a thin film. The pictorial image of a typical vacuum evaporation unit is shown in Fig. 3.1[Image has been taken from the laboratory of solar photovoltaic division under School of Energy Studies, Jadavpur University]. Here the heating is performed by maintaining a large current through a filament that has a finite resistance. Here the evaporated material produces a vapour that collides with the gas molecules inside the chamber, and the fraction of scattered vapour transfers through the ambient gas by maintaining a specified distance to provide a contamination-free deposition of the thin film [9,10].

Fig. 3.1: Pictorial Image of Vacuum Coating Unit

Vacuum evaporation units are used in the semiconductor and microelectronic industries for the purpose of thin film deposition to produce various electronic or optoelectronic-based devices. Apart from this, it can also be used in wastewater treatment and the food processing industry. This is very useful deposition technique for the development of thin film semiconducting device.

3.2.1.2 Radio Frequency (R.F) Sputtering

The Radio Frequency Sputtering (R.F.) method is used to develop thin films for the semiconductor industry. In this technique, the substrate, target material, and R.F. electrode is kept in a vacuum chamber. Here material is released from the source at a lower temperature compared to the evaporation process. The pictorial image of a typical R.F Sputtering unit is shown in Fig. 3.2. [Image has been taken from the laboratory of the solar photovoltaic division under the School of Energy Studies, Jadavpur University].

Fig. 3.2: Pictorial Image of R.F Sputtering Unit

Here, at first, source or target material and an inert gas such as argon have been introduced inside the vacuum chamber in the range of less than 15 mTorr. The gas plasma has been struck by the R.F. source, and thus gas becomes ionized. Now the ions have been accelerated in the direction of the surface of the target to break the atoms in the form of vapor and it has been condensing on total surfaces of the substrate. This coating technology has been used in solar cells, lasers, LEDs, optical filters, medical devices, etc. for application purposes [11,12].

3.2.2 Chemical Deposition Techniques

Chemical deposition is one of the fabrication techniques in which materials are allowed to react with various chemicals by maintaining different conditions to perform specific reactions in a way that coatings form successfully on a suitable substrate. The details of the different process are given in the text below.

3.2.2.1 Chemical Bath Deposition (CBD)

Chemical Bath Deposition (CBD) is a simple technique for the deposition of thin films by using an aqueous precursor solution. This process of forming thin film by deposition of aqueous ions on a solid substrate is called heterogeneous nucleation. On the other hand, here also form homogeneous thin film metal chalcogenides (basically oxides, sulphides, and selenides) and some ionic compounds. The pictorial image of a typical Chemical Bath Deposition (CBD) unit is shown in Fig. 3.3 [Image has been taken from the laboratory of the solar photovoltaic division under the School of Energy Studies, Jadavpur University].

Fig. 3.3: Pictorial Image of Chemical Bath Deposition (CBD) Unit

This deposition process is affected by some factors, such as the nature and concentration of reactant, concentration of complexing agents, reaction temperature, pH of solution, duration of reaction, and nature of substrate. This technique of thin film deposition is very much suitable for industrial applications because it is a very simple, cheap, and reliable process compared to other methods of deposition [13,14].

3.2.2.2 Spray Pyrolysis

Spray pyrolysis is a simple and low-cost technique in material science for thin film deposition. The term pyro means heat, and lysis means breaking, and thus pyrolysis signifies breaking the chemical molecules into simple units by applying heat. This method of fabricating thin film is performed by spraying a precursor solution on a heated surface. The temperature and pressure of this method depend on the specific application. The substrate temperature and compressed air pressure of 300-500^{0}C and 0.5 atm. have generally been maintained here. This process introduces a chemical reaction between a clutch of liquid or vapour atoms with the influence of the heating effect. Here, each of the sprayed droplets generates an endothermic decomposition by reaching the hot substrate and provides a single or polycrystalline thin film. The excess solvent and undesired product should be volatile due to the effect of deposition temperature. The properties of film depend on several parameters, such as spray rate, substrate temperature, droplet size, solution concentration, distance between spraying nozzle and substrate, etc., during the time of deposition [15,16].

This process provides a very easy path to dope a high-quality and adherent thin film of uniform thickness. This deposition technique can be used in various fields such as sensors, solar cells, and solid oxide fuel cell development purposes.

3.2.2.3 Spin Coating

The spin coating technique is used to develop thin films on flat substrates. In this process, a fluid resin has been deposited on the surface of a substrate by spinning the substrate using a spin coater while maintaining a high speed of around 3000 rpm. The resin flows rapidly

throughout the surface of the substrate by introducing a centrifugal force. The pictorial image of a typical spin coating unit is shown in Fig. 3.4 [17]. The properties and thickness of the film depend on different resin parameters such as viscosity, surface tension, drying rate, percent solids, etc. On the other hand, the properties of coated film also depend on parameters like rotational speed, acceleration, concentration of solution, etc. The suitable change in these parameters can provide drastic variation in the property of coated film. This process can provide a faster rate of deposition and easy control of chemicals as well as the substrate.

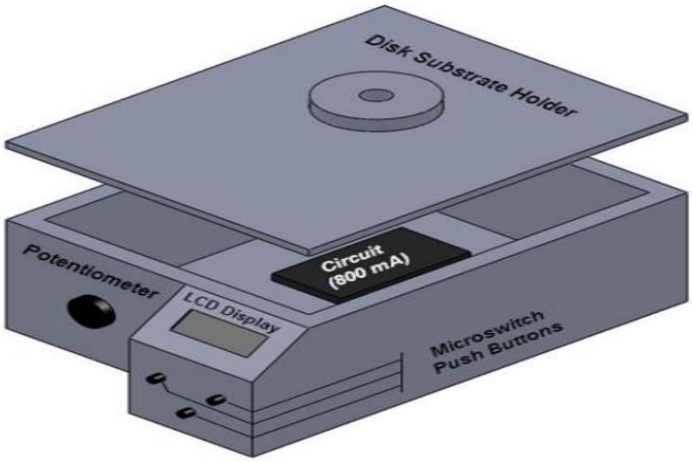

Fig. 3.4: Pictorial Image of Spin Coating Unit

In the microelectronics industry, it is mostly used for the development of photosensitive materials, which have generally thickness in the micron range. This technique is often used for the fabrication of TiO_2 on glass or quartz substrates [18, 19].

3.2.2.4 Successive Ionic Layer Adsorption and Reaction (SILAR)

Successive Ionic Layer Adsorption and Reaction (SILAR) is a chemical deposition technique for the formation of thin films by developing ionic layers on the surface of a substrate. In this method, the substrate is immersed in two different solutions containing anions and cations, respectively. Here, an electrostatic force develops to attract ions within the solution to the opposite charge ions that belong to the surface layer. Thus, an in situ chemical reaction takes place on the substrate for the development of the desired materials. Here a layer-by-layer deposition has been implemented to achieve a solid thin film material. The sub-monolayer of the film has been obtained by maintaining the proper ratio of cations and anions during each step of SILAR deposition and thus achieving an ultrathin layer of the desired sample. This method introduces simple equipment, low operating temperature, atmospheric pressure, and large-area deposition, making it low cost compared to other in situ deposition technology [20].

SILAR technology has been used for the development of different inorganic-semiconductor-modified electrodes, and it can also be used for the formation of PbSe and CdSe-based thin films on mesoporous TiO_2. This process is suitable for the development of well-defined quantum dot (QD) layers on mesoporous metal oxides [21].

3.2.2.5 Electroless Deposition

Electroless deposition of metals is a spontaneous electrochemical deposition process. This process is an autocatalytic process which involves deposition of metal on a conductive or a non-conductive substrate by chemical reduction of a metallic salt by a suitable reducing agent. The reaction of prime interest is the cathodic reaction which involves reduction of metallic ions followed by simultaneous anodic oxidation of hydrogen ions [22]. The advantage of electroless deposition is that this process can be applied to deposit metals on the surface of non-conductive substrate as well as irregularly shaped objects. One disadvantage is that the chemical bath needs often replenishment with electron transfer. Electroless deposition finds several applications in the field of microelectronics, aerospace industries, oil and natural gas sector etc. [23].

Electroless deposition comprises of mainly four basic steps [24]:

(a) Substrate Pre-treatment: The substrate is cleaned thoroughly for removing any grease, contaminants etc.

(b) Substrate Sensitization: The sensitizer is an ionic layer which serves as initial catalytic site for active metal deposition. Generally, a thin layer of tin (Sn) is grown on the surface of the substrate which acts as a sensitizer layer.

(c) Substrate Activation: The activator is another ionic layer which accelerates the final metal deposition by acting as catalytic seed over surface of the substrate. Generally, a thin layer of palladium (Pd) is grown on the Sn layer which acts as an activator layer.

(d) Electroless Deposition: The activated solution is washed in distilled water and then electroless deposition is performed. Electroless deposition is the process by which metallic ions in the salt solution are reduced by a powerful reducing agent and the metallic layer is deposited on the surface of the substrate.

Flowchart of electroless deposition:

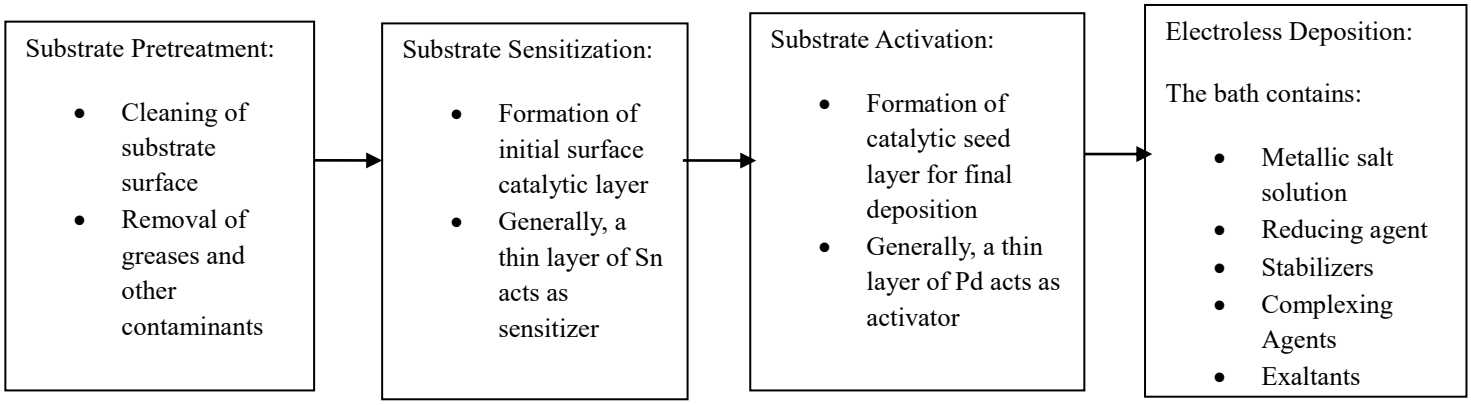

The philosophy behind electroless deposition is not exact but tentative such that an electrical potential is built up along the substrate periphery in the solution which sets up two ionic

currents in the potential zone (one cathodic and other anionic) resulting in a couple of ionic reactions. These ions neutralize their charges on the surface of the substrate and thus initiate deposition. To set up the build-in potential, the surface of the substrate requires pre-conditioning (i.e. sensitization and activation) for autocatalytic conversion. The reducing agent induces the ionic currents by releasing a large number of ions in the solution. Under equilibrium conditions the cathodic current (i_c) becomes equal to the anionic current (i_a) when the deposition process begins through charge transfer mechanism. The rate of metal deposition is a function of ionic current flow. The ionic current flow depends upon various parameters such as solution temperature, pH and various additives added to the solution. These parameters control the ionization rate and also influence the built-in potential along the substrate surface.

3.2.2.6 Electroplating or Electrochemical Deposition

Electroplating, or electrochemical deposition, is a technique to form a metal coating on the surface of a solid substrate. Electroplating consists of two terms, i.e., electro and plating, where electro signifies electric current (D.C.), and plating means coating the surface area of some solid substrate with implementing another material. This process is conducted by the application of an electrolytic cell, which consists of an anode (positive electrode), a cathode (negative electrode), and electrolytic solutions. The metal in which electroplating is carried out is connected to the cathode, and the metal that should be deposited is connected to the anode. The D.C. current is provided here by implementing an external power source. The pictorial image of a typical electroplating unit is shown in Fig. 3.5 [Image has been taken from the laboratory of the solar photovoltaic division under the School of Energy Studies, Jadavpur University].

Fig. 3.5: Pictorial Image of Electroplating Unit

If, for example, copper is deposited to some other metal, then copper (Cu) sulphate should be taken as an electrolyte, which splits up Cu^{2+} cations andSO_4^{2-} anions in the solution. Finally,

Cu^{2+} cations reduce metallic copper (Cu) at the cathode material. This technique is used to improve the surface behaviours of any object, such as resistance to corrosion, minimize friction, uniformity, reflectivity, electrical conductivity, lubricity, etc., in industry [25].

3.2.2.7 Hydro thermal Synthesis

Hydrothermal synthesis is a method in which the growth of materials occurs from aqueous solutions at higher temperature and pressure. Here, a heterogeneous reaction takes place by introducing aqueous solvents and complexing agents under elevated temperature (130-250^{0}C) and pressure (0.3-4 MPa) to dissolve and recrystallise the materials. This technique is a single crystal deposition process, and it depends on the solubility of raw materials in warm water under higher pressure. Here the formation of crystal occurs in a teflon- or steel-based pressure vessel named an autoclave. The substance is placed in an autoclave by introducing water supply during the time of fabrication. The temperature gradient is conserved at the opposite side of the deposition chamber. The solute has been dissolved in the hotter end while crystal growth occurred at the cooler end [26].

This method provides a stable crystalline phase at melting point and can grow materials that conserve higher vapour pressure at their melting point. It is very much suitable for the development of inorganic compounds, nanomaterials, as well as zeolites [27].

3.3 Characterization Techniques of thin film semiconductor

There are various characterization techniques to analyze thin-film semiconductors for performing as optoelectronic devices. The structural analysis by using different methods like XRD, SEM, EDX, etc. is used to observe the structure and surface morphology of the film, whereas optical analysis by using various methods like UV-VIS-NIR spectrophotometry, photoluminescence, etc. is used to determine different optical parameters like band gap, refractive index, absorption coefficient, optical constant, etc. of the semiconducting film. The details of the different structural and optical characterization techniques are mentioned in the text below.

3.3.1 Structural Analysis

The structural analysis of thin film samples by using various techniques such as XRD (X-ray Diffraction), SEM (Scanning Electron Microscopy), EDX (Energy-dispersive X-ray), FESEM (Field Emission Scanning Electron Microscopy), TEM (Transmission Electron Microscopy), and HRTEM (High-resolution Transmission Electron Microscopy) has been discussed in the present text.

3.3.1.1 X-ray Diffraction (XRD)

XRD, or X-ray diffraction, is a technique to determine atomic as well as molecular structure regarding the crystal of a certain material. This method introduces constructive interference between monochromatic X-ray and sample. These incident monochromatic rays are produced from a cathode ray tube and incident towards the sample. Thus, constructive interference between a sample and incident ray has occurred when it satisfies the principle of Bragg's

Law, i.e., nλ = 2d sinθ, where n is diffraction order, λ is wavelength of incident radiation, d is grating constant, and θ is glancing angle. Here every possible diffraction direction of the crystalline lattice should be obtained due to the arbitrary orientation of the sample by maintaining the scanning range of 2θ angles. The angle between incident and diffracted rays is a key factor in all diffraction. Finally, the diffracted rays have been detected and finally processed as well as counted [28]. The pictorial image of a typical XRD unit is shown in Fig. 3.6 [29].

Fig. 3.6: Pictorial Image of XRD Unit

The following microstructural parameters obtain from XRD analysis were calculated below to analyze the crystalline nature of the prepared samples using Scherrer method [30] as shown from eqn. (1) to eqn. (3).

Crystallite Size, $D = K\lambda/ß Cos\Theta$ …….(1)

where, λ= wavelength, ß is the full-width-at-half maximum (FWHM) of the peaks, Θ is the Bragg angle (in radian)

Dislocation Density,$\rho = 1/D^2$…….(2)

Microstrain,$\epsilon = ß cot\Theta/4$……(3)

This method is used to determine the phase of crystalline materials, and it can also be implemented to gather information about unit cell dimensions.

3.3.1.2 Scanning Electron Microscope (SEM) and Energy Dispersive X-ray (EDX)

Scanning Electron Microscopy (SEM) technique can produce high-resolution and magnified images of a material by releasing a focused electron beam on the surface of a sample. This incident beam can interact with the molecular composition of the materials. Thus, this interaction can provide a measurable electron energy, which should be analyzed by a scanning microscope to produce a three-dimensional image. Here the secondary electrons, which are emitted from the atoms and excited by the beam of electrons, are detected by the instrument named energy dispersive x-ray (EDX), and the detected rays are converted properly to gather some valuable information about the materials. EDX is used to determine the elements as well as their composition within the materials. EDX generally shows peaks of the spectrums that correspond to the different energy levels. These peaks are unique for individual elements, and a higher peak corresponds to a higher concentration of a particular element of the material. The SEM and EDX systems are generally associated within the same instrument [31]. The pictorial image of a typical SEM & EDX unit is shown in Fig. 3.7 [32].

Fig. 3.7: Pictorial Image of SEM & EDX Unit

The SEM micrographs can produce the magnifying images, which are useful for better understanding of the surface morphology of the materials. On the other hand, EDX can provide elemental analysis, which is very much useful for chemical characterisation of the sample material.

3.3.1.3 Field Emission Scanning Electron Microscope (FESEM)

Field Emission Scanning Electron Microscope (FESEM) is an upgraded microscopic system that can provide improved magnification and the ability to determine very minute features regarding the surface of the sample in comparison to the SEM unit. FESEM produces higher-resolution images at low accelerating voltage than SEM images. The operating principle of this method is similar to the conventional SEM microscopic system, which is described in the present text. The main difference between SEM and FESEM systems is their electron

generation source, in which FESEM uses a field emission gun (FEG) and SEM uses thermionic emission, respectively. This technique is suitable to determine fine surface morphology with higher magnification, structural uniformity, advanced coating thickness, corrosion features, minute contamination feature geometry, etc. [33,34].

3.3.1.4 Transmission Electron Microscopy (TEM)

Transmission Electron Microscopy (TEM) is a very powerful microscopic tool that can be used in the areas of high-resolution imaging, diffraction, and spectroscopy. This technique provides much greater magnification regarding the surface morphology of any material compared to the FESEM system. It has the ability to produce detailed surface structure with 1-2 angstrom resolutions of any sample. The pictorial image of a typical TEM unit is shown in Fig. 3.8 [35].

Fig. 3.8: Pictorial Image of TEM Unit

In this method, a highly focused electron beam is transmitted through a very thin sample specimen whose thickness is less than 100 nm to obtain an image. The interaction between the electron beam and sample material provides a formation of an image. Some electrons are transmitted while some are diffracted or scattered during the transmission through the sample depending on the thickness and properties of the material. Now these transmitted electrons are directed through projector lenses to achieve magnified images. Finally, the image is focused on a fluorescent screen to observe the image for the users. This method has the ability to analyse nanostructures, crystallography, defect analysis, etc., in the field of material science [36].

3.3.1.5 High Resolution Transmission Electron Microscopy (HRTEM)

High-Resolution Transmission Electron Microscopy (HRTEM) is a portrayal mode of TEM that permits direct imaging at the atomic level of a material structure. HRTEM provides higher magnification as well as resolution (around 0.5 angstrom) in comparison to TEM. The working principles of HRTEM and TEM are almost identical, based on the interaction of the

electron beam with the sample material as discussed in the present text. The image formation occurred by only transmitted electrons in the case of TEM, while the image can be created by utilising both transmitted as well as scattered electrons in the case of HRTEM.

This system requires a brighter electron source and a more stable goniometer in comparison to the TEM. This technique is used to study the morphology as well as the composition of nanomaterials. It is also used to determine the atomic-level defects in metals, semiconductors, etc [37].

3.3.2 Optical Analysis

The optical analysis of thin film samples by using various techniques such as UV-VIS-NIR spectrophotometry and photoluminescence has been discussed in the present text.

3.3.2.1 UV-VIS-NIR Spectrophotometer

UV-VIS-NIR spectrophotometer is an analytical instrument that can be used to determine the number of distinct wavelengths of UV or visible (VIS) or near-infrared (NIR) light when it is transmitted or absorbed or reflected through a sample material with reference to a blank sample. The wavelength ranges of UV, visible, and NIR light belong in between 100 nm-400 nm, 400 nm-700 nm, and above 700 nm, respectively. The shorter wavelength bears more energy, whereas longer wavelengths bear less energy. This instrument consists of a light source section, a wavelength selection system, and a detection unit. Here generally xenon lamps, tungsten lamps, halogen lamps, etc., are used as sources of light. The light is passed through a wavelength selection system where some wavelengths are directed, which is suited for the specific sample. This system consists of a monochromator, an absorption filter, an interference filter, a cutoff filter, a bandpass filter, etc. The absorption filter is used to absorb specific wavelengths of light, whereas the interference filter is used to eliminate unwanted wavelengths that occur due to destructive interference. The cutoff or bandpass filter is used to pass certain wavelengths, and it is generally implemented as an interference filter. Finally, a detector unit is used to convert the light wave, which is passed through the sample, into the electrical signal, and the output data is taken from the computer system. The pictorial image of a typical UV-VIS-NIR spectrophotometer unit is shown in Fig. 3.9 [Image has been taken from the laboratory of the solar photovoltaic division under the School of Energy Studies, Jadavpur University].

Fig. 3.9: Pictorial Image of UV-VIS-NIR spectrophotometer Unit

This unit has been used for the analysis of optical parameters of a semiconductor, such as transmittance, absorption, reflectance, band gap, etc. On the other hand, it is also used for sunscreen evaluation, DNA as well as RNA analysis, glass analysis, etc. purposes [38].

3.3.2.2 Photoluminescence

Photoluminescence is a technique in which the emission of light from any material has been measured by absorption of photons of the sample material. The electron can move from the valence band to the conduction band of a semiconducting material when it absorbs photon energy greater than its bandgap energy. This electron loses its excess energy after a certain period of time during the photoexcitation process and comes back to the valence band. The luminescent photon has been emitted from the material when the energy of the electron eventually falls back down. Thus, the energy of the emitted photon is a measure of the bandgap energy of the material. The optical absorption has occurred by atoms and molecules as a function of wavelength in UV-VIS-NIR spectrophotometers, whereas in photoluminescence, optical fluorescence of atoms and molecules as a function of wavelength has been performed. The pictorial image of a typical photoluminescence unit is shown in Fig. 3.10 [39].

Fig. 3.10: Pictorial Image of Photoluminescence Unit

A light wave having energy matching with material band gap energy directed towards sample material through the excitation monochromator, and it has been absorbed by the material. Then the wave is transmitted to the input of emission monochromator where emitted light has been selected for further processing. After it is directed towards the input of detector where this wave is converted into electrical signal. Finally, it is amplified and observed the output in the recorder. The output of the photoluminescence can give the information about optical band gap, impurity, exciton energy, excitation lifetime etc. of the semiconducting material [40].

3.4 Conclusion

Thin-film semiconductors play an important role in the development of optoelectronic devices and sensors in the industry. In the present chapter, various physical and chemical

deposition techniques regarding thin film semiconductor fabrication and their different characterization methods, such as structural as well as optical, have been discussed elaborately. Physical deposition methods involved higher capital equipment, whereas chemical deposition processes require minimum laboratory setup. In this present work, a copper nitride-based semiconducting film has been developed by a low-cost chemical deposition process, and the feasibility of the film in optoelectronic sensors and devices applications has been detailed described in chapters 4 and 5, respectively.

References:

1. E. Acosta, Thin Film Properties and Applications, Thin Films (2021), DOI: 10.5772/ intechopen.95527.

2. W. D. Nix, Mechanical Properties of thin films, Springer, Metallurgical Transactions A 20 (1989) pp. 2217-2245.

3. N.D. Arora, J.R. Hauser, D.J. Roulston, Electron and hole mobilities in silicon as a function of concentration and temperature, IEEE Transactions on Electron Devices 29(2) (1982) pp. 292-295.

4. J. Y. W. Seto, The electrical properties of polycrystalline silicon films, Journal of Applied Physics 46(12) (1975) pp. 5247-5254.

5. A. Ignatiev, P. O'Neill., G. Zajac, The surface microstructure optical properties relationship in solar absorbers: black chrome, Solar Energy Materials 1(1-2) (1979) pp. 69-79.

6. M. Pelliccione, T.M. Lu, Evolution of Thin Film Morphology: Modeling and Simulations, Springer Series in Materials Science (2008), 1st Edition, DOI :10.1007/978-0-387-75109-2.

7. K.L. Choy, Chemical vapour deposition of coatings, Progress in Materials Science 48 (2), (2003) pp. 57-170.

8. M.S. Dresselhaus, G.Chen, M.Y. Tang, R.G. Yang, H. Lee, D.Z. Wang, Z.F. Ren, J. P. Fleurial, P.Gogna, New Directions for Low-Dimensional Thermoelectric Materials, Advanced Materials 19 (8) (2007) pp. 1043-1053.

9. K. L. Chopra, I. Kaur, Thin Film Device Applications, Spinger (1983), DOI:10.1007/978-1-4613-3682-2.

10. R. V. Stuart, Vacuum Technology, Thin Film and Sputtering, Academic Press (2012), 1st edition.

11. R. Garg, S. Gonuguntala, M. S. Iqbal, A. Oluwasogo, U. pal, M. Ahmadipour, Sputtering thin films: Materials, applications, challenges and future directions, Advances in Colloid and Interface Science 330 (2024)103203.

12. A. Baptista, F. Silva, J. Porteiro, J. Míguez, Gustavo Pinto, Sputtering Physical Vapour Deposition (PVD) Coatings: A Critical Review on Process Improvement and Market Trend Demands, Coatings 8 (11) (2018) 402.

13. S. Pal, D. Patil, S. Tayade, Review on Chemical Bath Deposition Technique, Asian J. Adv. Basic Sci. 6(3) (2018) pp.55-57.

14. B. A. Ezekoye, P.O. Offor, V. A. Ezekoye, F. I. Ezema, Chemical Bath Deposition Technique of Thin Films: A Review, International Journal of Scientific Research 2 (8) (2013).

15. D. Perednis, L. J. Gauckler, Thin Film Deposition Using Spray Pyrolysis, Journal of Electroceramics 14 (2005) pp.103–111.

16. V. K. Singh, Thin film deposition by spray pyrolysis techniques, Journal of Emerging Technologies and Innovative Research 4 (11) (2017).

17. R. G. Aguilar, J. O. López, Low-cost instrumentation for spin-coating deposition of thin films in an undergraduate laboratory, Lat. Am. J. Phys. Educ. 5 (2) (2011).

18. M.D. Tyona, A theoretical study on spin coating technique, Advances in Materials Research 2 (4) (2013) pp. 195-208.

19. D. B. Hall, P. Underhill, J. M. Torkelson, Spin Coating of Thin and Ultrathin Polymer Films, Polymer Engineering and Science 38 (12) (1998).

20. B. Ghosh, M. Das, P. Banerjee, S. Das, Fabrication of SnS thin films by the successive ionic layer adsorption and reaction (SILAR) method, Semiconductor Science and Technology 23 (12) (2008).

21. G. Chen, J. Seo, C. Yang, P. N. Prasad, Nano chemistry and nanomaterials for photovoltaics, Chemical Society Review 21 (2013).

22. A.M. Tarditi, M.L. Bosko, L.M. Cornaglia, Electroless Plating of Pd Binary and Ternary Alloys and Surface Characteristics for Application in Hydrogen Separation, Reference Module in Materials Science and Materials Engineering, Comprehensive Materials Finishing 3(2017) pp. 1-24.

23. P. Siddikali, P.S. Rama Sreekanth, Performance Evaluation of CNT Reinforcement on Electroless Plating on Solid Free-Form-Fabricated PETG Specimens for Prosthetic Limb Application Polymers 14 (2022) 3366.

24. M. Paunovic, M. Schlesinger, Modern Electroplating (Edition:5), Wiley, The Electrochemical Society Series (2010), ISBN: 978-0-470-16778-6.

25. N. A. Hamza1, A. S. Majeed, S. M. Jawd, Review on Types and Methods of Electroplating on Metals, Journal of Power Electronics and Devices 7(1) (2021) pp. 44-51.

26. P. Sirajudheen, N. C. Poovadhumkuzhi, S. Vigneshwaran, B. M. Chelaveettil, S. Meenakshi, Applications of chitin and chitosan-based biomaterials for the adsorptive removal

of textile dyes from water: A comprehensive review, Carbohydrate Polymers 273 (2021) 118604.

27. Y. X. Gan, A. H. Jayatissa, Z. Yu, X. Chen, M. Li, Hydrothermal Synthesis of Nanomaterials 8917013 (2020).

28. V. Gonzalez, M. Cotte, F. Vanmeert, W. de Nolf, K. Janssens, X-ray Diffraction Mapping for Cultural Heritage Science: a Review of Experimental Configurations and Applications, Chemistry- A European Journal 26(8) (2020).

29. T F. Veliseicik, R. Zurauskiene, M. Valentukeviciene, Determining the Impact of High Temperature fire Conditions on Fibre Cement Boards Using Thermogravimetric Analysis, Symmetry 12 (2020)1717.

30. A.L. Patterson, The Scherrer Formula for X-Ray Particle Size Determination, Physical Review 56 (10) (1939) pp.978–982.

31. M. Abd Mutalib, M.A Rahman, M.H.D Othman, A.F.Ismail, J. Jaffar, Scanning Electron Microscopy (SEM) and Energy-Dispersive X-Ray (EDX) Spectroscopy, Membrane Characterization (2017), Chapter 9, pp. 161-179.

32. Material Science & Engineering, IIT-Kanpur, website: https://www. iitk.ac.in /mse/sem /index.html.

33. R. Senthil Prabhu, R. Priyanka, M. Vijay, G.R. Kaviya Vikashini, Field Emission Scanning Electron Microscopy (FESEM) with A Very Big Future in Pharmaceutical Research, International Journal of Pharmacy and Biological Sciences-IJPBSTM 11 (2) (2021) pp. 183-187.

34. Overview of FESEM system, Tutorial of IIT Kanpur, website: https://www.iitk.ac.in /meesa /SEM/ tutorial/SEM_MS.pdf.

35. Jeol Ltd., website: https://www.jeolbenelux.com/JEOL-BV-News/Tag/3d-edx.

36. T. G. Rukari, B. R. Alhat, Transmission Electron Microscopy- an overview, International Research Journal for Inventions in Pharmaceutical Sciences 1 (2) (2013).

37. J. C. H. Spence, High-Resolution Electron Microscopy (4^{th} edition), Oxford University Press (2013), ISBN 978-0-19-966863-2.

38. C. W. Brown, Ultraviolet, Visible, Near-Infrared Spectrophotometers, Applied Spectroscopy Reviews 35 (3) (2007) pp 151-173.

39. Edinburgh Instrument, (web:https://www.edinst.com/product/fls1000-photoluminescence-spectrometer/).

40. U. Shukla, S. Bari, Study on the Photoluminescence, Journal of Pure Applied and Industrial Physics 8(5) (2018) pp. 25-31.

Chapter 4

A Novel method for fabricating semiconducting monocrystalline Copper Nitride Nanowires for Optoelectronic Applications

4.1 Introduction

Exploration on the use of II-VI and III-V group compound semiconductors in device fabrication gained attention since 1954 due to their several advantages over the elemental semiconductors like Si and Ge. Transition metal nitrides are also attractive class of semiconducting materials for their several technological applications [1]. Copper nitride (Cu_3N) is one such compound semiconductor in this class because of its tremendous potential in applications such as recording and electronics sectors [2, 3]. Copper nitride exhibits cubic anti- ReO_3 type crystal structure (a = 3.807Å) having several interstitial sites. If appropriate atoms are made to occupy these interstitial sites, then optical and electrical properties of Cu_3N could be enhanced [4]. Copper nitrides have relatively low thermal stability allowing these compounds to decompose into copper [5]. This encourages further research on copper nitrides in the field of electronics.

In earlier works the Cu_3N films had been deposited by atomic layer deposition (ALD) technique on Ru and SiO_2 substrates. The film was reduced to metallic Cu after annealing at 200°C. The ALD Cu_3N as well as reduced Cu films were found to exhibit smooth surface and outstanding step coverage. The resistivity of the 4.2 nm thick film was obtained to be 30 μΩ-cm [6]. Previously Cu_3N films were developed by depositing copper from an electron gun in ambience of atomic nitrogen obtained from a RF plasma source up to thickness of 10 μm. It was observed that the N_2 adsorption on the Cu <100> surface at room temperature and also at 100°C altered the Cu surface morphology drastically, probably due to presence of dislocations for relieving the stress caused due to difference in lattice parameters between Cu and Cu_3N [7]. The copper nitride films had been deposited in the past by pulsed laser ablation process by ablating a copper target at various pressures of nitrogen. The [N]/ [Cu] ratio i.e. x varied between 0 and 0.33 for a corresponding variation of N_2 pressure in the range of $9x10^{-2}$ to $1.3x10^{-1}$ torr. It was feasible to obtain sub, over as well as stoichiometric films by simply controlling N_2 pressure. The lattice constants were 3.85 À for x=0.25 and found to vary between 3.81 À to 3.83 À for x=0.33. The electrical resistivity of the film with x=0.25 was found to be lower than that of x=0.33 [8]. In the past Cu_3N films were developed by DC magnetron sputtering of Cu target in ambience of nitrogen. Cu_3N crystallites with anti-ReO_3 structure were observed. The preferential direction of growth of films was along the <111> plane at low flow rate of N_2 gas while it was along the <100> plane for higher flow

rates respectively. The flow rate of N_2 gas also influenced the rate of deposition, resistivity as well as micro-hardness [9]. Cu_3N films had been prepared previously by reactive RF magnetron sputtering at different N_2 partial pressures. The films were found to possess cubic anti-ReO_3 structure with lattice constant being 0.3855 nm. When N_2 flow increased the films exhibited stronger texture along the crystal direction <100> with subsequent increase in lattice constant. The optical band-gap of the deposited films was 1.75 eV which increased with increase in N_2 flow rate. The films were found to be thermodynamically stable at 473K with decomposition temperature ranging from 516 K to 547 K [10]. Cu_3N thin films were developed on by reactive High-Power Impulse Magnetron Sputtering (HiPIMS). The films displayed anti-ReO_3 type uniform structures with low defects. Significant absorbance was recorded in UV and visible range. The improved surface properties and development of exquisite ITO-Cu_3N-ITO heterostructures exhibited formation of excellent p-n junction with high performance and ultrafast electron-hole recombination making Cu_3N a perfect candidate for photodetector applications [11]. Metastable copper nitride layers were synthesized using the plasma magnetron sputtering method. Layers with different chemical composition could be obtained by altering the process parameters viz. power and modulation frequency with the most stable ones being formed at lower power. A single phase Cu_3N structure was achieved for each individual frequency. It was evident from obtained results that electronic properties of the layers formed were in good agreement with their chemical composition [12]. N-rich copper nitride films were prepared using dc triode sputtering. It was observed that N_2 started migrating from bulk to film surface leading to two different chemical phases with dissimilar atomic N_2 composition, lattice constants and crystallographic orientation without any change in crystal structure. It was also confirmed that the excess nitrogen accommodated in interstitial locations within the lattice structure [13]. The feasibility study of Cu_3N thin films obtained by reactive sputtering for optical recording media application was conducted. Thermal decomposition of Cu_3N films into Cu detected at 470°C. The copper film hence obtained exhibited a huge difference in reflectance [14]. Cu_3N was obtained by a novel direct nitridation of Cu films. A highly undoped Cu_3N was found to be n-type semiconductor whereas interstitial fluorine doping resulted in the formation of p type semiconductor. The bipolar doping thus observed in the prepared films making it promising in PV applications as an alternate absorber layer [15]. Cu_3N films were fabricated by both Plasma Immersion Ion Implantation (PIII) and Reactive Magnetron Sputtering (RMS) methods respectively. A metal-rich conductive phase of Cu_4N was formed along with Cu_3N in the film developed by PIII method. The resistive switching properties were examined by growing Ni as top

electrode. The PIII deposited Ni/Cu_xN/Cu memory devices exhibited excellent DC and AC endurance performance surpassing that of RMS deposited device which was unstable in nature [16]. Copper nitride nanoparticles were prepared by microwave irradiation process. Copper nitride powder thus obtained was milled and converted to ink by adding ethylene glycol to it followed by annealing. Comparing the Cu_3N ink with the similarly prepared Cu_2O and CuO inks the copper conversion rate was found to be highest and sheet resistance the lowest for Cu_3N, making copper nitride an aspiring candidate for pulsed light sintering-based printed circuit board production processes [17]. Cu_3N films were prepared by spin coating a solution of copper nitride formed by ammonolysis of copper (II) trifluoroacetate at 300–310°C on a silicon substrate. The formation of Cu_3N microstructures was confirmed. The films were found to be stoichiometric narrow band gap semiconductors in nature [18]. Cu_3N nanowires were conformally transferred onto Li metal foil by a one-step roll-press process. In the process Li_3N was formed by reaction of Li and Cu_3N. The Li_3N@Cu nanowire layers thus obtained assisted homogeneous 3D channel structured Li-ion flux exhibiting high Li-ion conductivity of Li_3N. The nanowires could guide lithium to grow into a dense, planar structure without dendrite growth thus exhibiting excellent cycling properties even at high current density making it a suitable candidate for metal ion batteries and fuel cells [19].

It was inferred from previous works that most methods for fabrication of copper nitride involve sputtering, atomic layer deposition and other physical deposition methods. But in the current work copper nitride thin films have been fabricated by a relatively simple and inexpensive spray deposition method. The present deposition process involves meager capital equipment and low recurring input. In this work copper nitride formed by spraying an anionic precursor solution on the surface of copper foil placed over a hot-plate has been reported. The variation of structural properties of the samples with different molar concentration of the precursor solution has been studied. Optical and electrical analysis of the best optimized sample obtained so far has been performed to analyze its potential as a photoresistor or light dependent resistor (LDR).

4.2 Fabrication Methodology

The development of the Cu_xN thin film has been performed here by utilizing a simple and low-cost spray deposition method. The details of the fabrication process have been described in the text below.

4.2.1 Introduction to the present deposition method

The current technique of semiconductor fabrication is a convenient one for conversion of metals into semiconductors. Transition metals are suitable for this purpose as they have the ability to absorb chemical reagents at their surfaces. In this method a precursor solution containing a suitable anion (it can be a group 15 element or a group 16 element) was discretely sprayed on to the surface of a cleaned metallic film placed over a hot-plate. The rate of deposition is dependent upon the rate of chemical sprayed on the film as well as the temperature of the hot plate. Both these factors influence oxidation state and stoichiometry of the elements as well as chemical kinetics of the reaction.

4.2.2 Experimental Details

A. Cleaning of the substrate

A 5cm x 2cm copper strip (film) was cut from a 99.9999% pure copper foil by a pair of large scissors. The strip was washed in concentrated hydrochloric acid (HCl) in a beaker for about 3 minutes for removal of grease and oxides on its surface. Then the strip was washed in distilled water to remove the traces of acid followed by an acetone wash when it was finally ready for deposition.

B. Preparation of the anionic precursor solution

At first thiourea powder was weighed on a cleaned and dried borosilicate glass as per the molarity of the aqueous solution. Then 25 ml of distilled water was poured in a cleaned and dried 500ml beaker to which the thiourea was added for preparation of the aqueous solution. After 5ml of ammonium hydroxide solution was added to the solution. The molarity of the thiourea solution was varied as 0.2(M), 0.4(M), 0.6(M), 0.8(M) and 1.0(M) respectively.

C. Deposition Process

The cleaned copper strip was placed on the hot plate, maintaining it at a temperature range of 50°C to 60°C. Next, the syringe was immersed into the anionic precursor solution, and a very small amount of the solution almost about one-fourth of the total volume of the syringe, was sucked into the syringe. The liquid sucked into the syringe was then carefully sprayed onto the copper strip. The painter's brush was used to spread the liquid evenly over the entire mass of the copper strip. Care was taken to ensure that the liquid was not sprayed anywhere else on

the hotplate except the copper strip. This process of spraying of the liquid on the metallic copper strip was carried out for precursor solutions of varied molarities i.e. 0.2(M), 0.4(M), 0.6(M), 0.8(M) and 1(M) respectively.

D. Post deposition heat treatment

The set of five Cu_xN samples prepared by the above-mentioned technique for variable molarities i.e. 0.2(M), 0.4(M), 0.6(M), 0.8(M) and 1(M) respectively were placed inside a vacuum annealing furnace at a constant temperature of 90°C for 3 hrs. for the purpose of post deposition annealing.

E. Chemical Reaction of the Deposition Process

The entire deposition process involved the following chemical reactions described in eqn. (1-5).

Step I: Ammonium hydroxide (NH_4OH) when added to thiourea solution ammonium sulfide and urea are formed as shown in eqn. (1)

$$CS(NH_2)_2 + 2NH_4OH \rightarrow (NH_4)_2S \text{ (ammonium sulfide)} + CO(NH_2)_2\text{(urea)} + H_2O \quad \ldots\ldots(1)$$

Step II: When the above-mentioned solution was sprayed on metallic copper film placed on hot-plate, urea formed in step I tautomerized to ammonium isocyanate (NH_4NCO) which decomposes into ammonia and cyanic acid (HNCO) at high temperature as shown in eqn. (2).

$$CO(NH_2)_2 \rightleftharpoons NH_4NCO \text{ (ammonium isocyanate)} \xrightarrow{\triangle} NH_3 + HNCO \text{ (isocyanic acid)} \quad \ldots\ldots(2)$$

Step III: The ammonium sulfide formed in step I and ammonium isocyanate (NH_4NCO) formed in step II underwent chemical reaction with the hot metallic copper film to form amorphous copper sulfide as shown in eqn. (3) and copper isocyanate (CuNCO) in eqn. (4) respectively.

$$2Cu + (NH_4)_2S \rightarrow Cu_2S \text{ (amorphous)} + 2NH_3 + H_2 \quad \ldots. (3)$$

$$2Cu + 2NH_4NCO \rightarrow 2CuNCO + 2NH_3 + H_2 \quad \ldots. (4)$$

Step 4: Copper isocyanate being unstable thermally decomposes into crystalline copper nitride, amorphous copper carbide and copper oxide respectively as shown in eqn. (5).

$$CuNCO \xrightarrow{\triangle} Cu_3N \text{ (crystalline)} + Cu_2C_2 \text{ (amorphous)} + Cu_2O \text{ (amorphous)} \ldots.(5)$$

The formation of as-prepared as well as annealed Cu_xN samples has been accomplished with varied molarities by a low-cost spray deposition technique. The deposition technique has been described pictorially in Fig 4.1.

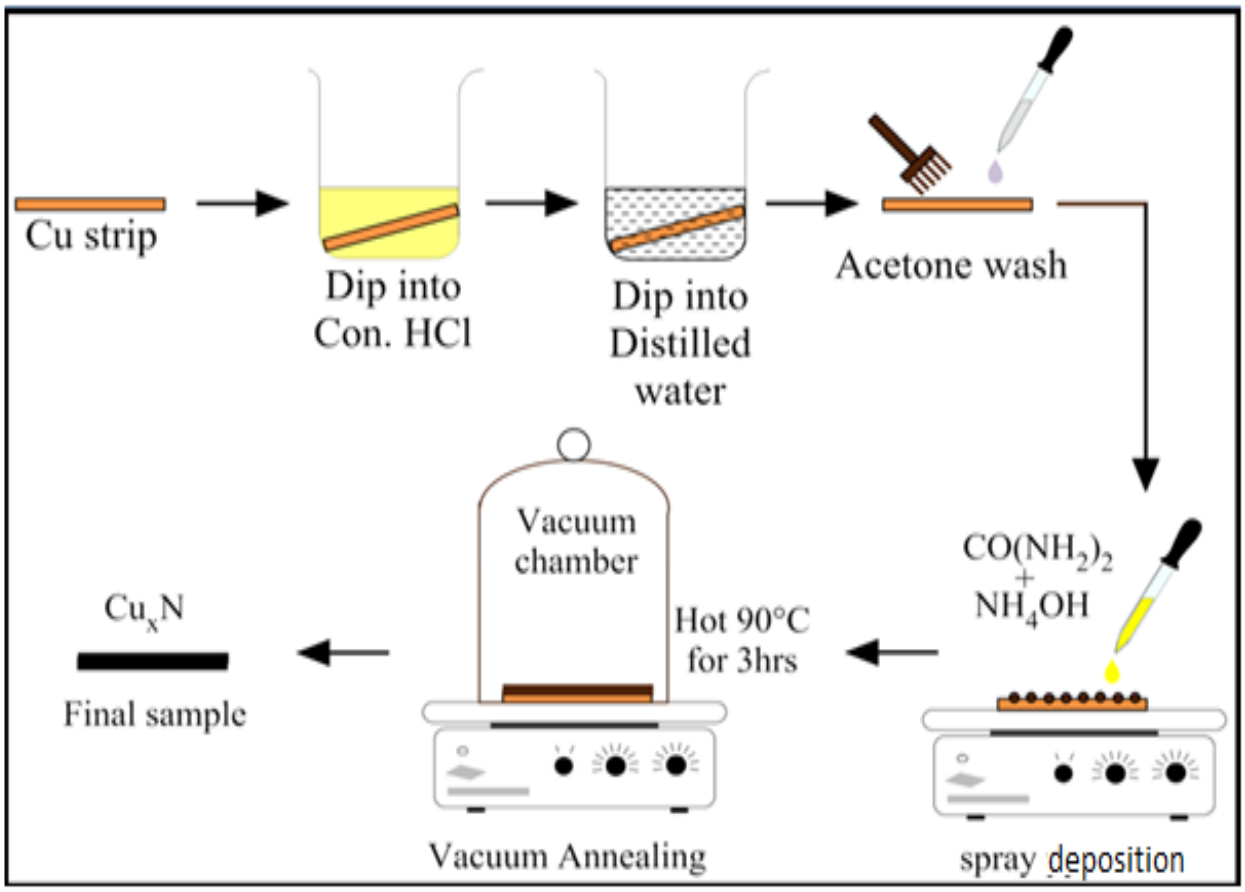

Fig. 4.1: Pictorial Description of Copper Nitride fabrication process by low-cost spray deposition technique

For performing electrical analysis, metallic silver (Ag) was used as contact material on the fabricated samples. Here dot contacts of Ag paste were painted on the sample followed by heat treatment at 90°C for 30 mins. The images of the as-prepared and annealed samples with varied molarities, i.e., 0.2(M), 0.4(M), 0.6(M), 0.8(M) and 1(M), respectively, have been shown in fig. 4.2 given below.

	Cu_xN As-prepared Samples		Cu_xN Annealed Samples
0.2(M)			
0.4(M)			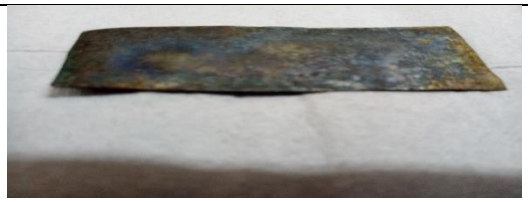
0.6(M)	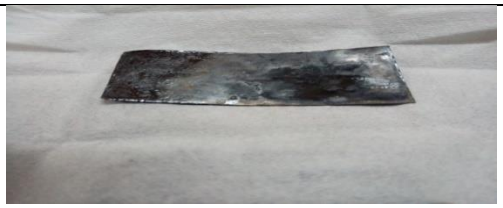		
0.8(M)			
1(M)			

Fig. 4.2: Pictorial Images of As-prepared and Annealed Copper Nitride (Cu_xN) Films of different molarities

4.3. Results & Discussion

The structural, optical and electrical performance analysis regarding copper nitride thin film sample have been studied elaborately in the following text.

4.3.1 Structural Analysis:

A. Structural analysis from XRD spectroscopy

X-ray diffraction (XRD) system is a technique which is used to determine crystalline phases as well as microstructural parameters of a material. Here constructive interference has occurred between the mono chromatic X-ray and sample. The monochromatic rays are produced from a cathode ray tube and incident towards the sample. The constructive interference between a sample and incident ray has occurred when it satisfies the principle of Bragg's Law, i.e., $n\lambda = 2d \sin\theta$, where n is diffraction order, λ is wavelength of incident radiation, d is grating constant, and θ is glancing angle. The angle between incident and diffracted rays is a key factor in all diffraction. Here every possible diffraction direction of the crystalline lattice has been obtained due to the arbitrary orientation of the sample by maintaining the scanning range of 2θ angles. At last, diffracted rays have been detected and processed to obtain the desired information [20]. In this present study copper nitride (Cu_xN) based thin film has been fabricated by utilizing a simple and low-cost spray deposition process. The Cu_xN samples have been prepared with varied molarities, i.e., 0.2(M), 0.4(M), 0.6(M), 0.8(M) and 1(M), respectively. Here both as-prepared as well as annealed samples have been produced to observe the effect of annealing on the optoelectronic performances of the fabricated Cu_xN samples. The XRD patterns have been determined here with varied molarities for both as-prepared and annealed samples. The various microstructural parameters, such as crystallite size, FWHM, dislocation density, microstrain etc., have also been cultivated by considering both as-prepared and annealed samples in this present study. The structural analysis accomplished from the XRD technique is very useful to determine optimum Cu_xN film to be used in optoelectronic applications.

In this present work, XRD patterns of both as-prepared and annealed samples, when compared with standard crystallographic data, the best fit was obtained from the reference XRD pattern of cubic Cu_3N crystal phase [chemical formula Cu_3N, lattice constant (a) = 3.815] corresponding to JCPDS Card no. 02:1156. The XRD patterns of the as-prepared and annealed samples of all molarities displayed a single modest peak at $2\Theta = 50.5°$ along the crystalline plane (0 0 2) indicating formation of excellent copper nitride (Cu_3N) mono-crystalline samples along that plane. The XRD pattern of Copper Nitride as-prepared and annealed samples of different molarities is shown in Fig. 4.3(a,b). XRD Patterns for 0.6 (M)

Cu_xN as-prepared and annealed samples together are shown separately in Fig. 4.4 to observe the effect of annealing regarding the fabricated samples.

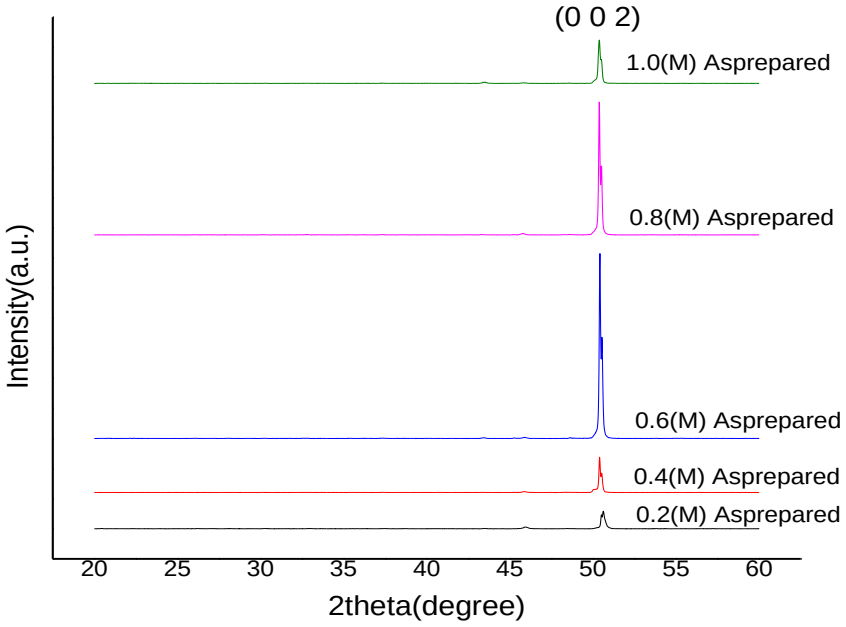

(a): XRD patterns of Cu_xN As-prepared samples of different molarities

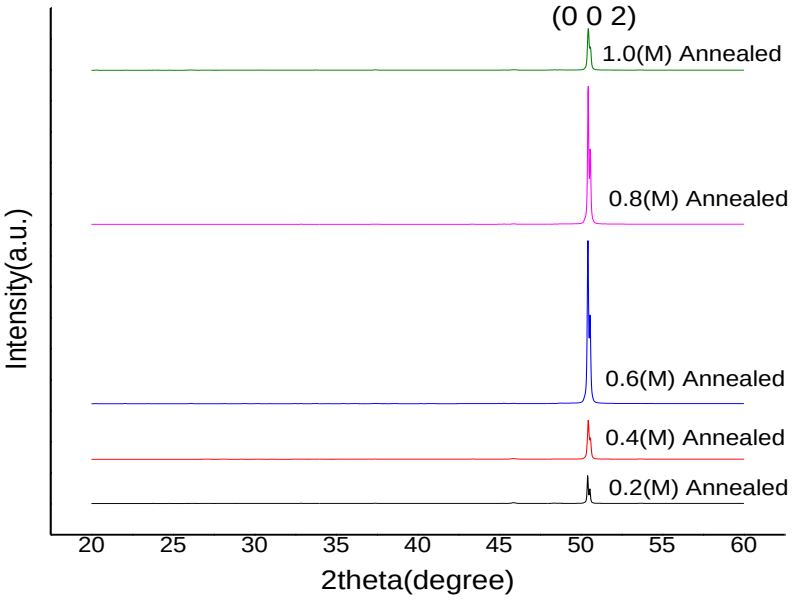

(b): XRD Pattern of Cu_xN Annealed samples of different molarities

Fig. 4.3(a, b): XRD Patterns for As-prepared and Annealed copper nitride (Cu_xN) samples of respective molarities

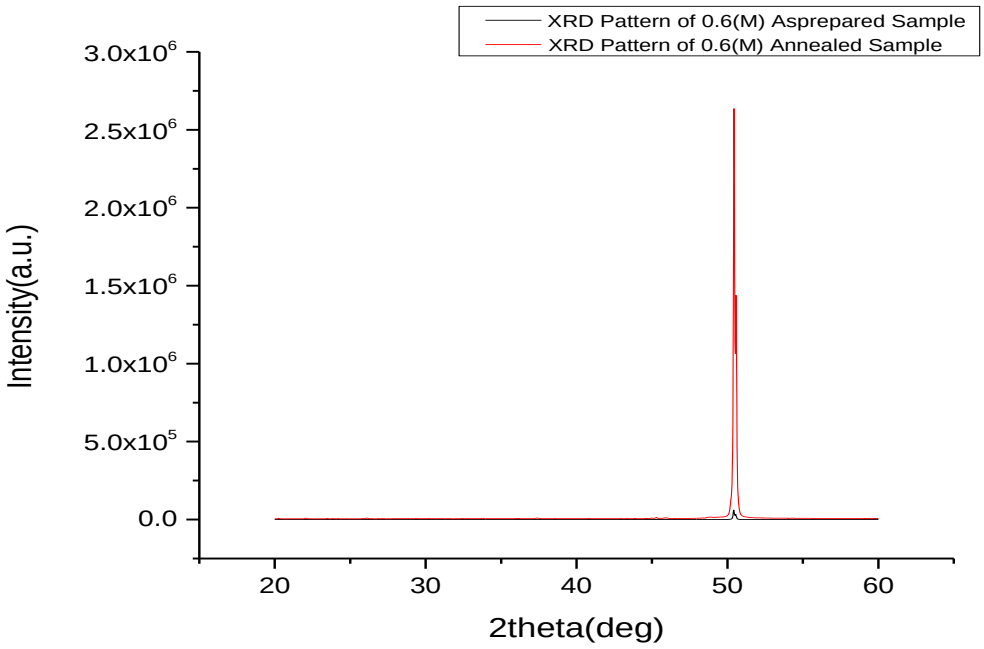

Fig. 4.4: XRD Patterns for 0.6 (M) Cu_xN As-prepared and Annealed samples respectively

It has been inferred from the Fig. 4.3(a,b) that copper nitride samples of all molarities have been shown to be monocrystalline in nature. The same trend has also been observed in annealed samples. Here annealing has improved the peak height and the increment of maximum peak height is observed in Fig. 4.4 for 0.6 (M) Cu_xN sample among all. This increment of peak height indicates that the crystallinity of the Cu_xN sample has improved by the effect of annealing, and the same trend has also occurred for other samples.

The following microstructural parameters for both as-prepared and annealed samples were calculated below to analyze the crystalline nature of the prepared samples using Scherrer method [21] as shown from eqn. (6) to eqn. (8).

Crystallite Size, $D = K\lambda/ß Cos\Theta$…….(6)

where, K=0.9, λ=CuKα wavelength=1.5406Å, ß is the full-width-at-half maximum (FWHM) of the peaks, Θ is the Bragg angle (in radian)

Dislocation Density,$\rho = 1/D^2$…….(7)

Microstrain,$\epsilon = ß cot\Theta/4$……(8)

XRD microstructural parameters for both as-prepared and annealed Cu_xN samples have shown in Tables 4.1&4.2 respectively.

Table 4.1: XRD microstructural parameters analysis of the Cu_xN as-prepared samples

Molarity	**2Ɵ(deg.)**	**FWHM ß(deg.)**	**Peak height (a.u)**	**Crystallite Size D(nm.)**	**Dislocation Density ρ (m^{-2})**	**Micro-strain (ε)**
0.2(M)	50.5	0.291	5215	30.2513	$1.0927x10^{-3}$	0.002680497
0.4(M)	50.5	0.2285	8864	38.5063	$0.6744x\ 10^{-3}$	0.002112841
0.6(M)	50.5	0.2179	45704	40.3481	$0.6143\ x\ 10^{-3}$	0.002016514
0.8(M)	50.5	0.2147	32287	40.9737	$0.5956x\ 10^{-3}$	0.001986488
1.0(M)	50.5	0.2328	12539	37.743	$0.702x\ 10^{-3}$	0.002156867

Table 4.2: XRD microstructural parameters analysis of the Cu_xN annealed samples

Molarity	**2Ɵ(deg.)**	**FWHM ß(deg.)**	**Peak height (a.u)**	**Crystallite Size D (nm.)**	**Dislocation Density ρ (m^{-2})**	**Micro-strain (ε)**
0.2(M)	50.5	0.0788	435674	111.4323	$8.0533x10^{-5}$	$0.730299\ x\ 10^{-3}$
0.4(M)	50.5	0.1169	581980	75.1253	$1.7718x10^{-4}$	$1.063123\ x\ 10^{-3}$
0.6(M)	50.5	0.0933	2560881	94.1167	$1.1289x10^{-4}$	$0.864972\ x\ 10^{-3}$
0.8(M)	50.5	0.0781	2230699	112.443	$7.9092x10^{-5}$	$0.723345\ x\ 10^{-3}$
1.0(M)	50.5	0.116	651815	75.707	$1.7447x10^{-4}$	$1.075565\ x\ 10^{-3}$

It can be observed from Tables 4.1& 4.2 that particle size of both as-prepared and annealed Cu_xN samples was in nanometer range i.e. it can be said that copper nitride nanostructures had been formed. For the as-prepared samples, 0.6(M) sample exhibited highest peak height i.e., it was the most crystalline in nature, whereas the dislocation density and microstrain were minimum for 0.8(M) sample i.e. it was the least strained. The same trend had been observed for the annealed samples. The post-deposition heat treatment resulted in a significant increase of peak height and decrease in FWHM values. In other words, post deposition annealing rapidly improved crystallinity of samples of all molarities. It can also be observed that post deposition annealing led to a significant increase in particle size along with an equivalent decrease in other parameters such as dislocation density and micro-strain thus resulting in formation of less strained structures for samples of all molarities. The highest peak height has obtained for 0.6(M) annealed sample among all and least strain has observed for 0.8(M) annealed sample among all. XRD patterns of 0.6(M) as-prepared and annealed

samples together are shown separately in Fig 4.4 to observe the improvement of peak height as well as sample crystallinity by annealing more clearly. The same trend will be observed for other samples too.

B. Structural analysis from SEM-EDX

Scanning Electron Microscopy (SEM) system is a technique which is used to produce high-resolution and magnified images of a thin film material. On the other hand, Energy Dispersive X-ray (EDX) is used to determine the elements as well as their composition within the materials. In SEM, incident electron beam can interact with the molecular composition of the materials. This interaction can provide a measurable electron energy, which has analyzed by a scanning microscope to produce a three-dimensional image. This image can provide surface morphology of the material. In this method the secondary electrons, which are emitted from the atoms and excited by the beam of electrons are detected and the detected rays are converted properly to provide some valuable information about the materials. The compositional ratio of the material has been obtained from here. EDX generally shows peaks of the spectrums that correspond to the different energy levels, and these peaks are unique for individual elements. The higher peak indicates the higher concentration of a particular element of the material. The SEM and EDX are generally associated within the same instrument [22]. Here copper nitride (Cu_xN) film has been fabricated with varying molarities, i.e., 0.2(M), 0.4(M), 0.6(M), 0.8(M) and 1(M), by spray deposition technique. It has been observed from XRD analysis that all molarity samples have exhibited crystalline nature, and post-deposition annealing has improved the crystallinity of all samples. Here it was also observed that the 0.6(M) Cu_xN sample exhibited the highest peak height, i.e., it was the most crystalline in nature, and on the other hand, the dislocation density and microstrain were minimum for the 0.8(M) Cu_xN sample, i.e., it was the least strained. It has also been observed that annealing has improved the overall structural parameters of the fabricated samples. Thus, 0.6(M) and 0.8(M) Cu_xN samples have shown to be the most optimum among all. Therefore, in this present study, SEM and EDX analysis have been performed for 0.6(M) and 0.8(M) Cu_xN fabricated samples. The SEM micrographs have been taken for both as-prepared and annealed samples. The SEM images have been produced along three different orientations for each sample. These images indicate the parameters, such as particle size, surface morphology, cracks or any dislocation, etc., about the fabricated films. On the other hand, EDX can provide the compositional ratio (Cu:N) of the material. The compositional ratio of the material has influenced the electronic properties of the semiconducting materials. In this present work, the optimum compositional ratio of Cu_xN has been determined to be used for optoelectronic applications.

SEM images of 0.6 (M) Cu_xN as-prepared samples along different orientation as represent in Fig. 4.5 [I(a), II(a), III(a)]. SEM images of 0.6 (M) Cu_xN annealed samples along different orientation as represent in Fig. 4.6 [I(b), II(b), III(b)]. SEM images of 0.8 (M) Cu_xN as-prepared samples along different orientation as represent in Fig. 4.7 [I(c), II(c), III(c)]. SEM

images of 0.8 (M) Cu_xN annealed samples along different orientation as represent in Fig. 4.8 [I(d), II(d), III(d)].

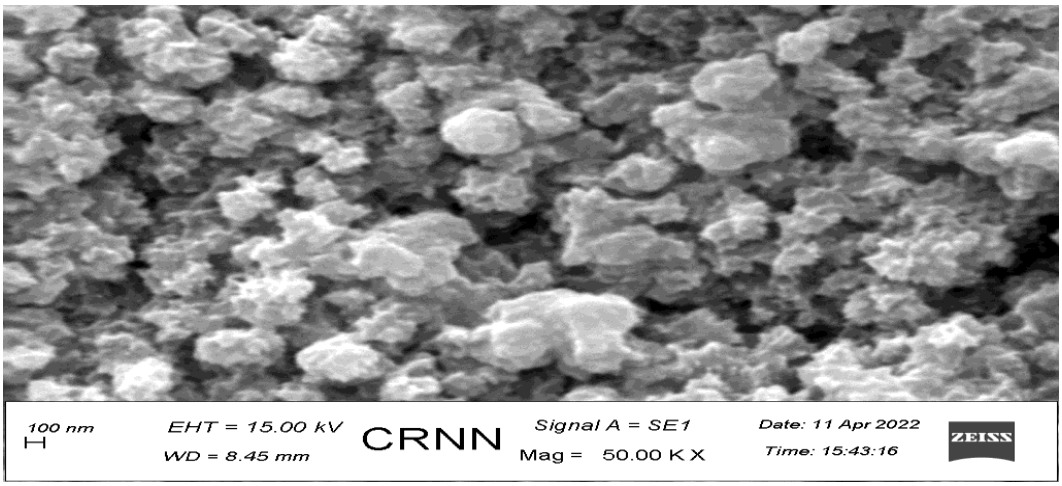

I(a): 0.6(M) Cu_xN as-prepared sample

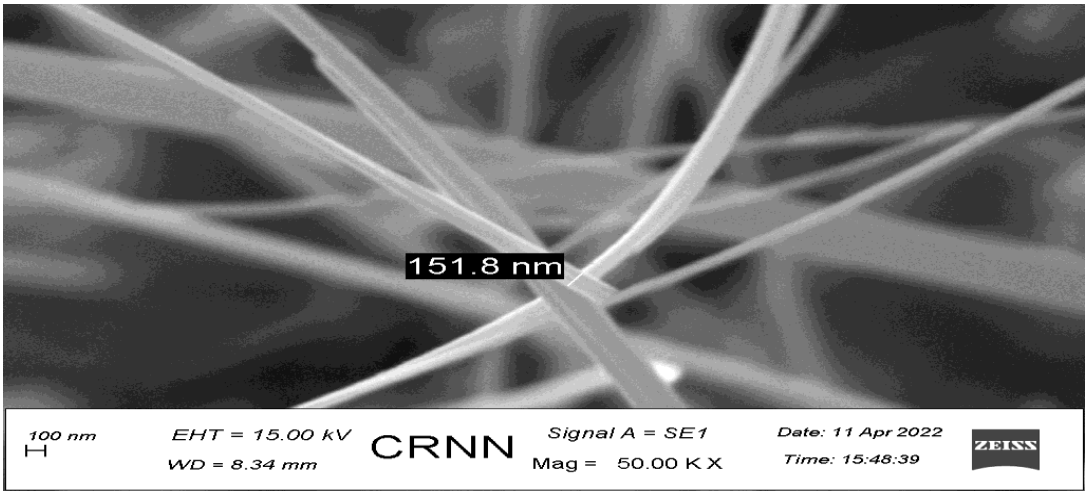

II (a): 0.6(M) Cu_xN as-prepared sample

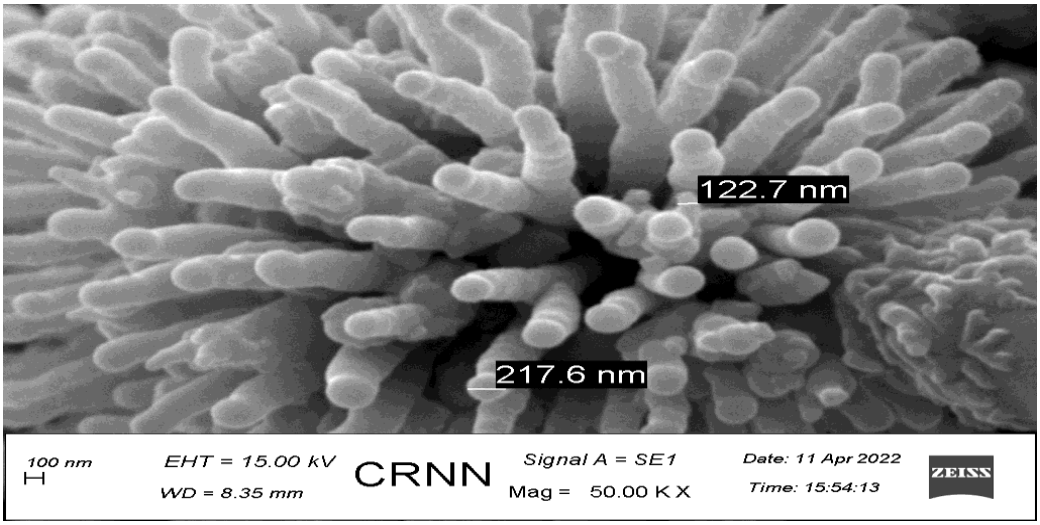

III (a): 0.6(M) Cu_xN as-prepared sample

Fig. 4.5[I(a), II(a), III(a)]: SEM Images of 0.6(M) Cu_xN As-prepared Sample along different orientations.

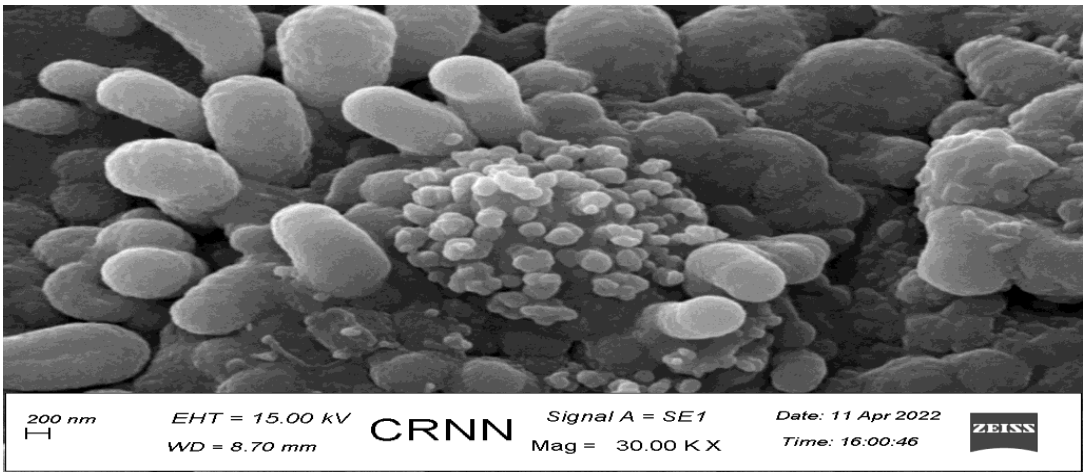

I(b): 0.6(M) Cu_xN annealed sample

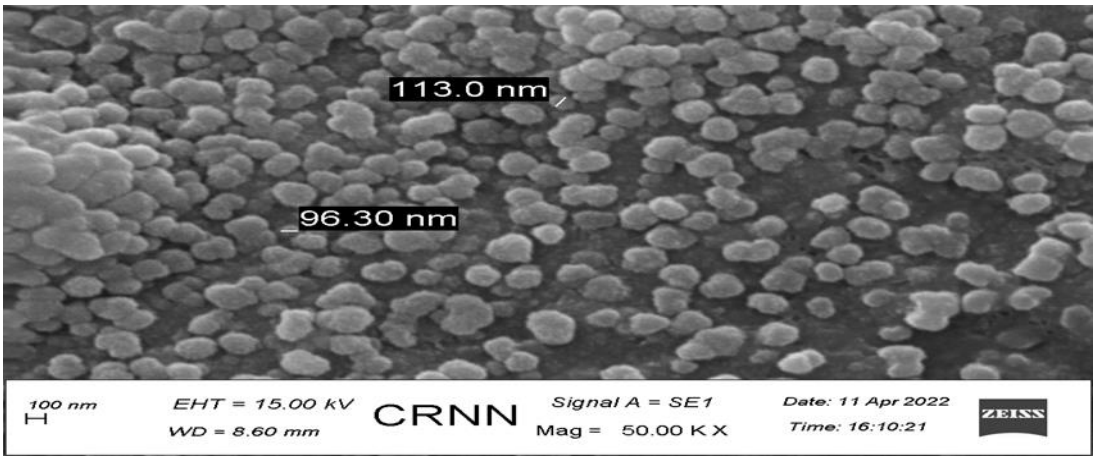

II(b): 0.6(M) Cu_xN annealed sample

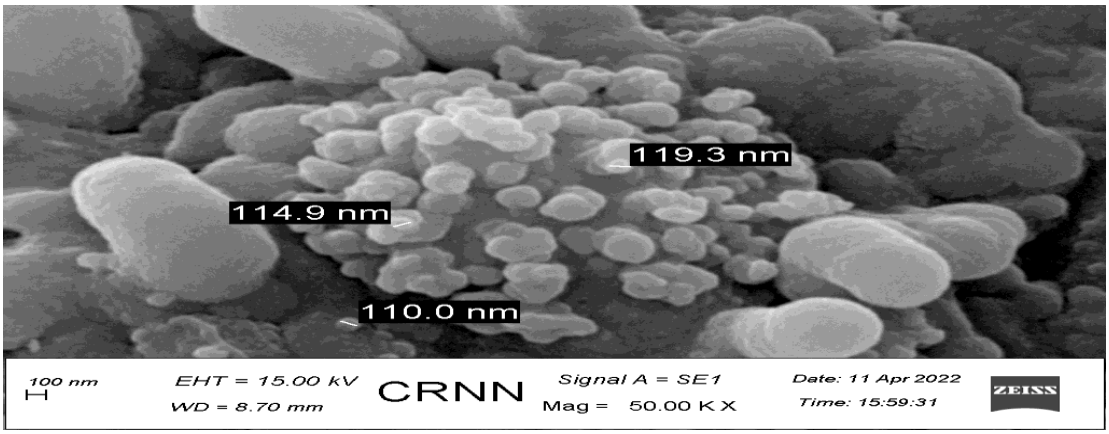

III(b): 0.6(M) Cu_xN annealed sample

Fig. 4.6 [I(b), II(b), III(b)]: SEM Images of 0.6(M) Cu_xN Annealed Sample along different orientations

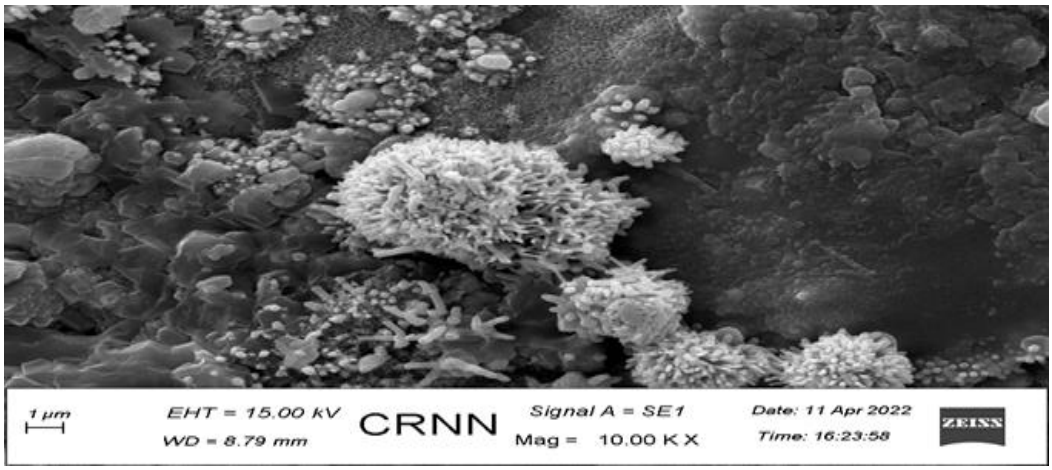

I(c): 0.8(M) Cu_xN as-prepared sample

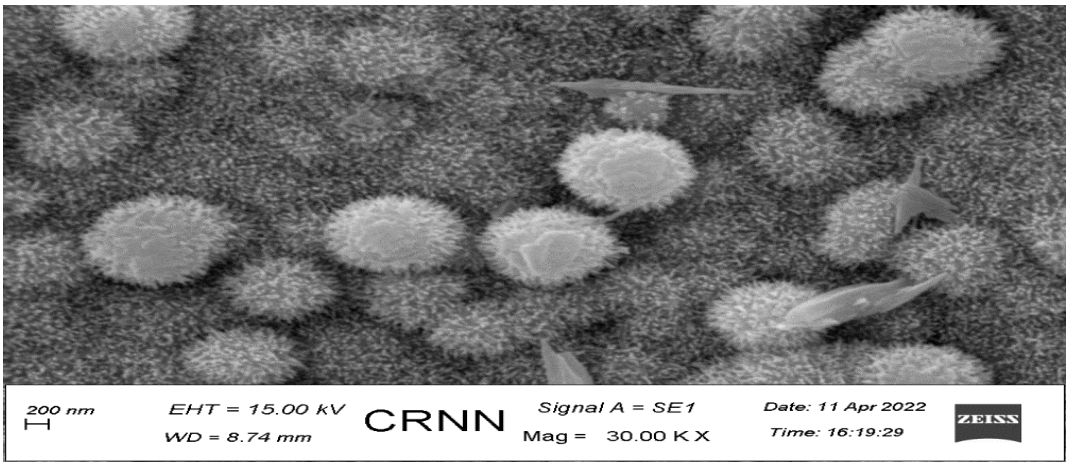

II(c):0.8(M) Cu_xN as-prepared sample

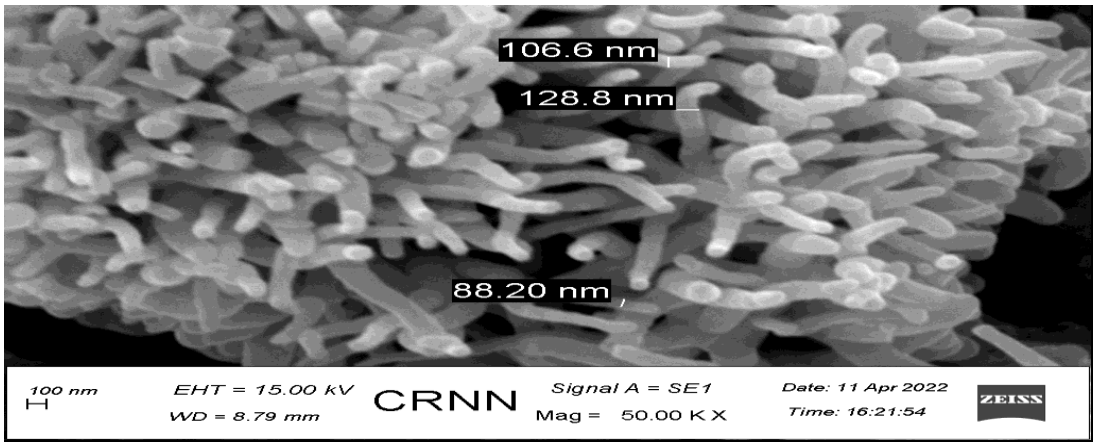

III(c): 0.8(M) Cu_xN as-prepared sample

Fig. 4.7 [I(c), II(c), III(c)]: SEM Images of 0.8(M) Cu_xN As-prepared Sample along different orientations

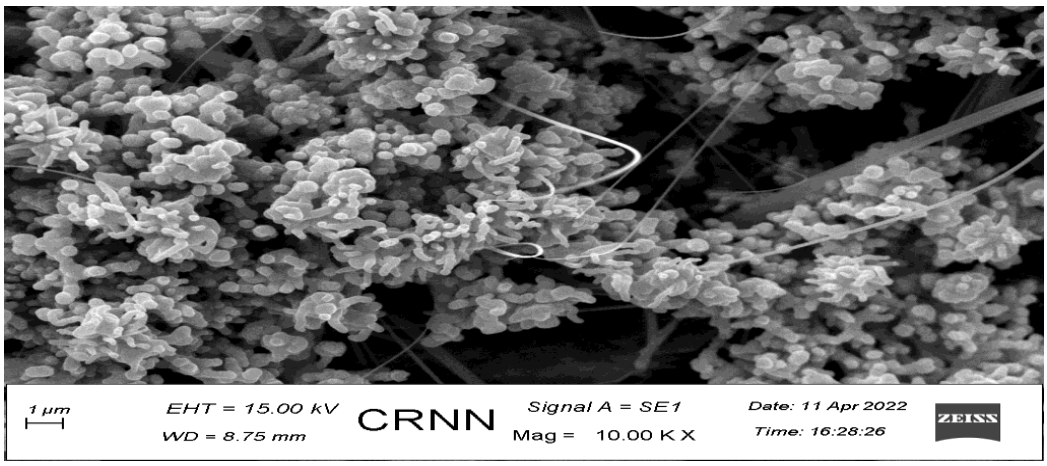

I(d): 0.8(M) Cu_xN annealed sample

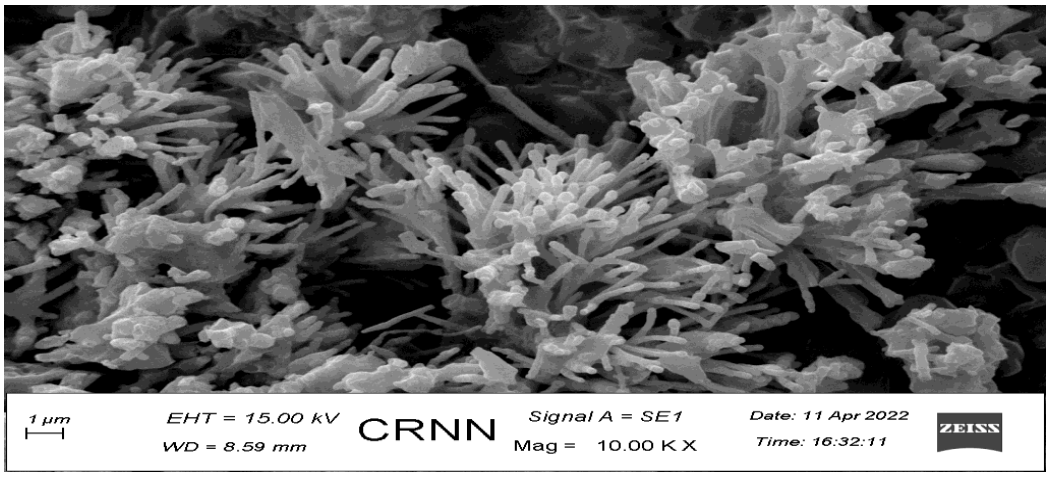

II(d): 0.8(M) Cu_xN annealed sample

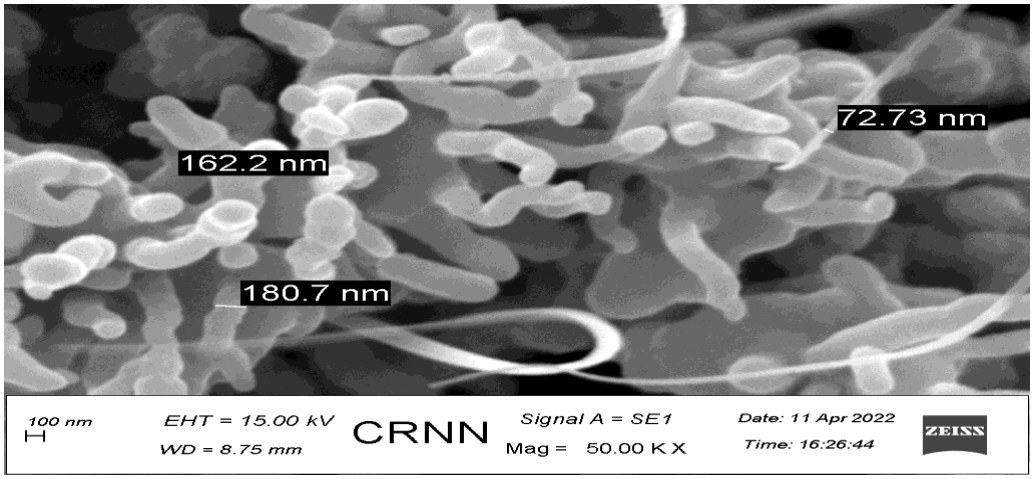

III(d): 0.8(M) Cu_xN annealed sample

Fig. 4.8 [I(d), II(d), III(d)]: SEM Images of 0.8(M) Cu_xN Annealed Sample along different orientations

The SEM micrographs of 0.6(M) and 0.8(M) Cu_xN as-prepared and annealed samples as taken from various orientations are shown in Fig. 4.5 [I(a), II(a), III(a)] to 4.8[I(d), II(d), III(d)]. The crystals were compact, well distributed and found to be of uniform size. The crystallite size was found to vary from 72.73 nm to 217.6 nm. Any crack or pinhole were not found in SEM images. The SEM images in Figs. 4.5[I(a), II(a), III(a)],4.7[I(c),II(c),III(c)]and 4.8[I(d), II(d), III(d)] clearly indicate formation of copper nitride nanowires, thus in accordance with XRD results. However, SEM image for 0.6(M) annealed sample i.e. Fig. 4.6 [I(b), II(b), III(b)] indicates that nanowires were about to grow. The uniform growth of nanowires is discernible from the SEM images. The formation of these nanowires indicates improved semiconducting properties as well as structural stability of the samples.

The percentage analysis of the elements of the 0.6(M) and 0.8(M) Cu_xN as-prepared as well as annealed samples from EDX studies have shown in a tabular form below (Table 4.3).

Table 4.3: Percentage analysis of the elements of the Cu_xN samples from EDX studies

Sample Number	Cu_xN Sample Type	Copper (Cu) Atomic %	Nitrogen (N) Atomic %	Carbon (C) Atomic %	Sulfur (S) Atomic %	Oxygen (O) Atomic %	Cu: N Atomic Ratio
1	0.6(M) Asprepared	34.44	34.1	18.74	3.66	6.81	1.008
2	0.6(M) Annealed	36.56	27.1	19.27	6.76	7.58	1.349
3	0.8(M) Asprepared	31.27	30.31	19.78	9.31	7.04	1.032
4	0.8(M) Annealed	28.74	35.49	20.43	6.99	6.36	0.809

Energy Dispersive X-Ray (EDX) Analysis had been performed here to determine the compositional ratio of the elements in the fabricated nanostructured copper nitride samples, as shown in Table 4.3. It had been previously reported that deposited Cu_xN films were not always consistent in their optimum stoichiometry to be used for optoelectronic devices. Films thus apparently existed as stoichiometric (Cu_3N) or either in non-stoichiometric nitrogen-rich or copper-rich forms [23, 24, 25]. Present EDX studies revealed the samples to be mostly non-stoichiometric in nature. The average Cu:N ratio of the samples was found to vary between 0.8 and 1.35. Here it is perceived that non-stoichiometric crystallographic defects (specifically metal deficiency defects) are present which have altered the overall Cu:N atomic ratio in the crystalline sample. Therefore, surface morphology and compositional ratio of the 0.6(M) and 0.8(M) Cu_xN as-prepared and annealed samples have been determined from the SEM and EDX studies.

4.3.2 Optical Analysis

UV-VIS-NIR (Ultraviolet-Visible-NearInfrared) spectrophotometer system is a technique which is used to determine various optical parameters such as transmittance, absorption, reflectance, band gap, etc., of a thin film semiconducting material. The wavelength ranges of UV, visible, and NIR light belong in between 100 nm-400 nm, 400 nm-700 nm, and above 700 nm respectively. The shorter wavelength has more energy, whereas longer wavelengths bear less energy. This system consists of three sections such as light source section, wavelength selection section and a detection section. The light is passed through a wavelength selection system where some wavelengths are directed, which is suited for the specific sample. Here absorption filter is used to absorb specific wavelengths of light, whereas the interference filter is used to eliminate unwanted wavelengths. The cutoff or bandpass filter is used to pass certain wavelengths, and it is generally implemented as an interference filter. Finally, a detector unit is used to convert the light wave, which is passed through the sample, into the electrical signal, and the output data is taken from the computer system [26]. In this present work, at first the absorption spectrum within the wavelength range of 200 to 1200 nm of the highest crystalline 0.6(M) Cu_xN as-prepared and annealed

samples has been determined to observe its performance in the visible range spectrum. The absorption spectrum curve of 0.6(M) Cu_xN as-prepared and annealed samples is shown in Fig. 4.9.

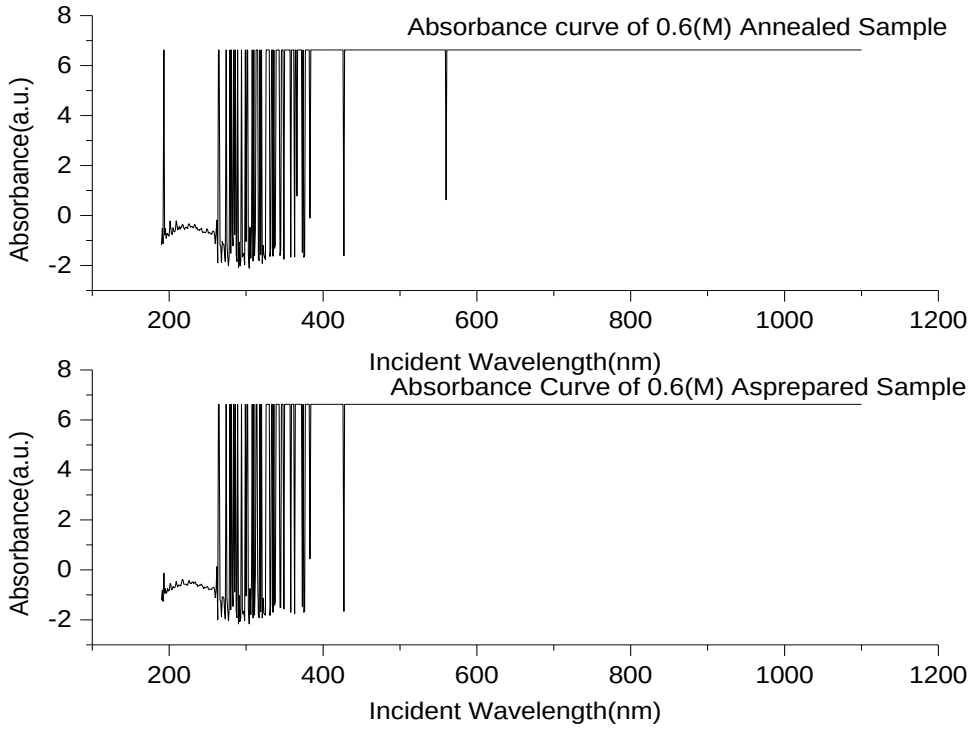

Fig. 4.9: Absorption curves of 0.6(M) Cu_xN As-prepared and Annealed samples

The samples exhibited very low values of transmittance since they were formed by spraying nitride anionic precursor solution directly on the metallic copper substrate. The UV-Vis-NIR absorption spectra of both 0.6(M) Cu_xN as-prepared and annealed samples were observed respectively. From the absorption spectra as shown in Fig. 4.9, the absorption in the UV range i.e. 200nm-280nm was found to be very low (around zero) meaning that the reflectance of UV radiation from the surface of the films was very high. Noise signal was recorded in the wavelength range of 280nm-380nm because of instrumental error. The absorbance values of both samples were exceptionally high in the visible range i.e. 400nm-700nm as well as in the NIR range i.e. 700nm-1200nm.

The optical bandgap of a semiconductor is defined as that minimum energy difference between the highest energy in the valence band and the lowest energy in the conduction band. On the other hand, the highest energy in the valence band and the lowest energy in the conduction band lie in the same momentum value for direct bandgap semiconductors,

whereas a different momentum value is for indirect bandgap semiconductors. The light is absorbed by the semiconducting material when the incident photon energy is greater than or equal to the band gap energy of a material. Thus, the bandgap of a semiconducting material is a very important parameter for optoelectronic applications. The value of direct and indirect bandgaps has been obtained by the following equations [27,28].

Bandgaps were evaluated from the absorption spectra using the following relation as per eqn. (9):

$ahv = Ac(hv - Eg)^n$ ……..(9)

where A_c is a constant, hv is photon energy, E_g is bandgap, a is absorption coefficient and n = 1/2 for direct bandgap semiconductors and n = 2 for indirect bandgap semiconductors

The absorption coefficient can be calculated from the relation as per eqn. (10):

$a = \left(\frac{1}{t}\right).\ln(\frac{100}{T})$……(10)

where t is the thickness of the films and T is the percentage transmitted.

Direct and Indirect band gap curves of 0.6(M) Cu_xN as-prepared and annealed samples are shown in Figs. 4.10(a,b) and 4.11(a,b) respectively.

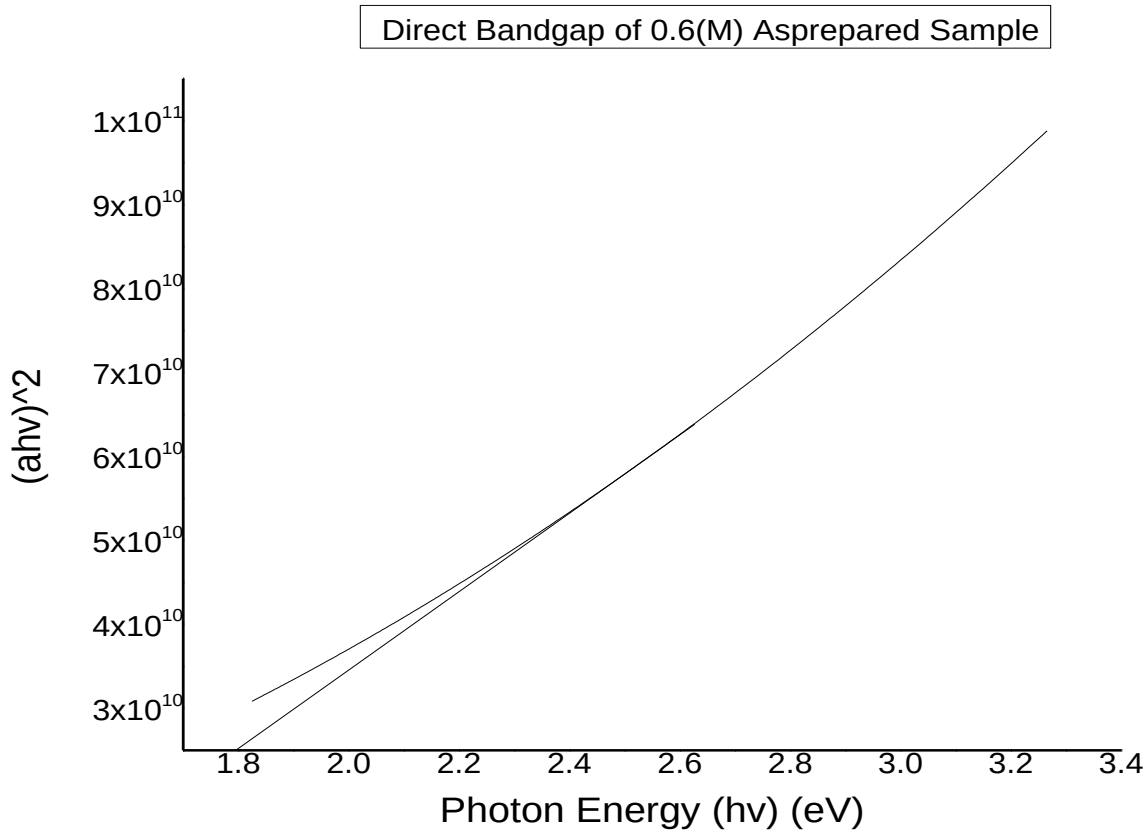

(a): Direct band gap curve of 0.6(M) Cu_xN As-prepared sample

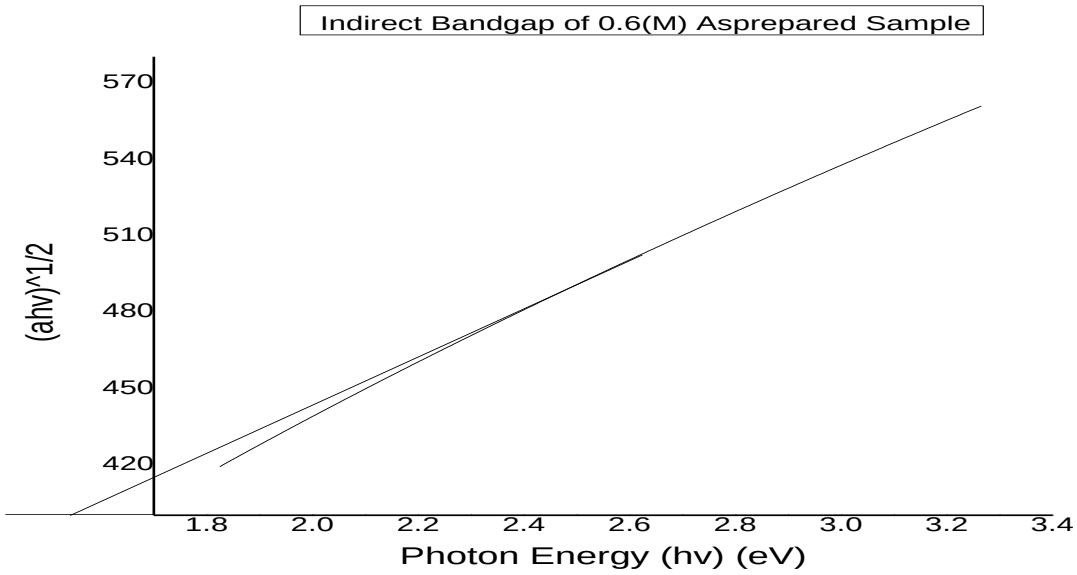

(b): Indirect band gap curve of 0.6(M) Cu_xN As-prepared sample

Fig. 4.10 (a,b): Direct and Indirect Bandgap Curves of 0.6(M) Cu_xN As-prepared Sample

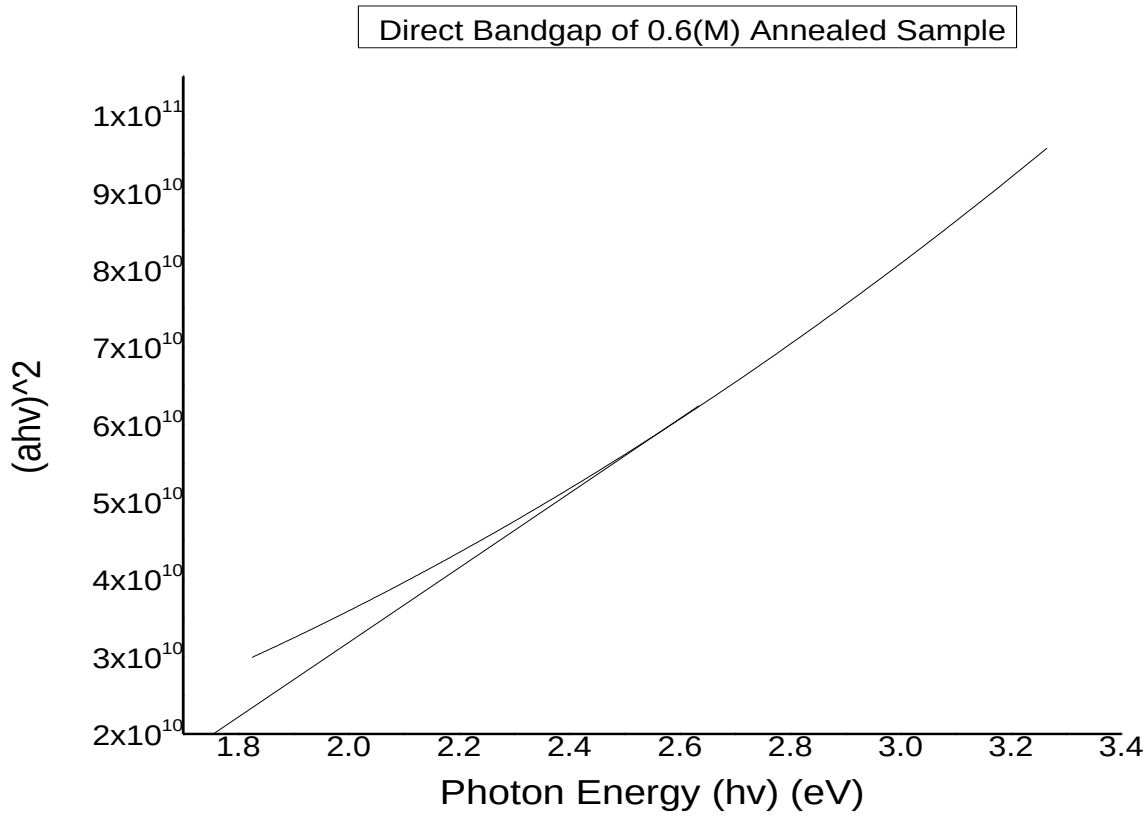

(a): Direct band gap of 0.6(M) Cu_xN Annealed sample

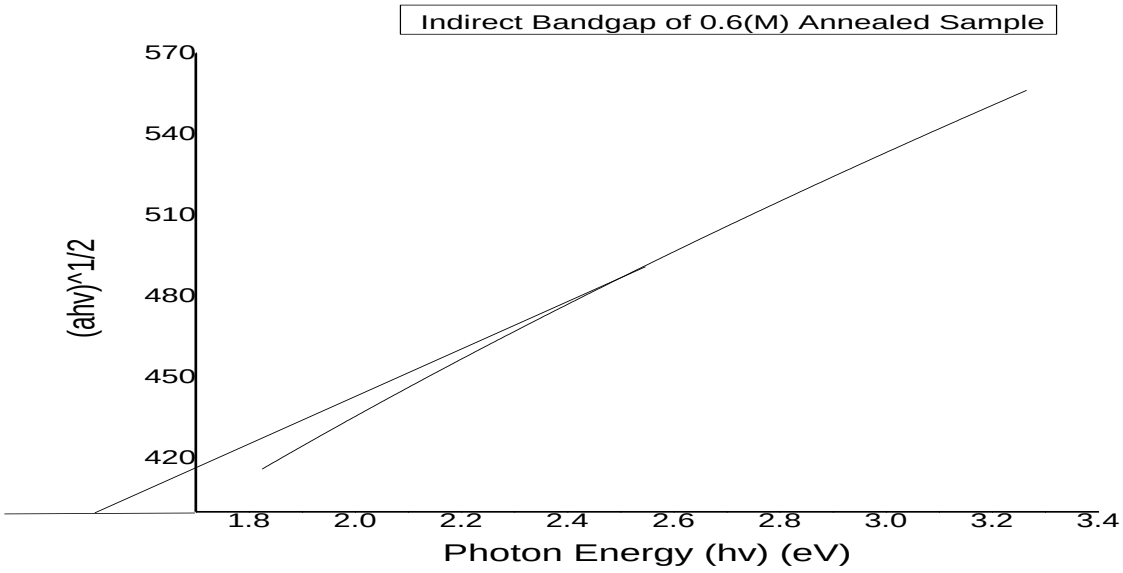

(b): Indirect band gap of 0.6(M) Cu_xN Annealed sample

Fig. 4.11 (a,b): Direct and Indirect Bandgap Curves of 0.6(M) Cu_xN Annealed Sample

Copper nitride exhibits both direct as well as indirect optical band-gaps [27, 28]. The direct and indirect band-gaps were obtained for both 0.6(M) Cu_xN as-prepared and annealed samples respectively from Tauc's plot as shown in Fig. 4.10(a,b) and Fig.4.11(a,b) respectively. The values of direct and indirect band-gaps of 0.6(M) asprepared sample were found to be 1.79 eV and 1.54 eV while those of 0.6(M) annealed sample were 1.75 eV and 1.5 eV respectively. The experimental values of optical bandgap of copper nitride were found to vary within the range of 1.2–1.9 eV [29, 30, 31]. The band-gap values obtained in the present work were in good agreement with previously obtained results. The lower value of indirect band-gap of both as-prepared and annealed samples was indicative of the fact that an indirect transition from valence band to conduction band occurs due to absorption of a photon and a phonon at lower energy regime whereas a direct transition from valence band to conduction band occurs due to absorption of a photon at higher energy regime [32]. However, it was observed that annealing improved both direct and indirect bandgaps of the samples. Thus, it is a promising material in the application as an optical sensor.

4.3.3 Electrical Analysis

Copper nitride compounds have very high values of work function of around 4eV [33]. When a metal having low work function is brought in contact with large work function materials such as copper nitride, a space charge carrier accumulation at the metal semiconductor barrier

is induced which is called bound charge polarization effect. This polarization effect hinders carrier conduction. However, when a metal with high work function is used as a contact on copper nitride, the bound charge polarization effect is minimum and thus carrier conduction will be increased. It is known that silver (Ag) has high work function ranging between 4.26eV-4.73eV [34]. Hence silver having work function value close to that of Cu_xN could form a low barrier Schottky contact or even an Ohmic contact in this metal-semiconductor junction [35]. Therefore, silver can be a good contact material to be fabricated on copper nitride compounds. Accordingly, the same was done in the present work for performing the electrical analysis. The thermal and photoconductive responses of the 0.6(M) Cu_xN annealed sample were observed in Figures 4.12(a,b) and 4.13 (a,b) respectively.

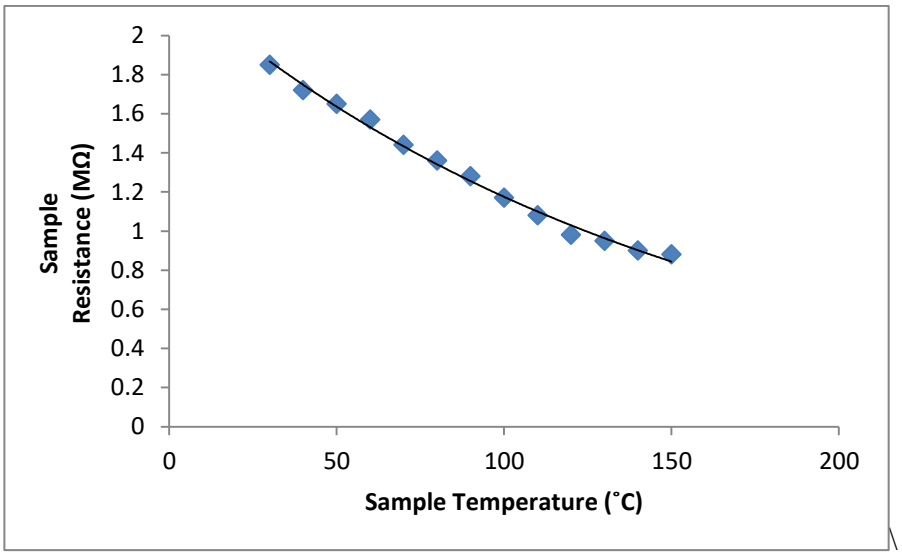

(a): Curve of Sample Resistance vs Sample temperature

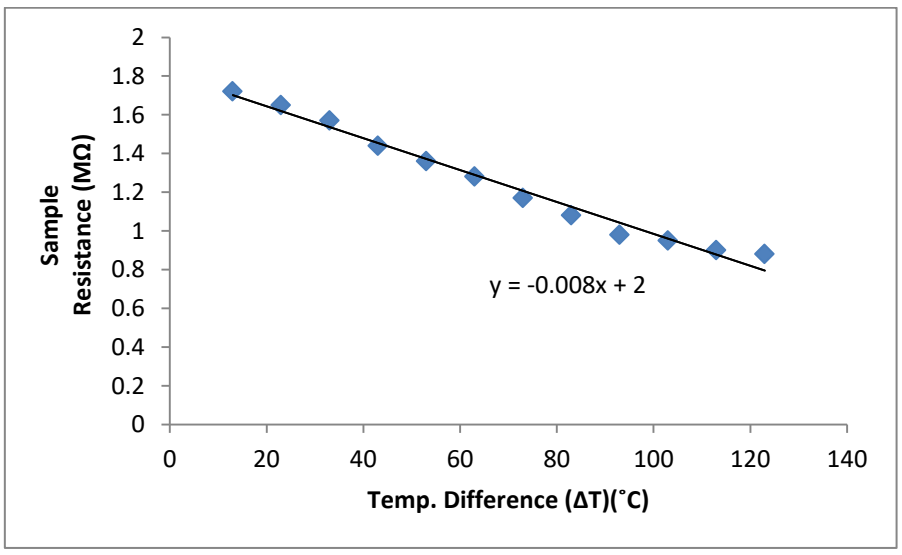

(b): Curve of Sample Resistance vs Temperature difference

Fig. 4.12 (a,b): Thermal response curves of the 0.6 (M) Cu_xN Annealed sample

From the thermal response curve in Fig.4.12.(a), it was revealed that sample resistance exponentially decreased with increasing temperature. We know that $R = R_0 + \alpha R_0(\Delta T)$, where α is the temperature coefficient of resistance of the sample material, R is the sample resistance at temperature T_2, R_0 is the sample resistance at room temperature $T_1 = 27^{\circ}C$ i.e. 2 MΩ and temperature difference is $\Delta T = T_2 - T_1$. In Fig.4.12.(b) the linear curve fitting of the sample resistance (R) vs temperature difference (ΔT) curve was obtained. The value of α of the sample material was obtained from the slope of the fitted linear plot in Fig. 4.12.(b). The value of α obtained was $-0.004/^{\circ}C$. The negative temperature coefficient of resistance of the formed material indicated semiconductor formation.

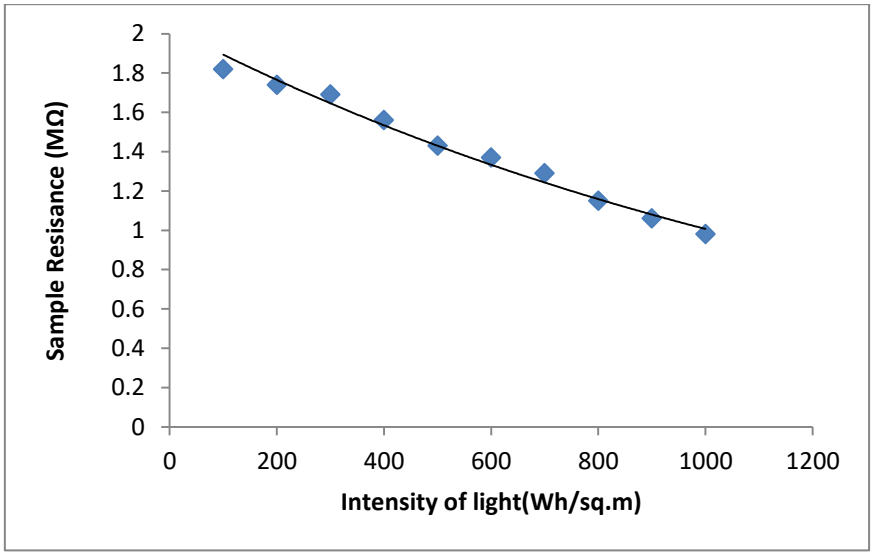

(a): Curve of Sample Resistance vs Intensity of light

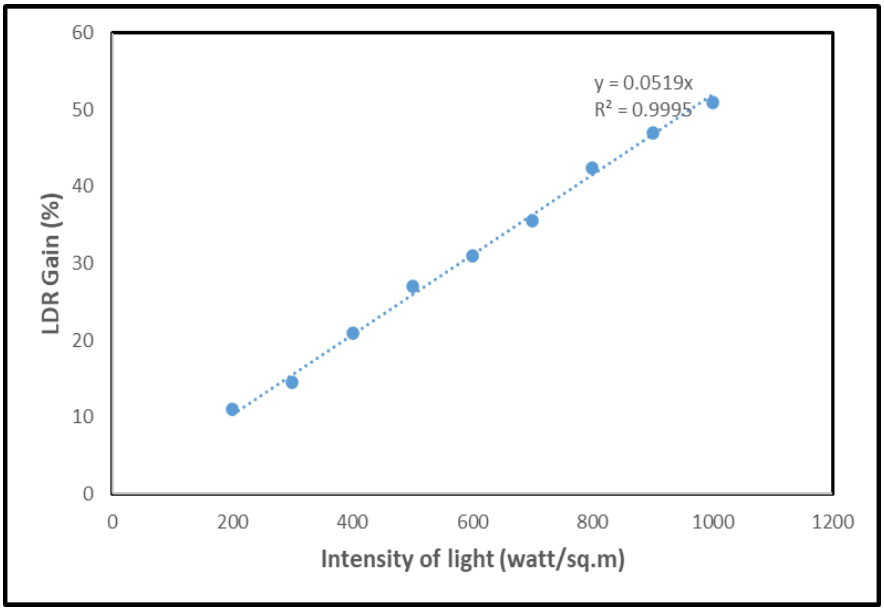

(b): Curve of LDR gain vs Intensity of light

Fig. 4.13(a,b): Photoconductive response curves of the 0.6(M) Cu_xN Annealed sample

From the photoconductive response curve of the 0.6(M) Cu_xN annealed sample as in Fig. 4.13.(a), it was revealed that the value of the sample resistance decreased exponentially with increasing luminous intensity, which is a typical characteristic of a photoconductive sensor like a light dependent resistor (LDR). The % gain of the LDR material was calculated by the formula viz. LDR Gain (%) = [1– (R_{light}/ R_{dark})] *100, where R_{dark} is dark resistance at room temperature i.e. 2MΩ and R_{light} is the material resistance at room temperature exposed to various light intensities (from 100 watt/sq.m to1000 watt/sq.m). The LDR Gain (%) was plotted against intensity of light in Fig. 4.13.(b) and it was revealed that the gain (%) was maximum i.e. 51% at 1000 watt/sq.m. light intensity. The graph reveals highly precise results, with measurements closely aligned with each other and the fitted line. The error margin of a linear curve signifies the uncertainty associated with the measurement and the line of the best fit. The error bars represent the uncertainty in the individual measurement that is plotted on the graph. The length of the bar signifies the dispersion of the data, or it quantifies how much the experimental results might differ from the actual or true, and it can be represented by the formula for standard deviation. This study reveals that the results closely align with both the true value and the fitted line. All the data are clustering around the regression line drawn with optimum standard deviation. Therefore, it can be concluded that the error margin lies within experimental range.

4.4 Conclusion

Detailed fabrication process of device grade Cu_xN nanowire mentioned in the text of the present work is simple and a low cost one. The XRD structural analysis indicated about the formation of monocrystalline cubic Cu_3N and post deposition annealing resulted in the significant improvement in crystallinity and structural parameters. The sample formed by spraying 0.6(M) anionic precursor solution exhibited the best crystallinity whereas the other structural parameters were best for that prepared using 0.8(M) solution. The same trend was observed post annealing. The SEM micrographs indicated formation of copper nitride nanowires. The EDX analysis revealed ratio of Cu and N to vary from 0.8 to 1.35. The absorption spectra of 0.6(M) as-prepared and annealed samples revealed excellent absorption in the visible and NIR range respectively and low absorption in the UV range, indicating that the prepared samples could find applications as propitious optical and NIR sensors. The direct and indirect bandgaps of 0.6(M) Cu_xN as-prepared sample were 1.79 eV and 1.54 eV while those for 0.6(M) Cu_xN annealed samples were 1.75 eV and 1.5 eV respectively. It has been revealed that annealing can improved overall structural as well as optical parameters. The resistance temperature curve of 0.6(M) Cu_xN annealed sample exhibited negative temperature coefficient of resistance of -0.004/˚C, thus revealing its semiconducting characteristics. Therefore, the suitable compositional ratio (Cu: N) of the optimally fabricated 0.6(M) Cu_xN annealed sample is 1.35, for which it has been used for optoelectronic applications. The photo response curve of the same sample revealed its resistivity to be decreasing exponentially with increasing input luminous intensity. This property is an essential parameter in using this material in fabricating opto-electronic devices and sensors. Here Cu_xN based photoresistor or light dependent resistor (LDR) performances have been studied, and maximum LDR gain of 51% at 1000 watt/sq.m light intensity has been achieved.

Now the optoelectronic performance, i.e., photoconductive and photovoltaic analysis of the fabricated optimized 0.6(M) Cu_xN annealed film, has been performed to observe its feasibility for solar cell application. It has been executed by utilizing numerical simulations using Oghma-Nano software (8.1.020) and here providing experimental data of UV-Vis-NIR spectroscopy as input to the simulation software. The detailed study has been accomplished in Chapter 5 of this present thesis.

References:

1. S.T. Oyama (Ed.), The Chemistry of Transition Metal Carbides and Nitrides, 1996, pp. 1–27, DOI:10.1007/978-94-009-1565-7_1.

2. T. Maruyama, T. Morishita, Copper nitride and tin nitride thin films for write-once optical recording media, Applied Physics Letter 69 (1996) 890.

3. R. Cremer, M. Witthaut, D. Neuschutz, C. Trappe, M. Laurenzis, O. Winkler, H.Kurz, Deposition and Characterization of Metastable Cu_3N Layers for Applications in Optical Data Storage, Microchimica Acta 133 (2000) pp.299-302.

4. JCPDS-ICSS, International Centre for Diffraction Data, Newtown Square, PA, USA.

5. S. Terada, H. Tanaka, K. Kubota, Heteroepitaxial growth of Cu_3N thin films, Journal of Crystal Growth 94 (1989) pp.567-568.

6. J. M. Park, K. Jin, B. Han, M. J. Kim, J. Jung, J. J. Kim, W.J. Lee, Atomic layer deposition of copper nitride film and its application to copper seed layer for electrodeposition, Thin Solid Films 556 (2014) pp.434–439.

7. D. Ecija, J. M. Gallego, R. Miranda, The adsorption of atomic N and the growth of copper nitrides on Cu (1 0 0), Surface Science 603 (2009) pp.2283–2289.

8. C. Gallardo-Vega, W.de la Cruz, Study of the structure and electrical properties of the copper nitride thin films deposited by pulsed laser deposition, Applied Surface Science 252 (2006) pp.8001–8004.

9. X. Li, Q. Bai, J. Yang, Y. Li, L. Wang, H. Wang, S. Ren, S. Liu, W. Huang, Effect of N_2-gas flow rates on the structures and properties of copper nitride films prepared by reactive DC magnetron sputtering, Vacuum 89 (2013) pp.78-81.

10. J. Xiao, Y. Li, A. Jiang, Structure, Optical Property and Thermal Stability of Copper Nitride Films Prepared by Reactive Radio Frequency Magnetron Sputtering, Journal of Material Science & Technology **27**(5) (2011) pp.403-407.

11. S. Sakalley, A. Saravanan, W. C. Cheng, S. C. Chen, H. Sun, C. L. Hsu, B. R. Huang, High power impulse magnetron sputtering growth processes for copper nitride thin film and its highly enhanced UV - visible photodetection properties, Journal of Alloys and Compounds 896 (2022) 162924.

12. K. Nowakowska- Langier, L. Skowronski, R. Chodun, S. Okrasa, G. W. Strzelecki, M. Wilczopolska, B. Wicher, R. Mirowski, K. Zdunek, Influence of generation control of the magnetron plasma on structure and properties of copper nitride layers, Thin Solid Films 694 (2020) 137731.

13. R. Gonzalez-Arrabal, N. Gordillo, M. S. Martin-Gonzalez, R. Ruiz-Bustos, F. Agulló-López, Thermal stability of copper nitride thin films: The role of nitrogen migration, Journal of Applied Physics107 (2010)103513.

14. T. Maruyama, T. Morishita, Copper nitride and tin nitride thin films for write-once optical recording media, Applied Physics Letter 69 (1996) 890.

15. K. Matsuzaki, K. Harada, Y. Kumagai, S. Koshiya, K. Kimoto, S. Ueda, M. Sasase, A. Maeda, T. Susaki, M. Kitano, F. Oba, H. Hosono, High-Mobility p-Type and n-Type Copper Nitride Semiconductors by Direct Nitriding Synthesis and In Silico Doping Design, Advanced Materials 30 (2018) 1801968.

16. Q. Zhou, Q. Lu, Y. Zhou, Y. Yang, X. Du, X. Zhang, X. Wu, Influences of preparation methods on bipolar switching properties in copper nitride films, Surface & Coatings Technology 229 (2013) pp.135–139.

17. T. Nakamura, H. J. Cheong, M. Takamura, M. Yoshida, S. Uemura, Suitability of Copper Nitride as a Wiring Ink Sintered by Low-Energy Intense Pulsed Light Irradiation, Nanomaterials 8 (2018) 617.

18. R. Szczesny, E. Szłyk, M. A. Wisniewski, T. K. A. Hoang, D. H. Gregory, Facile preparation of copper nitride powders and nanostructured films, Journal of Material Chemistry C 4 (2016) pp.5031-5037.

19. D. Lee, S. Sun, J. Kwon, H. Park, M. Jang, E. Park, B. Son, Y. Jung, T. Song, U. Paik, Copper Nitride Nanowires Printed Li with Stable Cycling for Li Metal Batteries in Carbonate Electrolytes, Advanced Materials 32 (2020) 1905573.

20. T F. Veliseicik, R. Zurauskiene, M. Valentukeviciene, Determining the Impact of High Temperature fire Conditions on Fibre Cement Boards Using Thermogravimetric Analysis, Symmetry 12 (2020)1717.

21. A.L. Patterson, The Scherrer Formula for X-Ray Particle Size Determination, Physical Review. 56 (10) (1939) pp. 978–982.

22. M. Abd Mutalib, M.A Rahman, M.H.D Othman, A.F.Ismail, J. Jaffar, Scanning Electron Microscopy (SEM) and Energy-Dispersive X-Ray (EDX) Spectroscopy, Membrane Characterization (2017), Chapter 9, pp. 161-179.

23. C.M. Caskey, R.M. Richards, D.S. Ginley, A. Zakutayev, Thin film synthesis and properties of copper nitride, a metastable semiconductor, Material Horizons. 1 (4) (2014) pp.424–430.

24. R. Gonzalez-Arrabal, N. Gordillo, M.S. Martin-Gonzalez, R. Ruiz-Bustos, F. Agulló-López, Thermal stability of copper nitride thin films: The role of nitrogen migration, Journal of Applied Physics 107 (2010) 103513.

25. Q. Lu, X. Zhang, W. Zhu, Y. Zhou, Q. Zhou, L. Liu, X. Wu, Reproducible resistive-switching behavior in copper-nitride thin film prepared by plasma-immersion ion implantation, Physics Status Solidi. 208 (4) (2011) pp.874–877.

26. C.W. Brown, Ultraviolet, Visible, Near-Infrared Spectrophotometers, Applied Spectroscopy Reviews 35 (3) (2007) pp 151-173.

27. G.Sahoo, S. R. Meher, M. K. Jain, Room temperature growth of high crystalline quality Cu_3N thin films by modified activated reactive evaporation, Material Science Engineering. B 191 (2015) pp. 7−14.

28. D. Dorranian, L. Dejam, A. H. Sari, A. Hojabri, Structural and optical properties of copper nitride thin films in a reactive Ar/N_2 magnetron sputtering system, The European Physical Journal Applied Physics 50 (2010) 20503.

29. D.Y. Wang, N. Nakamine, Y. Hayashi, Properties of various sputter-deposited Cu–N thin films, Journal of Vacuum Science & Technology A 16 (1998) 2084.

30. K.J. Kim, J.H. Kim, J.H. Kang, Structural and optical characterization of Cu_3N films prepared by reactive RF magnetron sputtering, Journal of Crystal Growth 222 (2001) pp.767-772.

31. S. Ghosh, F. Singh, D. Choudhary, D.K. Avasthi, V. Ganesan, P. Shah, A. Gupta, Effect of substrate temperature on the physical properties of copper nitride films by r.f. reactive sputtering, Surface Coating Technology (142–144) (2001) pp.1034-1039.

32. B. Wang, T.R. Harris, M.R. Hogsed, Y.K. Yeo, M. Y. Ryu, J. Kouvetakis, Comparison study of temperature dependent direct/indirect bandgap emissions of $Ge_{1-x-y}Si_xSn_y$ and $Ge_{1-y}Sn_y$ grown on Ge buffered Si, Thin Solid Films 673 (2019) pp.63-71.

33. A. Tilemachou, M. Zervos, A. Othonos, T. Pavloudis, J. Kioseoglou, p-Type Iodine-Doping of Cu_3N and Its Conversion to γ-CuI for the Fabrication of γ-CuI/Cu_3N p-n Heterojunctions**,** Electronic Materials 3(1) (2022) pp.15–26.

34. A. W. Dweydari, C. H. B. Mee, Work function measurements on (100) and (110) surfaces of silver, Physicia Status Solidi 27 (1975) pp.223-230.

35. B. Ghosh, Electrical contacts for II–VI semiconducting devices, Microelectronic Engineering, 86 (2009) pp.2187–2206.

Chapter 5

Investigation on Optoelectronic response of crystalline copper nitride (Cu_xN) thin film semiconducting material

5.1 Introduction

In the present era, commercial electronics and the solar photovoltaic industry are dominated by silicon. Silicon is plentiful, chemically stable, non-toxic and exhibits an indirect optical bandgap, making it ideal for application in optoelectronic industries [1] in general and as a solar cell absorber layer in the photovoltaic market with more than 93% share until now [2]. Despite these advantages the cost of fabrication of silicon solar cells remains very high. The lion's share of the silicon solar cell cost remains embedded in the silicon wafer [3] and wafers also account for 46% of the module costs [4]. However, fabrication of highly efficient silicon solar cells remains difficult because of the presence of high impurity content in polycrystalline silicon [5]. On the other hand, inadequate light absorption takes place at longer wavelengths, leading to a requirement of thick c-Si substrate for the fabrication of highly efficient solar cells, thus increasing fabrication costs [6]. Several low-cost inorganic optoelectronic materials have gained prominence for substituting silicon for PV cell development and a lot of research has been conducted in this domain [7].

The crystalline structures of various inorganic materials can be modeled by using modern software simulation techniques. A high-temperature superconductor compound yttrium barium cobalt oxide (YBCO) i.e. $YBa_2Cu_3O_{7-x}$ was modeled by performing numerical simulations using Gaussian Process Regression in MATLAB software and the superconductor transition temperature i.e. critical temperature was predicted based upon lattice parameters. A high critical temperature is an important aspect of a superconductor for practical applications and hence predicting the same by software simulations is an area of key interest. The simulated results were similar to the experimentally obtained values of superconductor critical temperature thus explaining the accuracy and stability of the numerical simulation technique [8]. Lattice misfit between two crystalline phases of Ni-based single crystal superalloys (Ni-SXs) (i.e. γ and γ' phases) was predicted by developing a computational Gaussian process regression model based upon alloy chemical composition, deposition temperature and morphological factors. Ni-SXs exhibit very high mechanical strength, but their mechanical behavior is dependent upon the crystalline phases and the lattice mismatch between these phases must be determined for predicting their deformation mechanism. The developed regression model was very accurate and stable, required low computation time and the prediction output was comparable with practical results [9]. Modern simulation techniques are accurate and can be used to predict the response of conventional materials.

Optoelectronic devices based on inorganic materials have been simulated before and such works have been comprehensively reviewed. CdTe-based solar cells with a ZnO window layer and various buffer layers such as CdS, ZnO, ZnS and ZnSe were modeled using the Silvaco-Atlas semiconductor device simulator with the ZnS-based cell being the most efficient [10]. A solar cell configuration consisting of Ag/ZnO: Al/intrinsic ZnO/ $CdS/Sb_2Se_3/Mo$ was modeled using SCAPS-1D software with Ag as front contact and Mo as back contact respectively. It was found that several parameters like Sb_2Se_3 layer thickness, carrier concentration and work function of the back contact metal influenced solar cell performance [11]. A solar cell with Cu_2Te absorber layer, WS_2 window layer, Al top contact and Ni back contact was simulated using SCAPS-1D software. The WS_2 buffer layer

displayed better performance than the CdS buffer layer [12]. A $CuSbS_2$-CdS solar cell was simulated using SCAPS-1D software. Cell output was found to be dependent upon numerous material/heterojunction properties and cell parameters were also dependent upon the optical bandgap and electron affinity of buffer and absorber layers [13]. A solar cell with Al/ZrS_2/$CuInS_2$/Au configuration with ZrS_2 as buffer and $CuInS_2$ as absorber layers and Al as front and Au as back contacts was simulated using SCAPS-1D software. Cell output was found to be dependent upon parameters like buffer and absorber layer thickness, optical bandgap, defect density, acceptor density, shunt and series resistance [14]. Two solar cells, the first one with $CuInS_2$ as the absorber layer and CdS as the buffer layer and a second one with an additional ZnO window layer were simulated using SCAPS-1D software. The addition of a ZnO layer led to an improvement in cell performance [15]. A solar cell with glass/ $CuGa(S,Te_2)$:Fe/In_2S_3/(Al-Zn-O) (AZO) configuration was simulated by SCAPS-1D software. The iron doping resulted in an improvement of cell efficiency with iron doping due to an intermediate band formation with iron incorporation [16]. A solar cell with configuration Al/AZO/CdTe/NiO/Ni was simulated using SCAPS-1D software. It was found that cell performance was dependent upon thickness and carrier concentration of window and absorber layers, series and shunt resistances and cell operating temperature [17]. A monoclinic Cu_2SnS_3-based solar cell was simulated using AMPS-1D software. Essential parameters like absorber and buffer layer thickness and carrier concentration, back contact metal work function and operating temperature were optimized for maximizing cell performance [18]. A $Cu_2BaSn(S,Se)_4$ (CBTS) - CdS based solar cell was simulated using SCAPS-1D software. The presence of a MoS_2 interlayer was vital for the performance of the solar cell. The solar cell performance was boosted due to the presence of p-type MoS_2, but it dwindled due to the presence of n-type MoS_2 [19]. A copper manganese tin sulfide (CMTS)-based solar cell with various buffer layers like CdS, Zn(O,S) and SnS_2 was simulated using SCAPS-1D software. Various parameters of the CMTS-SnS_2 solar cell like buffer and absorber layer thickness, CMTS layer acceptor density, SnS_2 layer donor density and defect density were optimized for better cell performance [20]. Copper gallium diselenide (CGS) and copper indium gallium diselenide (CIGS)-based single junction and double junction (or tandem) solar cells were simulated using Silvaco-Atlas software. Tandem cells showed better performance [21]. CdS-CdTe heterojunction solar cells were simulated by SCAPS-1D software. It was found that a film of low thickness was mandatory for proper functioning of the cell [22]. A solar cell with the configuration Cu_2SnS_3/$ZnO_{1-x}S_x$/ZnO/Al was modeled and simulated using SCAPS-1D software. It was observed that use of $ZnO_{1-x}S_x$ as buffer layer and ZnO as window layer improved cell performance [23]. Modelling and simulation of a ZnO/CdS/ $CuInGaSe_2$ (CIGS) was performed using wxAMPS software. Several parameters, such as ZnO i.e. window layer, CdS i.e. buffer layer and CIGS i.e. absorber layer thicknesses and carrier concentrations of the CdS layer, were optimized for proper functioning of the solar cell [24]. A ZnO/CdS/CIGS solar cell was simulated using SCAPS software with ZnO:Al i.e. TCO (transparent conductive oxide) and Mo were used as front and back contacts respectively. Several parameters such as optical bandgap, mismatch between buffer and absorber layers and CIGS and TCO layer thicknesses were optimized for proper functioning of the cell [25]. A solar cell with Mo/$CuSnS_3$ (CTS) /CdS/ZnO/TCO/Al configuration was simulated using AMPS-1D software. Absorber layer i.e. CTS layer thickness and work

function of the back contact metal was optimized for proper cell functioning [26]. Solar cells with Sb_2Se_3 and Sb_2S_3 absorber layers and CdS, ZnO, ZnS, ZnSe and In_2Se_3 as buffer layers were simulated using SCAPS-1D software. The absorber and window layer thicknesses were varied and it was found that solar cells with ZnS as a buffer layer were most efficient with both antimony chalcogenide absorber layers [27].

Thin film materials have become popular in recent times for a wide range of applications including semiconductors, integrated circuits, telecommunications, optoelectronics etc. Thin film refers to a very thin layer of material with thickness varying from a fraction of a nanometer to a few micrometers. Nanomaterials are thin film materials with particle sizes between 1nm and 100nm. Nanomaterials have several advantages over conventional bulk materials. Nanomaterials possess lightweight, high durability, high specific surface area, high mechanical strength, high energy storage capacity, high electrical conductivity and excellent magnetic properties [28]. Nanomaterials can be used for accurate and timely detection of pathogenic microbes. Pathogenic Acinetobacter baumannii (A. baumannii) phages p53 and pB3074 bacteria were accurately identified in one tube by the collection of contaminated wastewater samples, followed by the preparation of phage solution nanoparticles and phage buffer phage solutions and then bacteria content estimation by three different experimentation techniques. This process was rapid, sensitive, specific, inexpensive and capable of distinguishing between dead and live bacteria [29]. PL-$Dy_2Ce_2O_7$ nanoplates were synthesized by a fast and simple chemical technique using orange juice as a capping agent and then a screen-printed modified electrode based upon the synthesized nanocomposites (PL-$Dy_2Ce_2O_7$/SPE) was developed for electrochemical sensing of mesalazine (MEZ) displaying electrocatalytic oxidation of MEZ. The process exhibited exemplary repeatability and reproducibility [30]. Nanomaterials also display photocatalytic activity. $Nd_2Sn_2O_7$ and $Nd_2Sn_2O_7$-Nd_2O_3 nanoparticles were prepared by a novel eco-friendly calcination technique employing grape extract for photocatalytic destruction of contaminant erythrosine under ultraviolet illumination with 96% efficiency [31]. Nanostructured ZrO_2 prepared using zirconyl nitrate and ethylenediamine exhibited photocatalytic degradation of water contaminant eriochrome black T dye under UV light [32]. Pure hexagonal Nd_2O_3 nanostructures prepared by thermal conversion of hydrothermally synthesized nanostructured $Nd(OH)_3$ using Schiff base ligand also exhibited photocatalytic degradation of water contaminant eriochrome black T dye [33]. $Dy_2Sn_2O_7$ nanomaterials prepared by an environmentally friendly route using Ficus carica extract for photocatalytic degradation of crystal violet and Acid Violet 7 contaminants under the presence of visible light [34]. Nanomaterials also find several applications in medical and healthcare sectors. Nanostructured CeO_2 fabricated by a facile, eco-friendly sonochemical technique using cerium (III) hexahydrate as a cationic precursor and mentha extract as a capping agent displayed enhanced cytotoxicity against cancerous cell lines, thus explaining its potential for developing new medicines and drugs for treating cancer cell lines [35]. Several nanomaterials, such as CZTS (Cu_2ZnSnS_4), ZnO, TiO_2, CdTe, CISe ($CuInSe_2$) etc. have been found to be very promising for optoelectronic applications too. These nanomaterials can be fabricated by a plethora of physical and chemical deposition techniques. CZTS nanomaterials display a very high absorption coefficient in the visible range [36, 37] and are an earth

abundant, low-cost absorber layer material for thin-film solar cells [38]. CZTS (Cu_2ZnSnS_4) nanocrystals with particle sizes below 3nm are found to exhibit a quantum confinement effect, thus making them suitable for tunable bandgap solar cell applications [39]. ZnO nanomaterials are eco-friendly wide bandgap semiconductors that can act as electron transport layers in organic [40] and dye sensitized solar cells [41] respectively. They can also function as a photocatalyst [42], gas-sensor [43] and photodetector [44] respectively. TiO_2 nanomaterials exhibit high photo corrosion resistance, excellent thermal stability and a wide optical bandgap [45]. TiO_2 nanoparticles can be used as photosensitizers in dye sensitized solar cells [46] and as self-cleaning anti-reflection coatings in photovoltaic cells [47]. CdTe nanoparticles exhibit a large absorption coefficient [48] and can be used in thin-film solar cells, lenses, optical windows etc. [49]. CISe ($CuInSe_2$) nanoparticles exhibit a high optical absorption coefficient, direct optical bandgap, fine thermal stability and stability towards photodegradation [50] thus making it a suitable candidate for low-cost, highly efficient solar cells [51].

It was inferred from the previous chapter of this present thesis that Cu_xN nanostructure has been developed by a low-cost spray deposition method, and 0.6(M) Cu_xN annealed sample provides the best semiconducting properties as well as structural stability among all. Thus, 0.6(M) Cu_xN film has been considered for the analysis of photoconductive and photovoltaic studies in this present context. The optical spectroscopy data of the fabricated 0.6 (M) Cu_xN optimized film has been provided as input to Oghma-Nano software (8.1.020) for carrying out numerical simulations for solar cell modelling. This process of providing practical data as input to simulation software has been believed to produce accurate computational output compatible with real-time data. First software-simulated photoconductive response of the Cu_xN semiconductor with varying thicknesses (50μm, 50nm, 50Å) has been obtained. The detailed photoconductive analysis involving variation of thin film thickness is highly tedious while performing practical experimentation. However, performing the same analysis using the current technique has been assumed to produce results compatible with practical ones. Then the photovoltaic response of the Cu_xN film with optimized thickness has been noted for testing its feasibility for solar cell applications. The photovoltaic application was probed by modelling a device by using Cu_xN film as absorber and window layers in combination with various inorganic semiconductors that have been executed in the present work. Photovoltaic performance analysis by practical experimentation requires expensive infrastructure. However, performing the same using the current technique has been assumed to produce results compatible with practical ones and be adopted in places with lagging necessary infrastructure. The present study has been performed to observe the potential of Cu_xN material in solar cell applications.

5.2 Optical Analysis

Here a detailed optical analysis of the optimized 0.6(M) Cu_xN annealed sample obtained from previous study mentioned in Chapter 4 has been performed. The UV-Vis-NIR optical spectrum of the fabricated optimized 0.6(M) Cu_xN annealed film was obtained from a UV-Vis-NIR spectrophotometer in the wavelength range of 200–1200 nm. Various optical parameters such as transmittance, reflectance and absorbance were obtained from the optical

spectra. Due to instrumental error, noise has been recorded in the 280-380 nm wavelength range.

The transmittance of optical radiation through the fabricated film was negligible as illustrated by the transmittance curve as shown in Fig. 5.1, since the deposition was performed directly on a metallic copper substrate.

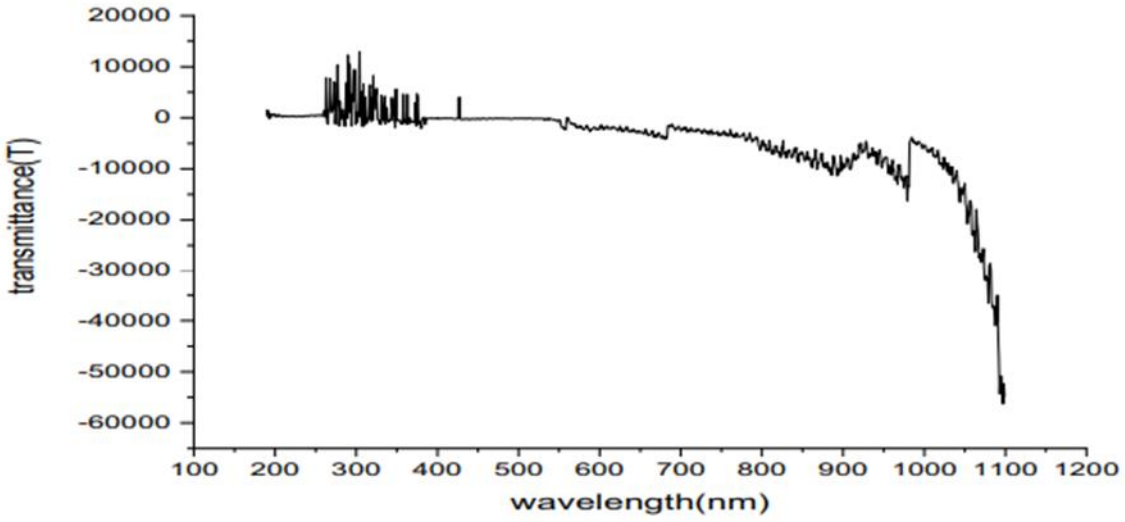

Fig. 5.1: Transmittance vs Wavelength curve of fabricated 0.6 (M) Cu_xN annealed sample (within 100nm-1200nm range)

The optical radiation would therefore either be reflected or absorbed. The value of reflectance as obtained from the reflectance curve as shown in Fig. 5.2, was found to be high in the UV range (200nm – 300nm) and low in both the visible (400nm – 700nm) and NIR (700-1200) ranges respectively. On the other hand, absorption was found to be extremely high in the visible and NIR ranges respectively as shown in Fig. 5.3.

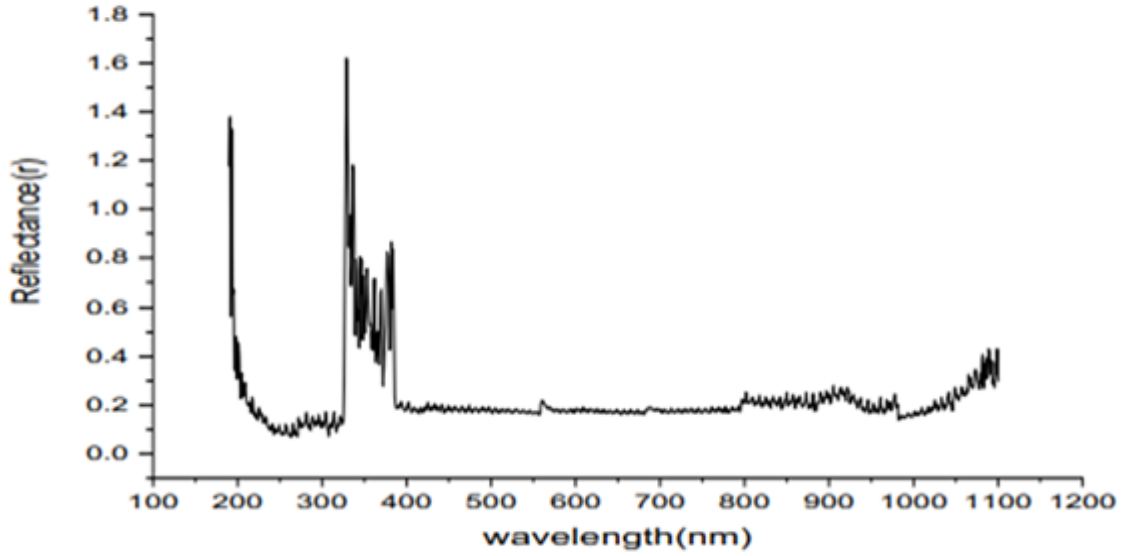

Fig. 5.2: Reflectance vs Wavelength curve of fabricated 0.6 (M) Cu_xN annealed sample (within 100nm-1200nm range)

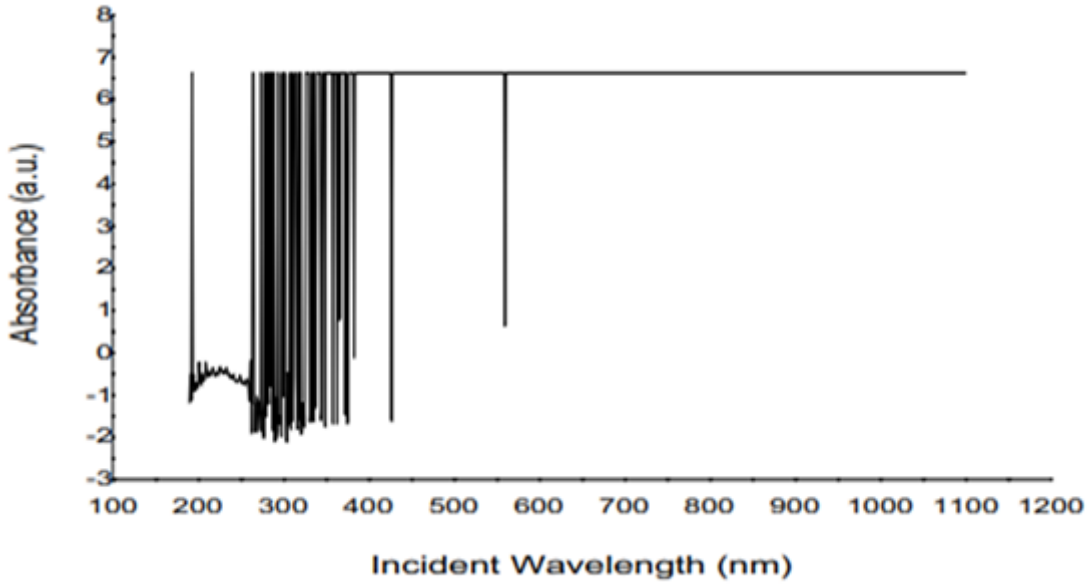

Fig. 5.3: Absorbance vs Wavelength Curve of fabricated 0.6 (M) Cu_xN annealed sample (within 100nm-1200nm range)

From the reflectance and absorbance data, the real refractive index (n), extinction coefficient (k) and absorption coefficient (a) were calculated using the following formulae [52, 53, 54].

Complex Refractive Index $N = n(\lambda) + j\,k(\lambda)$(4)

where $n(\lambda)$ is real refractive index, $k(\lambda)$ is imaginary refractive index and λ is wavelength of radiation

Real Refractive Index $n(\lambda) = \frac{1+\sqrt{r}}{1-\sqrt{r}}$……..(1)

Extinction Coefficient $k(\lambda) = \frac{a\lambda}{4\pi}$……..(2)

Absorption Coefficient $a(\lambda) = \frac{2.303A}{t}$ ……(3)

where *r*, *A* and t are the reflectance, absorbance and thickness of the thin film respectively.

Therefore, the values of the real refractive index, extinction coefficient and absorption coefficient have been obtained from here, and the plotting of these parameters with the variation of wavelength has been shown in Fig. 5.4, Fig. 5.5, and Fig. 5.6, respectively.

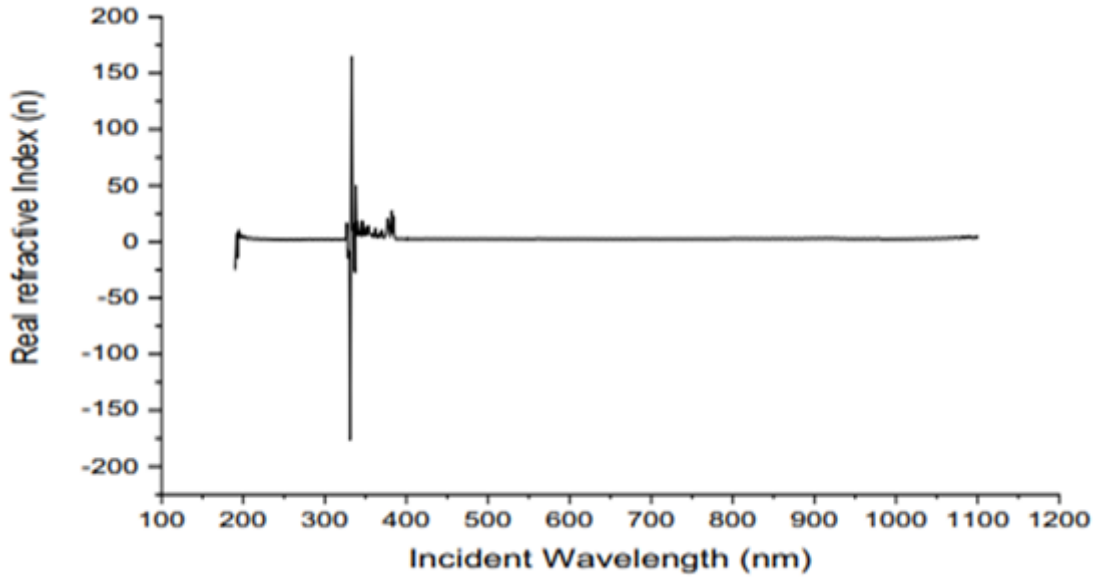

Fig. 5.4: Variation of Real refractive index with incident wavelength of fabricated 0.6 (M) Cu_xN annealed sample (within 100nm-1200nm range)

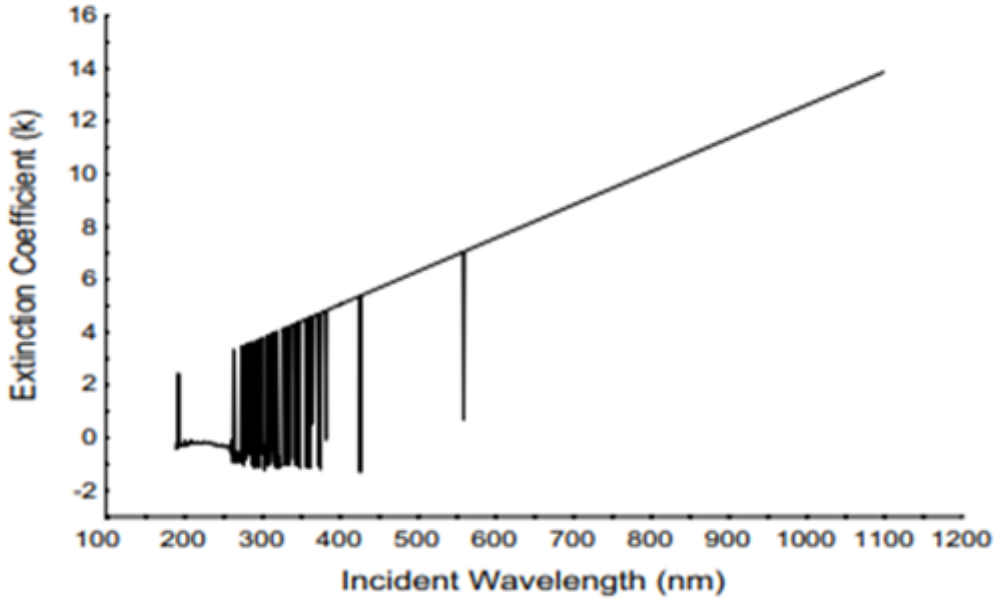

Fig. 5.5: Variation of Extinction coefficient with incident wavelength of fabricated 0.6 (M) Cu_xN annealed sample (within 100nm-1200nm range)

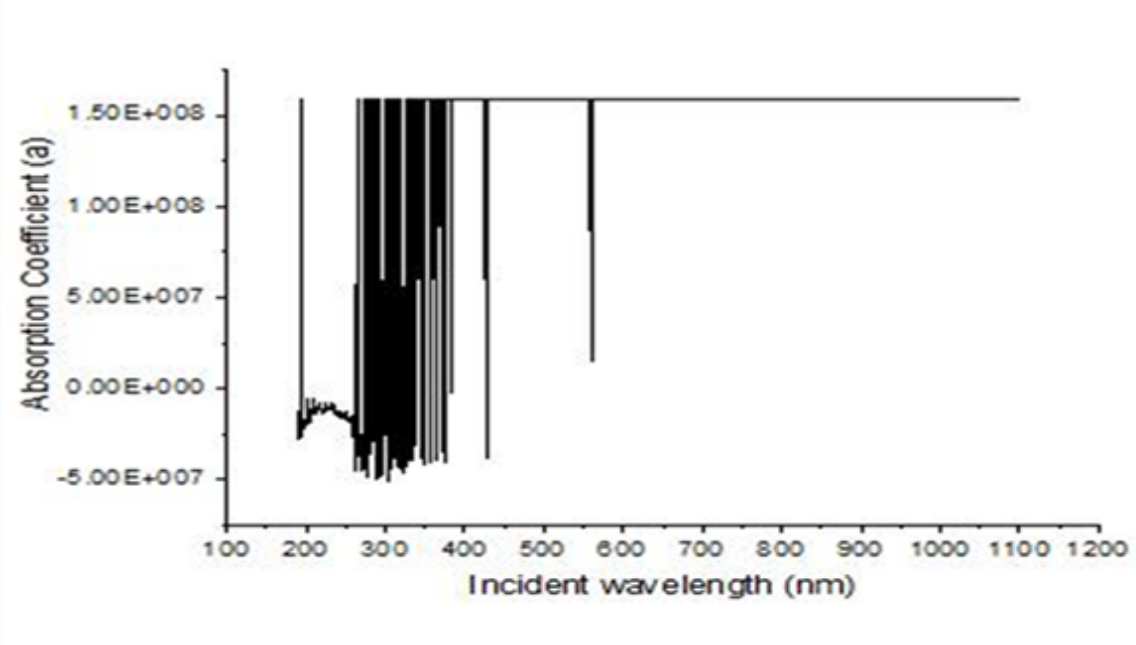

Fig. 5.6: Variation of Absorption coefficient with incident wavelength of fabricated 0.6 (M) Cu_xN annealed sample (within 100nm-1200nm range)

The variation of real refractive index (n), extinction coefficient (k) and absorption coefficient (α) with respect to incident radiation wavelength (λ) is plotted in Figs. 5.4, 5.5 and 5.6 respectively. From the curves, very high values of absorption coefficient and optimum values of real refractive index and extinction coefficient were observed.

5.3 Optoelectronic Performance Analysis

The optoelectronic (photoconductive and photovoltaic) performance of the fabricated copper nitride sample was analyzed by performing numerical simulations using Oghma-Nano software (8.1.020) and providing UV-Vis-NIR spectroscopy data (band gap, refractive index, extinction coefficient and absorption coefficient data) of the optimized 0.6 (M) Cu_xN annealed sample as input to the simulation software. The variation in photoconductive response by tuning film thickness from 50μm to 50nm and 50Å at different light intensities has been observed. Then the optimized film thickness of Cu_xN material has been considered to accomplish photovoltaic performances. The feasibility of solar cells has been examined by using Cu_xN both as absorber and window layers respectively. First two solar cells with Cu_xN as an absorber layer and CdS and ZnO as window layers have been simulated and photovoltaic performance has been noted. Then two solar cells with Cu_xN as a window layer and PbSe and InAs as absorber layers have been simulated and photovoltaic performance has been cultivated. Thereafter, the simulated results have been compared with the experimental results of other conventional CdS-based solar cells like CdS-Cu_2S, CdS-PbS, CdS-CdTe etc. It is assumed that obtained results should be comparable with real time data. Optoelectronic performance analysis for solar cell device applications using present techniques is simple and can be adopted in places lagging high-grade fabrication and characterization infrastructure.

5.3.1 Device Simulation Technique

Oghma-Nano stands for Organic and Hybrid Material Nano simulation software. Oghma-Nano is a general-purpose model used for the simulation of photovoltaic devices such as inorganic, organic and perovskite solar cells, organic field effect transistors (OFET), organic light-emitting diodes (OLED), photonic crystals, optical filters, etc. [55]. In the present work, Oghma-Nano software (8.1.020) was used for simulating the photoconductive characteristics of the fabricated copper nitride semiconductor and the photovoltaic characteristics of corresponding optical devices have been studied using the band gap, refractive index, extinction coefficient and absorption coefficient data of the fabricated film. The optoelectronic properties could be simulated using Oghma-Nano software (8.1.020). Poisson's equation, electron-hole drift equation and electron-hole continuity equation were employed by the software for carrying out the simulations by solving the following equations (4)-(8):

$$\frac{d}{dx} \in_0 \in_r \frac{d\emptyset}{dx} = q(n - p) \quad \ldots\ldots\ldots\ldots\ldots\ldots(4)$$

$$\frac{\partial J_n}{\partial x} = q\left(R_n - G + \frac{\partial n}{\partial t}\right) \quad \ldots\ldots\ldots\ldots\ldots\ldots(5)$$

$$\frac{\partial J_p}{\partial x} = q\left(R_p - G + \frac{\partial p}{\partial t}\right) \quad \ldots\ldots\ldots\ldots\ldots\ldots(6)$$

$$J_n = q\mu_n \frac{\partial E_c}{\partial x} + qD_n \frac{\partial n}{\partial x} \quad \ldots\ldots\ldots\ldots\ldots\ldots(7)$$

$$J_p = q\mu_p \frac{\partial E_v}{\partial x} + qD_p \frac{\partial p}{\partial x} \quad \text{.....(8)}$$

where$\in_0$ is permittivity of free space, $\in_r$ is relative permittivity, n is total electron density, p is total hole density, q is elementary charge on an electron, G is generation rate per unit volume, $J_{n,p}$ is electron and hole current flux density, $D_{n,p}$ is electron and hole diffusion coefficients, $R_{n,p}$ is net recombination rate for electrons and holes, μ_n is electron mobility and μ_h is hole mobility.

Table 5.1: Materials parameters used in the simulation [56, 57, 58, 59, 60]

Material Properties	**Cu_xN**	**CdS**	**ZnO**	**PbSe**	**InAs**
Electron Mobility ($m^2.V^{-1}.s^{-1}$)	$1.63x10^{-4}$	$2.65x10^{-4}$	$3.5x10^{-4}$	$1.7x10^{-4}$	$1.4x10^{-4}$
Hole Mobility ($m^2.V^{-1}.s^{-1}$)	$0.1x10^{-4}$	$1.5x10^{-4}$	$1.66x10^{-4}$	$0.65x10^{-4}$	$0.5x10^{-4}$
Effective Concentration of Free Electrons (at 300K) (m^{-3})	$1.62x10^{23}$	$7.8x10^{23}$	$3.7x10^{23}$	$3.6x10^{23}$	$2.0x10^{23}$
Effective Concentration of Holes (at 300K) (m^{-3})	$5.56x10^{23}$	$3.9x10^{23}$	$1.8x10^{23}$	$2x10^{23}$	$0.8x10^{23}$
Electron Affinity (eV)	4	4.2	4.5	4.5	4.93
Optical Bandgap (eV)	1.75	2.42	3.3	0.27	0.36
Relative Permittivity	15	5.7	10.4	23	14.6

The above parameters, namely electron mobility, hole mobility, effective free electron concentration, effective hole concentration, electron affinity, optical bandgap and relative permittivity, as mentioned in Table 5.1 are accumulated from previous research works and used for carrying out numerical simulations for obtaining photoconductive and photovoltaic analysis using Oghma-Nano software (8.1.020).

5.3.2 Study of Photoconductive Characteristics

The photoconductive characteristics of the fabricated optimized 0.6 (M) Cu_xN annealed film were obtained by performing computer simulations using Oghma-Nano software. Silver (Ag) metal (10nm thick) was used as contact to the copper nitride semiconductor while performing the simulation. The thickness of the semiconductor layer was varied as 50µm, 50nm and 50Å respectively, to observe the variation of photoconductive characteristics of Cu_xN based photoconductors. The variation of film thickness in the micro, nano and angstrom ranges is very tedious while performing the chemical deposition method. Therefore, in this present study, variation of film thickness has been performed by providing experimental data as input to the simulation software to observe the photoconductive performances of the fabricated film. The schematic representation of copper nitride semiconductor under 1Sun intensity is shown in Fig. 5.7.

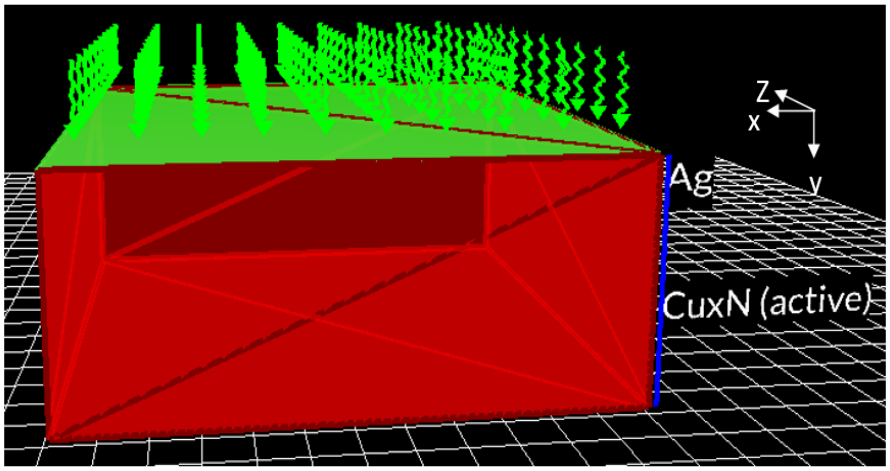

Fig.5.7 Image of Cu_xN based photoconductor under 1 Sun light intensity

The photoconductive characteristics of Cu_xN semiconductor with varying film thickness are described in the present work. The total charge density vs applied voltage, current vs applied voltage, recombination prefactor vs excess carrier density, and charge carrier generation rate vs Y-position characteristics have been studied for the films with thicknesses of 50µm, 50nm and 50Å under dark conditions and 0.1 $W.cm^{-2}$, 1 $W.cm^{-2}$ and 10 $W.cm^{-2}$ light intensities, respectively.

Total Charge Density (Y-axis) vs Applied Voltage (X-axis) Curves at different light intensities for 50µm, 50nm and 50Å films have shown in Fig.5.8 (A) [(I.a),(II.a),(III.a),(IV.a)], Fig.5.8 (B) [(I.b),(II.b),(III.b),(IV.b)] and Fig.5.8 (C) [(I.c), (II.c),(III.c),(IV.c)] respectively.

Total Charge Density (Y-axis) vs Applied Voltage (X-axis) Curves at different light intensities with variation of film thickness

For 50µm film thickness:

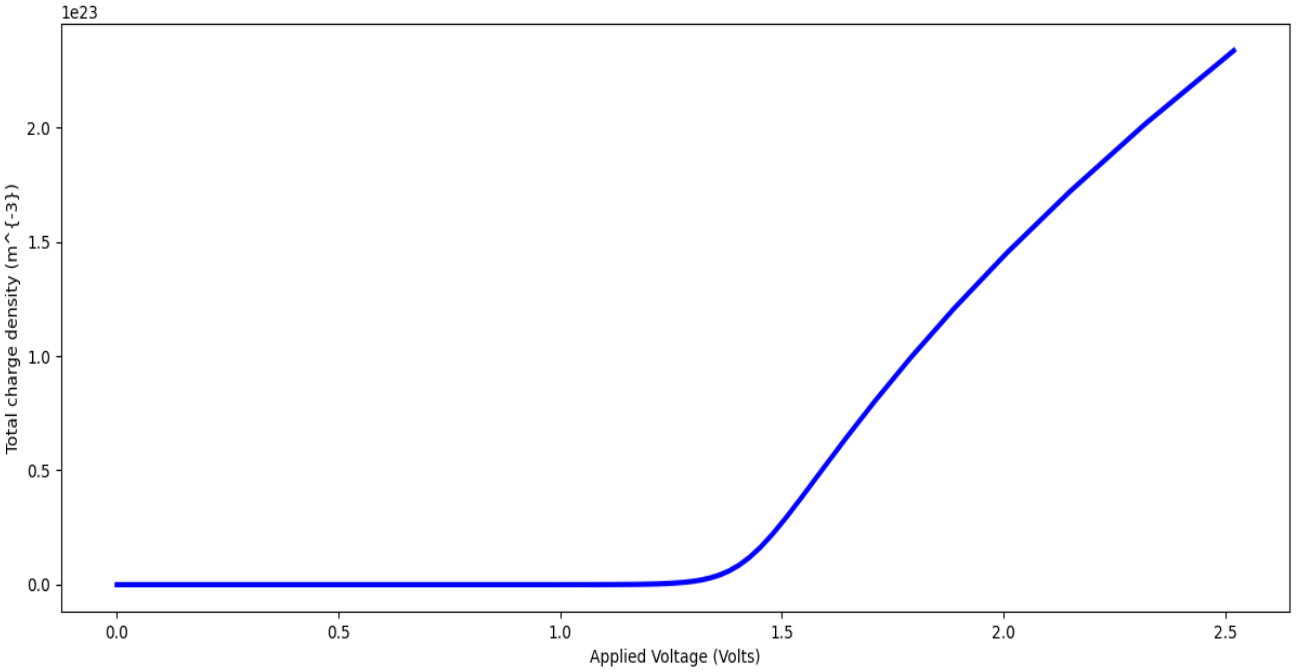

(I.a): At light intensity 0 W.cm^{-2} (Dark Condition)

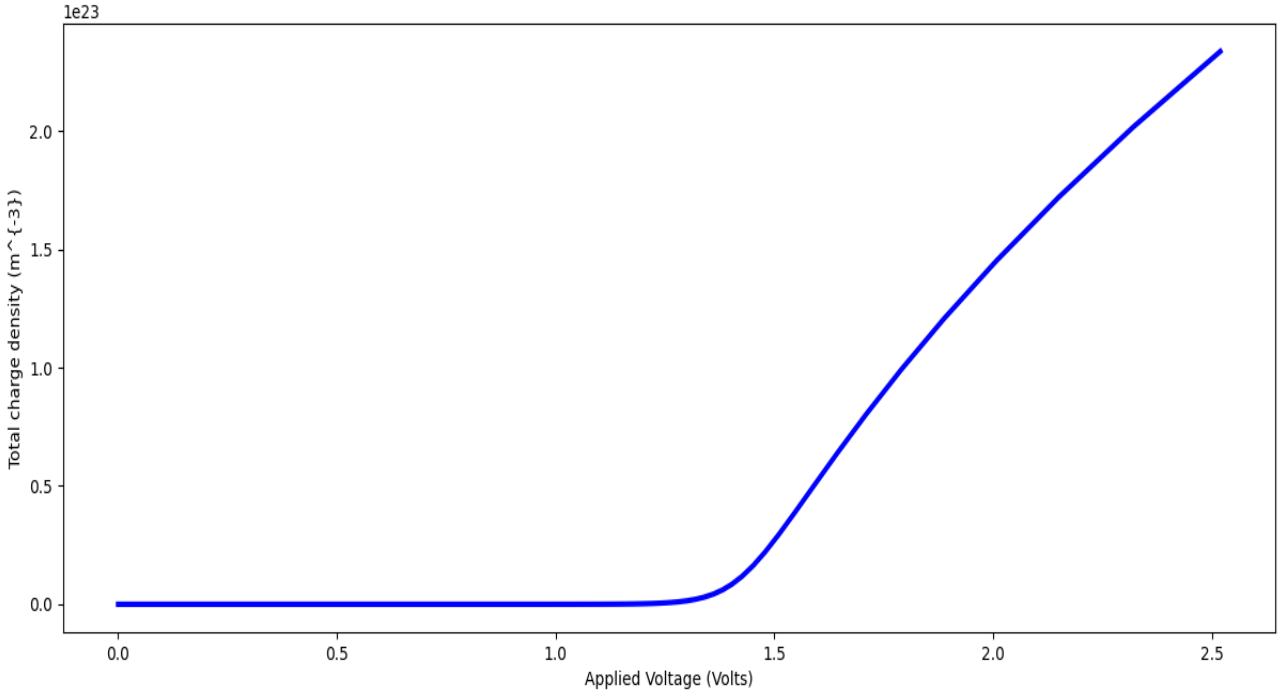

(II.a): At light intensity 0.1 W.cm^{-2}

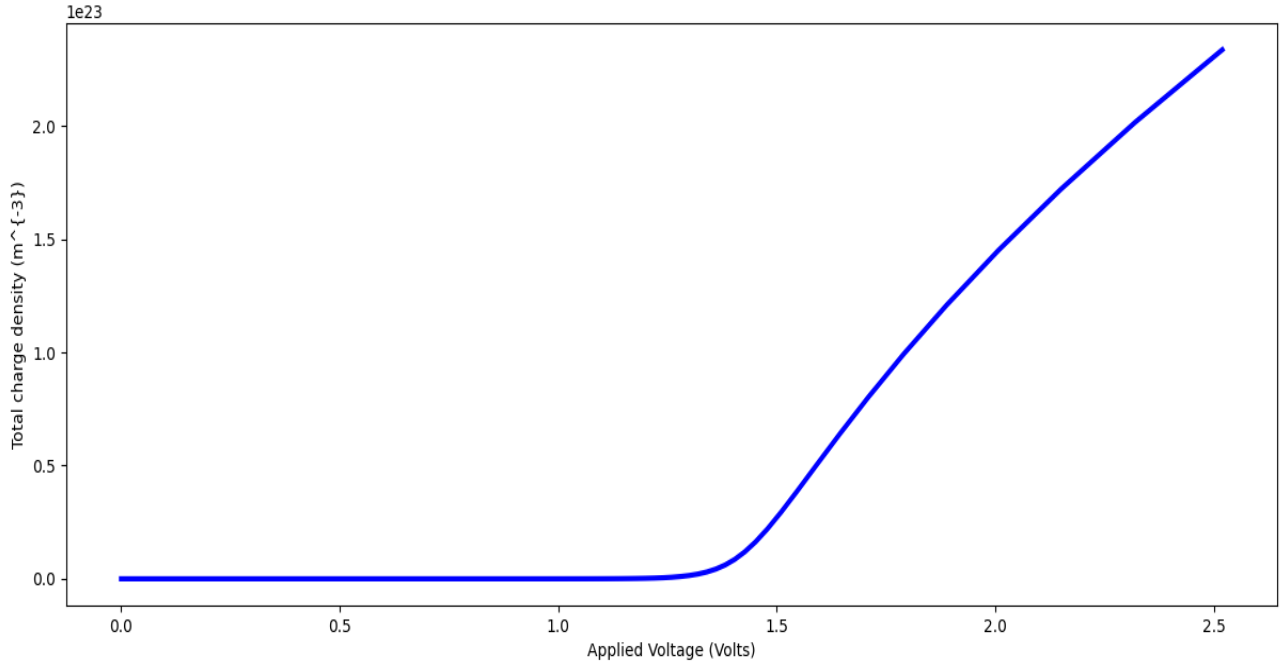

(III.a): At light intensity 1 W.cm^{-2}

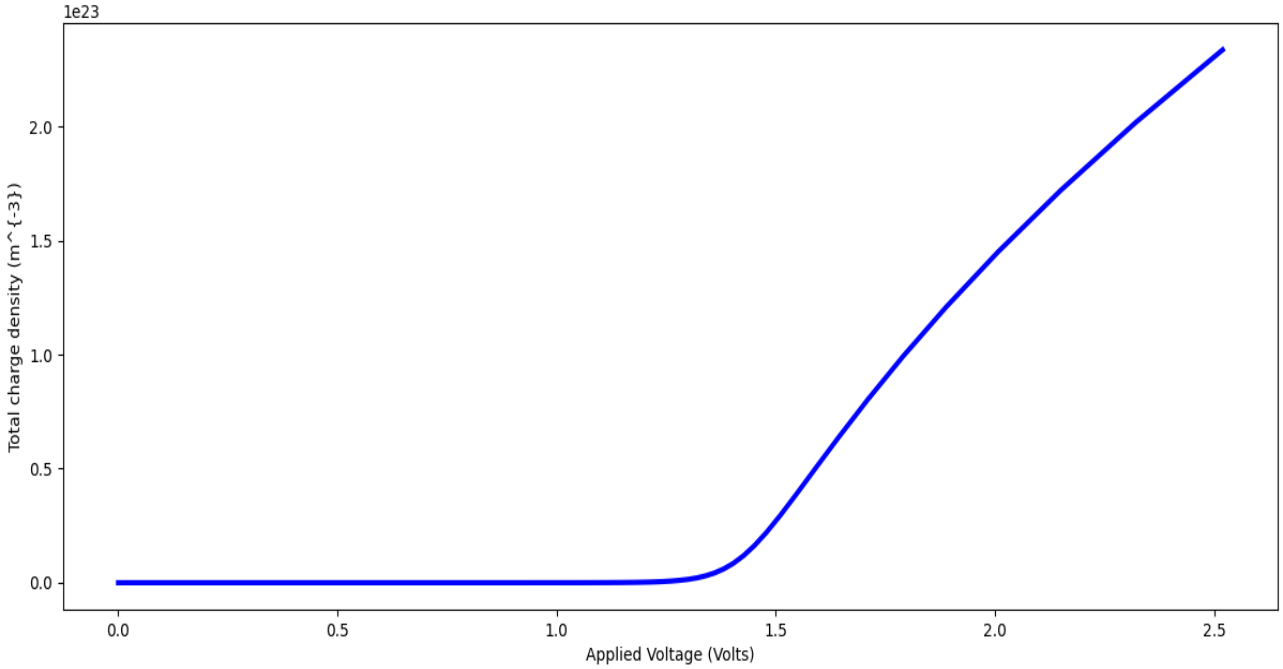

(IV.a): At light intensity 10 W.cm^{-2}

Fig.5.8 (A) [(I.a),(II.a),(III.a),(IV.a)]: Curves of Total charge density (Y-axis) vs Applied voltage (X-axis) for film thickness 50µm of Cu_xN sample for different input light intensities i.e.0W.cm^{-2},0.1W.cm^{-2},1W.cm^{-2}, and 10W.cm^{-2} as represent (I.a),(II.a),(III.a),and (IV.a)respectively.

For 50 nm film thickness:

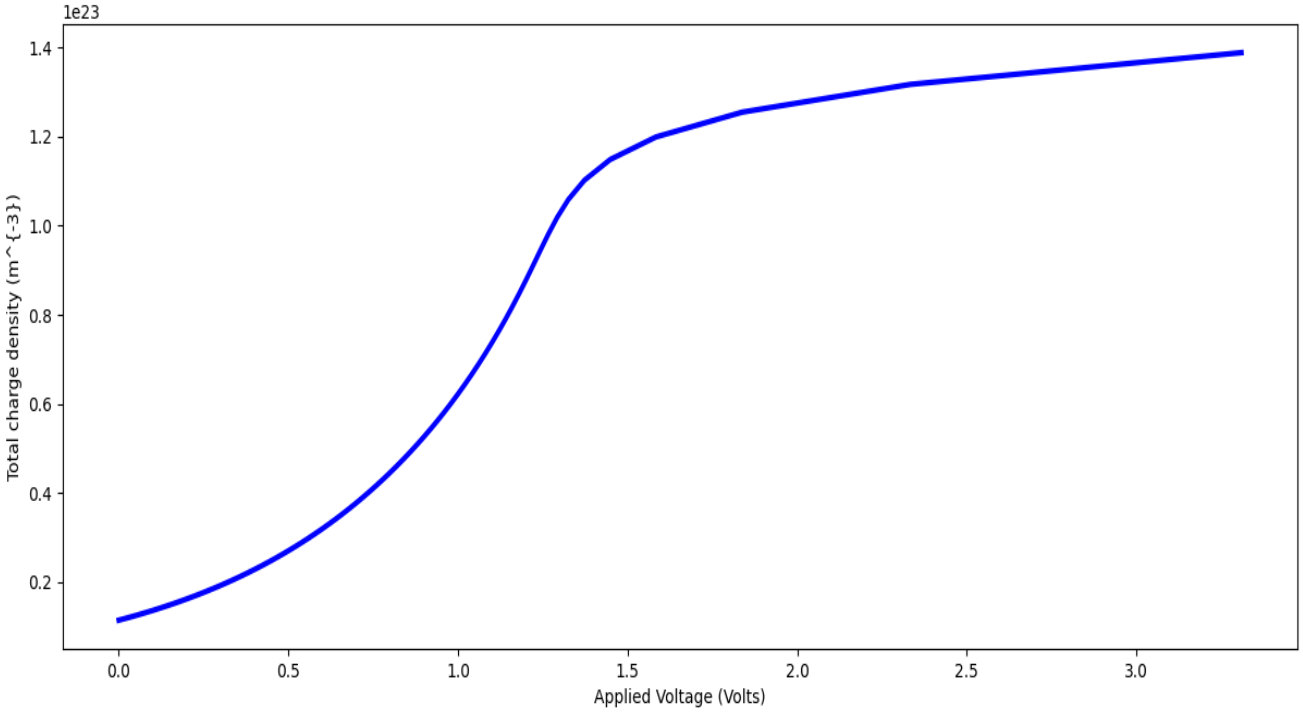

(I.b): At light intensity 0 W.cm^{-2} (Dark Condition)

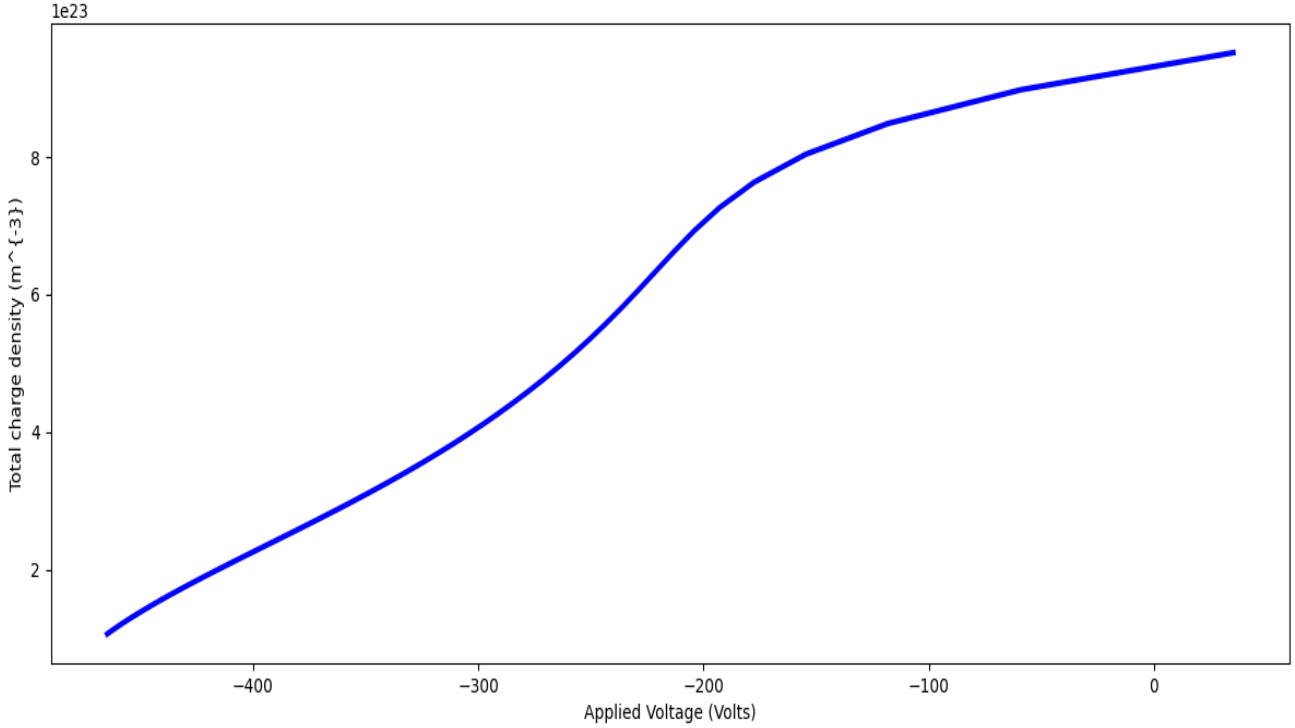

(II.b): At light intensity 0.1 W.cm^{-2}

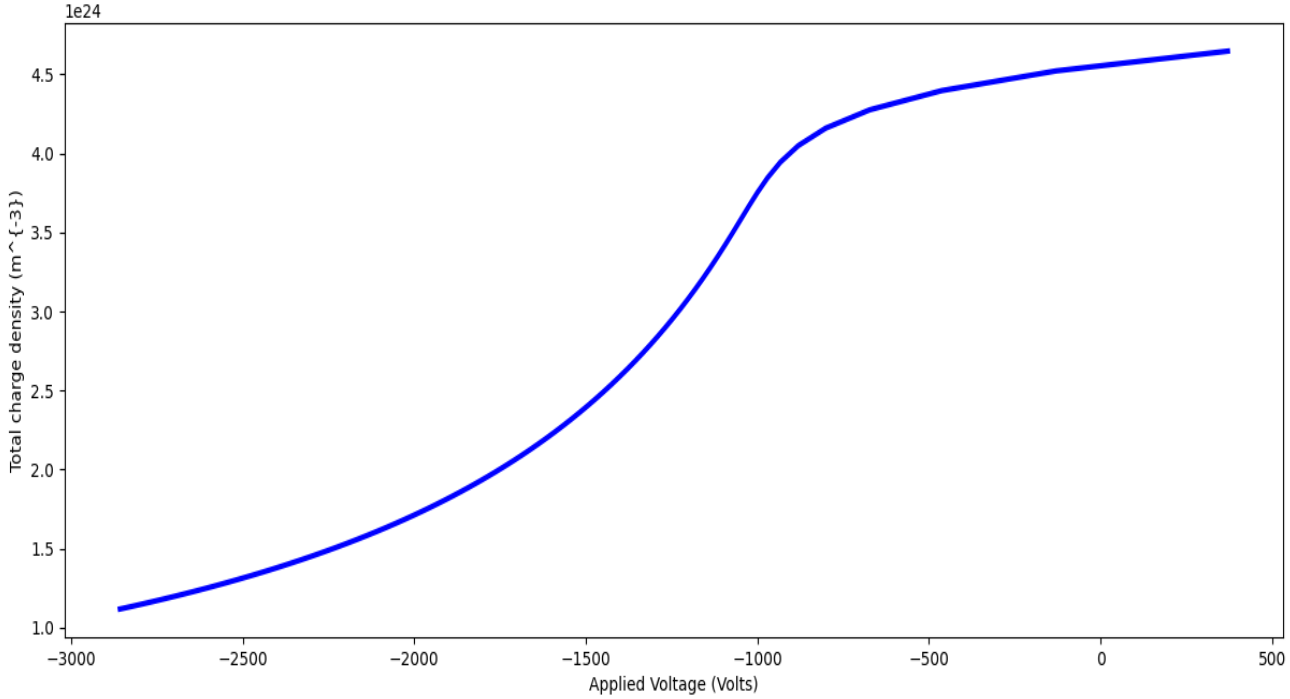

(III.b): At light intensity 1 W.cm^{-2}

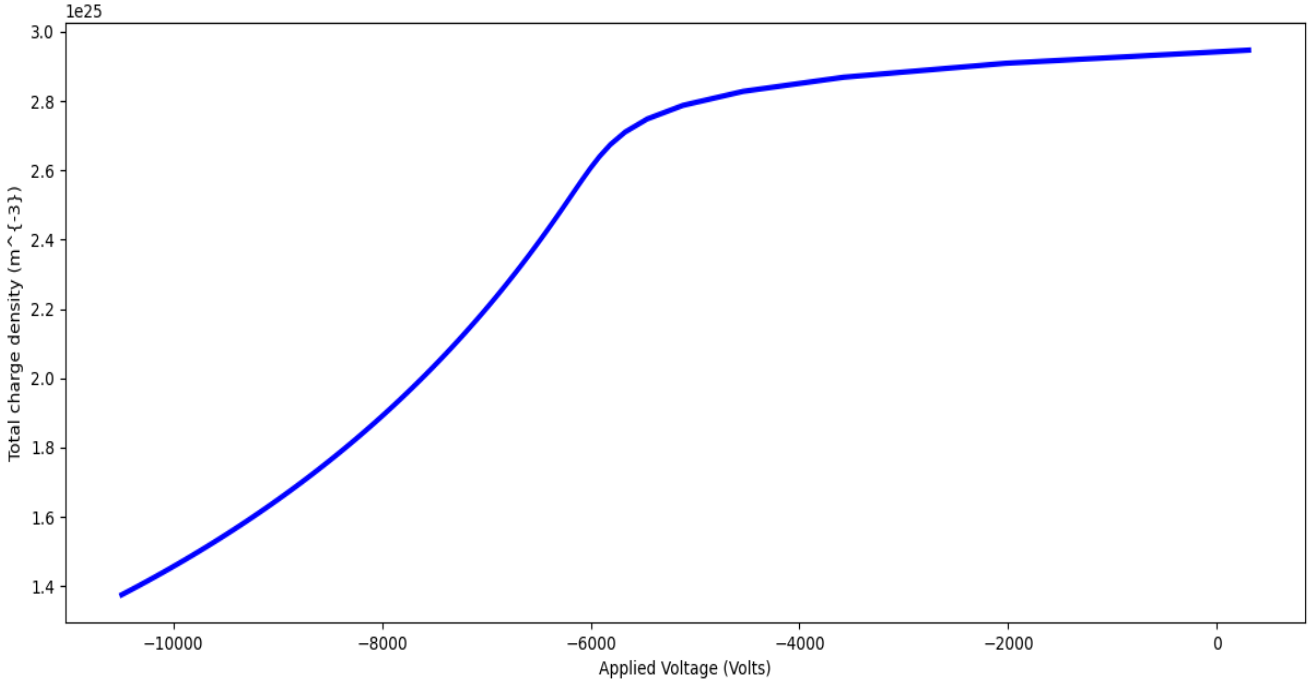

(IV.b): At light intensity 10 W.cm^{-2}

Fig.5.8 (B) [(I.b),(II.b),(III.b),(IV.b)]: Curves of Total charge density (Y-axis) vs Applied voltage (X-axis) for film thickness 50 nm of Cu_xN sample for different input light intensities i.e. 0W.cm^{-2}, 0.1W.cm^{-2}, 1W.cm^{-2} and 10W.cm^{-2} as represent (I.b),(II.b),(III.b), and (IV.b) respectively.

For 50Å film thickness:

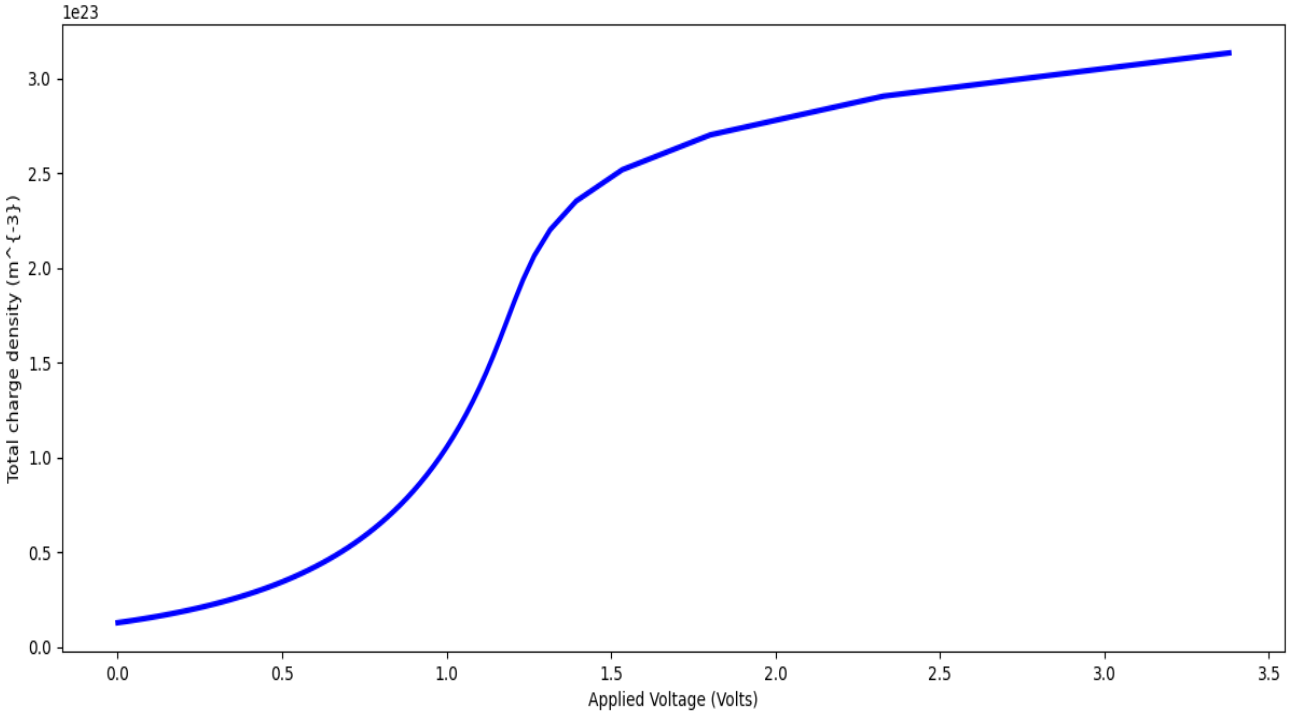

(I.c): At light intensity 0 W.cm^{-2} (Dark Condition)

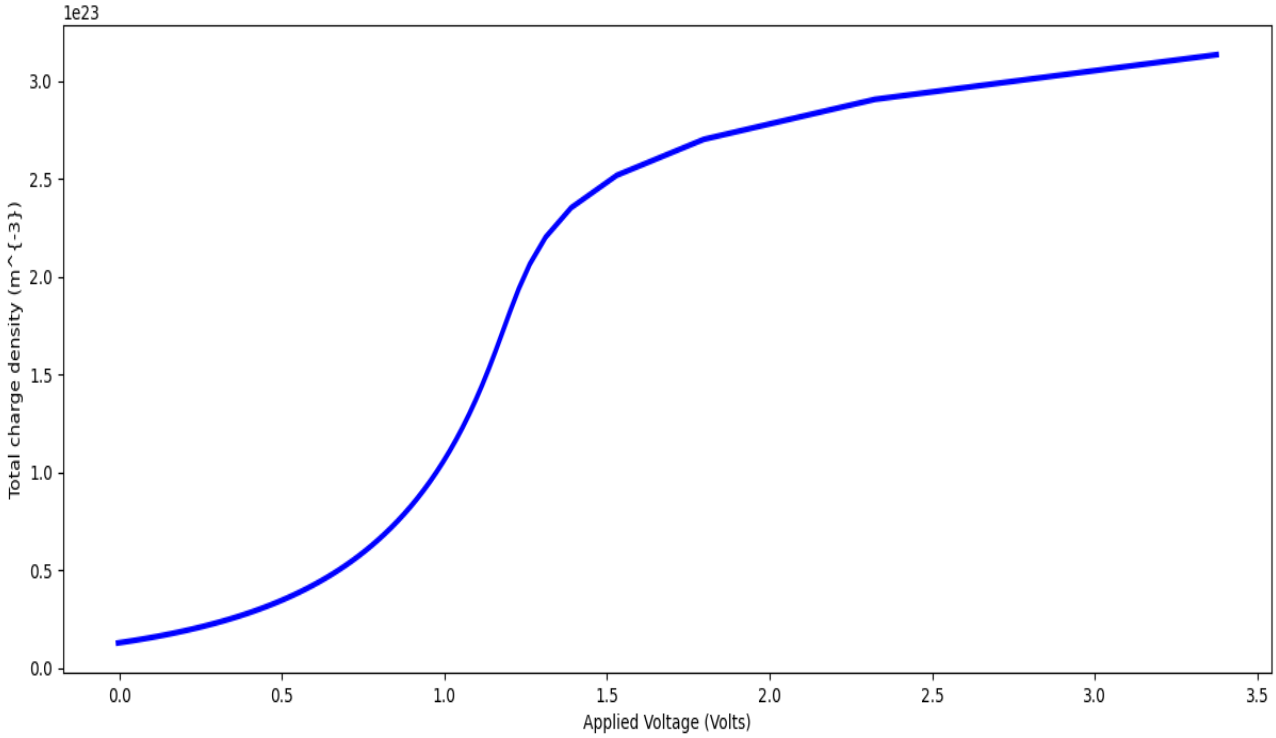

(II.c): At light intensity 0.1 W.cm^{-2}

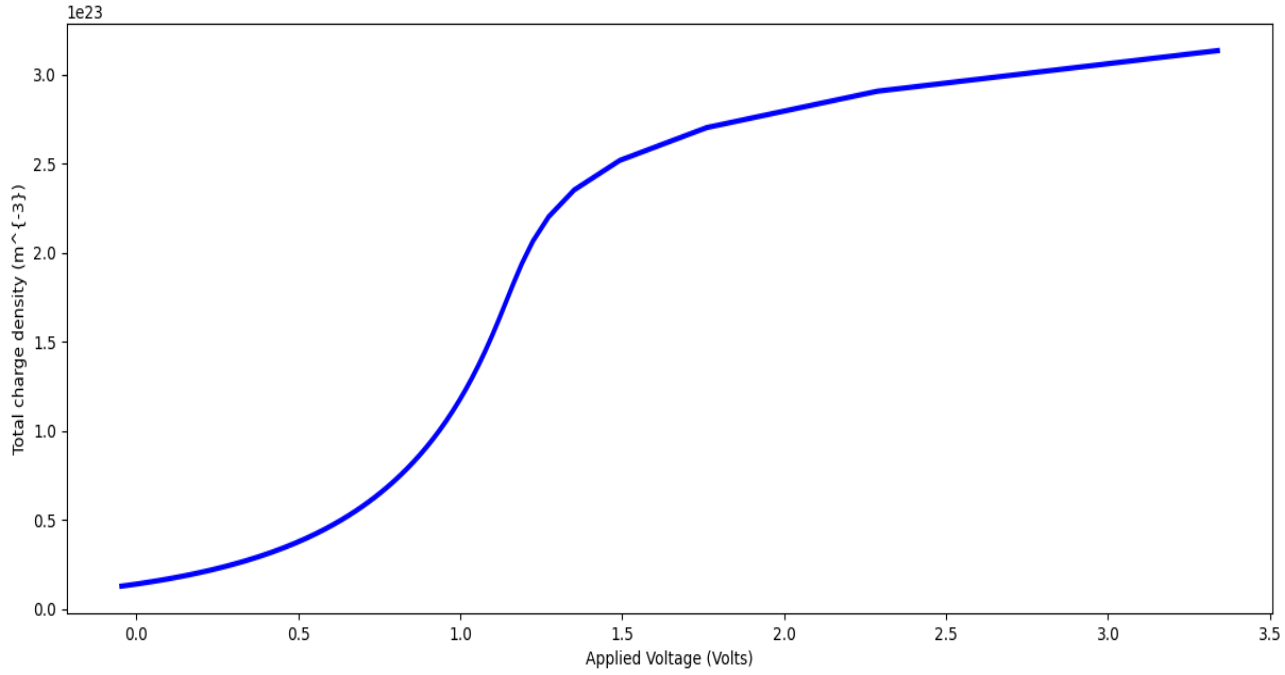

(III.c): At light intensity 1 W.cm^{-2}

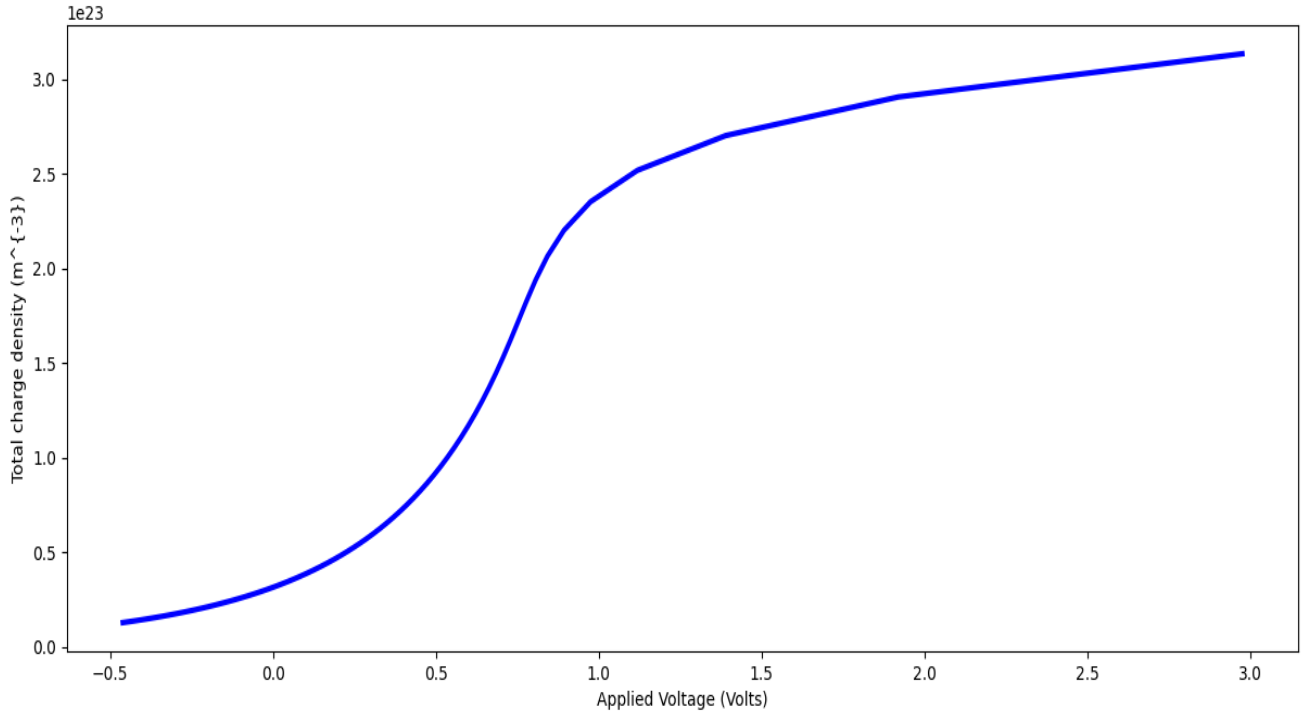

(IV.c): At light intensity 10 W.cm^{-2}

Fig. 5.8 (C) [(I.c), (II.c),(III.c),(IV.c)]: Curves of Total charge density (Y-axis) vs Applied voltage (X-axis) for film thickness 50Å of Cu_xN sample for different input light intensities i.e. 0W.cm^{-2}, 0.1W.cm^{-2}, 1W.cm^{-2} and 10W.cm^{-2} as represent (I.c), (II.c),(III.c),and (IV.c) respectively.

The total charge density refers to the volume charge density, i.e. charge induced in the copper nitride semiconductor per unit volume with the application of an external voltage. In metal-semiconductor junctions, charge carriers have transferred either metal to semiconductor or vice versa. The charge has transferred from metal to semiconductor in the case of n-type semiconductors and vice versa in the case of p-type semiconductors. A potential barrier is created at the metal-semiconductor junction known as a Schottky barrier, and here exists a bound charge polarization effect which opposes current flow at the junction. The built-in potential plays a major role for the conduction of current in metal-semiconductor junctions. The barrier height is dependent on the work function difference between metal and semiconductor. This barrier affects the current flow as well as the overall characteristics of the junction. The total charge density vs applied voltage characteristics have been studied regarding Cu_xN film thicknesses 50µm, 50nm and 50Å in present context. When the thickness of the film was 50µm, the charge density-applied voltage curve was found to be rectifying in nature, i.e. the charge began to be induced after a certain voltage (or cut-in voltage), which was at around 1.4V for all light intensities. The charge density vs applied voltage curves for the 50µm thin film similar in nature due to similar bound charge polarization with a maximum induced charge density of $2x10^{23}C.m^{-3}$ at dark conditions as seen from Fig.5.8(A) (I.a.), at $0.1W.cm^{-2}$ light intensity as seen from Fig.5.8(A) (II.a), at $1W.cm^{-2}$ light intensity as seen from Fig.5.8(A) (III.a) and at $10W.cm^{-2}$ light intensity as seen from Fig. 5.8(A) (IV.a) respectively. This bound charge polarization occurred at the metal-semiconductor junction that opposed the charge flow, and it has been the same with varying light intensities in micrometer range thickness. In the case of microstructure at a metal-semiconductor junction, high density interface states are present, and these states can act as a scattering and trapping centres for the charge carriers [61]. Thus, the greater number of charge carriers is lost, and the total number of charge density, which is responsible for conduction, does not overcome the bound charge polarization at the junction. Therefore, the value of charge density in the case of 50µm thickness is the same instead of different light intensities. However, once the applied voltage exceeded the cut-in voltage, the bound charge polarization could be overcome, and the charge density started varying linearly with the applied voltage. The cut-in voltage is a threshold voltage value that the applied voltage must exceed for the conduction process to begin, i.e. material resistivity to fall significantly, whereas bound charge polarization is the space charge accumulation per unit volume at the metal-semiconductor junction. The charge density-applied voltage curve for the 50µm was found to remain unaltered with varying light intensity intensity as clear from Fig. 5.8(A) (I.a), Fig. 5.8(A) (II.a), Fig. 5.8(A) (III.a), and Fig. 5.8(A) (IV.a) respectively. The dark characteristics of the 50nm film displayed initial near linear variation and saturation after applied voltage of 1.4V as evident from Fig. 5.8(B) (I.b) whereas the charge density-applied voltage curve became almost linear under various luminous irradiation. The maximum induced charge density increasing from $10x10^{23}C.m^{-3}$ to $4.5x10^{24}C.m^{-3}$ and finally to $3x10^{25}C.m^{-3}$ for light intensities of $0.1W.cm^{-2}$, $1W.cm^{-2}$ and $10W.cm^{-2}$ as obtained from Fig. 5.8(B)(II.b), Fig.5.8(B)(III.b), and Fig. 5.8(B)(IV.b), respectively and finally it displayed saturation at positive applied voltage. This is happened in 50 nm film due to negligible bound charge polarization at this thickness.

The presence of cut-in voltage in the 50μm and its absence in the 50nm thin film could be observed which was indicative of the fact that the bound charge polarization at the metal-semiconductor junction which opposed charge flow fell when the film thickness decreased from 50μm to 50nm from Fig.5.8(A)(I.a) and Fig. 5.8(B) (I.b) respectively. This was also possibly because the dielectric constant for 50nm film is generally higher for 50μm film resulting in greater charge polarization. In nano level thickness, the surface-to-volume ratio is high, and thus surface is more controlled and passivated. Therefore, it leads to improved impact on surface charge polarization at the metal-semiconductor interface [61]. A further reduction in film thickness to 50Å resulted in the same characteristics with a maximum charge density of $3x10^{23}C.m^{-3}$ at dark conditions as seen from Fig.5.8(C) (I.c), at $0.1W.cm^{-2}$ light intensity as seen from Fig. 5.8(C) (II.c), at $1W.cm^{-2}$ light intensity as seen from Fig.5.8(C) (III.c) and at $10W.cm^{-2}$ light intensity as seen from Fig.5.8(C) (IV.c) respectively. The charge conduction was almost linear at first and then reached saturation after 1.5V at dark conditions as seen from Fig.5.8(C) (I.c), at $0.1W.cm^{-2}$ light intensity as seen from Fig.5.8(C) (II.c) and $1W.m^{-2}$ light intensity as seen from Fig.5.8(C)(III.c) respectively whereas saturation was reached much earlier after 1V at $10W.cm^{-2}$ light intensity as seen from Fig.5.8(C)(IV.c) respectively. When film thickness decreased from 50nm to 50Å, the energy band spectrum became discrete instead of being continuous. The optical bandgap remained at the original level during the continuous energy state, but when the band spectrum became discrete, the bandgap became size-dependent. As a result, when film thickness was reduced to 50Å then proximity between the free electron and its corresponding hole became greater [62] and so more energy was required to separate them, i.e. the more energy required for charge induction increased. The increased defects and trap states are present at this thickness due to the discrete energy band spectrum, and a greater number of carriers are lost here. Therefore, the value of charge density in the case of 50 Å thickness is the same instead of different light intensities. So, in a comparison among three different range thicknesses, maximum charge density is obtained in 50 nm and minimum in 50μm thickness-based film. After studying total charge density vs applied voltage characteristics, the corresponding current vs applied voltage characteristics have been cultivated here. The current vs applied voltage characteristics at different light intensities (dark condition, $0.1W.cm^{-2}$, $1W.cm^{-2}$, and $10W.cm^{-2}$) with variation of three different thicknesses, i.e. 50μm, 50 nm and 50 Å have been studied in this present context.

Current (Y-axis) vs Applied Voltage (X-axis) Curves at different light intensities for 50μm, 50nm and 50Å films have shown in Fig.5.9(A)[(I.a),(II.a),(III.a),(IV.a)], Fig.5.9(B) [(I.b),(II.b), (III.b),(IV.b)], and Fig.5.9(C) [(I.c), (II.c), (III.c), (IV.c)] respectively.

Current (Y-axis) vs Applied Voltage (X-axis) Curves at different light intensities with variation of film thickness

For 50µm film thickness:

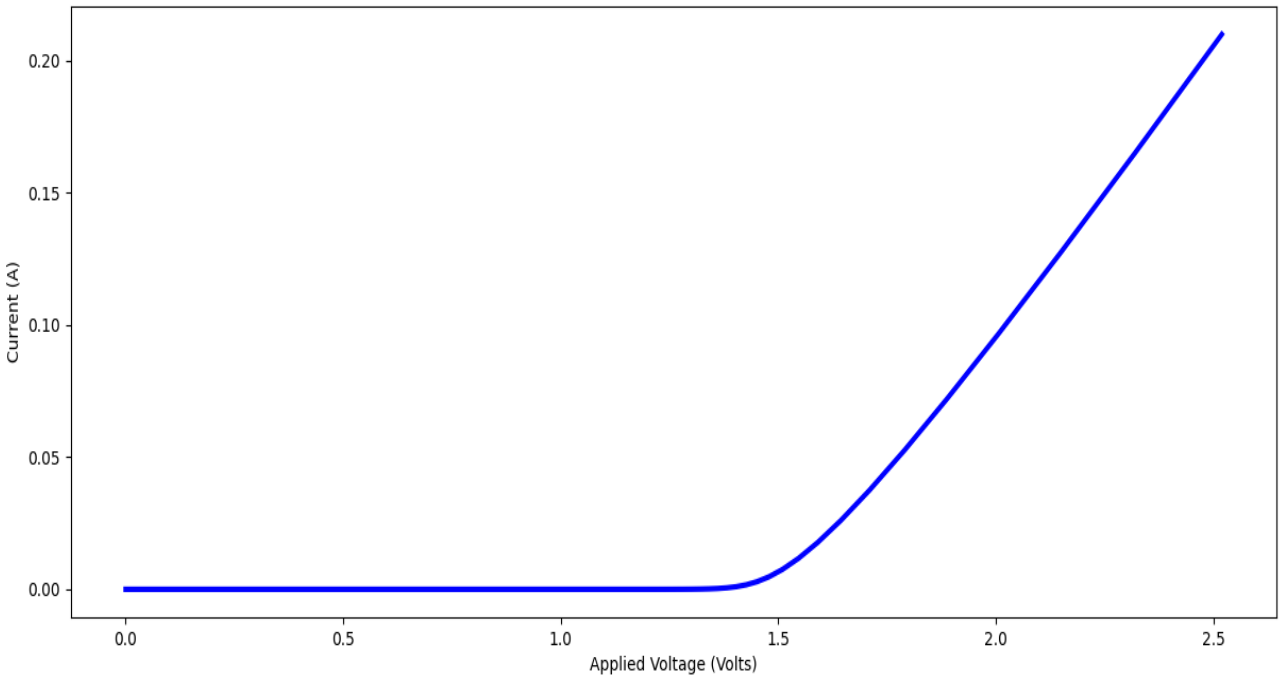

(I.a): At light intensity 0 W.cm^{-2} (Dark Condition)

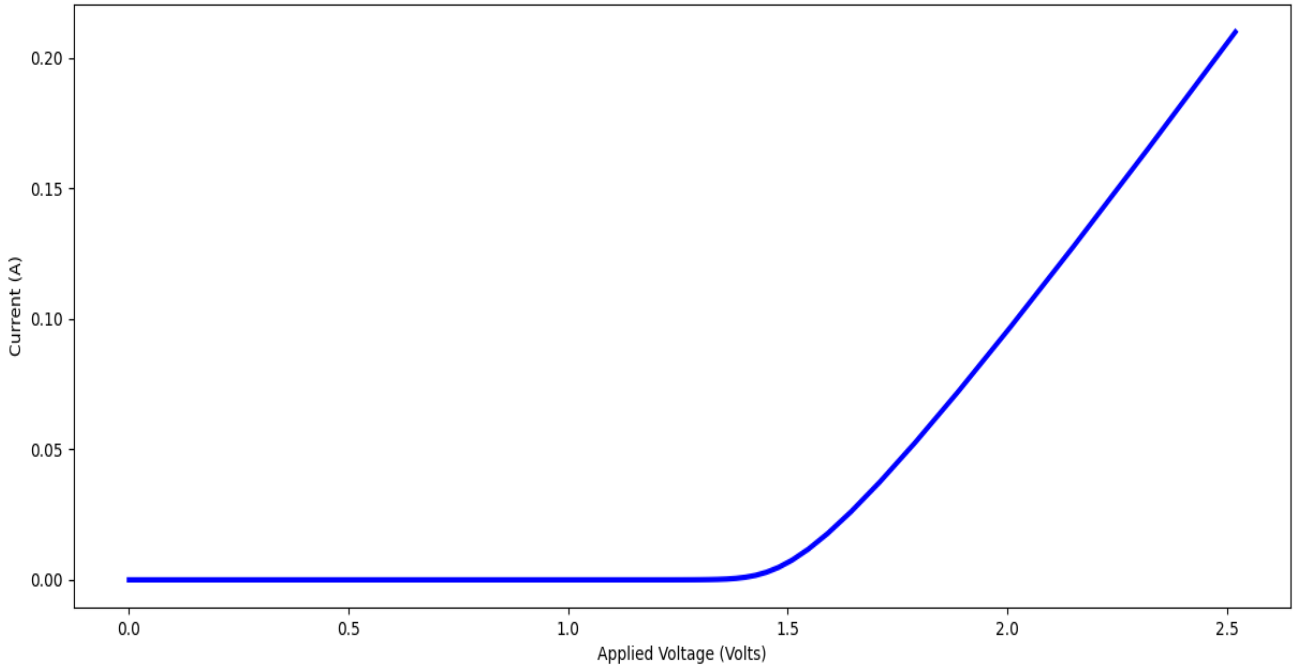

(II.a): At light intensity 0.1 W.cm^{-2}

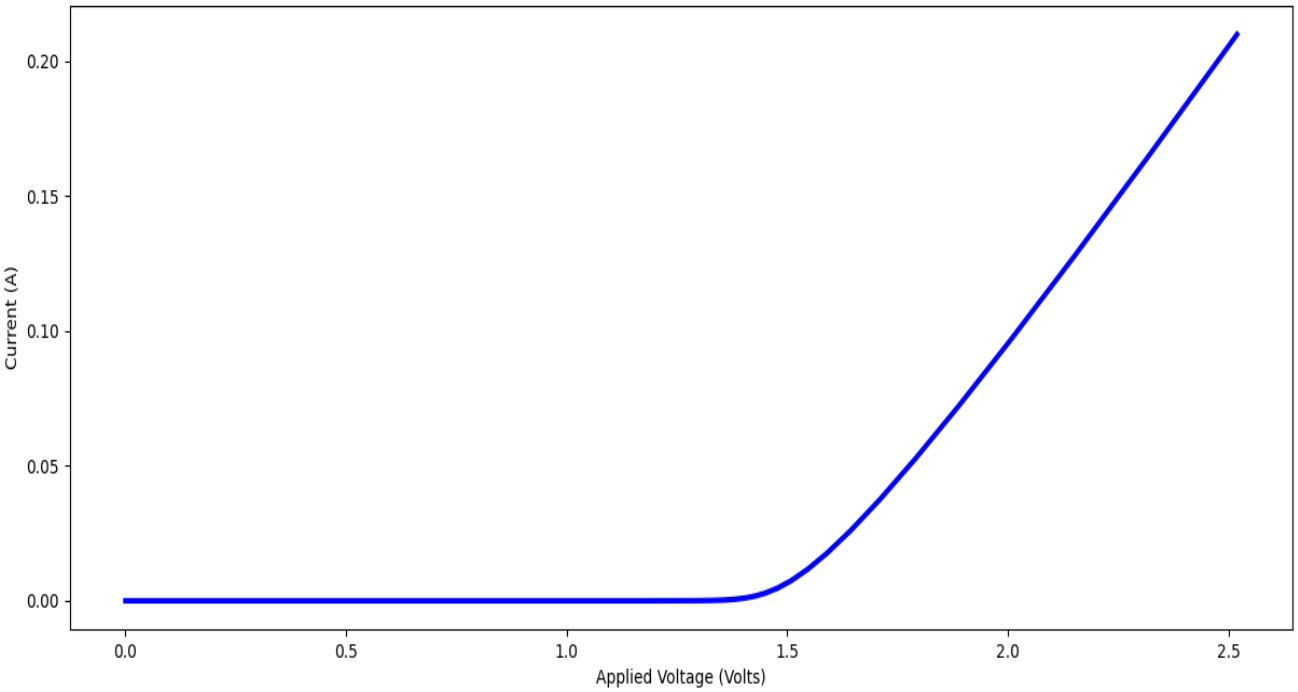

(III.a): At light intensity 1 W.cm^{-2}

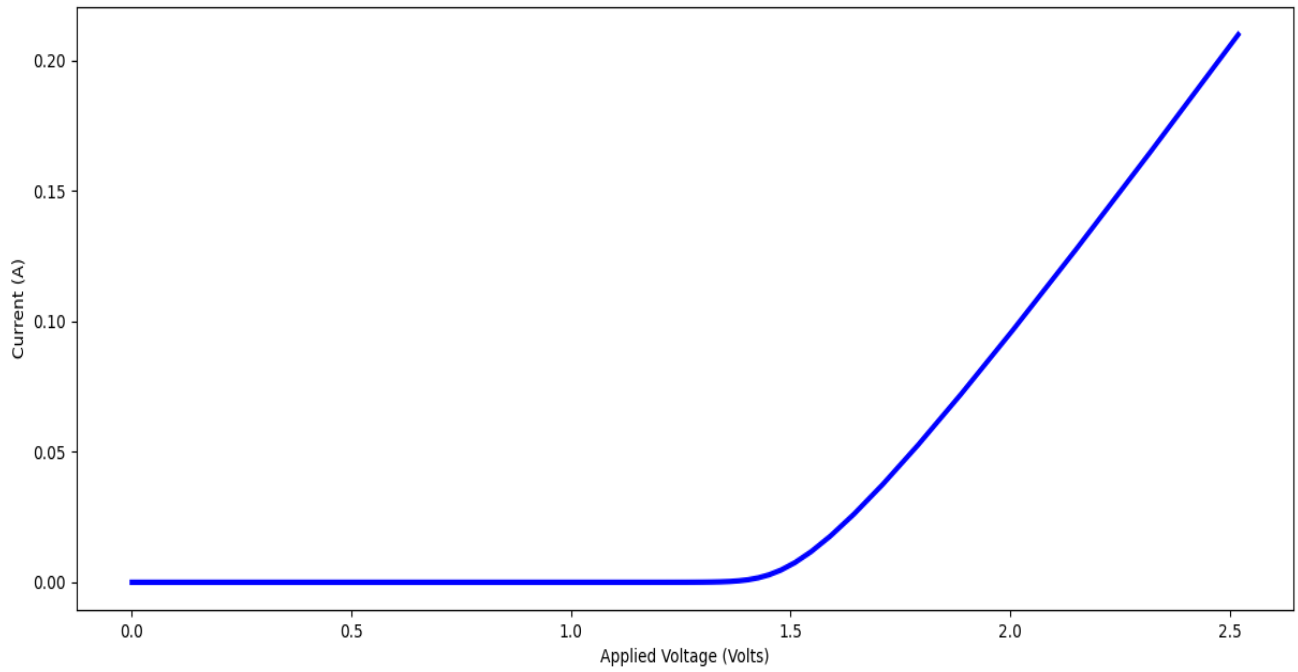

(IV.a): At light intensity 10 W.cm^{-2}

Fig. 5.9(A) [(I.a),(II.a),(III.a),(IV.a)] : Curves of Current (Y-axis) vs Applied voltage (X-axis) for film thickness 50µm of Cu_xN sample for different input light intensities i.e. 0W.cm^{-2}, 0.1W.cm^{-2}, 1W.cm^{-2} and 10W.cm^{-2} as represent (I.a),(II.a),(III.a), and (IV.a) respectively.

For 50 nm film thickness:

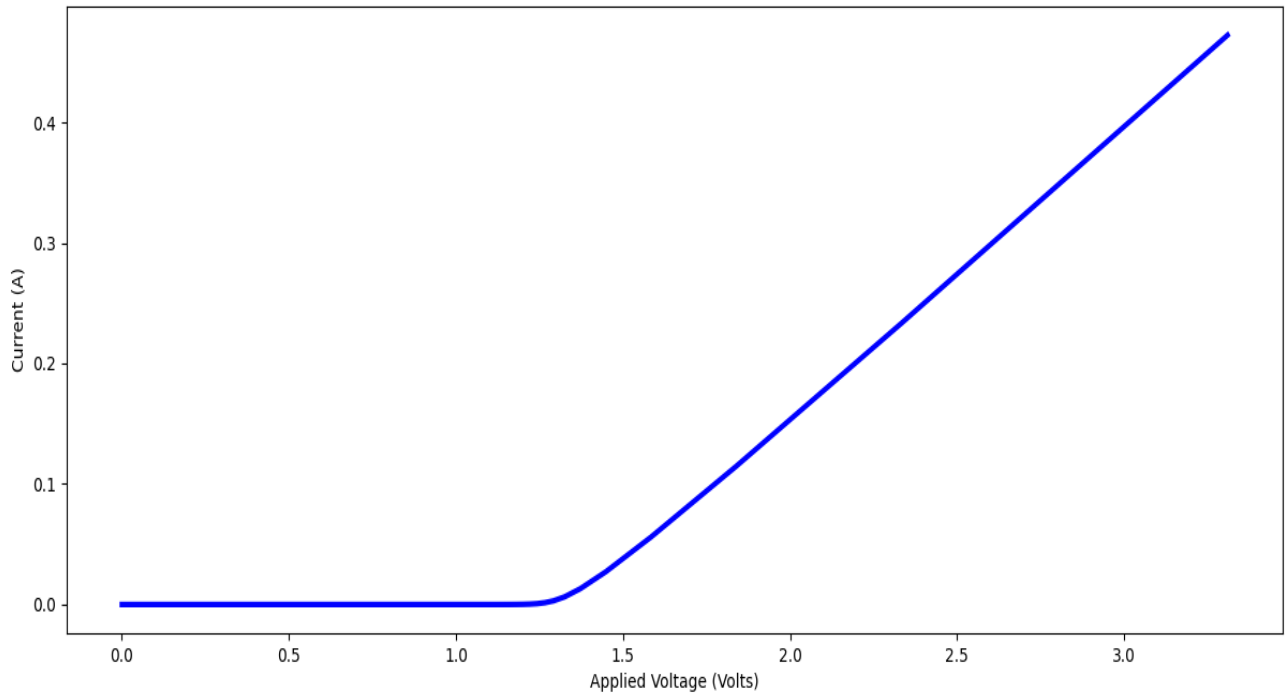

(I.b): At light intensity 0 W.cm^{-2} (Dark Condition)

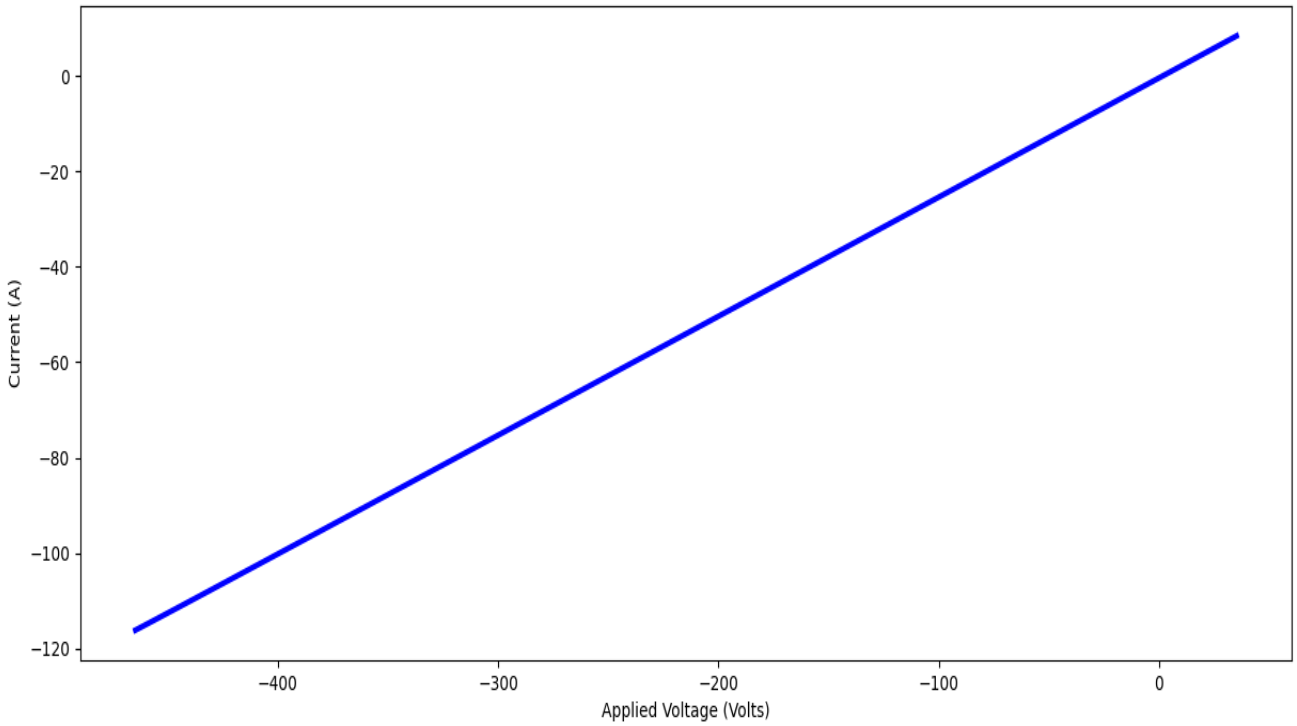

(II.b): At light intensity 0.1 W.cm^{-2}

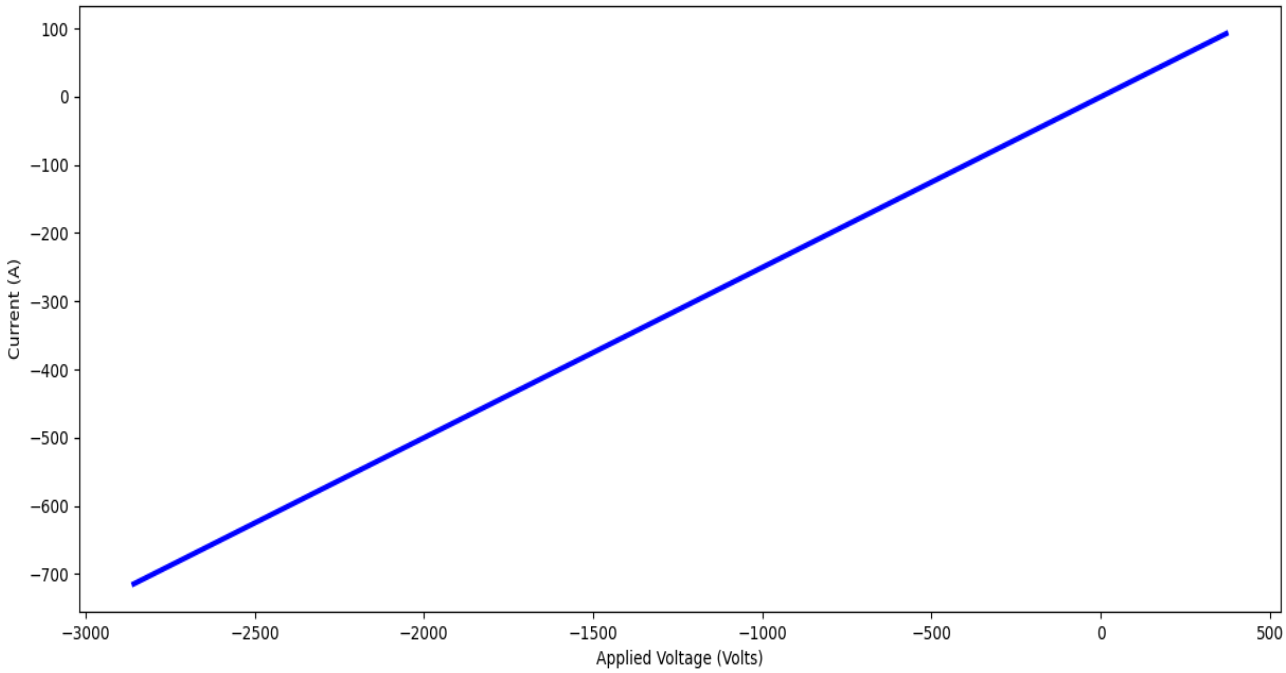

(III.b): At light intensity 1 W.cm^{-2}

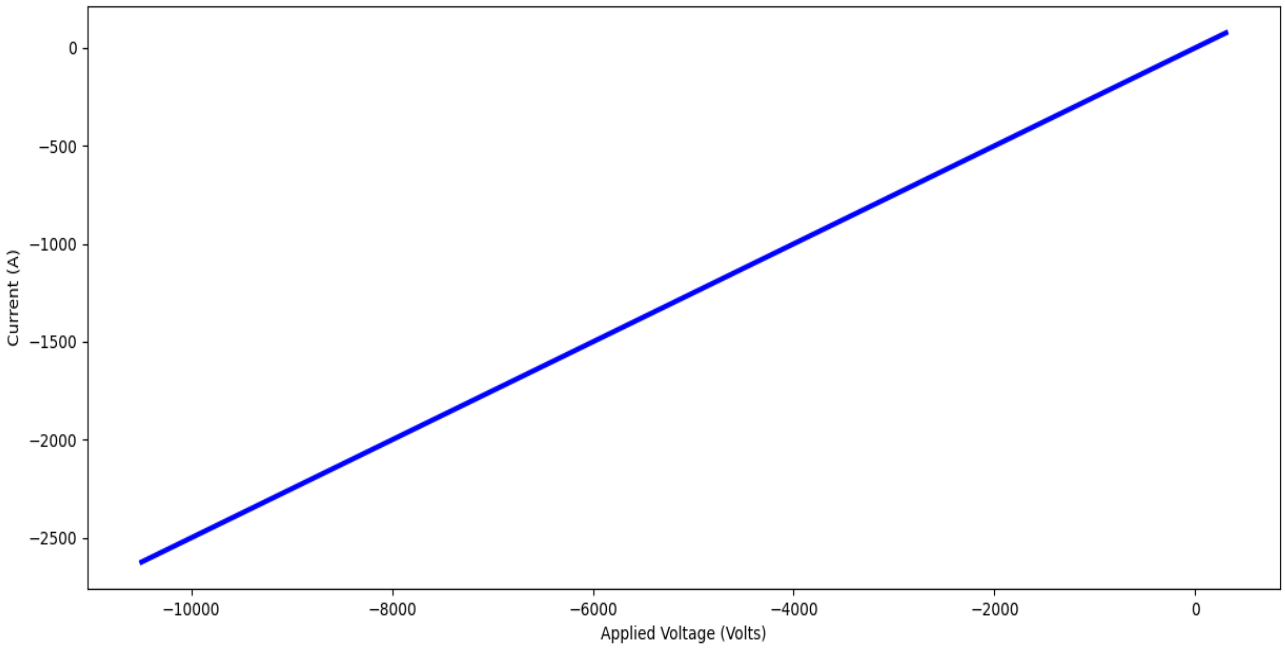

(IV.b): At light intensity 10 W.cm^{-2}

Fig.5.9(B) [(I.b),(II.b),(III.b), (IV.b)]: Curves of Current (Y-axis) vs Applied voltage (X-axis) for film thickness 50 nm of Cu_xN sample for different input light intensities i.e. 0W.cm^{-2}, 0.1W.cm^{-2}, 1W.cm^{-2} and 10W.cm^{-2} as represent (I.b),(II.b),(III.b), and (IV.b) respectively.

For 50Å film thickness:

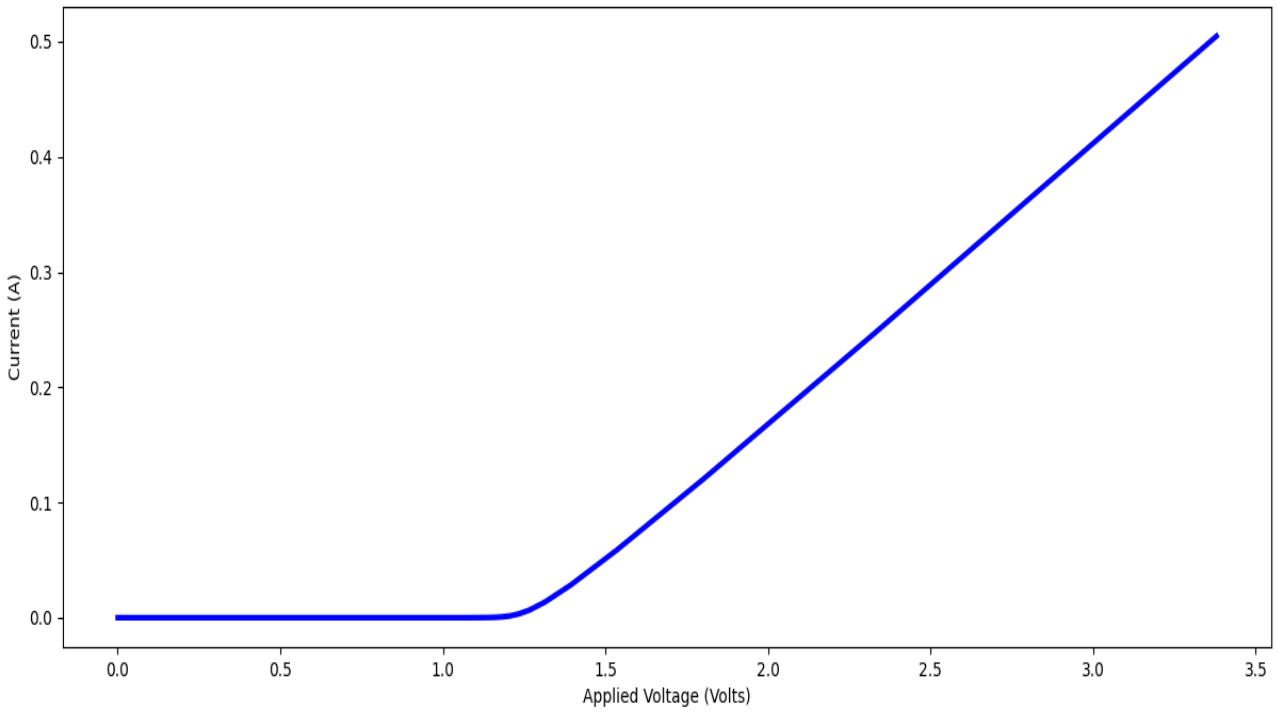

(I.c): At light intensity 0 W.cm^{-2} (Dark Condition)

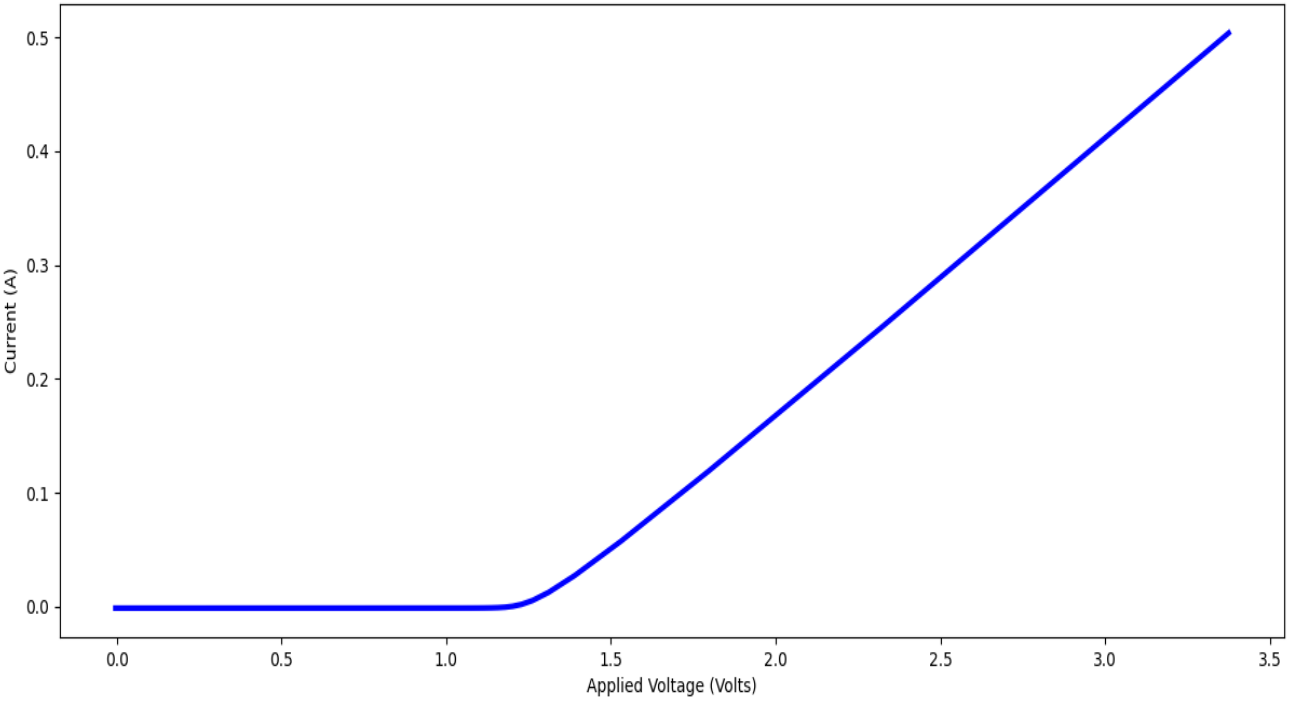

(II.c): At light intensity 0.1 W.cm^{-2}

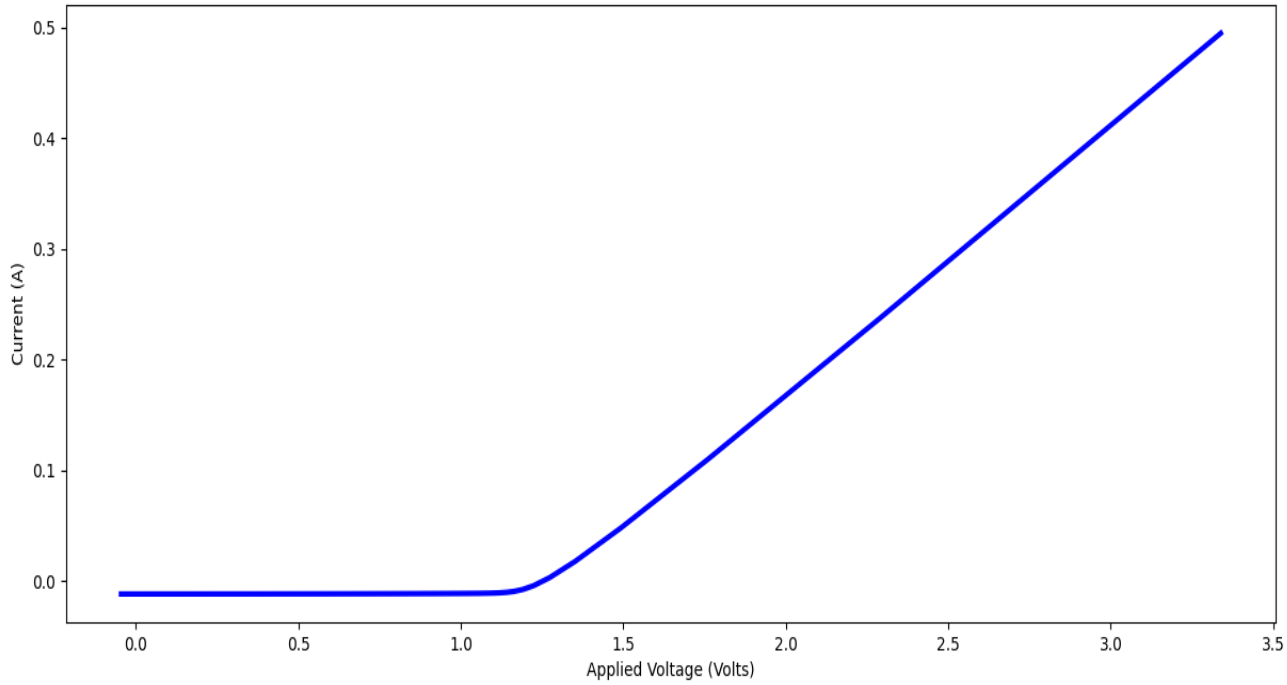

(III.c): At light intensity 1 W.cm^{-2}

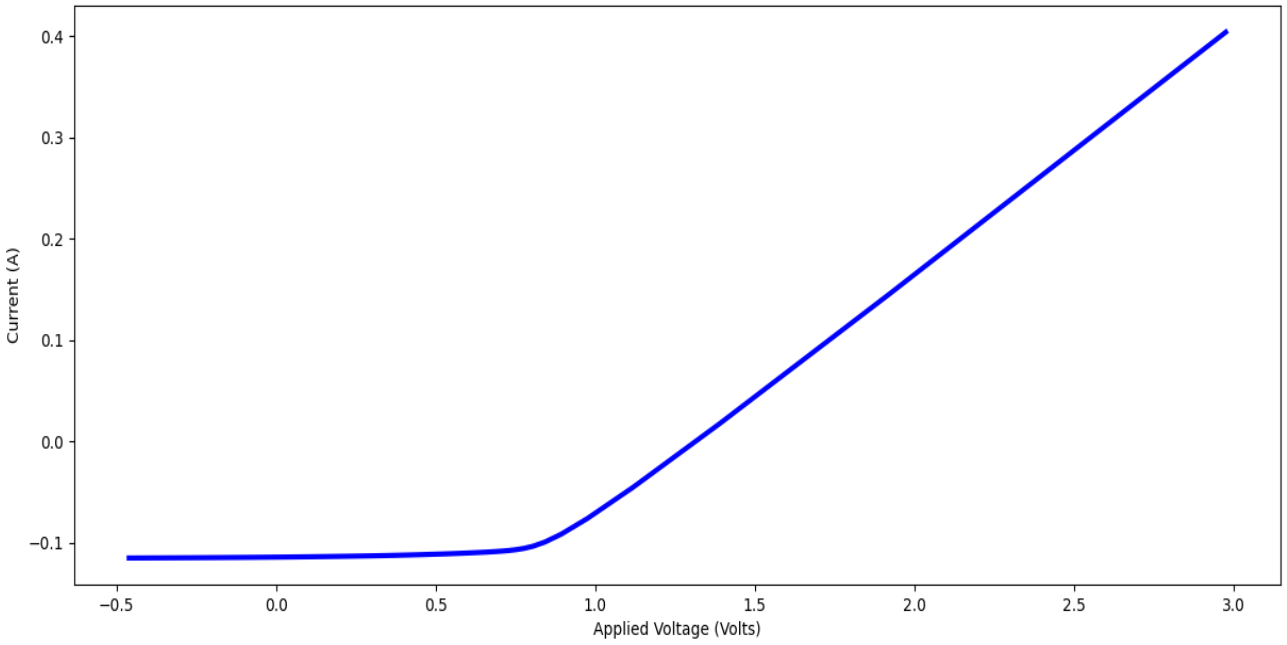

(IV.c): At light intensity 10 W.cm^{-2}

Fig. 5.9(C) [(I.c),(II.c),(III.c),(IV.c)]: Curves of Current (Y-axis) vs Applied voltage (X-axis) for film thickness 50Å of Cu_xN sample for different input light intensity i.e. 0W.cm^{-2}, 0.1W.cm^{-2}, 1W.cm^{-2} and 10W.cm^{-2} as represent (I.c),(II.c),(III.c), and (IV.c) respectively.

Current-applied voltage (I-V) characteristics of an electronic component are generally used to define its operation in an electrical circuit. I-V characteristic curves are used as tools for the determination of basic parameters of the component and mathematically model its behaviour in a circuit. The I-V characteristics of the 50μm thin film are rectifying and similar in nature with the same cut-in voltage of 1.4V due to similar bound charge polarization as seen under dark conditions from Fig.5.9(A)(I.a), at 0.1W.cm^{-2} light intensity as seen from Fig.5.9(A)(II.a), at 1W.cm^{-2} light intensity as seen from Fig.5.9(A)(III.a) and at 10W.cm^{-2} light intensity as seen from Fig.5.9(A)(IV.a) respectively. It is also clear that the value of cut-in voltage as well as corresponding bound charge polarization effect for the 50μm film remained the same for varying light intensities because, in the case of micro structure, more carriers are lost due to the higher number of trapping centres present at high density interface states at the metal-semiconductor junction [61] and thus net charge carriers, which are responsible for conduction, do not overcome the bound charge polarization effect. However, when the applied voltage exceeded the cut-in voltage then the charge carriers gained sufficient energy to overcome the bound charge polarization effect and then current conduction has started. These facts about the 50μm film can be observed from Fig.5.9(A)(I.a), Fig.5.9(A)(II.a), Fig.5.9(A)(III.a) and Fig.5.9(A)(IV.a) respectively. The I-V characteristic of the 50nm thin film at dark conditions was rectifying in nature with a cut-in voltage of 1.25V as seen from Fig.5.9(B)(I.b). However, the I-V characteristics became linear at 0.1W.cm^{-2} light intensity as seen from Fig.5.9(B)(II.b), at 1W.cm^{-2} light intensity as seen from Fig.5.9(B)(III.b) and at 10W.cm^{-2} light intensity as seen from Fig.5.9(B)(IV.b) respectively, thus negating the effect of bound charge polarization for all cases. This bound charge polarization has been reduced in nano level thickness due to a higher surface-to-volume ratio, i.e., the surface is more controlled and passivated, and thus greater charges are induced in the metal-semiconductor junction. On the other hand, dielectric constant is also higher in nanostructure, which induces greater charge polarization at the metal-semiconductor interface [61]. In the case of 50 Å thickness, it was evident that the cut-in voltage remained the same i.e. 1.25V for dark, 0.1W.cm^{-2} and 1W.cm^{-2} light intensities but decreased to 0.75V with an increase in light intensity to 10W.cm^{-2} as observed from Fig.5.9(C)(I.c), Fig.5.9(C)(II.c), Fig.5.9(C)(III.c) and Fig.5.9(C)(IV.c) respectively. The value of cut-in voltage has reduced to 0.75V at 10W.cm^{-2} light intensity as observed from Fig.5.9(C)(IV.c), implying the charge carriers requiring lesser energy to overcome the electron-hole pair binding energy. However, when the film thickness was further reduced to 50Å, the electronic band structure became discrete in nature and proximity between electron-hole pair increased resulting in requirement of more energy for separation of free charges [62]. Here also a greater number of carriers is lost in the trap state due to the discrete energy band spectrum which is present at this thickness, and thus the effect of bound charge polarization is also present here. Thus, free charge availability remained low, which impeded overall current conduction. However, when the applied voltage exceeded the cut-in voltage then the charge carriers gained sufficient energy to overcome the electron-hole pair binding energy as well as the bound charge polarization effect and then the I-V curve became linear.

Recombination pre-factor (Y-axis) vs Excess carrier density (X-axis) Curves at different light intensities for 50μm, 50nm and 50Å films have shown in Fig.5.10(A)[(I.a),(II.a),

(III.a),(IV.a)], Fig.5.10(B)[(I.b),(II.b),(III.b),(IV.b)], and Fig.5.10(C) [(I.c),(II.c),(III.c),(IV.c)] respectively.

Recombination pre-factor (Y-axis) vs Excess carrier density (X-axis) Curves at different light with variation of film thickness

For 50µm film thickness:

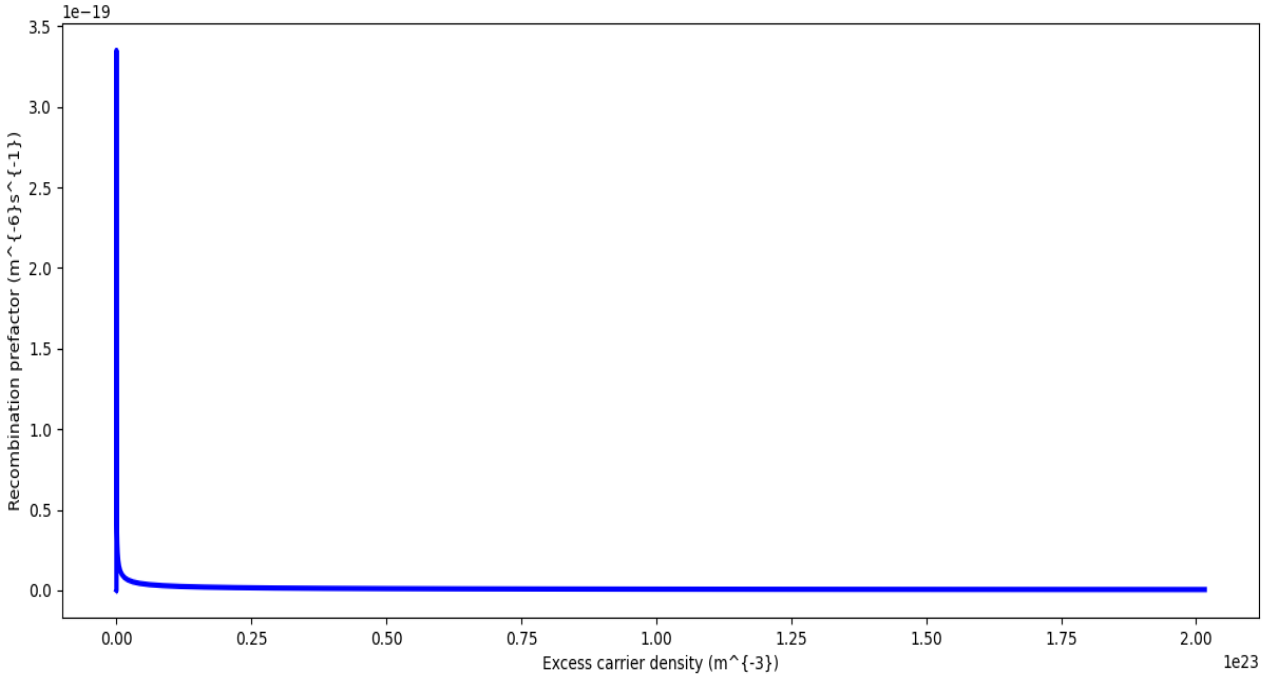

(I.a): At light intensity 0 W.cm^{-2} (Dark Condition)

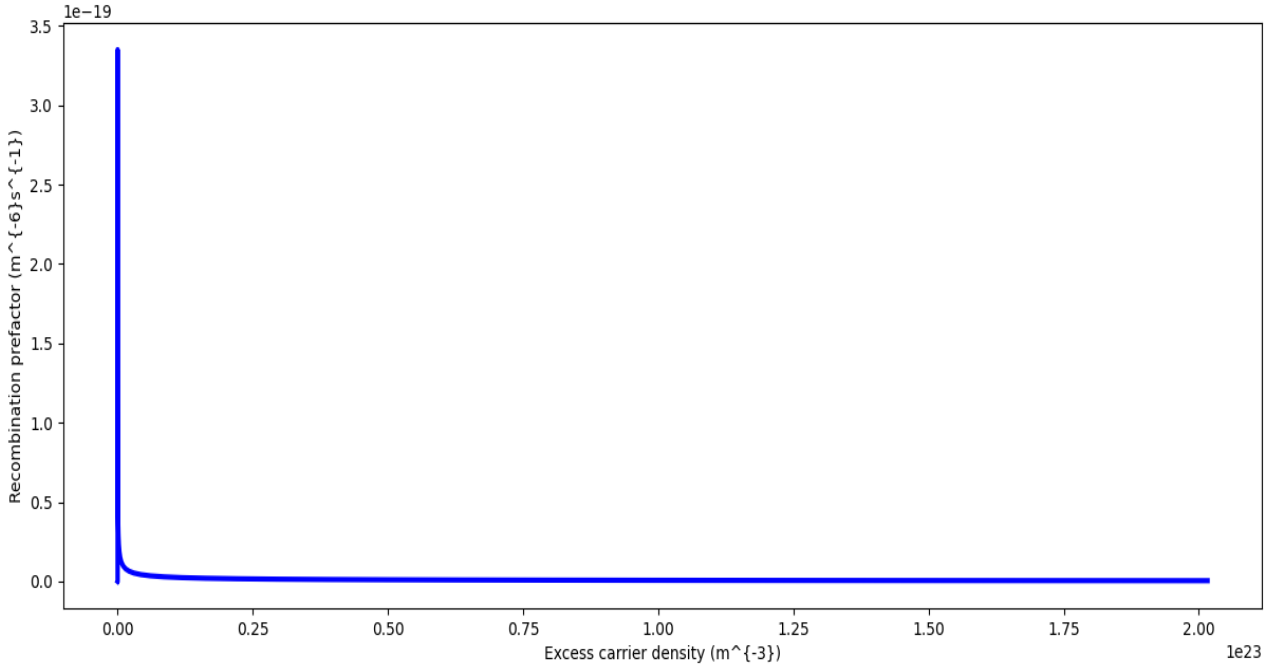

(II.a): At light intensity 0.1 W.cm^{-2}

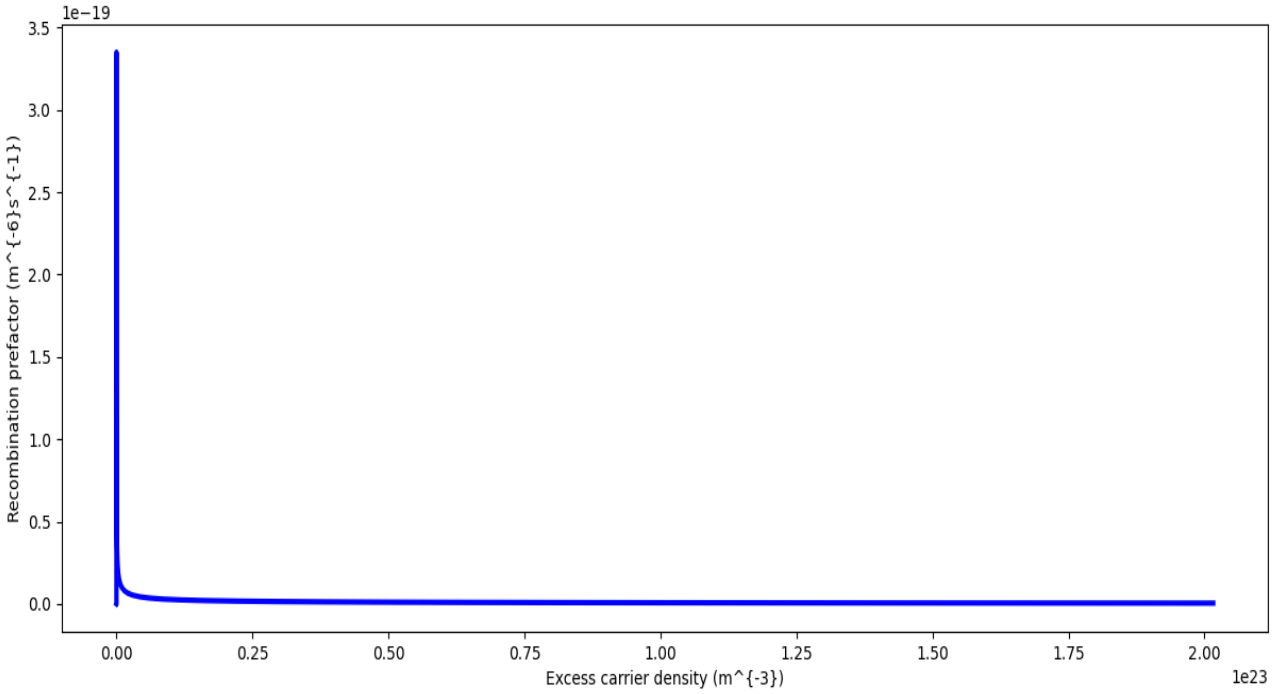

(III.a): At light intensity 1 W.cm^{-2}

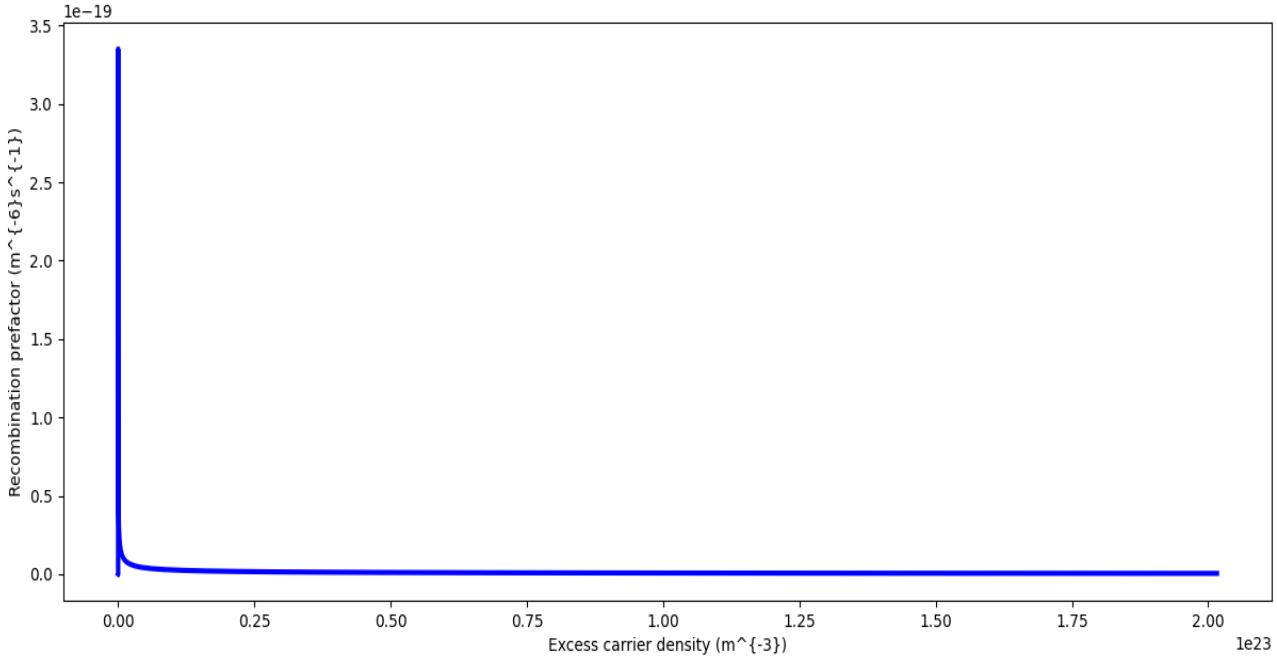

(IV.a): At light intensity 10 W.cm^{-2}

Fig. 5.10(A) [(I.a),(II.a),(III.a),(IV.a)]: Curves of Recombination prefactor (Y-axis) vs Excess carrier density (X-axis) for film thickness 50µm of Cu_xN sample for different input light intensities i.e. 0W.cm^{-2}, 0.1W.cm^{-2}, 1W.cm^{-2} and 10W.cm^{-2} as represent (I.a),(II.a),(III.a), and (IV.a) respectively.

For 50 nm film thickness:

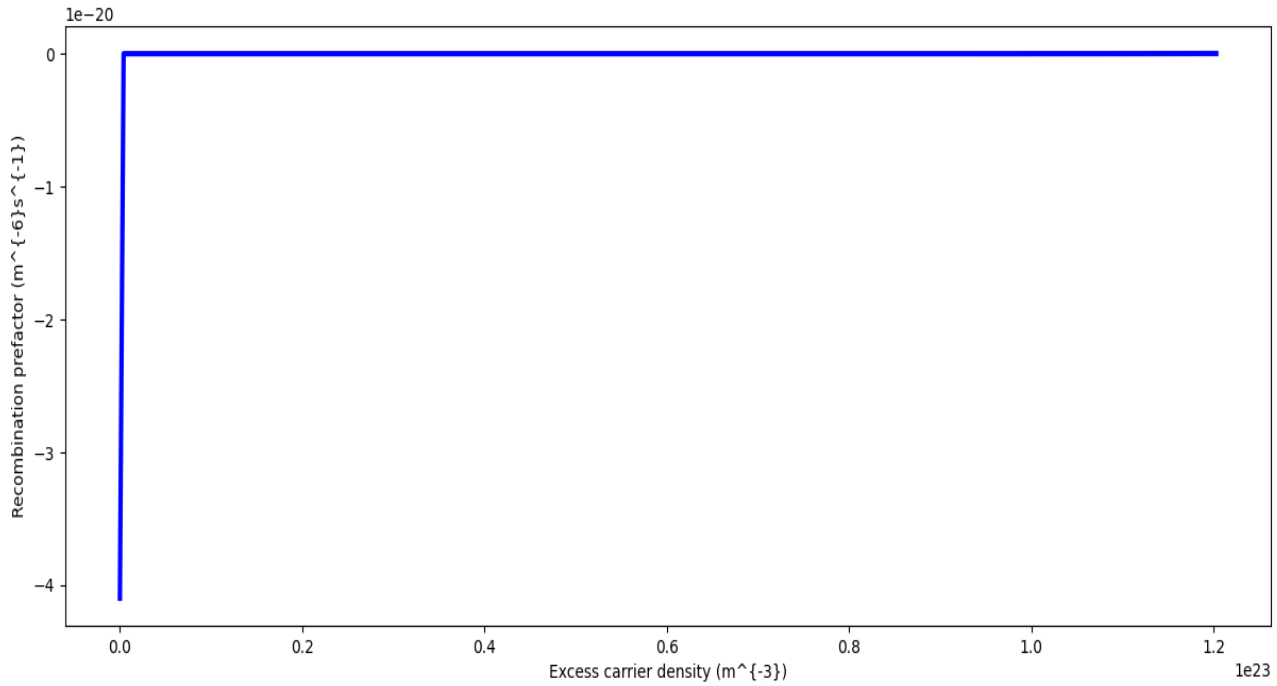

(I.b): At light intensity 0 W.cm^{-2} (Dark Condition)

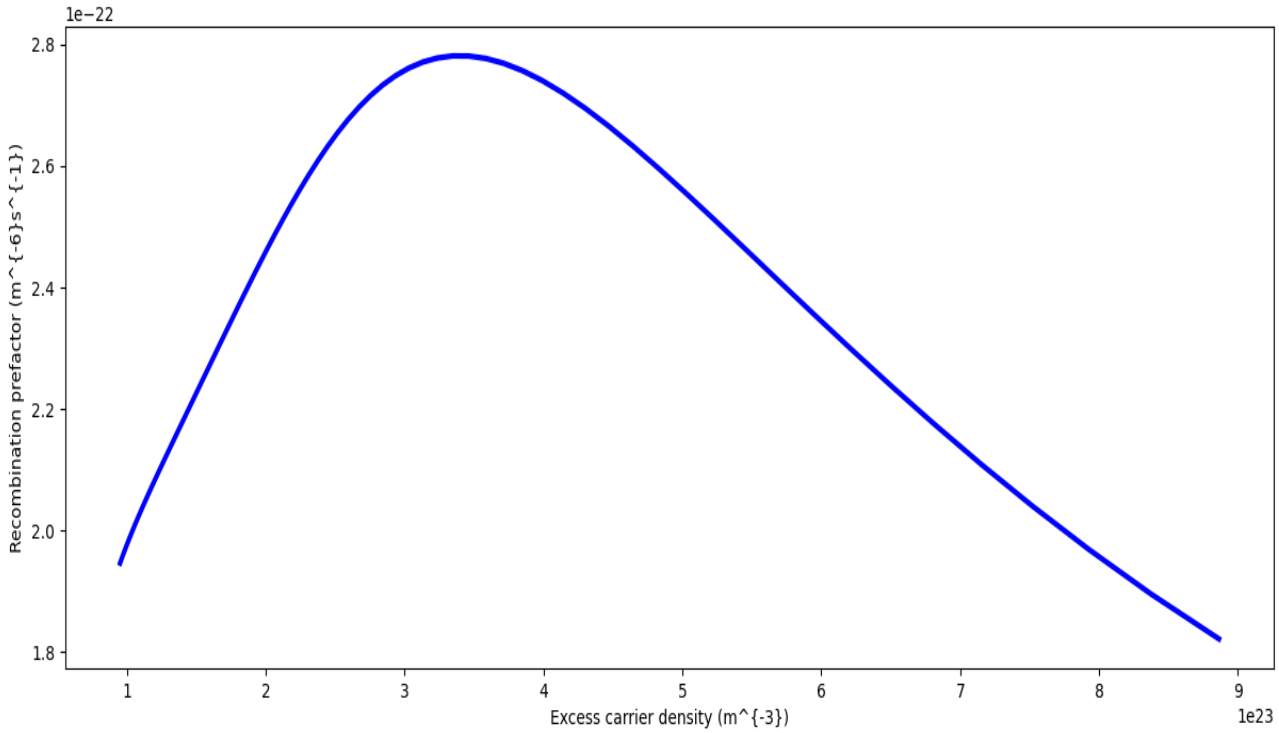

(II.b): At light intensity 0.1 W.cm^{-2}

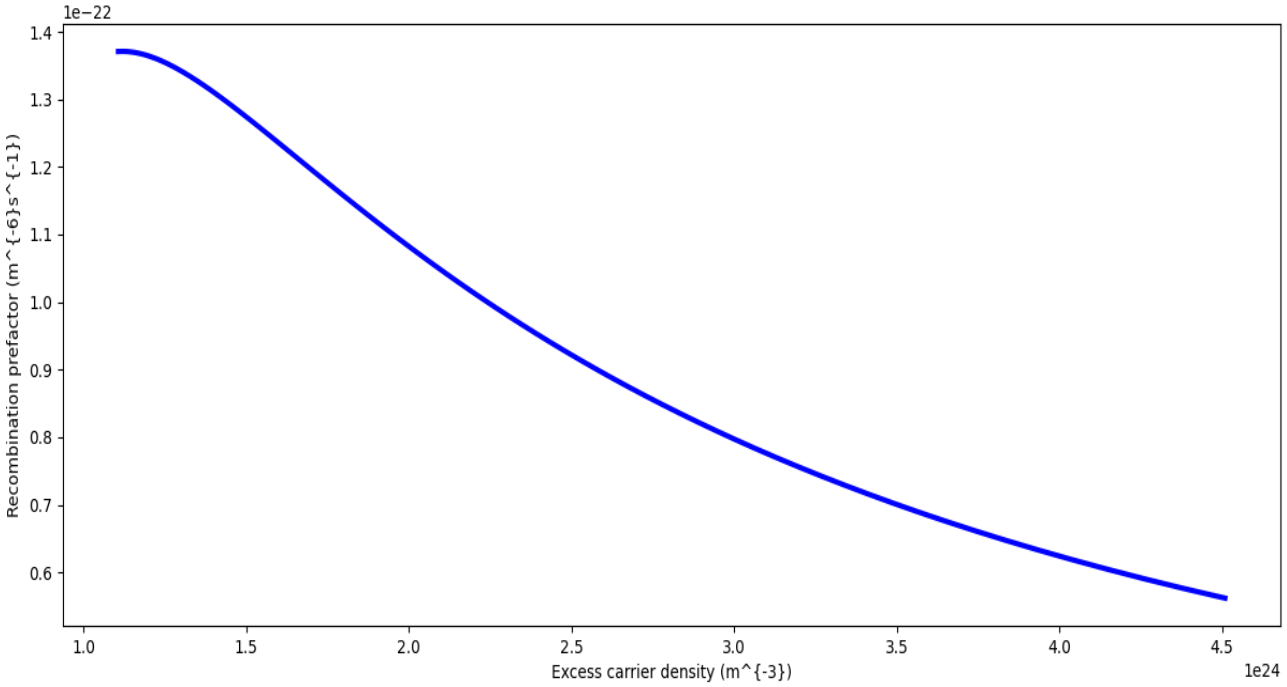

(III.b): At light intensity 1 W.cm^{-2}

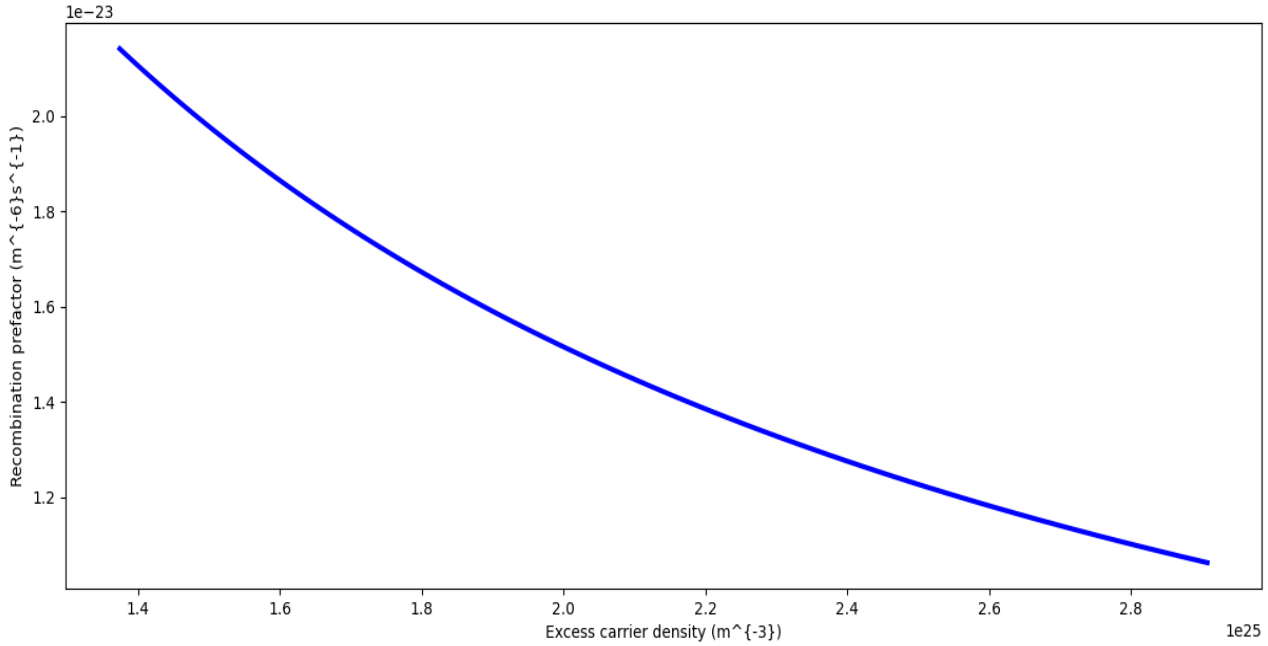

(IV.b): At light intensity 10 W.cm^{-2}

Fig. 5.10(B) [(I.b),(II.b),(III.b),(IV.b)]: Curves of Recombination prefactor (Y-axis) vs Excess carrier density (X-axis) for film thickness 50 nm of Cu_xN sample for different input light intensities i.e. 0W.cm^{-2}, 0.1W.cm^{-2}, 1W.cm^{-2} and 10W.cm^{-2} as represent (I.b),(II.b),(III.b),and (IV.b) respectively.

For 50Å film thickness:

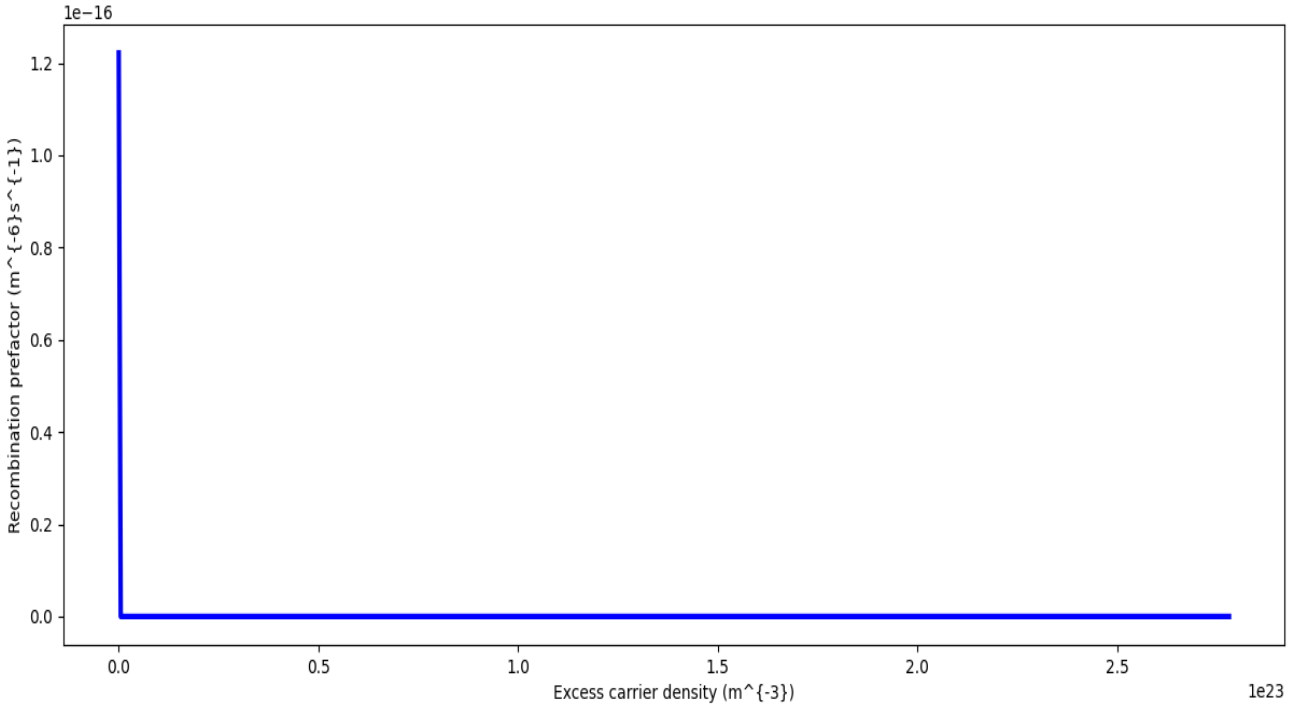

(I.c): At light intensity 0 W.cm^{-2} (Dark Condition)

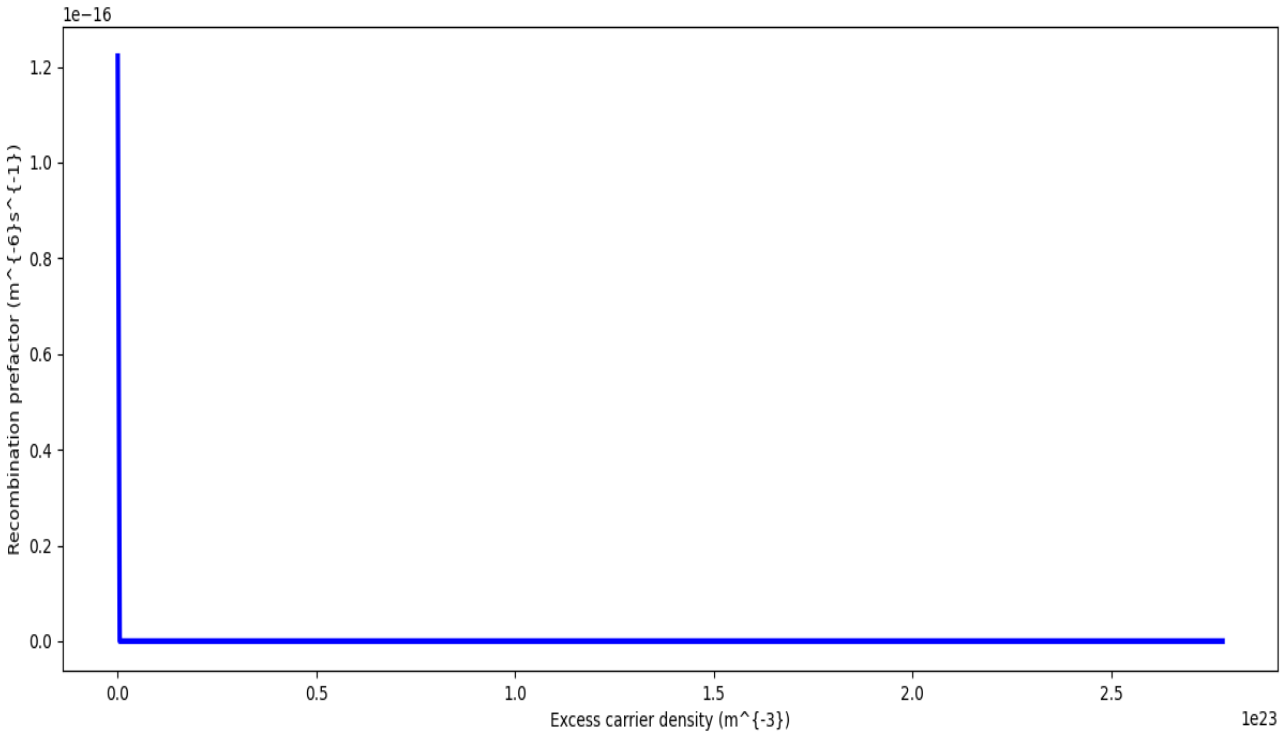

(II.c): At light intensity 0.1 W.cm^{-2}

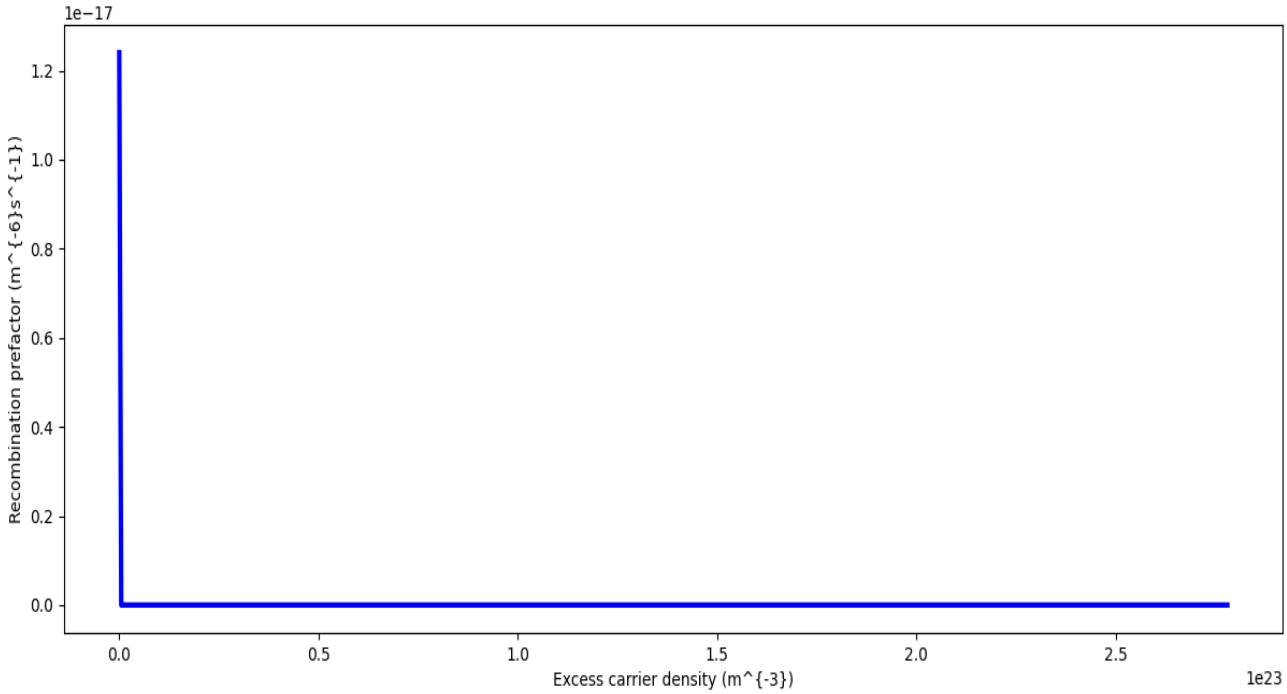

(III.c): At light intensity 1 W.cm^{-2}

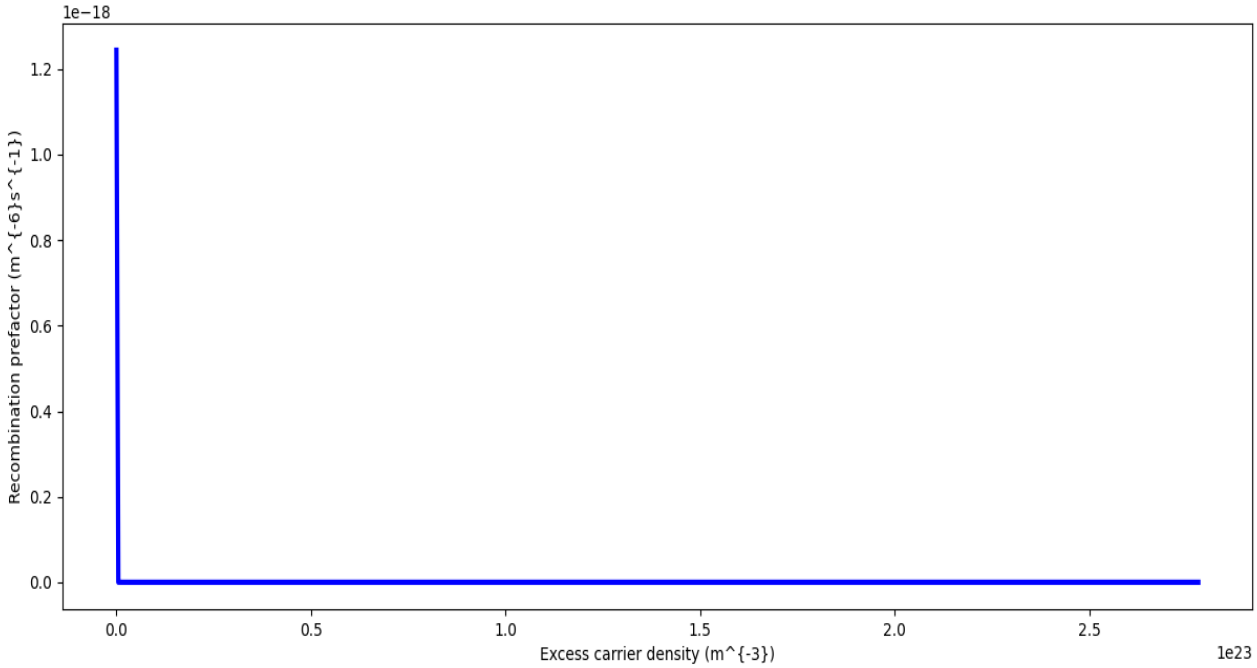

(IV.c): At light intensity 10 W.cm^{-2}

Fig. 5.10(C) [(I.c),(II.c),(III.c),(IV.c)] : Curves of Recombination prefactor (Y-axis) vs Excess carrier density (X-axis) for film thickness 50Å of Cu_xN sample for different input light intensities i.e. 0W.cm^{-2}, 0.1W.cm^{-2}, 1W.cm^{-2} and 10W.cm^{-2} as represent (I.c),(II.c),(III.c),and (IV.c) respectively.

Recombination prefactor is an important parameter of an optoelectronic material. The recombination prefactor can be recognized as recombination current density at thermal equilibrium. However, under external illumination the recombination prefactor can be used to express charge carrier recombination. The process of reaction of free electrons and holes is known as charge carrier recombination. The rate of recombination can be expressed in two alternate forms. First, an empirical expression was developed to express minority carrier lifetime as a mathematical function of excess carrier density. and the rate of recombination (R_{rate}) was defined as

$$R_{rate} = \frac{W}{\tau}\Delta n \quad \text{.....(9)}$$

where the W is film thickness, τ is effective minority carrier lifetime and Δn is excessive carrier concentration [63]

The rate of recombination can be expressed as a function of the recombination prefactor as [64]

$$R_{rate} = R_p \frac{np}{{n_i}^2} \quad \text{.....(10)}$$

where np is the product of free electron and hole concentrations and n_i^2 is its normalized value

From the two above equations the recombination prefactor can thus be expressed in terms of excess carrier concentration as

$$R_p = (\frac{{n_i}^2}{np})(\frac{W}{\tau})\Delta n \quad \ldots\ldots\ldots\ldots\ldots\ldots\ldots\ldots \quad (11)$$

In case of microstructure when optical radiation was incident upon the Cu_xN semiconductor, then an overwhelming part of the incident radiation was attenuated. Attenuation resulted in the radiation being either effectively absorbed or being scattered [65]. The value of recombination prefactor was found to be same i.e. $3.5x10^{-19}m^{-6}.s^{-1}$for the 50µm thin film at dark conditions as seen from Fig.5.10(A) (I.a), at $0.1W.cm^{-2}$ light intensity as seen from Fig. 5.10(A)(II.a), at $1W.cm^{-2}$ light intensity as seen from Fig.5.10(A)(III.a) and at $10W.cm^{-2}$ light intensity as seen from Fig. 5.10(A)(IV.a) respectively. Here maximum excess carrier concentration remained $2x10^{23}m^{-3}$ for all light intensities. In the case of microstructure recombination takes place due to the presence of more defects and trapping centres at high density interface states of metal-semiconductor junctions. The recombination prefactor is same for 50µm film in the absence of excess carrier concentration for an increase in light intensity from $0.1W.cm^{-2}$ to $1W.cm^{-2}$ and $10W.cm^{-2}$ respectively because here net absorption is less, i.e., carrier generation is also less resulted in smaller increase in average carrier lifetime [65] as seen from Fig. 5.10(A)(II.a), Fig. 5.10(A)(III.a) and Fig.5.10(A)(IV.a) respectively. The recombination prefactor for the 50nm film under dark conditions remained zero as seen from Fig.5.10(B)(I.b). While the recombination prefactor for the 50nm film gradually increased to $2.8x10^{-22}m^{-6}.s^{-1}$ up to an excess carrier concentration value of $3.5x10^{23}m^{-3}$ and then started gradually decreasing to $1.8x10^{-22}m^{-6}.s^{-1}$ for excess carrier concentration of $9x10^{23}m^{-3}$ at $0.1W.cm^{-2}$ light intensity as evident from Fig.5.10(B)(II.b). At first, an increase in excess carrier concentration resulted in more recombination and hence a higher recombination prefactor, but after excess carrier concentration of $3.5x10^{23}m^{-3}$, the increase in charge carriers was so rapid that it resulted in a higher average carrier lifetime and reduced recombination, hence a low recombination prefactor for the 50nm film at $0.1W.cm^{-2}$ light intensity. The recombination prefactor decreased exponentially from $1.4x10^{-22}m^{-6}.s^{-1}$ to $0.6x10^{-22}m^{-6}.s^{-1}$ with an increase in excess carrier density from $1.0x10^{24}m^{-3}$ to $4.5x10^{24}m^{-3}$ at a light intensity of $1W.cm^{-2}$ as seen from Fig.5.10(B)(III.b). The recombination prefactor decreased exponentially from $2.0x10^{-23}m^{-6}.s^{-1}$ to $1.2x10^{-23}m^{-6}.s^{-1}$ with an increase in excess carrier density from $1.4x10^{25}m^{-3}$ to $2.8x10^{25}m^{-3}$ at a light intensity of $10W.cm^{-2}$ light intensity as seen from Fig. 5.10(B)(IV.b). This trend of exponential decrease of recombination prefactor at $1W.cm^{-2}$ and $10W.cm^{-2}$ light intensities is due to increased average carrier lifetime and hence reduced recombination at higher light intensities. The value of recombination prefactor was overall lower for the 50nm thin film than the 50µm film because of more optical absorption and lesser optical scattering for the former and vice versa for the latter. On the other hand, lesser defects and trap states are present in nanometer range thicknesses because the surface is more controlled and passivated. This has happened due to a higher surface-to- volume ratio occurring in the case of nanostructures. Therefore defects, grain boundaries and interface recombination have reduced in the case of nanostructure-based film [65]. Thus, carrier lifetime has increased as well as reduced recombination. When the film thickness was reduced to 50Å, then the value of recombination prefactor was $1.2x10^{-}$

$^{16}m^{-6}.s^{-1}$ at dark condition as seen from Fig.5.10(C) (I.c), , $1.2x10^{-16}m^{-6}.s^{-1}$ at $0.1W.m^{-2}$ light intensity as seen from Fig.5.10(C)(II.c), $1.2x10^{-17}m^{-6}.s^{-1}$ at $1W.m^{-2}$ light intensity as seen from Fig. 5.10(C)(III.c), and $1.2x10^{-18}m^{-6}.s^{-1}$ at $10W.m^{-2}$ light intensity as seen from Fig.5.10(C)(IV.c), respectively. When the film thickness was reduced to 50Å, then the maximum excess carrier concentration remained $3x10^{23}m^{-3}$ for all light intensities, however the recombination prefactor decreased from $1.2x10^{-16}m^{-6}.s^{-1}$ to $1.2x10^{-17}m^{-6}.s^{-1}$ and $1.2x10^{-18}m^{-6}.s^{-1}$ in the absence of excess carrier concentration for an increase in light intensity from $0.1W.cm^{-2}$ to $1W.cm^{-2}$ and $10W.cm^{-2}$ respectively because an increase in light intensity resulted in increased average carrier lifetime [66] as seen from Fig. 5.10(C)(II.c), Fig.5.10(C)(III.c) and Fig.5.10(C)(IV.c) respectively. The recombination prefactor was least for the 50nm film and maximum for the 50Å one, while that of the 50µm remained in between the two. The recombination prefactor was maximum for the 50Å film because at this thickness presence of higher defects and trap states due to discrete energy band structure and thus reduces carrier life time as well as increases recombination. On the other hand, in the nano range thickness, recombination was least due to lesser defects and trap states. In nanometer range thicknesses surface is more controlled and passivated, and thus, lesser defects as well as trap states are present here. Therefore, 50nm thickness-based film is the optimum in comparison with the other two thickness-based films, such as 50µm and 50Å.

Charge carrier generation rate (Y-axis) vs Y-position (X-axis) Curves at different light intensities for 50µm, 50nm and 50Å films have shown in Fig.5.11(A)[(I.a),(II.a),(III.a),(IV.a)], Fig.5.11(B)[(I.b),(II.b),(III.b),(IV.b)] and Fig.5.11(C)[(I.c),(II.c),(III.c),(IV.c)] respectively.

Charge carrier generation rate (Y-axis) vs Y-position (X-axis) Curves at different light intensities with variation of film thickness

For 50µm film thickness:

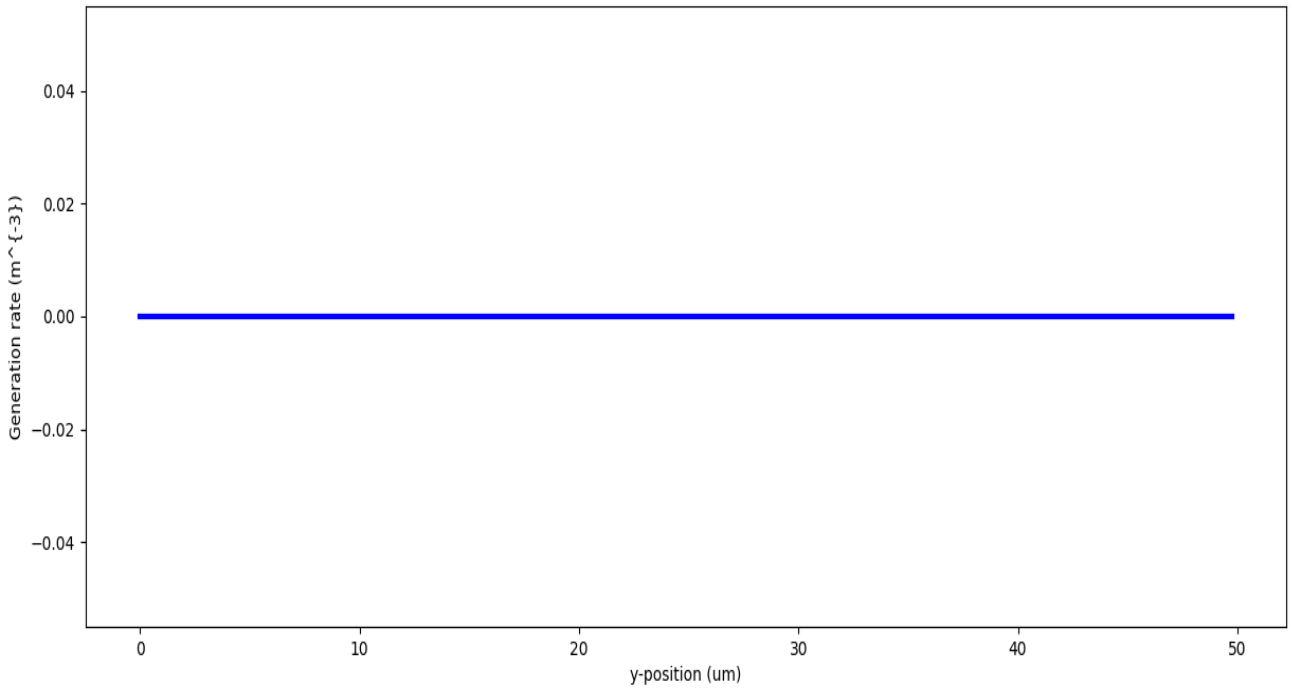

(I.a): At light intensity 0 W.cm^{-2} (Dark Condition)

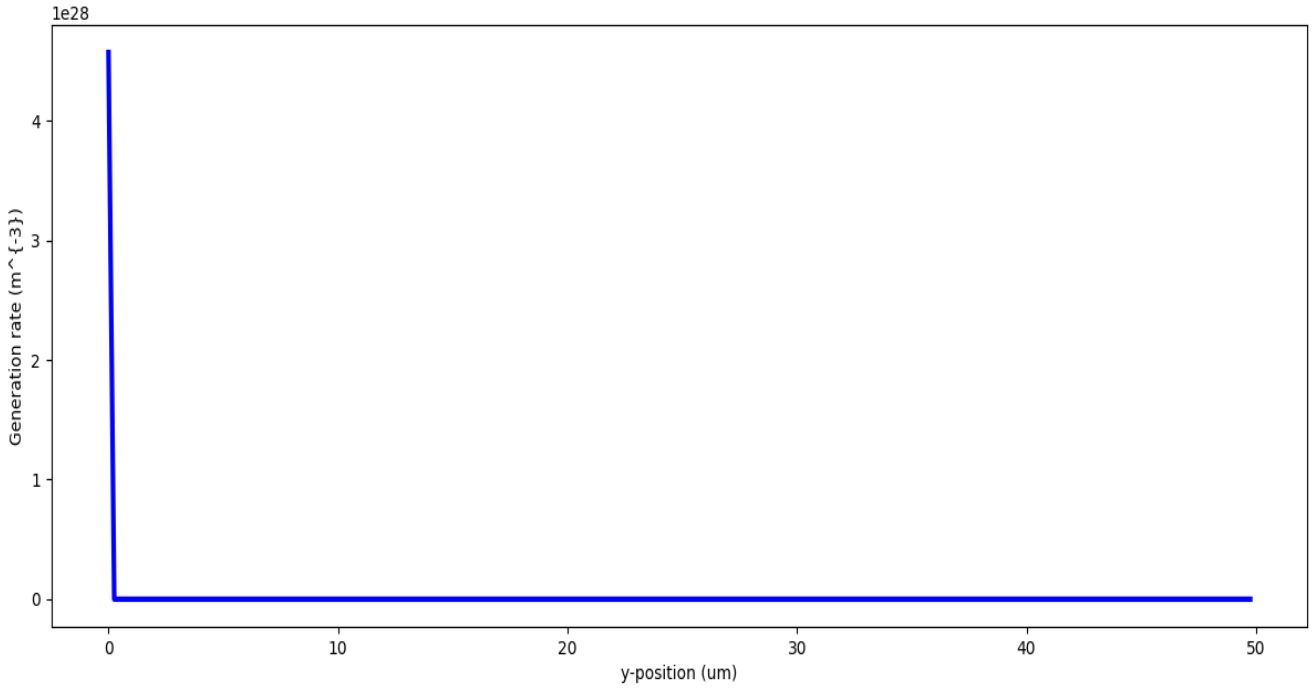

(II.a): At light intensity 0.1 W.cm^{-2}

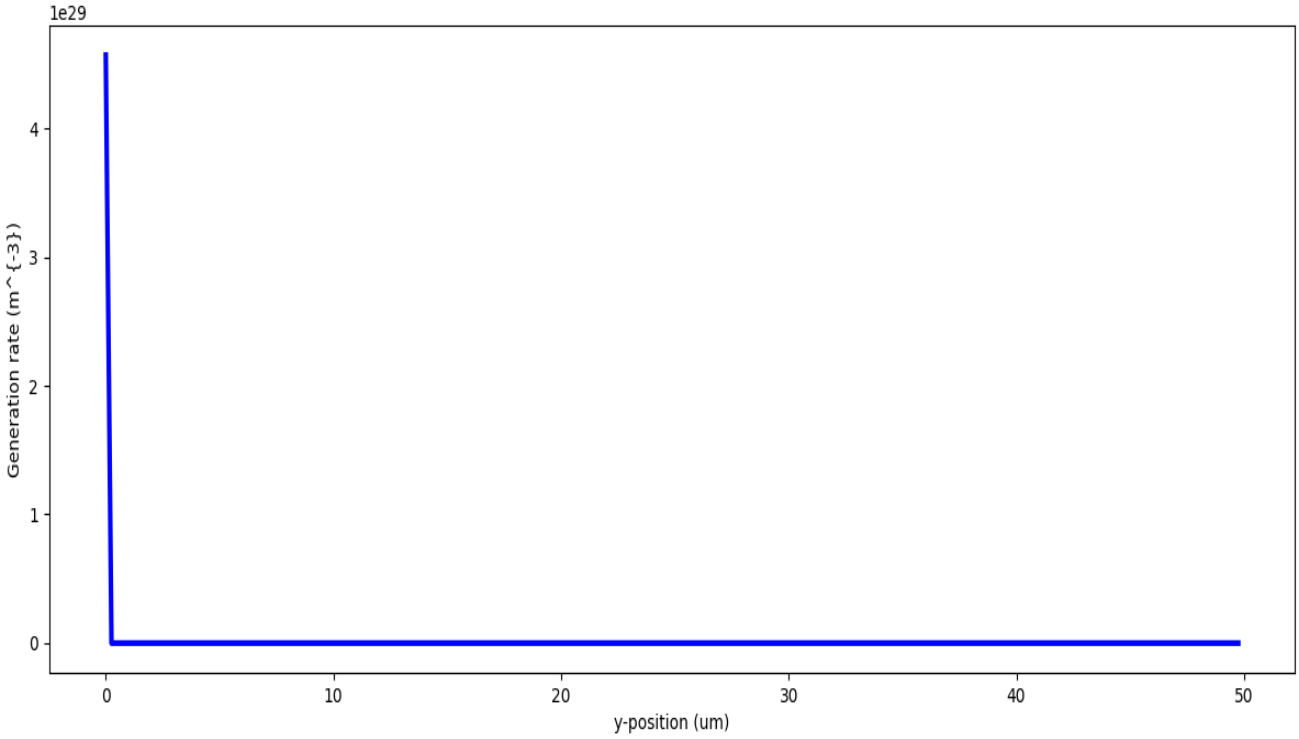

(III.a): At light intensity 1 W.cm^{-2}

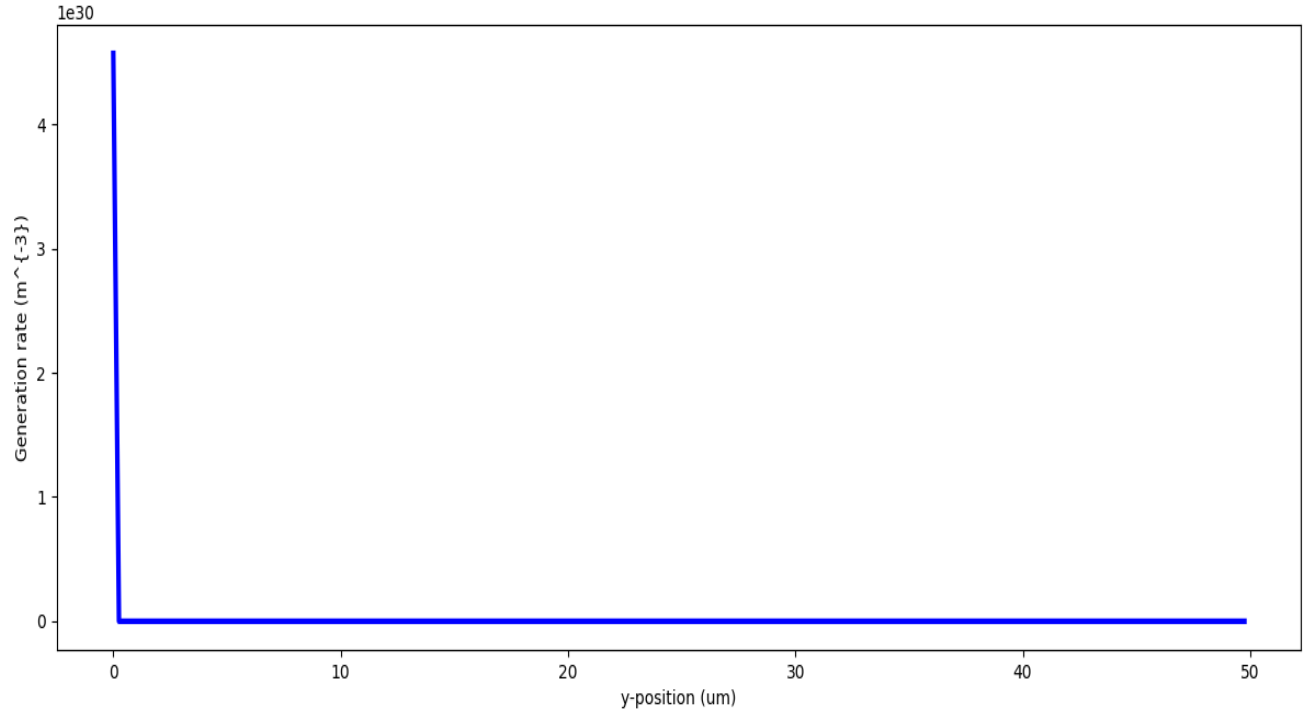

(IV.a): At light intensity 10 W.cm^{-2}

Fig. 5.11(A) [(I.a),(II.a),(III.a),(IV.a)]: Curves of Charge carrier generation rate (Y axis) vs Y-position (X axis) for film thickness 50µm of Cu_xN sample for different input light intensities i.e.0W.cm^{-2},0.1W.cm^{-2},1W.cm^{-2} and 10W.cm^{-2} as represent (I.a),(II.a),(III.a), and (IV.a) respectively.

For 50 nm film thickness:

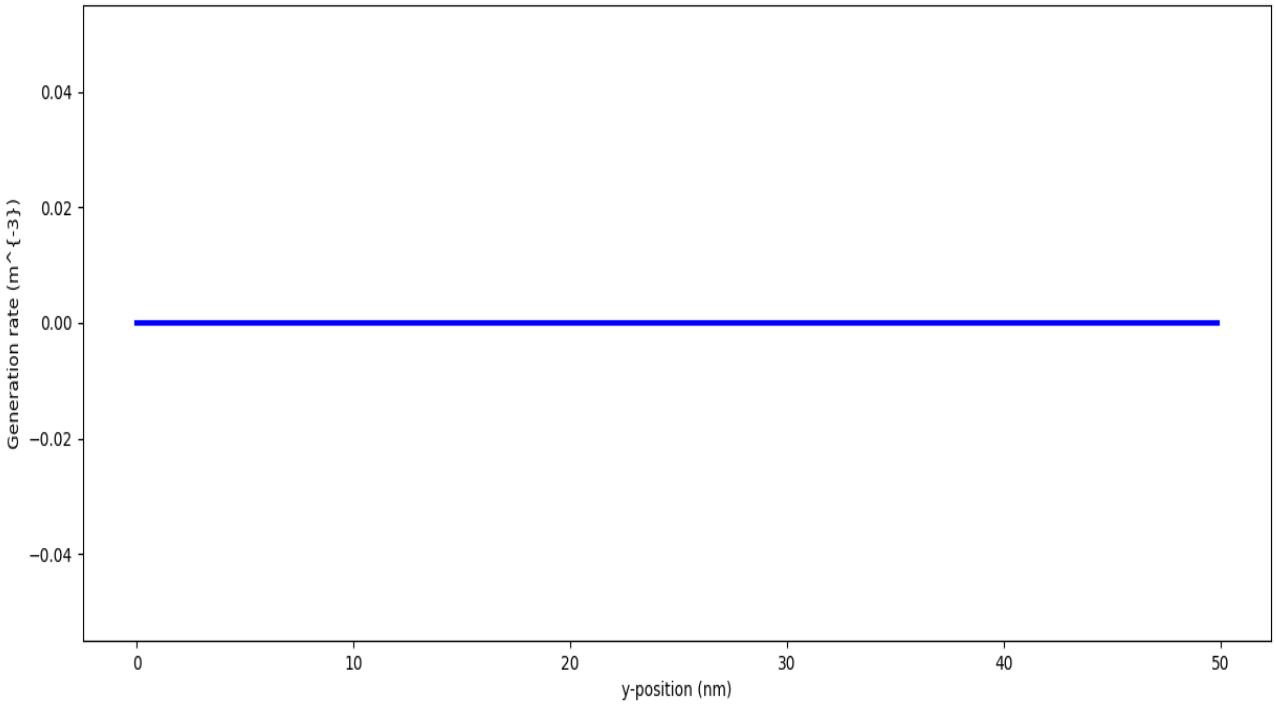

(I.b): At light intensity 0 W.cm^{-2} (Dark Condition)

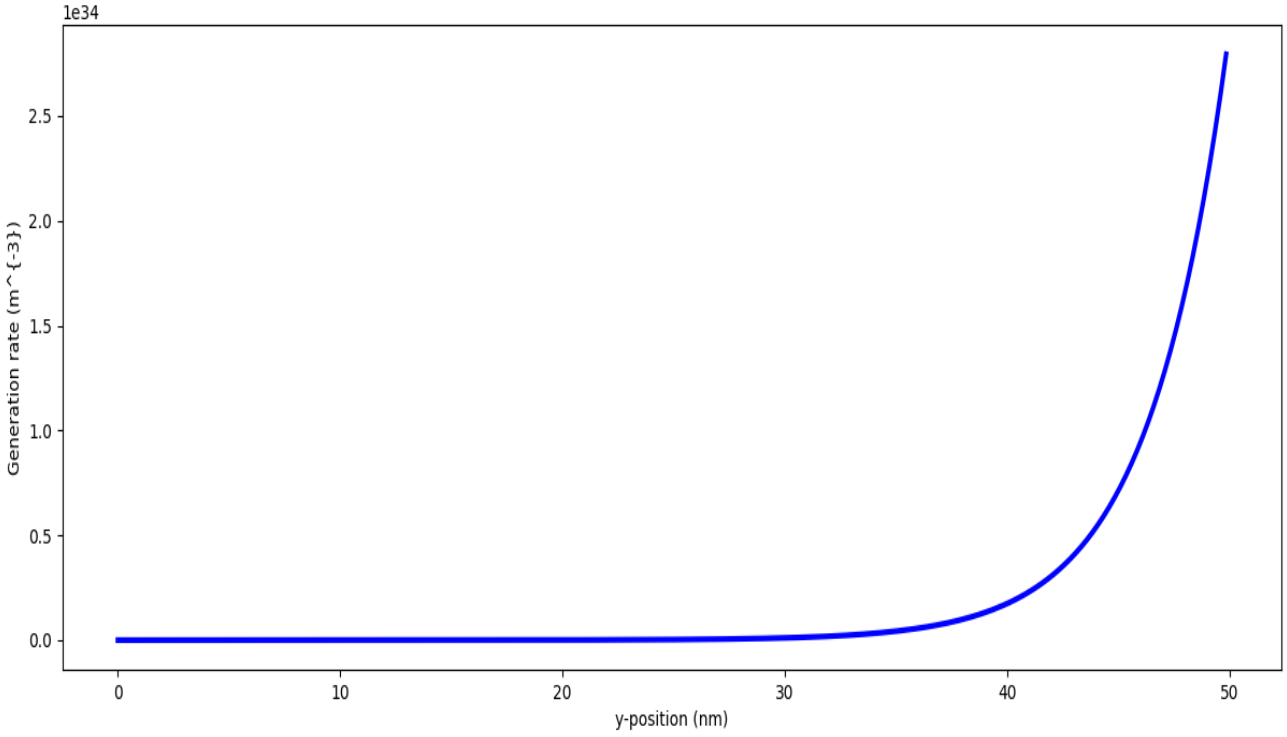

(II.b): At light intensity 0.1 W.cm^{-2}

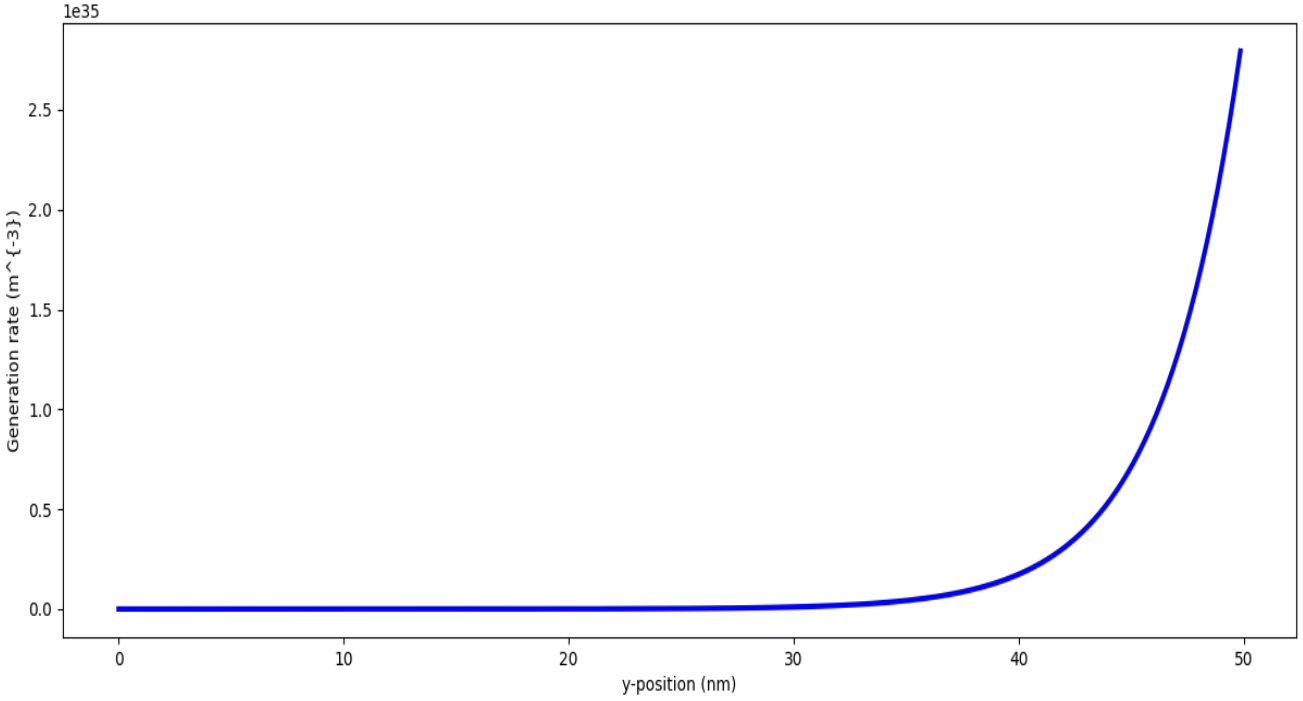

(III.b): At light intensity 1 W.cm^{-2}

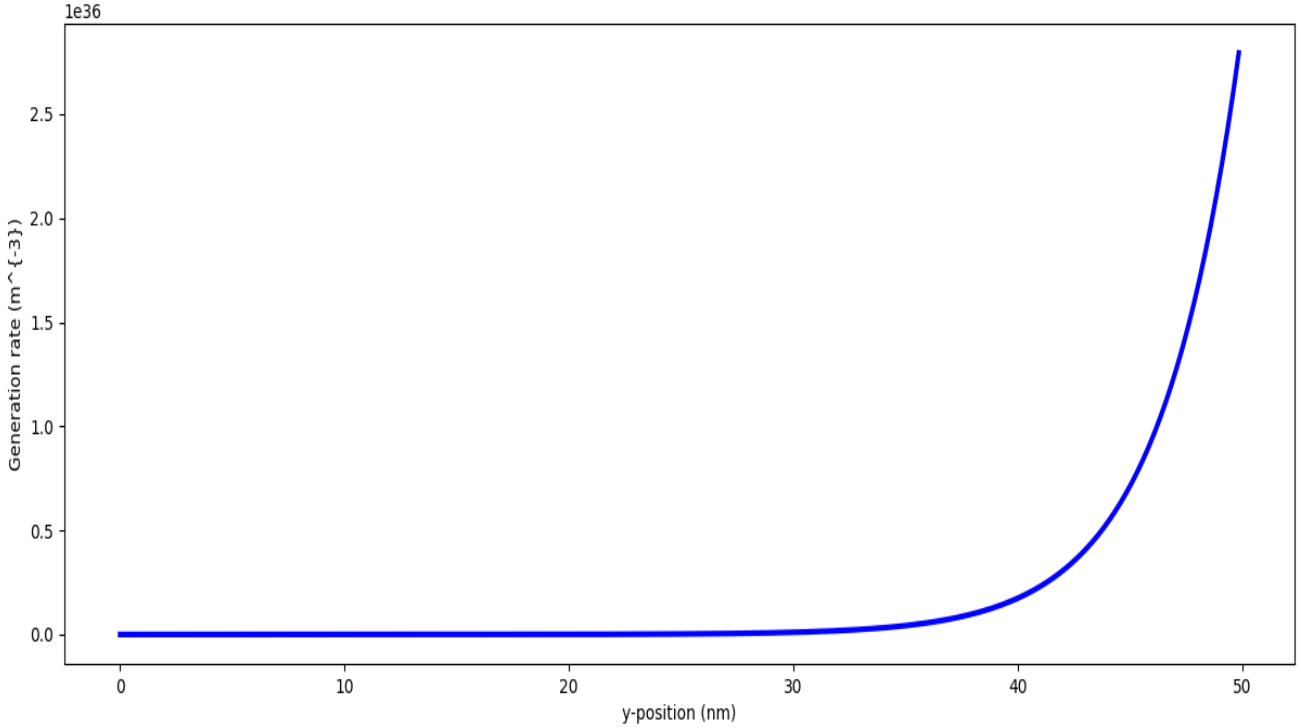

(IV.b): At light intensity 10 W.cm^{-2}

Fig. 5.11(B) [(I.b),(II.b),(III.b),(IV.b)]: Curves of Charge carrier generation rate (Y-axis) vs Y-position (X-axis) for film thickness 50 nm of Cu_xN sample for different input light intensities i.e. 0W.cm^{-2}, 0.1W.cm^{-2}, 1W.cm^{-2} and 10W.cm^{-2} as represent (I.b), (II.b), (III.b), and (IV.b) respectively.

For 50Å film thickness:

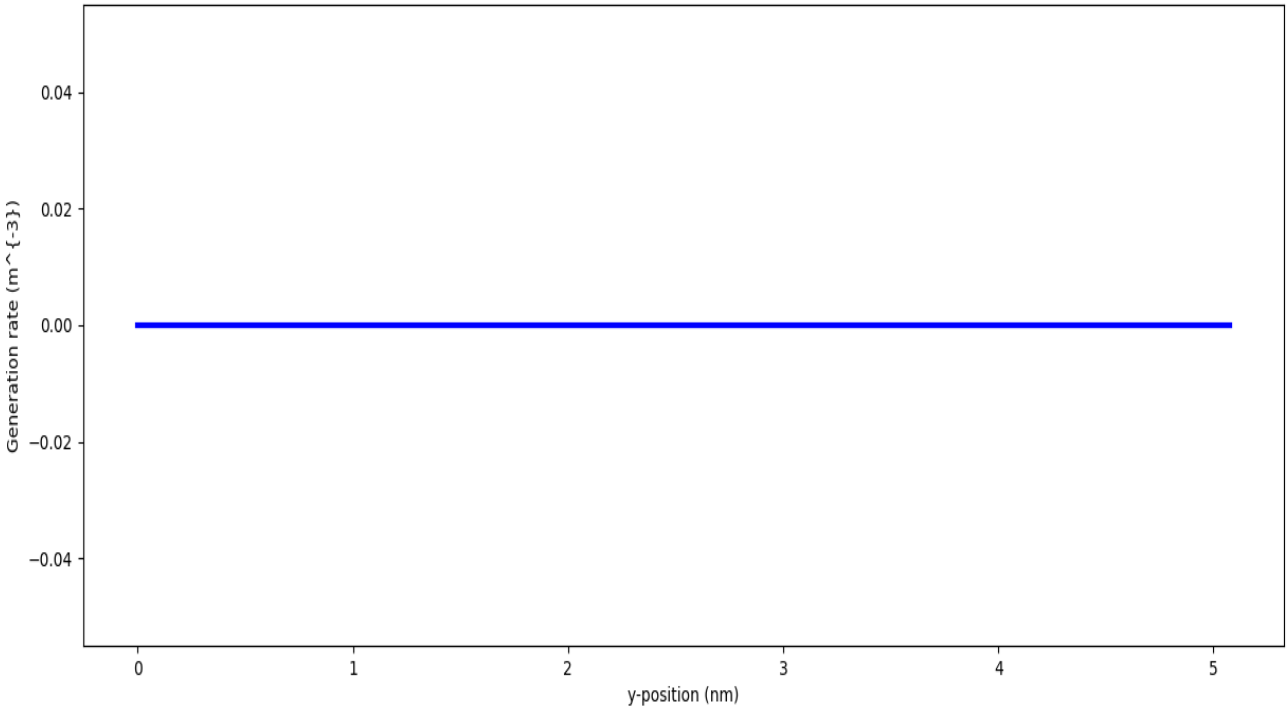

(I.c): At light intensity 0 W.cm^{-2} (Dark Condition)

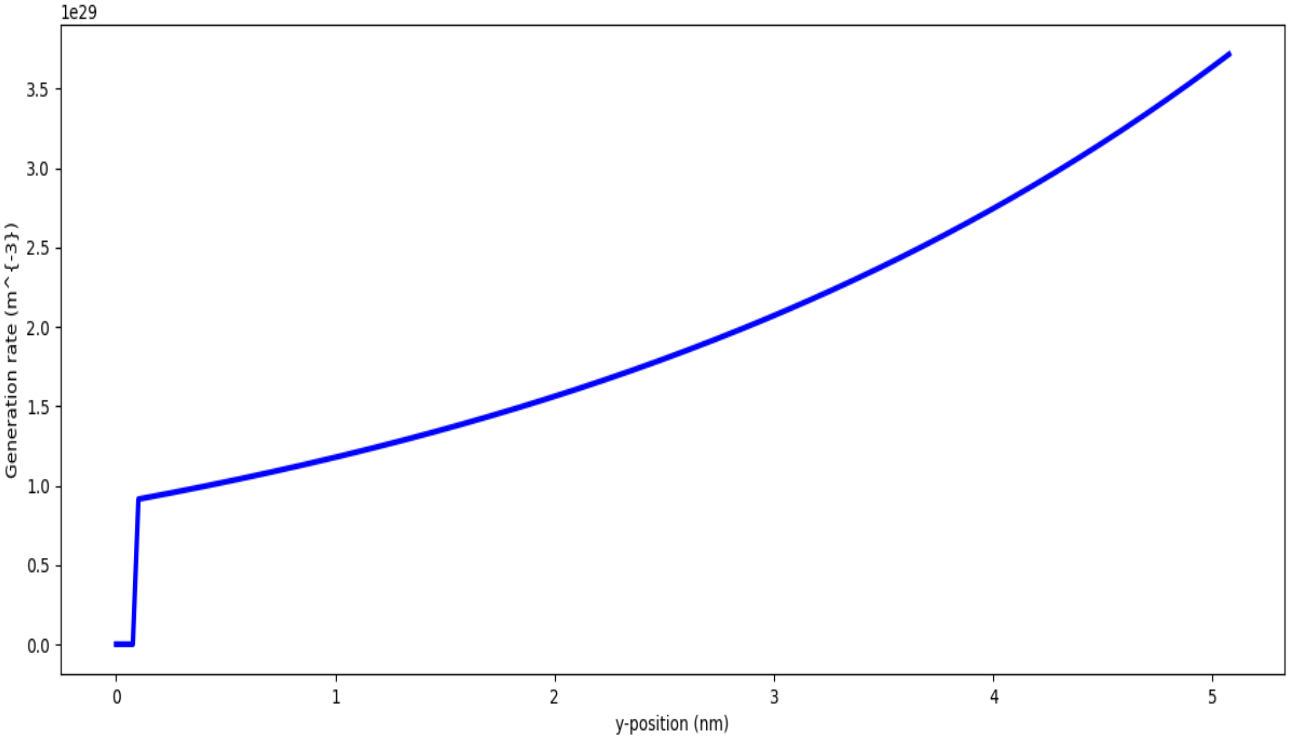

(II.c): At light intensity 0.1 W.cm^{-2}

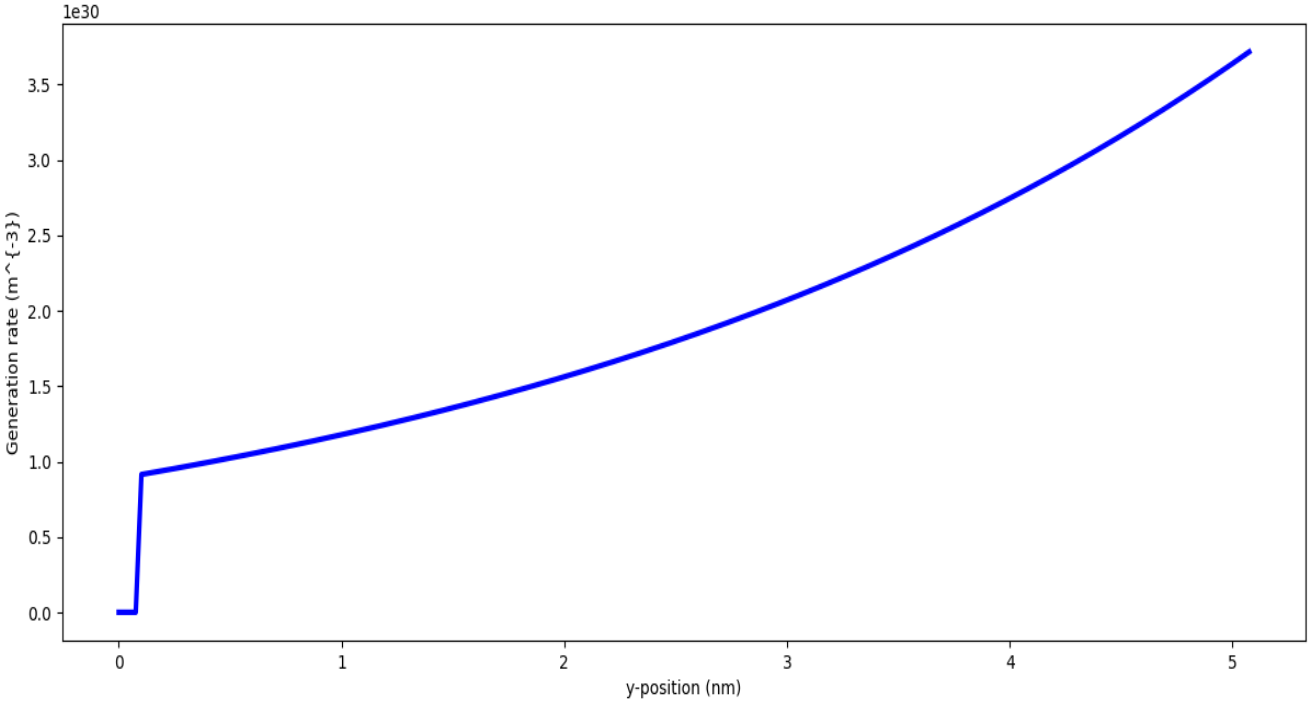

(III.c): At light intensity 1 W.cm^{-2}

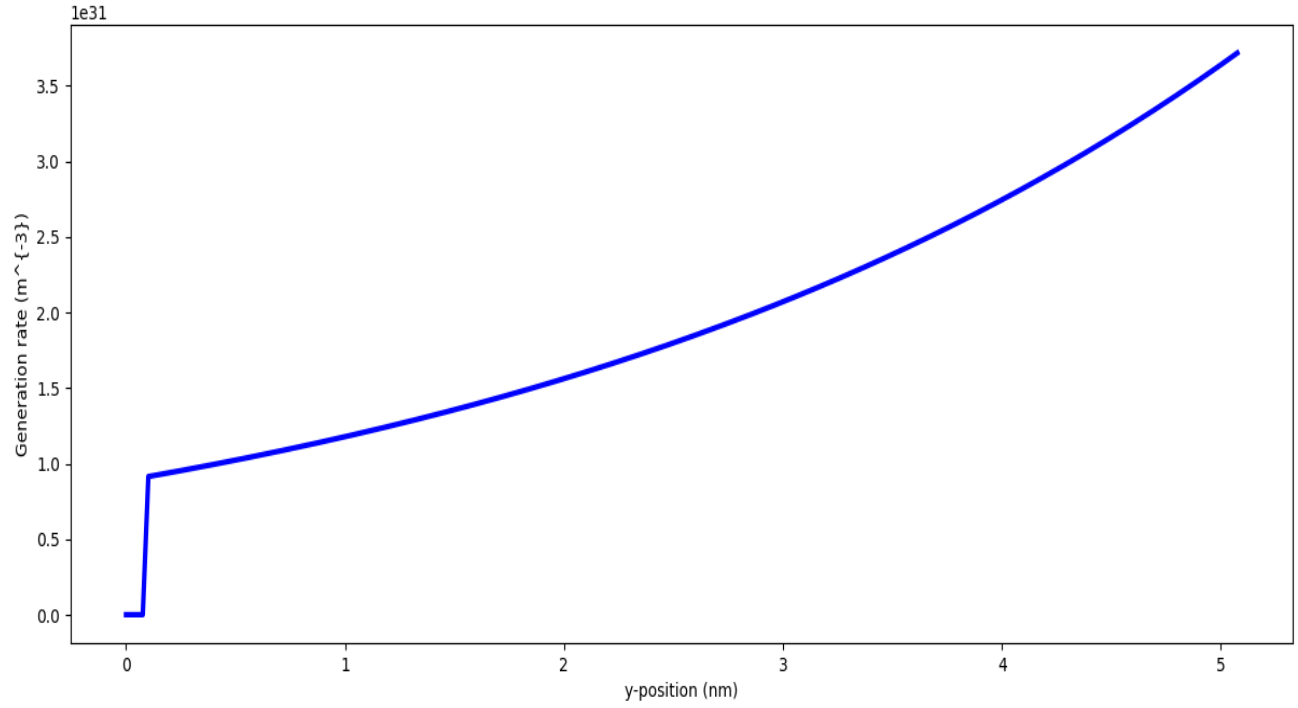

(IV.c): At light intensity 10 W.cm^{-2}

Fig. 5.11(C) [(I.c), (II.c),(III.c),(IV.c)] : Curves of Charge carrier generation rate (Y-axis) vs Y-position (X-axis) for film thickness 50Å of Cu_xN sample for different input light intensities i.e. 0W.cm^{-2}, 0.1W.cm^{-2}, 1W.cm^{-2} and 10W.cm^{-2} as represent (I.c), (II.c), (III.c), and (IV.c) respectively.

Generation of a free electron in the conduction band of a semiconductor results in the formation of a corresponding electron vacancy i.e. an equivalent positive charge or hole in its valence band. It was clear from the above characteristic curves that the generation rate of free electrons and holes (i.e. charge carriers) generated increased with an increase in light intensity for Cu_xN films of all thickness. The charge carrier generation rate is defined as the rate of electron-hole pair formation in a semiconducting material per unit volume and time. For the 50µm film, the maximum charge carrier generation rate was $4x10^{28}m^{-3}s^{-1}$ at $0.1W.cm^{-2}$ light intensity as seen from Fig.5.11(A)(II.a). The maximum carrier generation rate increased to $4x10^{29}m^{-3}s^{-1}$ and then finally to $4x10^{30}m^{-3}s^{-1}$ with an increase in light intensity from $1W.cm^{-2}$ as seen from Fig.5.11(A)(III.a) to $10W.cm^{-2}$ as seen from Fig. 5.11(A)(IV.a) respectively. For the 50µm film, carriers were found to be generated at the y=0µm plane for all light intensities as evident from Fig.5.11(A)(II.a), Fig. 5.11(A) (III.a) and Fig.5.11(A)(IV.a) respectively. The maximum charge carrier generation rate for the 50nm film was $2.5x10^{34}m^{-3}s^{-1}$ at y=50nm position at $0.1W.cm^{-2}$ light intensity as seen from Fig.5.11(B)(II.b), $2.5x10^{35}m^{-3}s^{-1}$ at y=50nm position at $1W.cm^{-2}$ light intensity as seen from Fig.5.11(B)(III.b) and $2.5x10^{36}m^{-3}s^{-1}$ at y=50nm position at $10W.cm^{-2}$ light intensity as seen from Fig.5.11(B)(IV.b) respectively. The charge generation rate remained zero up to the y=30nm position and then started increasing exponentially with a maximum value at y=50nm position i.e. at the surface of the film at all light intensities. The maximum charge carrier generation rate for the 50Å film was $3.5x10^{29}m^{-3}s^{-1}$ at $0.1W.cm^{-2}$ light intensity as seen from Fig.5.11(C)(II.c), $3.5x10^{30}m^{-3}s^{-1}$ at $1W.cm^{-2}$ light intensity as seen from Fig.5.11(C)(III.c) and $3.5x10^{31}m^{-3}s^{-1}$ at $10W.cm^{-2}$ light intensity as seen from Fig.5.11(C)(IV.c) respectively. The carrier generation rate increased parabolically from y=0Å position to y=50Å position and was maximum at the surface of the semiconductor for all light intensities. At a particular light intensity, the maximum carrier generation rate was observed for the 50nm thin film, while the least was observed for the 50µm thin film. The carrier generation rate was lowest for the 50µm film because the light incident upon that film got scattered and net light absorption was low in this case. The carrier generation was lower in the 50Å film as compared to the 50nm one because of higher electron-hole binding energy in the former as compared to the latter. The carrier generation is maximum in 50nm film because higher absorption of light since greater surface-to-volume ratio compare to others.

Various photoconductive parameters obtained by software simulation for 0.6(M) Cu_xN thin films of different thicknesses are mentioned in Table 5.2 given below.

Table 5.2: Simulation Results of Cu_xN film of Photoconductive Analysis

Parameters / **Sample Thickness**	**Charge Density ($C.m^{-3}$)**	**Cut-in Voltage (V)**	**Recombination Prefactor ($m^{-6}.s^{-1}$)**	**Carrier Generation Rate ($m^{-3}.s^{-1}$)**
50µm	$2x10^{23}$	1.4	$3.5x10^{-19}$	$4x10^{30}$
50nm	$3x10^{25}$	1.25	$1.2x10^{-23}$	$2.5x10^{36}$

50Å	$3x10^{23}$	1.25	$1.2x10^{-18}$	$3.5x10^{31}$

The photoconductive parameters (i.e. charge density, cut-in voltage, recombination prefactor and carrier generation rate) of the simulated Cu_xN semiconductor of varying thickness i.e. 50µm, 50nm and 50Å are mentioned in Table 5.2. The values of charge density, cut-in voltage, recombination prefactor and carrier generation rate of the 50µm thin film were $2x10^{23}C.m^{-3}$, 1.4V, $3.5x10^{-19}m^{-6}.s^{-1}$ and $4x10^{30}m^{-3}.s^{-1}$ respectively. The values of charge density, cut-in voltage, recombination prefactor and carrier generation rate of the 50nm thin film were $3x10^{25}C.m^{-3}$, 1.25V, $1.2x10^{-23}m^{-6}.s^{-1}$ and $2.5x10^{36}m^{-3}.s^{-1}$ respectively. The values of charge density, cut-in voltage, recombination prefactor and carrier generation rate of the 50Å thin film were $3x10^{23}C.m^{-3}$, 1.25V, $1.2x10^{-18}m^{-6}.s^{-1}$ and $3.5x10^{31}m^{-3}.s^{-1}$ respectively. The highest charge density, carrier generation rate and lowest recombination prefactor were observed for the 50nm thin film indicating maximum available free charge carriers and hence the best photoconductive performance compared to others. Thus 50 nm thickness is the optimum thickness and it has been considered to be used in photovoltaic applications in this present work.

5.3.3 Comparative Study of Photoconductive parameters of simulated Cu_xN film with conventional thin film semiconducting materials

The photoconductive parameters of the simulated 50nm Cu_xN thin film are compared with the experimental results of conventional semiconducting materials, as shown in Table 5.3.

Table 5.3: Photoconductive Parameters of Simulated 0.6(M) Cu_xN (50nm thickness) film: Comparison with Conventional Semiconducting Material

Parameters / **Semi-conducting Materials**	**Charge Density ($C.m^{-3}$)**	**Cut-in Voltage (V)**	**Recombination Prefactor ($m^{-6}.s^{-1}$)**	**Carrier Generation Rate ($m^{-3}.s^{-1}$)**
Cu_xN(50nm) (Simulated)	$3x10^{25}$	1.25	$1.2x10^{-23}$	$2.5x10^{36}$
Si	$1x10^{16}$ [67]	0.6 [68]	$2x10^{-22}$ [69]	$2.86x10^{27}$[70]
CdTe	$5x10^{14}$ [71]	0.8 [72]	$1.1x10^{-21}$ [73]	$7x10^{30}$ [74]
GaAs	$2.1x10^{15}$ [75]	1.2 [76]	$7.2x10^{-19}$ [77]	$1.2x10^{28}$ [70]

Silicon is the most abundant optoelectronic material currently used, while CdTe is a very efficient II-VI semiconductor and GaAs is a prominent III-V semiconductor. The values of charge density, cut-in voltage, recombination prefactor and carrier generation rate of the 50nm thin film were $3x10^{25}C.m^{-3}$, 1.25V, $1.2x10^{-23}m^{-6}.s^{-1}$ and $2.5x10^{36}m^{-3}.s^{-1}$ respectively. The experimental values of charge density, cut-in voltage, recombination prefactor and carrier generation rate of Si were $1x10^{16}C.m^{-3}$, 0.6V, $2x10^{-22}m^{-6}.s^{-1}$ and $2.86x10^{27}m^{-3}.s^{-1}$ respectively. The experimental values of charge density, cut-in voltage, recombination prefactor and carrier

generation rate of CdTe were $5x10^{14}C.m^{-3}$, 0.8V, $1.1x10^{-21}m^{-6}.s^{-1}$ and $7x10^{30}m^{-3}.s^{-1}$ respectively. The experimental values of charge density, cut-in voltage, recombination prefactor and carrier generation rate of GaAs were $2.1x10^{15}C.m^{-3}$, 1.2V, $7.2x10^{-19}m^{-6}.s^{-1}$ and $1.2x10^{28}m^{-3}.s^{-1}$ respectively. It can be observed from Table 5.3 that the charge density and carrier generation rate of the simulated Cu_xN thin film of 50nm thickness were significantly higher while its recombination prefactor was lower than those of other conventional semiconductors thereby making Cu_xN a promising semiconducting material for photoconductive applications. The detailed photoconductive analysis involving variation of thin film thickness in different units (i.e. 50 μm, 50 nm and 50 Å) is complicated while performing practical experimentation. However, performing the same analysis using the current technique produces accurate results compatible with practical ones and can be adopted instead of practical photoconductive performance analysis.

5.3.4 Study of Photovoltaic Characteristics

The optoelectronics characteristics of a photovoltaic cell formed by using the fabricated 0.6 (M) Cu_xN optimized annealed film first as an absorber layer (50nm thickness) and then as a window layer (20nm) have been obtained by performing computer simulations using Oghma Nano software.

The theory of the photovoltaic effect is used to predict the characteristics of a semiconductor which would operate with an optimum efficiency as a photovoltaic solar energy converter. The existence of such an optimum material results from the interaction between the optical properties of the semiconductor which determine what fraction of the solar spectrum is utilized and its electrical properties which determine the maximum efficiency of conversion into electricity. Considerable attention is devoted to the effect of the forbidden energy gap (Eg) of the semiconductor. It is shown that atmospheric absorption causes a shift in the solar spectrum which changes the value of the optimum forbidden energy gap between the limits 1.2 eV< Eg< 1.6 eV. The light is absorbed by the semiconducting material when the incident photon energy is greater than or equal to the band gap energy of a material. Thus, the bandgap of a semiconducting material is a very important parameter for photovoltaic applications. The high optical band gap of a material signifies only high-energy photons can be absorbed to excite electrons and lower-energy photons with less energy than the band gap pass straight through the material, leading to less of the solar spectrum being utilized as well as reduced efficiency. On the other hand, low band gap materials allow for the absorption of a wider range of photons, including lower-energy ones. However, if the photon energy is much higher than the band gap, the excess energy is quickly lost as heat energy. This phenomenon significantly reduces the energy that can be converted into electricity. Thus, the optimum band gap should be chosen such that it can absorb a significant portion of the solar spectrum while minimizing energy loss from high-energy photons. The optimum band gap for crystalline Si solar cells lies between 1.1 to 1.5 eV. The generation of photo-voltage depends on the fermi energy difference of the n-type and p-type sides of the junction. If considered, the values of the electron affinity of the n-type and p-type sides are almost the same, then the fermi energy difference (as well as the photo-voltage) of the p-n junction depends on the band gaps of the pair of the heterojunction. It has been observed that the increased band gaps (up to

an optimum limit) of a pair of heterojunctions increase the efficiency. However, photon energy with a value lower than the band gap cannot produce photo-voltage. The rate of change of drift velocity of the carriers with respect to. the rate of change of the electric field is called mobility. This electric field is produced due to built-in potential generated at the space charge region of the p-n junction of the cell. When photon energy is absorbed by the cell, then excess electron-hole pairs are generated, and these excess carriers produce current. The generated excess carriers separate and produce current through the circuit by the influence of the electric field at the space charge region. The recombination of the carriers may occur due to defects and impurities in the material. The recombination can reduce short-circuit current density as well as overall efficiency of the photovoltaic cell. If the mobility of the carriers is high, then charge carriers reach the electrodes faster, which reduces recombination and increases power output as well as efficiency. On the other hand, low carrier mobility results in lower current, reduced power output, and lower efficiency due to increased recombination losses [77.(1)].

When Cu_xN was used as the absorber layer of a photovoltaic cell, then a semiconductor having an optical bandgap greater than that of Cu_xN i.e. 1.75eV [78] was employed as its window layer. In the present work, CdS having a bandgap 2.42eV [79] and ZnO having a bandgap of 3.3eV [80] were used as window layers respectively for allowing electromagnetic radiation up to visible range to be transmitted into the absorber layer. The schematic representation of solar cells with Cu_xN as absorber layer with CdS and ZnO window layers under 1 Sun light intensity are shown in Fig. 5.12.a and Fig. 5.12.b respectively.

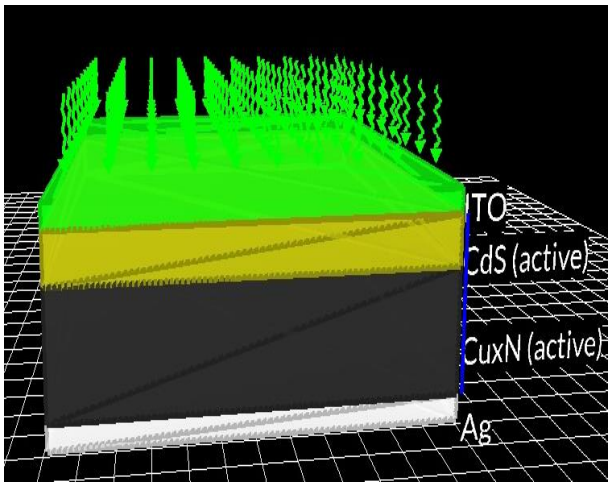

Fig. 5.12.a: CdS (window layer)-Cu_xN (absorber layer) based solar cell under 1Sun light intensity

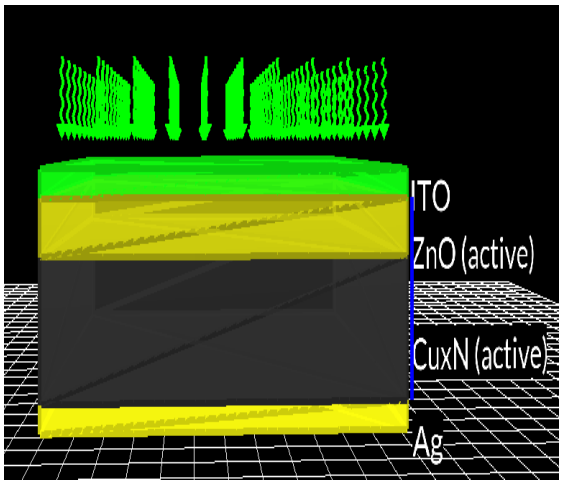

Fig. 5.12.b: ZnO (window layer)-Cu_xN (absorber layer) based solar cell under 1Sun light intensity

When Cu_xN was used as the window layer of a photovoltaic cell, then a semiconductor having an optical bandgap less than that of Cu_xN i.e. 1.75eV was employed as the cell's absorber layer. Here PbSe having a bandgap of 0.27eV [81] and InAs having a bandgap of

0.36eV [82] were used as absorber layers respectively for effectively producing charge carriers. The schematic representation of solar cells with Cu_xN as window layer with PbSe and InAs absorber layers under 1Sun light intensity are shown in Fig. 5.13.a and Fig. 5.13.b respectively.

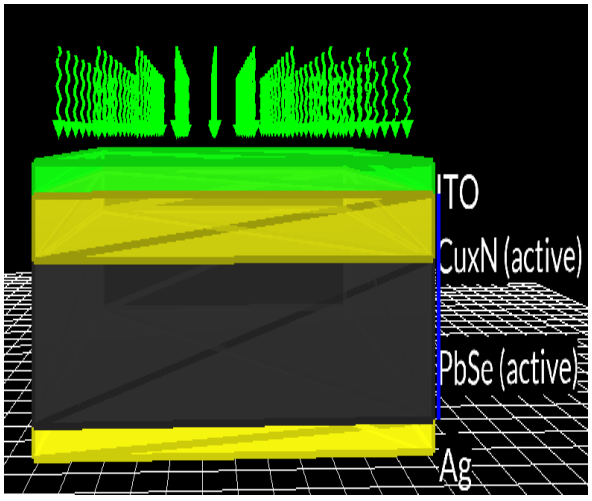

Fig. 5.13.a: Cu_xN (window layer) -PbSe (absorber layer) based solar cell under 1Sun light intensity

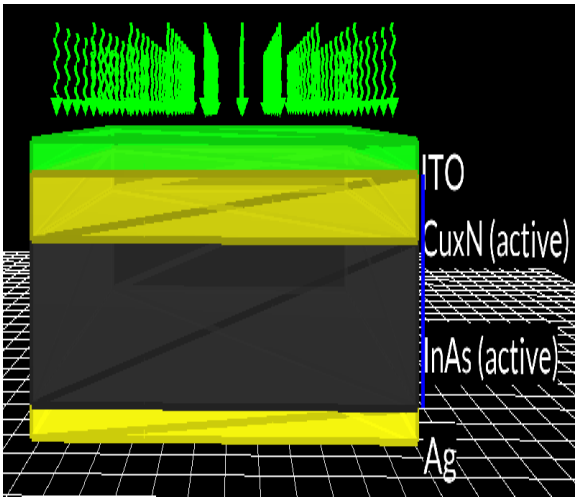

Fig. 5.13.b: Cu_xN (window layer) - InAs (absorber layer) based solar cell under1Sun light intensity

Indium tin oxide (ITO) and silver (Ag) were used as front contact and back contact of the solar cells respectively. The thickness of the window layer, absorber layer and contact layers were maintained at 20nm, 50nm and 10nm respectively. The detailed photovoltaic characteristics have been studied here by considering Cu_xN as an absorber layer in which CdS and ZnO act as a window layer, whereas Cu_xN acts as a window layer in which PbSe and InAs act as absorber layers. Finally, the optimum performance of Cu_xN, either as an absorber or window layer, has been determined in this present study.

The photovoltaic performances of the fabricated optimized Cu_xN film are described here. The total charge density vs applied voltage, current vs applied voltage, recombination prefactor vs excess carrier density, and charge carrier generation rate vs Y-position characteristics have been studied of Cu_xN based solar cells with various inorganic semiconductors at 1Sun light intensity.

The Total charge density (Y-axis) vs Applied voltage (X-axis) characteristics are shown in Figs. 5.14 [(a), (b), (c), (d)].

Total charge density (Y-axis) vs Applied voltage (X-axis) characteristics of Cu_xN based solar cells with various inorganic semiconductors

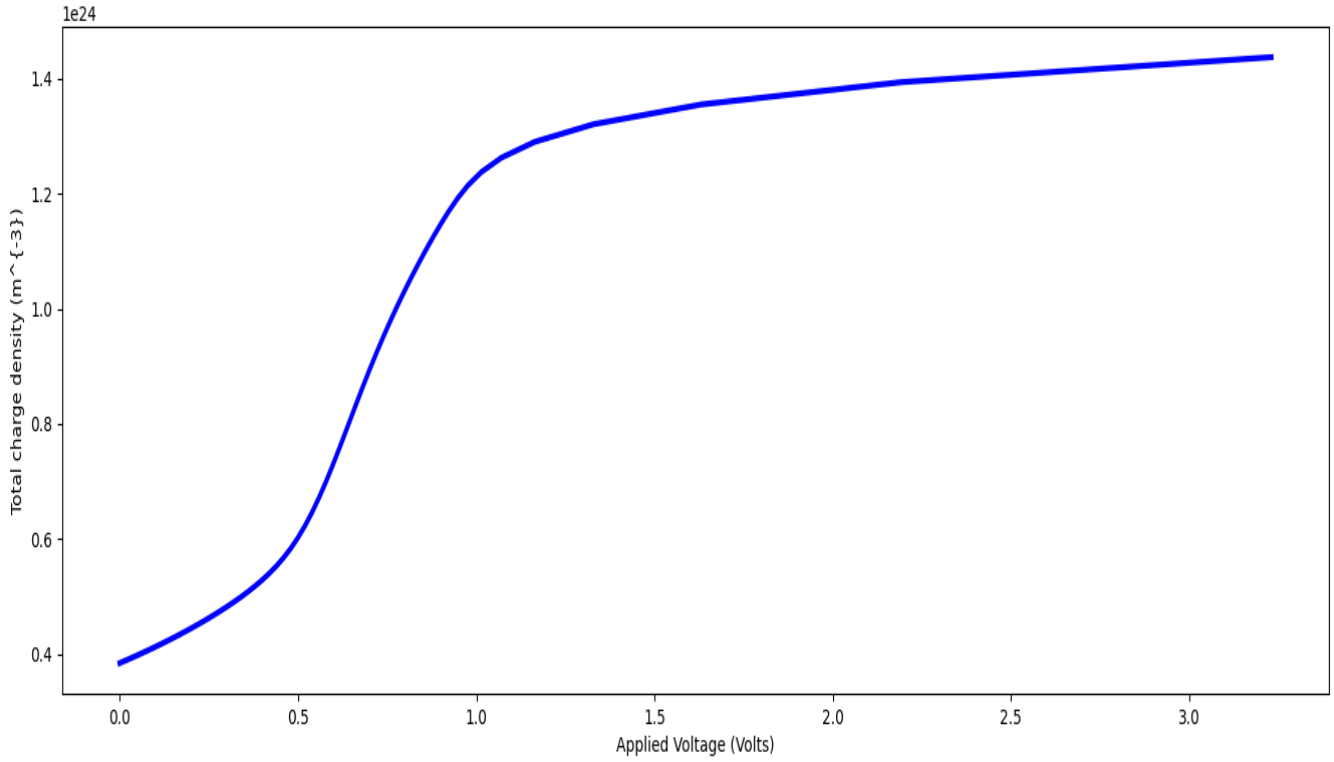

(a): CdS(window)-Cu_xN(absorber) Solar Cell

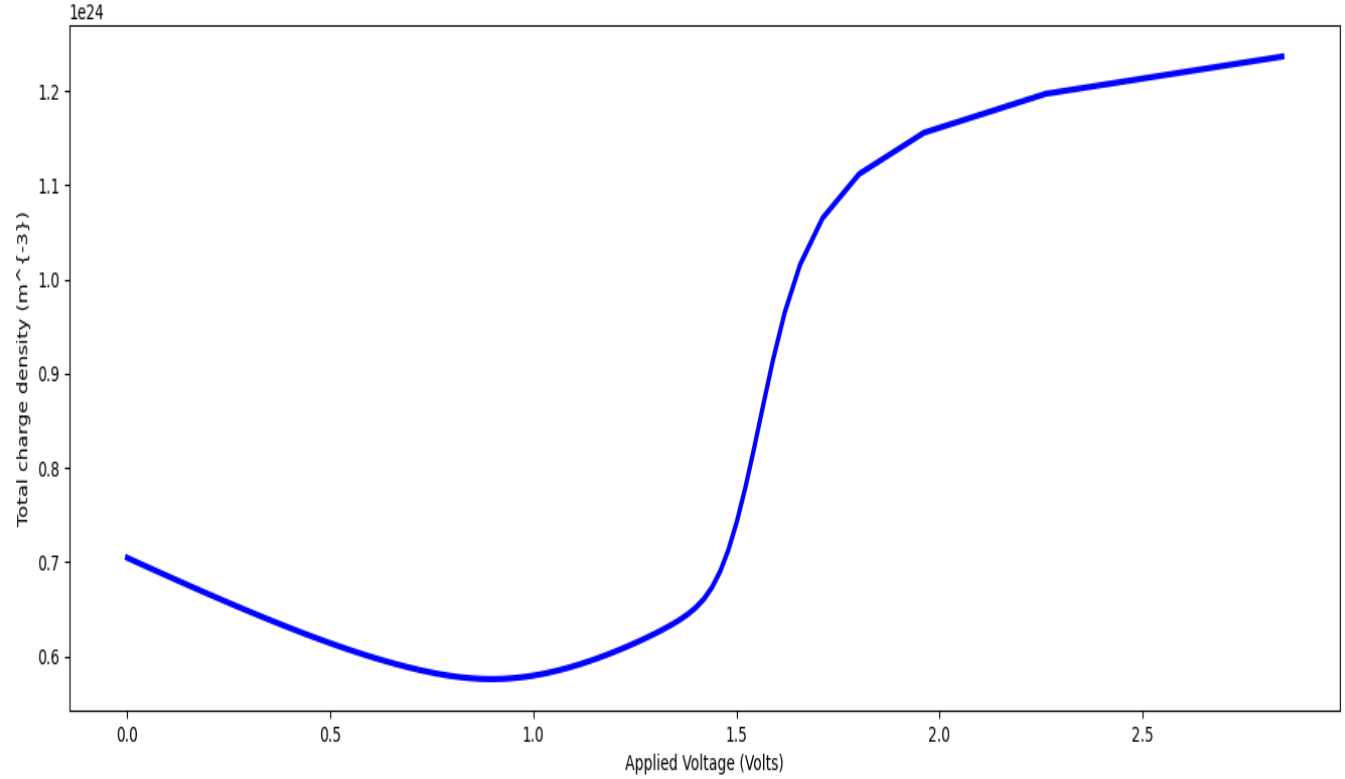

(b): ZnO(window)-Cu_xN(absorber) Solar Cell

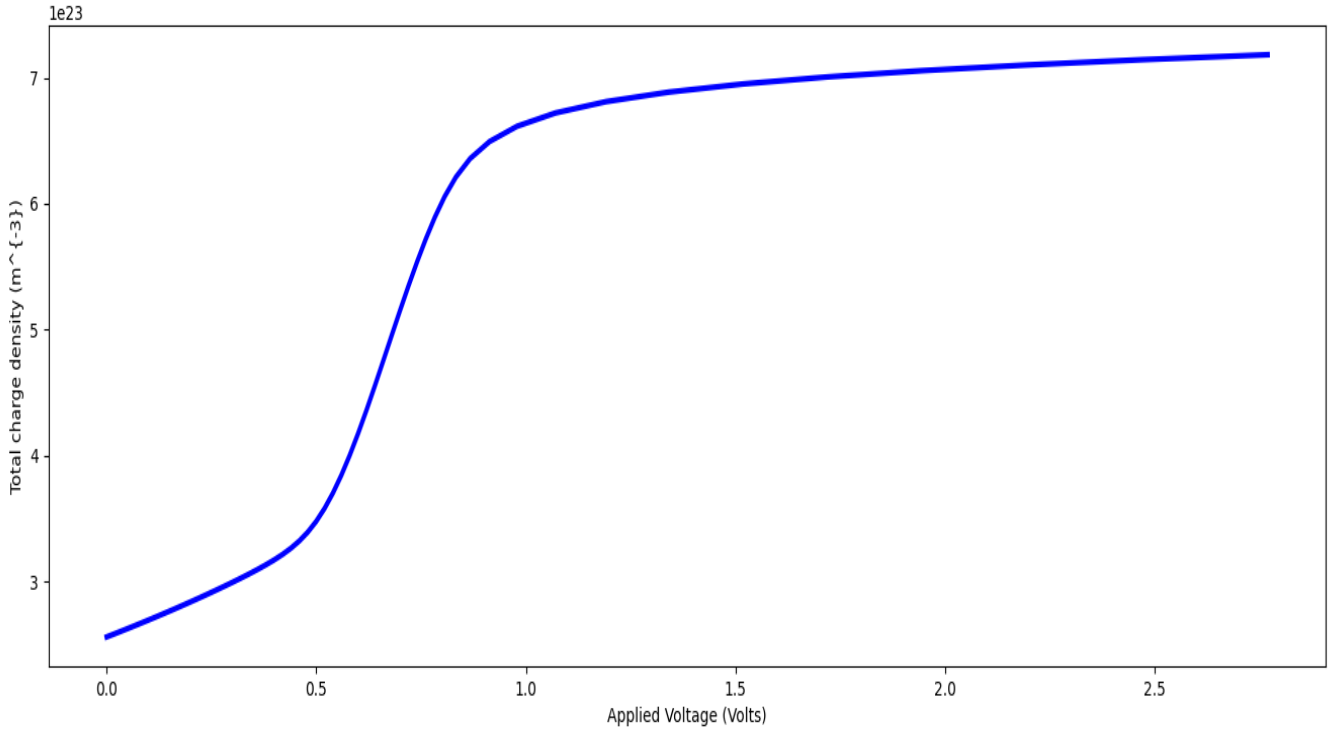

(c): Cu_xN(window)-PbSe (absorber) Solar Cell

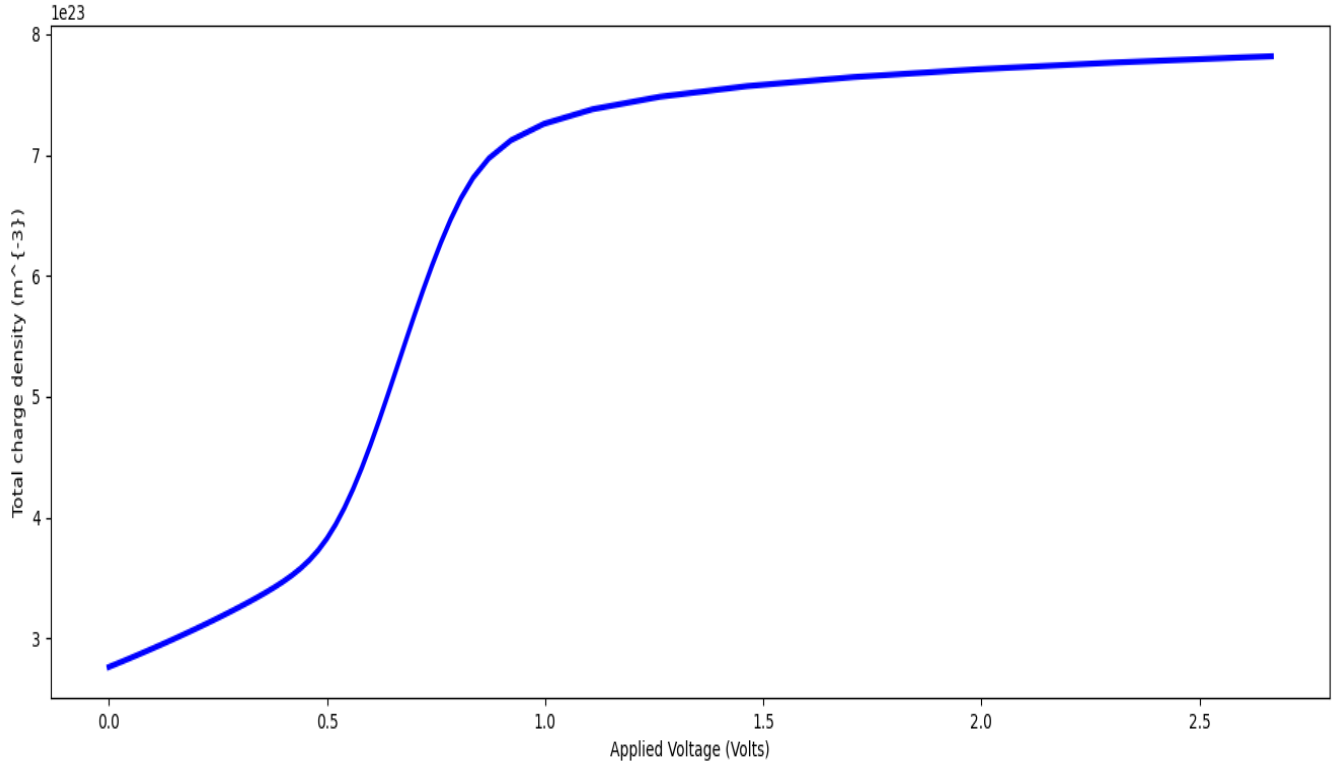

(d): Cu_xN(window)-InAs(absorber) Solar Cell

Fig. 5.14 [(a),(b),(c),(d)]: Total charge density (Y-axis) vs Applied voltage (X-axis) characteristics of Cu_xN based solar cells with various inorganic semiconductors at 1 Sun light intensity as represent (a), (b), (c) and (d) respectively.

The total charge density refers to the density of charges consisting of free electrons in the n-type semiconductor and holes in the p-type semiconductor of a solar cell. The total charge density is the charge accumulated per unit volume of a solar cell. The total charge density in a PV cell is dependent upon several factors like incident light intensity, absorber layer thickness, surface properties, mobility of charge carriers, carrier lifetime etc. The total charge density in a solar cell arises due to the presence of capacitance. Solar cell capacitance is contributed by mainly three factors: chemical capacitance arising from the response of charge carriers to an external optical or electrical perturbation, geometrical capacitance dependent upon the type and thickness of electrodes and solar cell architecture and capacitance contribution due to window and absorber layers [83, 84]. The nature of the total charge density vs applied voltage characteristics for the CdS-Cu_xN, Cu_xN-PbSe, Cu_xN-InAs solar cells is found to be similar. The total charge density vs applied voltage curve of the CdS-Cu_xN solar cell is described in Fig.5.14. (a). The charge density first increases linearly at a slower rate to $0.6x10^{24}C.m^{-3}$ with an increase in applied voltage from 0V to 0.5V. Then another linear increment in total charge density at a faster rate was observed from $0.6x10^{24}C.m^{-3}$ to $1.2x10^{24}C.m^{-3}$ with a corresponding increase in applied voltage from 0.5V to 1.0V followed by saturation at beyond applied voltage of 1.0V and finally reached at $1.4x10^{24}C.m^{-3}$.The total charge density vs applied voltage curve of the ZnO-Cu_xN solar cell is described in Fig.5.14.(b). The charge density first decreased linearly from $0.7x10^{24}C.m^{-3}$ to $0.6x10^{24}C.m^{-3}$ with an increase in applied voltage from 0V to 0.7V. Then a linear increase in charge density from $0.6x10^{24}C.m^{-3}$ to $0.7x10^{24}C.m^{-3}$ at a slower rate was observed with an increase in applied voltage from 1.0V to 1.5V. Then another linear increase in charge density but at a faster rate from $0.7x10^{24}C.m^{-3}$ to $1.2x10^{24}C.m^{-3}$ was observed with a corresponding increase in applied voltage from 1.5V to 2.0V beyond which saturation was reached. The total charge density vs applied voltage curve of the Cu_xN-PbSe solar cell is described in Fig.5.14.(c). The charge density first increased linearly at a slower rate from 0 $C.m^{-3}$ to $3x10^{23}C.m^{-3}$ with a corresponding increase in applied voltage from 0V to 0.5V, followed by another linear increase in total charge density at a fast rate from $3x10^{23}C.m^{-3}$ to $6x10^{23}C.m^{-3}$ with a rise in applied voltage from 0.5V to 1.0V and then finally saturation beyond 1.0V and finally reached at $7x10^{23}C.m^{-3}$. The total charge density vs applied voltage curve of the Cu_xN-InAs solar cell is described in Fig.5.14.(d). The charge density first increased linearly at a slower rate from $3x10^{23}C.m^{-3}$ to $4x10^{23}C.m^{-3}$ with an increase in applied voltage from 0V to 0.5V, followed by a further linear increase of total charge density at a faster rate from $4x10^{23}C.m^{-3}$ to $7x10^{23}C.m^{-3}$ with an increase in applied voltage from 0.5V to 1.0V and then finally saturation beyond the applied voltage of 1.0V and finally reached at $8x10^{23}C.m^{-3}$. The maximum charge density was highest for the CdS-Cu_xN solar cell, i.e., $1.4x10^{24}C.m^{-3}$ followed by the ZnO-Cu_xN solar cell, i.e., $1.2x10^{24}C.m^{-3}$, the Cu_xN-InAs solar cell, i.e., $8x10^{23}C.m^{-3}$, and the Cu_xN-PbSe solar cell, i.e., $7x10^{23}C.m^{-3}$. The charge accumulation was thus higher in solar cells with Cu_xN as an absorber layer than in the cells with Cu_xN as a window layer. Current (Y-axis) vs Applied voltage (X-axis) characteristics are shown in Figs.5.15 [(a), (b), (c), (d)].

Current (Y-axis) vs Applied voltage (X-axis) characteristics of Cu_xN based solar cells with various inorganic semiconductors

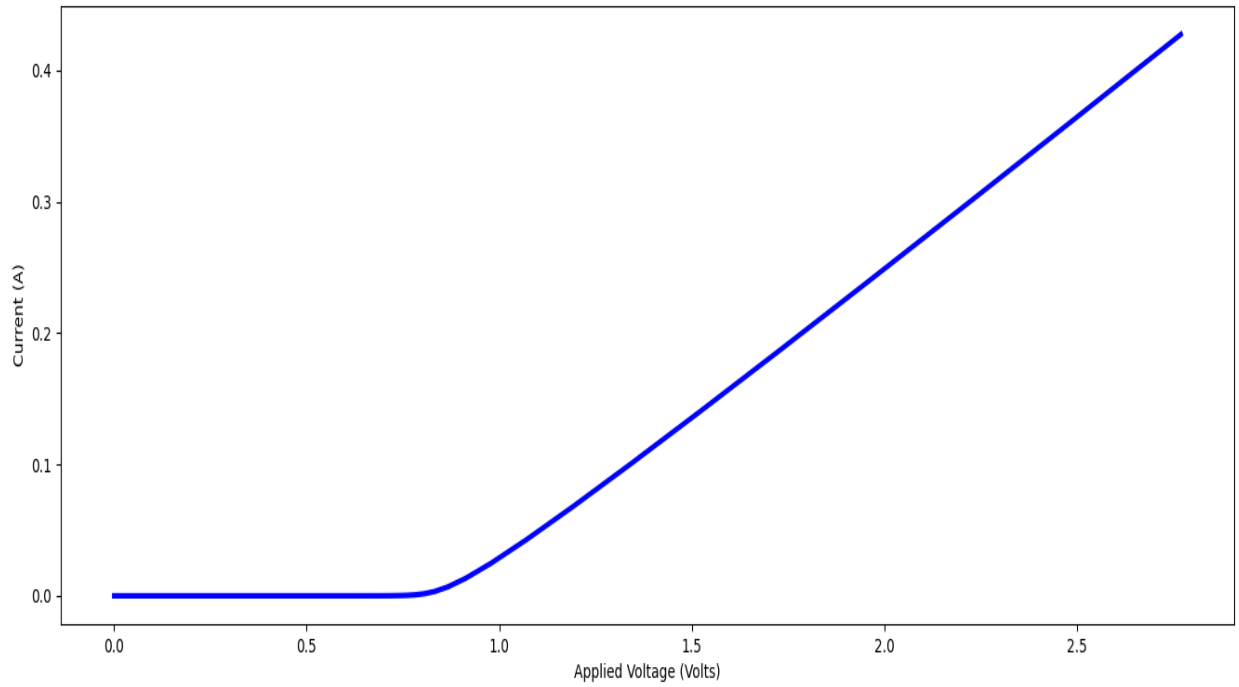

(a): CdS(window)-Cu_xN(absorber) Solar Cell

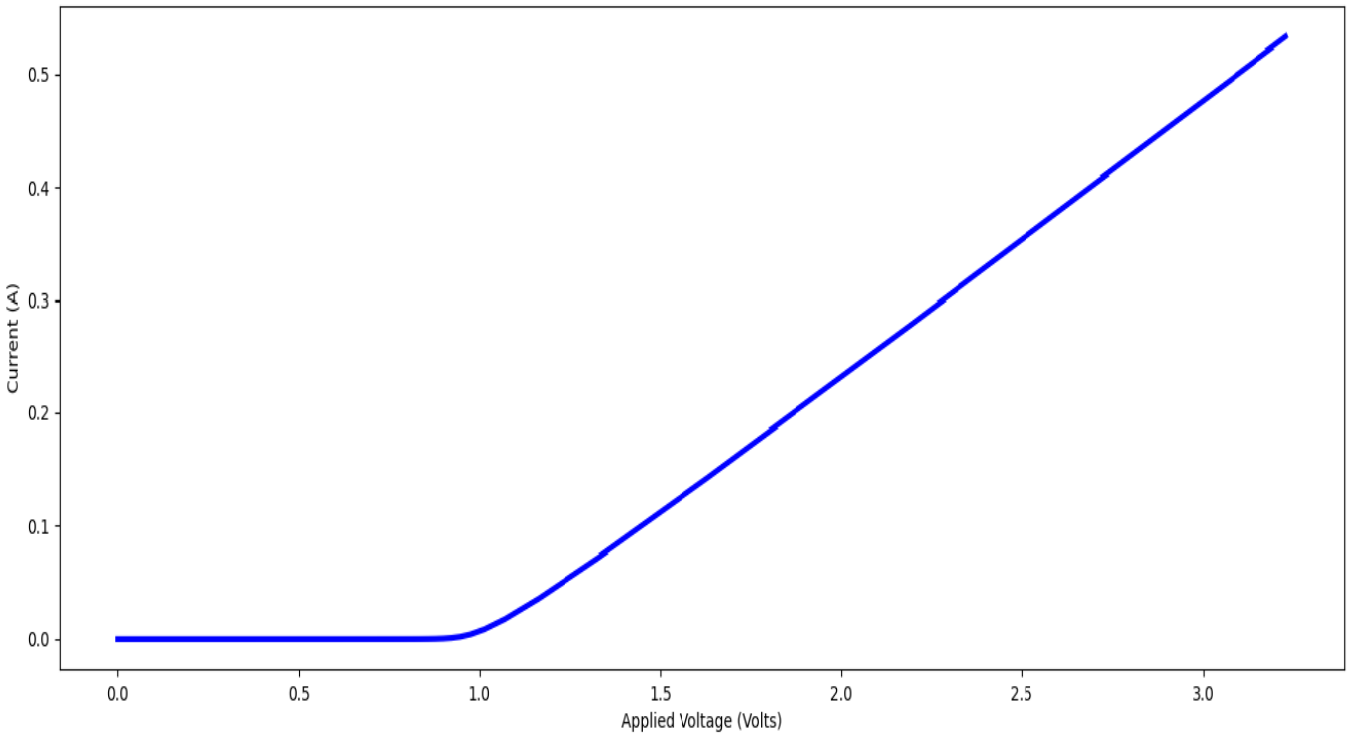

(b): ZnO(window)-Cu_xN(absorber) Solar Cell

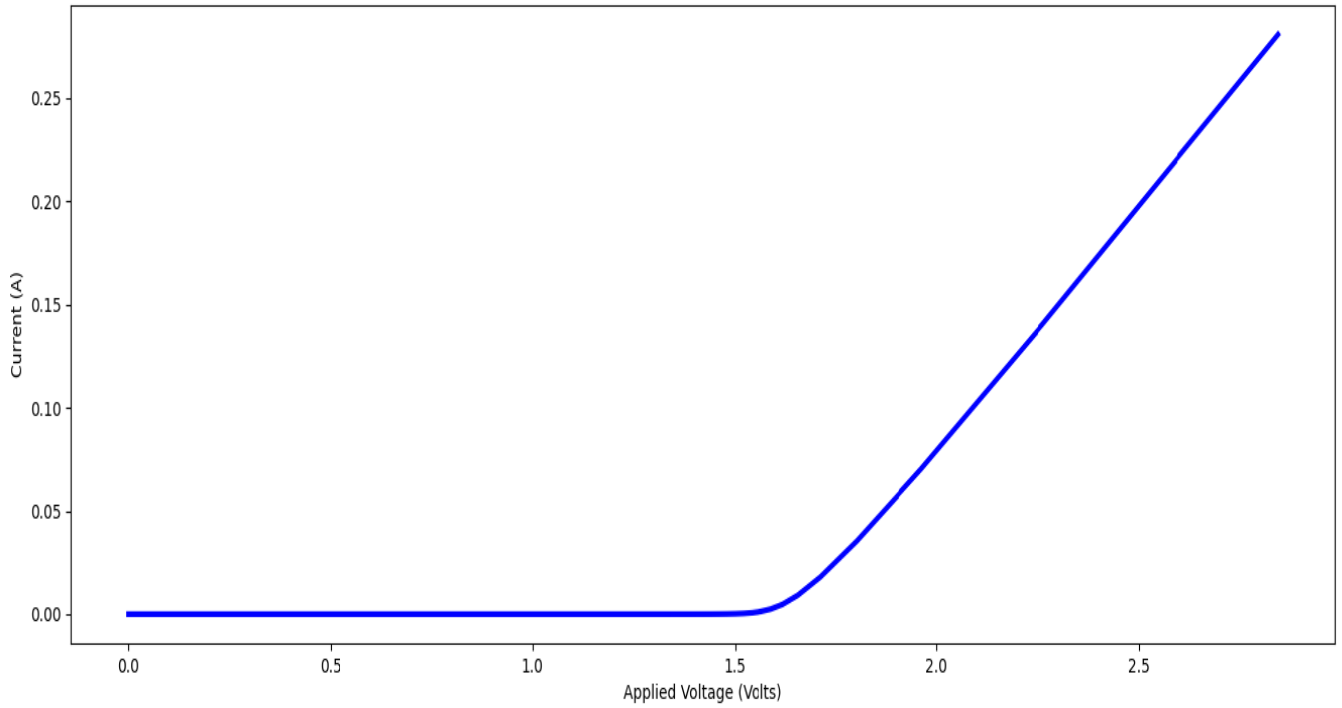

(c): Cu_xN(window)-PbSe(absorber) Solar Cell

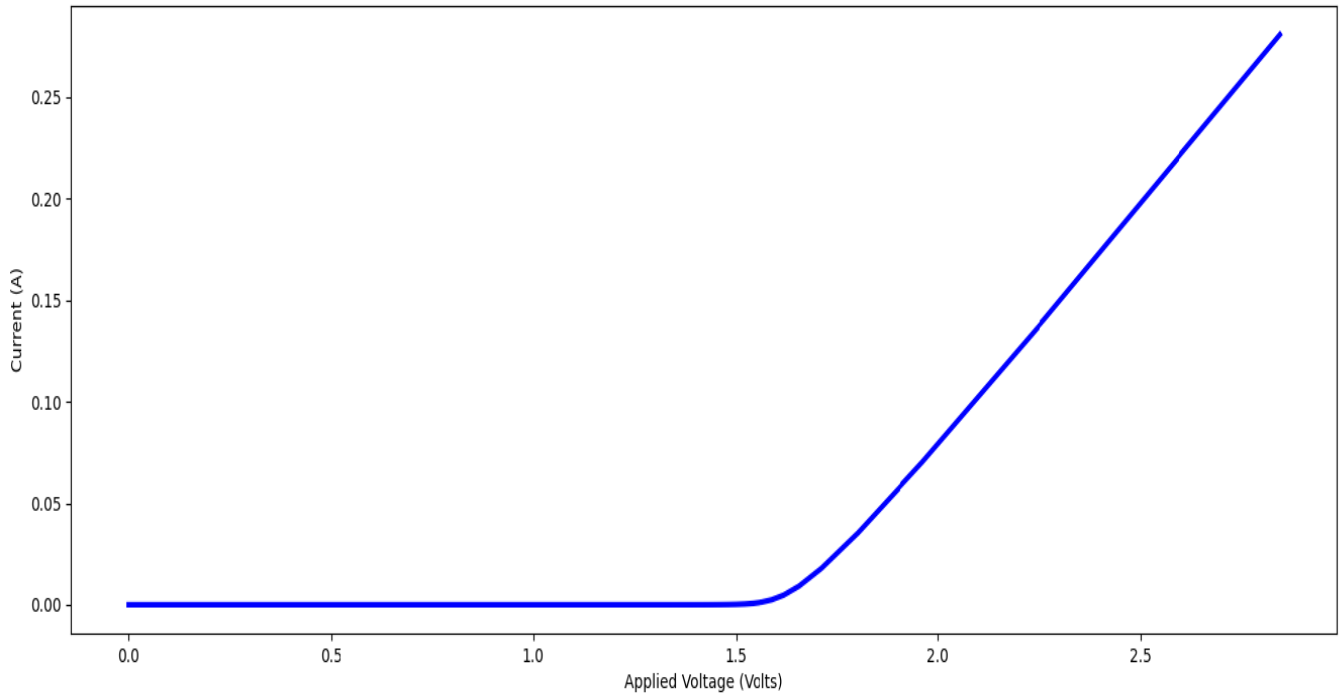

(d): Cu_xN(window)-InAs(absorber) Solar Cell

Fig. 5.15 [(a), (b), (c), (d)]: Current (Y-axis) vs Applied voltage (X-axis) characteristics of Cu_xN based solar cells with various inorganic semiconductors at 1Sun light intensity as represent (a), (b), (c) and (d) respectively.

The current-voltage (I-V) characteristic of a PV cell is basically a plot of all plausible working points within any suitable range. The I-V curve of a solar cell is basically a graphical representation of a solar cell operation. The I-V characteristics generally define the functionality of a solar cell at existing conditions of the environment and material characteristics in which the cell operates i.e. irradiance, temperature, material properties, cell design etc. The current-voltage characteristics in solar cells are generally rectifying in nature [85, 86]. The current-voltage (I-V) characteristics have been studied by considering Cu_xN as an absorber as well as window layers with various inorganic semiconductors in this present text. The I-V characteristics of the CdS-Cu_xN solar cell are mentioned in Fig.5.15.(a) from which it can be identified that after a cut-in voltage of 0.8V, the characteristics became linear in nature. From the I-V characteristics of the ZnO-Cu_xN solar cell in Fig.5.15.(b) it was clear that after a cut-in voltage of 1V, the characteristics became linear in nature. The I-V characteristics of the Cu_xN-PbSe solar cell are mentioned in Fig.5.15.(c) from which it was clear that the characteristics became linear after a cut-in voltage of 1.6V. The I-V characteristics of the Cu_xN-InAs solar cell are mentioned in Fig.5.15.(d) from which it was clear that the characteristics became linear after a cut-in voltage of 1.6V. The obtained I-V characteristics of the simulated solar cells were also found to be rectifying in nature. The current increases linearly with applied voltage after a certain threshold voltage known as cut-in voltage. The I-V characteristics specify the performance of a solar cell and the cell is turned on in the conduction mode after overcoming its cut-in voltage. The cut-in voltages of the cells with Cu_xN as the absorber layer were found to be much lower than the ones with Cu_xN as the window layers. The cut-in voltage of the CdS-Cu_xN cell was the lowest i.e. 0.8V as obtained from Fig. 5.15.(a) while that of the ZnO-Cu_xN cell was slightly higher i.e. 1V as obtained from Fig. 5.15.(b). The cut-in voltages of the two cells with the Cu_xN window layer were 1.6V as obtained from Fig.5.15.(c) and Fig.5.15.(d). The lowest cut-in voltage for the CdS-Cu_xN cell means that charge carriers in the cell required the least energy for achieving linear current conduction followed by the ZnO-Cu_xN cell and the maximum cut-in voltage for Cu_xN-PbSe and Cu_xN-InAs cells. The cut-in voltage was lower for the simulated solar cells with Cu_xN as an absorber layer than the ones with Cu_xN as a window layer. The cut-in voltage was minimum for the CdS-Cu_xN solar cell. The I-V characteristics of the simulated solar cells with Cu_xN as a window layer where PbSe and InAs act as absorber layers were similar in nature, with the same values of cut-in voltages, i.e., 1.6V. Thus, it can be concluded from the analysis of I-V characteristics that Cu_xN is more suitable for functioning as an absorber layer than the window layer of a solar cell.

Recombination prefactor vs Excess carrier density characteristics are shown in Figs.5.16 [(a), (b), (c), (d)].

Recombination prefactor vs Excess carrier density characteristics of Cu_xN based solar cells with various inorganic semiconductors

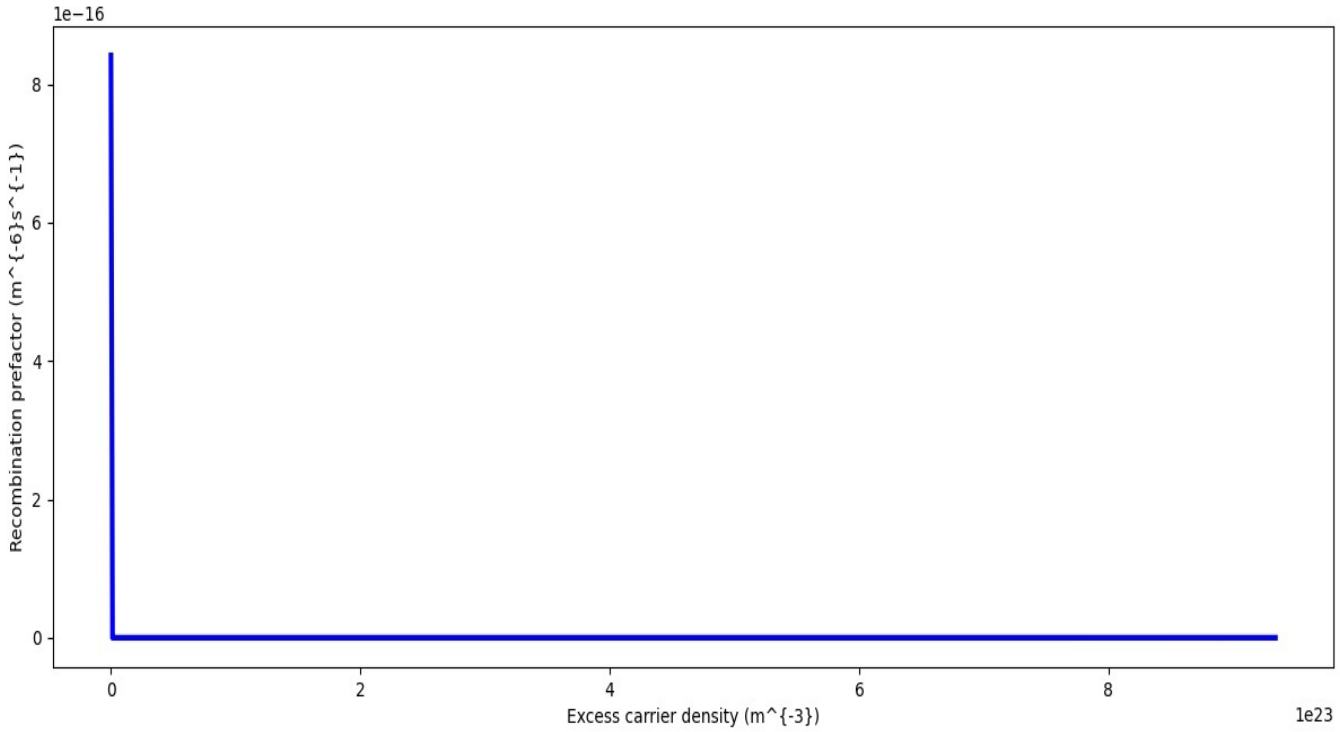

(a): CdS(window)-Cu_xN(absorber) Solar Cell

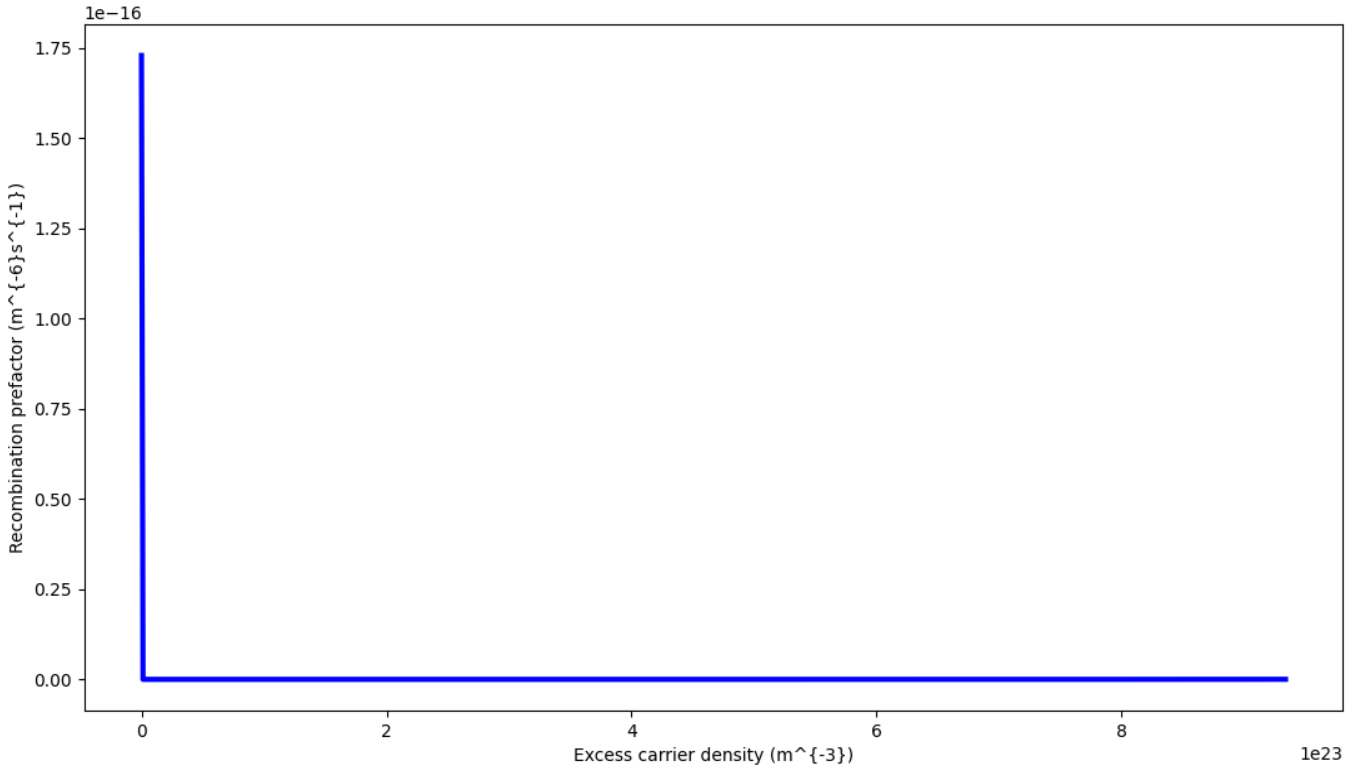

(b): ZnO(window)-Cu_xN(absorber) Solar Cell

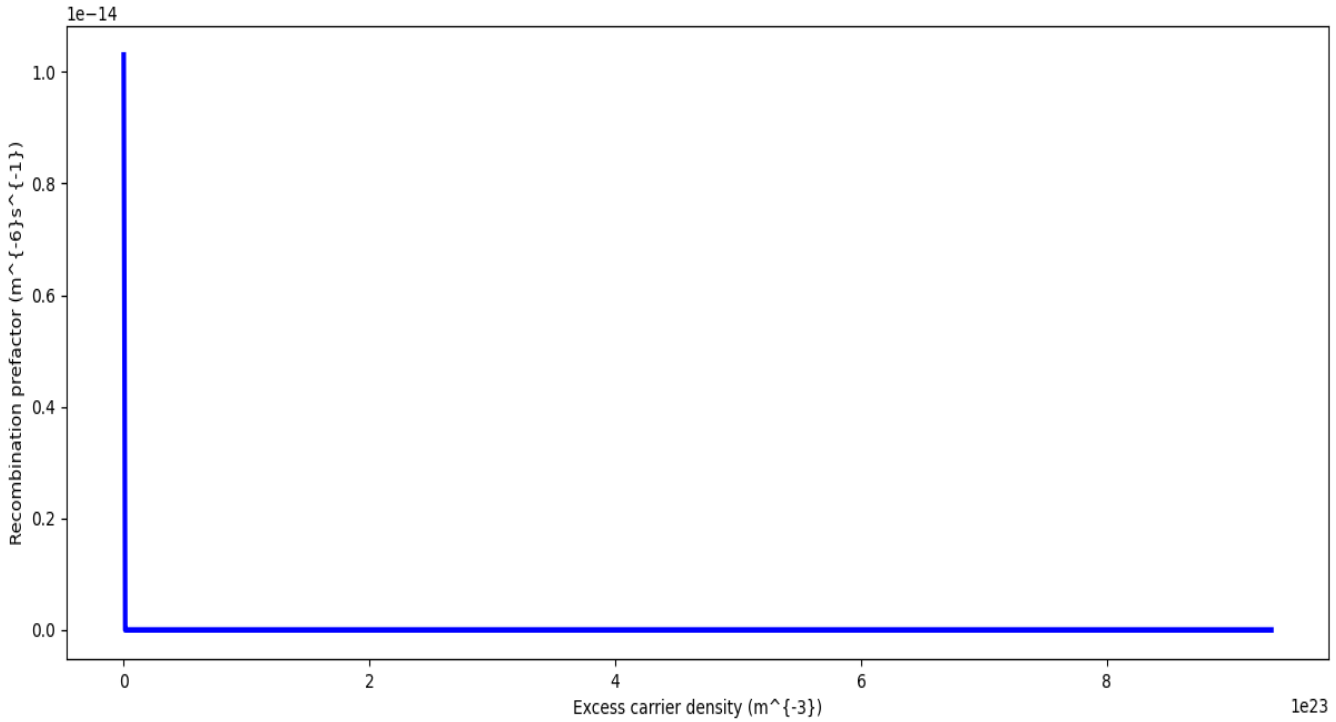

(c): Cu_xN(window)-PbSe(absorber) Solar Cell

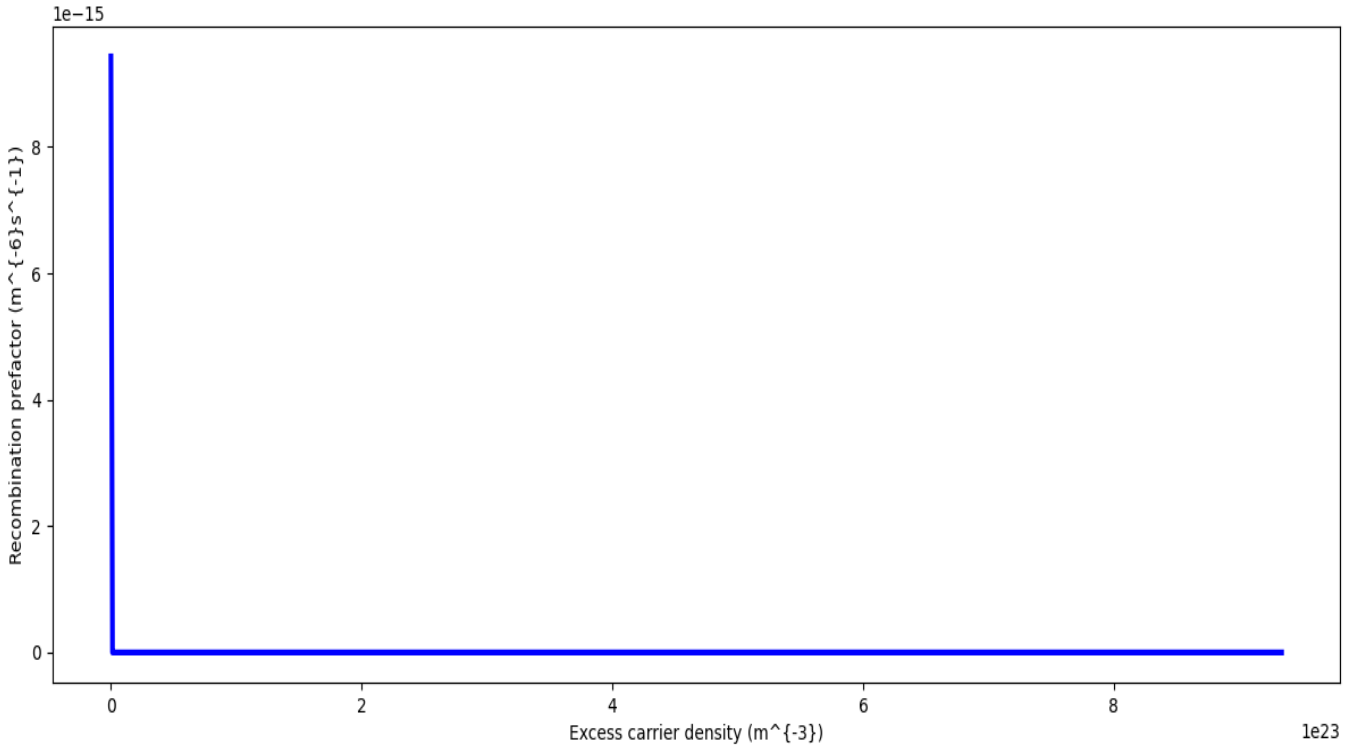

(d): Cu_xN(window)-InAs(absorber) Solar Cell

Fig.5.16[(a),(b),(c),(d)]: Recombination pre-factor (Y-axis) vs Excess carrier density (X-axis) characteristics of Cu_xN based solar cells with various inorganic semiconductors at 1Sun light intensity as represent (a), (b), (c) and (d) respectively.

Recombination in a solar cell result in the restoration of the non-equilibrium photogenerated free electron-hole pair population to its thermal equilibrium magnitude. Recombination in solar cells may be radiative or non-radiative in nature. Radiative recombination involves recombination of a free electron from the conduction band, and a hole in the valence band resulting in a decrease in electron energy level and a consequent photon emission. Non-radiative recombination involves dissipation of photogenerated carrier energy not by photon emission but by increasing the vibrational energy level of another charge carrier [87]. Recombination in solar cells results in increased voltage loss. Recombination prefactor is a measure of carrier recombination (both radiative and non-radiative) and hence a parameter of voltage loss analysis providing critical insights into energy conversion in solar cells [88]. Lower recombination prefactor results in enhancement of optical response by suppression of surface recombination velocity [89]. The recombination prefactor vs excess carrier density characteristics have been studied by considering Cu_xN as an absorber as well as window layers with various inorganic semiconductors in this present text. The recombination prefactor vs excess carrier density characteristics of the CdS-Cu_xN solar cell are mentioned in Fig.5.16.(a) with a recombination prefactor of $8x10^{-16}m^{-6}.s^{-1}$. The recombination prefactor vs excess carrier density characteristics of the ZnO-Cu_xN solar cell are mentioned in Fig.5.16.(b) with a recombination prefactor of $1.75x10^{-16}m^{-6}.s^{-1}$. The recombination prefactor vs excess carrier density characteristics of the Cu_xN-PbSe solar cell are mentioned in Fig.5.16.(c) with a recombination prefactor of $1x10^{-14}m^{-6}.s^{-1}$. The recombination prefactor vs excess carrier density characteristics of the Cu_xN-InAs solar cell are mentioned in Fig.5.16. (d) with a recombination prefactor of $9x10^{-15}m^{-6}.s^{-1}$. When charge carriers flow from their point of generation to a site of high recombination in a solar cell, then the recombination prefactor increases resulting in a decrease in carrier lifetime and photocurrent density respectively which alters solar cell operation from equilibrium. Recombination prefactor was lowest for the CdS-Cu_xN solar cell, i.e., $8x10^{-16}m^{-3}.s^{-1}$, as obtained from Fig.5.16.(a) whereas slightly higher in ZnO-Cu_xN, i.e., $1.75x10^{-16}m^{-3}.s^{-1}$ as obtained from Fig.5.16.(b) followed by Cu_xN-InAs, i.e., $9x10^{-15}m^{-3}.s^{-1}$ as obtained from Fig.5.16.(d) and highest for Cu_xN-PbSe, i.e.,$1.0x10^{-14}$ $m^{-3}.s^{-1}$ as obtained from Fig.5.16.(c). The recombination prefactor for all four simulated solar cells was recorded when excess carrier density was zero. However, in the presence of excess carrier density, the recombination prefactor of all four simulated solar cells was reduced to zero i.e. indicating increased carrier lifetime and hence sustained conduction. The recombination prefactor was lowest for the CdS-Cu_xN solar cell and highest for the Cu_xN-PbSe cell. It was also evident that recombination prefactors of the simulated solar cells with Cu_xN as the absorber layer were much less than the ones with Cu_xN as the window layer respectively. Thus, it can be concluded that solar cells with Cu_xN as an absorber layer must exhibit low recombination with better short-circuit current density and power conversion efficiency.

Charge carrier generation rate vs Y-position characteristics are shown in Figure 5.17 [(a), (b), (c), (d)].

Charge carrier generation rate vs Y-position characteristics of Cu_xN based solar cells with various inorganic semiconductors

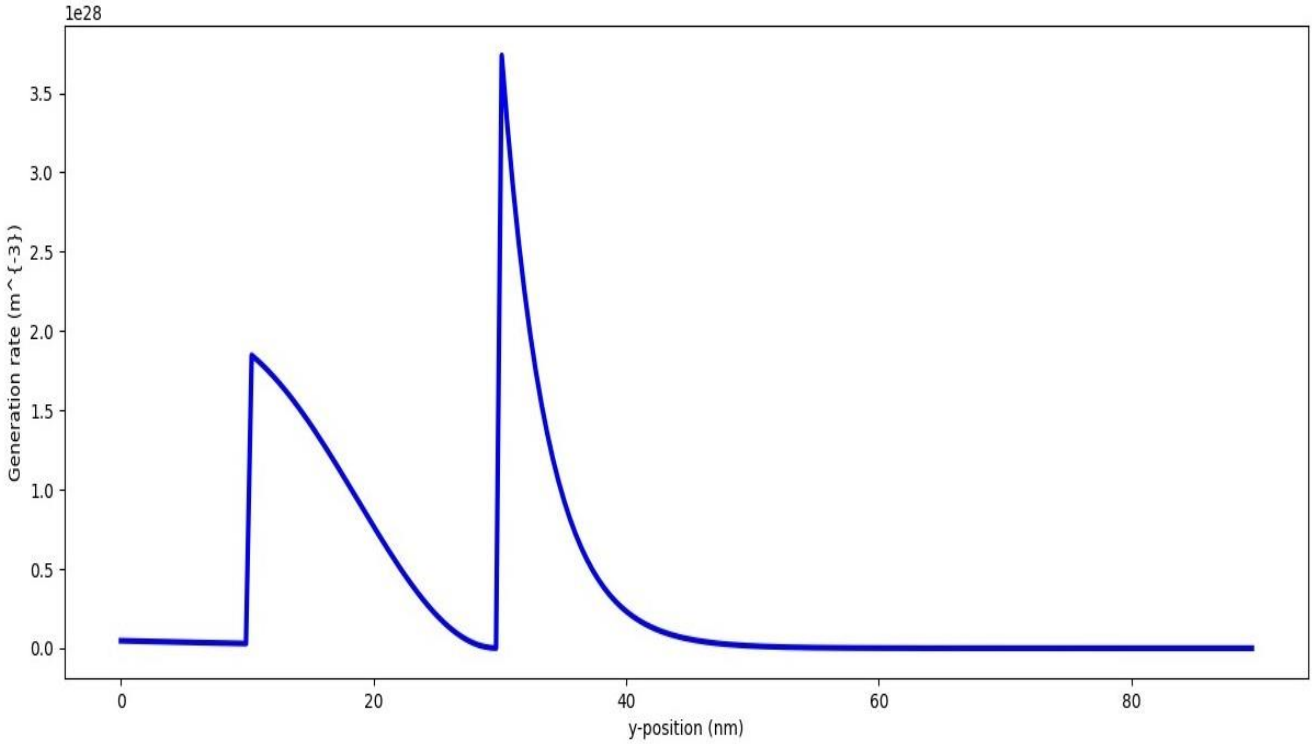

(a): CdS(window)-Cu_xN(absorber) Solar Cell

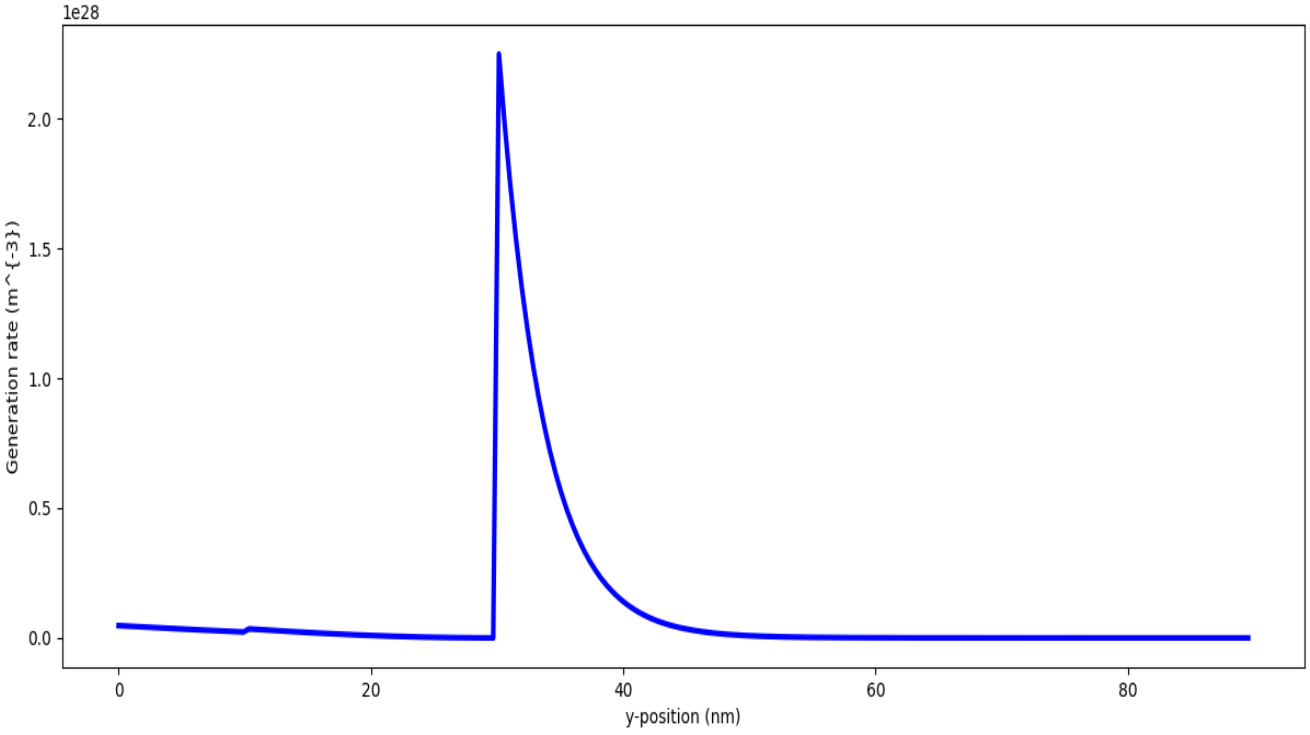

(b): ZnO(window)-Cu_xN(absorber) Solar Cell

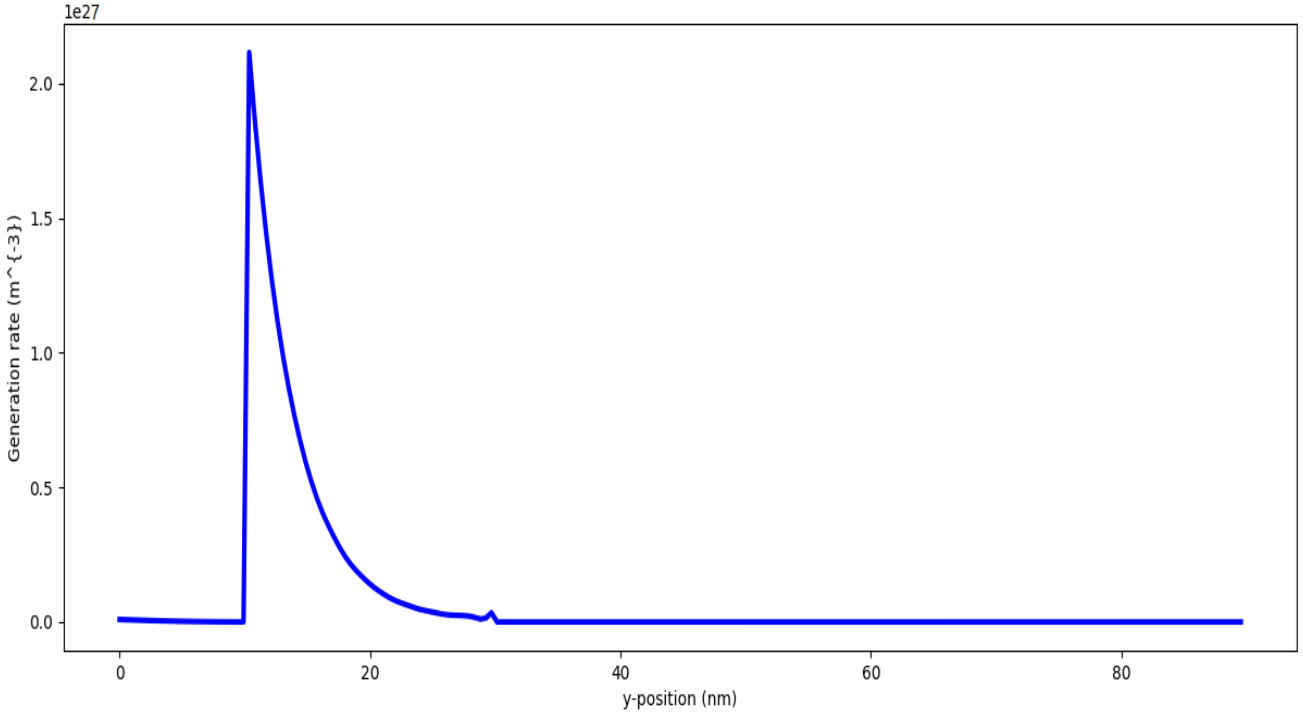

(c): Cu_xN(window)-PbSe(absorber) Solar Cell

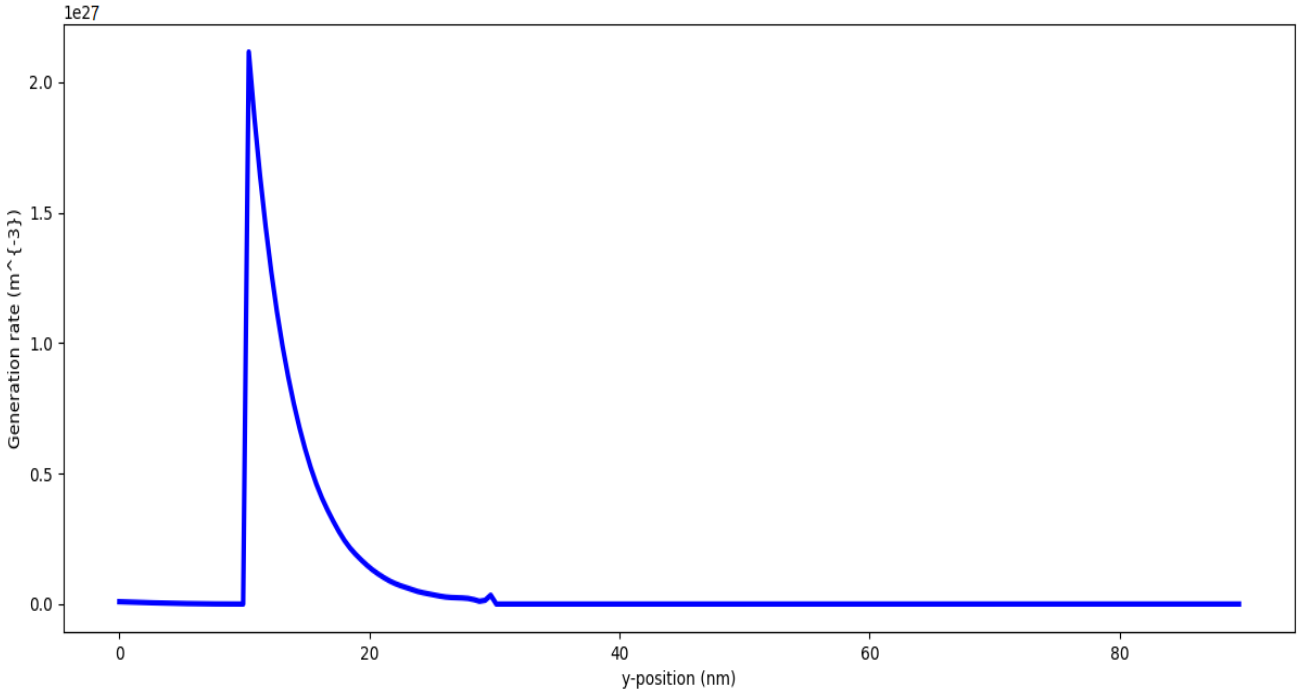

(d): Cu_xN(window)-InAs(absorber) Solar Cell

Fig.5.17[(a),(b),(c),(d)]: Charge carrier generation rate (Y-axis) vs Y-position (X-axis) characteristics of Cu_xN based solar cells with various inorganic semiconductors at 1Sun light intensity as represent (a), (b), (c) and (d) respectively.

Charge carrier (free electron and hole) generation occurs due to the absorption of the visible spectrum of light incident upon solar cells. The charge carrier generation rate in a solar cell is defined as the concentration of charge carriers per unit volume of the solar cell per unit time. The charge carrier generation rate of a PV cell depends on several factors, such as incident photon energy, thickness and absorption coefficient of the material, band gap of the window as well as absorber layers etc. The charge carrier generation vs Y-position characteristics have been studied by considering Cu_xN as an absorber as well as window layers with various inorganic semiconductors in this present text. The charge carrier generation rate vs Y-position of the simulated CdS-Cu_xN solar cell was found to be different from those of the remaining three simulated cells. The carrier generation rate of the CdS-Cu_xN cell first increased to $1.75x10^{28}m^{-3}s^{-1}$at y=15nm, declined exponentially to zero at y=30nm, then increased to a maximum i.e. $3.5x10^{28}m^{-3}s^{-1}$and finally decreased to zero exponentially as obtained from Fig.5.17.(a). The carrier generation rate of the ZnO-Cu_xN solar cell reached a maximum value i.e. $2.0x10^{28}m^{-3}s^{-1}$at y=30nm and then decreased exponentially to zero as obtained from Fig.5.17.(b). The characteristics of the Cu_xN-PbSe and Cu_xN-InAs cells were found to be exactly identical i.e. they reached a maximum value of $2.0x10^{27}m^{-3}s^{-1}$at y=10nm and then decreased exponentially to zero as obtained from Fig.5.17.(c) and Fig.5.17.(d) respectively. The maximum carrier generation rate was thus highest for the CdS-Cu_xN solar cell, i.e., $3.5x10^{28}m^{-3}s^{-1}$, followed by that of the ZnO-Cu_xN cell, i.e., $2.0x10^{28}m^{-3}s^{-1}$, and least for the Cu_xN-PbSe and Cu_xN-InAs cells, i.e.,$2.0x10^{27}m^{-3}s^{-1}$.

Absorption of photons in solar cells results in electrons gaining sufficient energy to transit from the valence band to the conduction band, thus leaving behind a hole in the valence band and giving rise to charge carriers. The generation of this excess electron-hole pair creates current and work done by the charge carriers creates voltage. The simultaneous presence of voltage and current gives rise to electric power in the solar cell. The charge carrier generation rate was maximum for the CdS-Cu_xN solar cell, followed by the ZnO-Cu_xN solar cell and minimum for both the Cu_xN-PbSe and Cu_xN-InAs solar cells respectively. The charge carrier generation rate was higher for the solar cells with Cu_xN as the absorber layer than for the ones with Cu_xN as the window layer.

The open circuit voltage (V_{OC}), short circuit current density (J_{SC}), voltage (V_m) and current density (J_m) at maximum power, maximum cell power (P_m), fill factor (FF) and power conversion efficiency (η) of two solar cells with Cu_xN as the absorber layer and CdS, ZnO as window layers and the other two with Cu_xN as the window layer and PbSe, InAs as absorber layers respectively are mentioned in Table 5.4 given below.

Table 5.4: Simulation Results of Photovoltaic Analysis

Sl. no.	Role of Cu_xN	Solar Cell Type	V_{OC} (V)	J_{SC} (mA/cm^2)	V_m (V)	J_m (mA/cm^2)	P_m (mW/cm^2)	FF	η (%)
1	Absorber Layer	CdS-Cu_xN	0.592	17.748	0.567	15.753	8.932	0.85	8.93
2		ZnO-Cu_xN	0.578	9.846	0.549	9.123	5.009	0.88	5.01
3	Window Layer	Cu_xN-PbSe	0.562	7.547	0.528	6.589	3.479	0.82	3.48
4		Cu_xN-InAs	0.567	7.849	0.537	6.88	3.695	0.83	3.69

The role of Cu_xN semiconducting material in photovoltaic applications and the performance parameters of Cu_xN-based solar cells have been summarized in Table 5.4. Here simulations were performed considering Cu_xN as absorber and window layers respectively. When Cu_xN was considered the absorber layer then CdS and ZnO were chosen as window layers whereas PbSe and InAs were chosen as absorber layers when Cu_xN was considered the window layer respectively. It is clear from Table 5.4 that all electrical parameters except fill factor were highest for the CdS-Cu_xN solar cell. This can be explained by the fact that the best current-voltage characteristics with the lowest cut-in voltage (i.e. 0.8Volt) were obtained for the CdS-Cu_xN solar cell i.e. the CdS-Cu_xN solar cell switched on to the conduction mode faster than the other solar cells considered. Additionally, it can be said that the CdS-Cu_xN solar cell has exhibited the lowest recombination prefactor (i.e. $8x10^{-16}m^{-6}.s^{-1}$) and highest charge carrier generation rate (i.e. $3.5x10^{28}m^{-3}.s^{-1}$) with a higher carrier lifetime leading to the highest maximum current density (i.e.15.753 mA/cm^2) and hence the highest photoconversion efficiency (i.e. 8.93%). The ZnO-Cu_xN solar cell showed the second-best photoconversion efficiency (i.e. η=5.01%) but was significantly lower than that of the CdS-Cu_xN solar cell (i.e. η=8.93%) because of the higher cut-in voltage (i.e.1Volt) as well as recombination prefactor (i.e. $1.75x10^{-16}m^{-6}.s^{-1}$) and lower carrier generation rate (i.e. $2.0x10^{28}m^{-3}$) than the CdS-Cu_xN solar cell. However, the fill factor was highest for the ZnO-Cu_xN solar cell (i.e. FF=0.88) i.e. this cell was found to operate closest to ideality. The solar cells with Cu_xN as window layer were underperforming compared to those with Cu_xN as an absorber layer. The maximum current density (i.e. 6.88 mA/cm^2) and efficiency of the Cu_xN-InAs solar cell (i.e. η=3.69%) were slightly higher than the short-circuit current density (i.e. 6.589 mA/cm^2) and efficiency (i.e. η=3.48%) of the Cu_xN-PbSe cell because of the slightly lower recombination prefactor in the former (i.e. $9x10^{-15}m^{-6}.s^{-1}$) than the latter (i.e. $1x10^{-14}m^{-6}.s^{-1}$). The total charge density in the Cu_xN-InAs cell (i.e.$8x10^{23}C.m^{-3}$) was also slightly higher than that in the Cu_xN-PbSe cell (i.e.$7x10^{23}C.m^{-3}$) further contributing to slightly higher maximum current density and solar cell efficiency in the former as compared to the later. However, the power conversion efficiency of the solar cells with Cu_xN as the window layer was much lower than that of the cells with Cu_xN as the absorber layer. Hence it can be inferred that Cu_xN is more suitable as an absorber layer than the window layer of a solar cell, and the performance of the

solar cell with Cu_xN as the absorber layer and CdS as the window layer was found to be the best among all the four simulated solar cells.

5.3.5 Comparative Study of photovoltaic parameters of simulated Cu_xN based cell with conventional thin film solar cell materials

The parameters of the simulated CdS-Cu_xN solar cell are compared with the experimental results of conventional solar cells with CdS as a window layer, as shown in Table 5.5.

Table 5.5: Solar Cell Parameters of Simulated CdS-Cu_xN based Cell: Comparison with Conventional CdS based Solar Cells

Solar Cell Para-meters / Solar Cell Type	V_{OC} (V)	J_{SC} (mA/cm^2)	V_m (V)	J_m (mA/cm^2)	P_m (mW/cm^2)	FF	η (%)
CdS-Cu_xN (Simulated)	0.592	17.748	0.567	15.753	8.932	0.85	8.93
CdS-Cu_2S [90]	0.516	19.3	0.39	18.2	7.098	0.71	7.09
CdS-PbS [91]	0.29	14	0.16	9.2	1.472	0.36	1.47
CdS-CdTe [92]	0.82	25.6	0.6	23	13.85	0.66	13.8
CdS-SnS [93]	0.346	20.53	0.296	14.42	4.26	0.60	4.2
CdS-ZnO [94]	0.77	4.65	0.55	2.22	1.21	0.34	1.2

The solar cell parameters of the simulated CdS-Cu_xN thin film were compared to those of conventional CdS-based solar cells (CdS-Cu_2S, CdS-PbS, CdS-CdTe, CdS-SnS, and CdS-ZnO solar cells) as shown in Table5.5. The values of maximum voltage, maximum current density, maximum power density, fill factor and efficiency of the simulated CdS-Cu_xN solar cell were 0.567V, 15.753mA/cm^2, 8.932 mW/cm^2, 0.85 and 8.93% respectively. The experimental values of maximum voltage, maximum current density, maximum power density, fill factor and efficiency of the CdS-Cu_2S solar cell were 0.39V, 18.2mA/cm^2, 7.098mW/cm^2, 0.71 and 7.09% respectively. The experimental values of maximum voltage, maximum current density, maximum power density, fill factor and efficiency of the CdS-PbS

solar cell were 0.16V, 9.2 mA/cm^2, 1.472 mW/cm^2, 0.36 and 1.47% respectively. The experimental values of maximum voltage, maximum current density, maximum power density, fill factor and efficiency of CdS-CdTe solar cells were 0.6V, 23 mA/cm^2, 13.85 mW/cm^2, 0.66 and 13.8% respectively. The experimental values of maximum voltage, maximum current density, maximum power density, fill factor and efficiency of CdS-SnS solar cells were 0.296V, 14.42mA/cm^2, 4.26mW/cm^2, 0.6 and 4.2% respectively. The experimental values of maximum voltage, maximum current density, maximum power density, fill factor and efficiency of CdS-ZnO solar cells were 0.55V, 2.22 mA/cm^2, 1.21mW/cm^2, 0.34 and 1.2% respectively. The fill factor of the simulated CdS-Cu_xN solar cell were highest among all the conventional solar cells mentioned while the maximum power density and efficiency of the simulated cell were lower than those of the CdS-CdTe solar cell but higher than those of CdS-Cu_2S, CdS-PbS, CdS-SnS, and CdS-ZnO solar cells respectively, thus making the CdS-Cu_xN solar cell a suitable candidate for photovoltaic applications. Photovoltaic performance analysis by practical experimentation requires expensive infrastructure. However, performing the same using the current technique produces accurate results compatible with practical ones and can be adopted in places lagging behind necessary infrastructure.

5.4 Conclusion

In this present study a modern computational analysis of the optoelectronic response of crystalline, nanostructured copper nitride (Cu_xN) semiconducting material fabricated by a simple, low-cost spray deposition technique has been performed. The optical data (band gap, refractive index, extinction coefficient and absorption coefficient data) of the semiconductor as obtained from UV-Vis-NIR spectroscopy was provided as input to Oghma-Nano software (8.1.020) for carrying out numerical simulations for obtaining photoconductive and photovoltaic responses of the fabricated 0.6(M) Cu_xN optimized annealed film. The photoconductive response was observed for the optimized film of varying thickness i.e. 50µm, 50nm and 50Å under different light intensities of 0W.cm^{-2}, 0.1W.cm^{-2}, 1W.cm^{-2} and 10W.cm^{-2}. The total charge density vs applied voltage, current vs applied voltage, recombination prefactor vs excess carrier concentration and charge carrier generation rate vs Y-position photoconductive characteristics were found to be best for the 50nm film with values of total charge density of $3x10^{25}$ C.m^{-3}, cut-in voltage of 1.25V, recombination prefactor of $1.2x10^{-23}$ m^{-6}.s^{-1} and carrier generation rate of $2.5x10^{36}$m^{-3}.s^{-1} respectively. These results were compatible with those of conventional semiconducting materials such as Si, GaAs and CdTe respectively. The photoconductive performance analysis by variation of film thickness while performing practical experimentation is complicated; however, performing the same analysis using the current technique can be adopted to significantly reduce the complexity. The photovoltaic characteristics were obtained by simulating solar cells with fabricated 0.6 (M) Cu_xN optimized film as the absorber layer of thickness 50nm with CdS and ZnO of thickness 20nm as window layers and the Cu_xN film as the window layer of thickness 20nm with PbSe and InAs of thickness 50nm as absorber layers respectively. The photovoltaic characteristics were observed for all the simulated solar cells at 1Sun light intensity and solar cell parameters were obtained. The best photovoltaic characteristics and

parameters were obtained for the solar cell with CdS as the window layer and Cu_xN as the absorber layer, i.e., maximum current density of 15.753 mA/cm^2, maximum power density of 8.932 mW/cm^2, fill factor of 0.85, photoconversion efficiency of 8.93% etc. These results are compatible with the experimental results of the conventional CdS-based solar cells such as CdS-Cu_2S, CdS-PbS and CdS-CdTe cells. The photovoltaic performance analysis of solar cells requires high-grade laboratory infrastructure. The analysis performed by the present computational technique provides outcomes similar to experimental results and hence can be adopted in places lagging proper infrastructure. This technique is simple, convenient and comparable to modern computational methods and can be used in optoelectronic device modelling applications. It can be thus concluded that the Cu_xN semiconductor of thickness in the nanometer range is most suitable for functioning as the absorber layer of solar cell and its photovoltaic performance is best with CdS as its window layer. However, the optimization of 0.6(M) Cu_xN semiconductor layer thickness in the nanometer range and the photovoltaic performance analysis of this optimized semiconductor layer remains a topic of future studies.

References:

1. M.D. Kelzenberg, D.B. Turner-Evans, M.C. Putnam, S.W. Boettcher, R.M. Briggs, J. Y. Baek, N.S. Lewis, H.A. Atwater, High-performance Si microwire photovoltaics, Energy Environ. Sci. 4 (2011) pp.866–871.

2. W. Yan, X. Tan, L. Guan, H. Zhou, X. Yang, P. Xiang, Z. Zhong, Solution of efficiency loss in thinned silicon PERC solar cells, Renew. Energy 165 (2021) pp.118–124.

3. P.K. Basu, A. Khanna, Z. Hameiri, The effect of front pyramid heights on the efficiency of homogeneously textured inline-diffused screen-printed monocrystalline silicon wafer solar cells, Renew. Energy 78 (2015) pp.590–598.

4. S.K. Dhungel, J. Yoo, K. Kim, S. Ghosh, S. Jung, J. Yi, Study of electrical properties of oxidized porous silicon for back surface passivation of silicon solar cells, Renew. Energy 33 (2008) pp.282–285.

5. E.L. Warren, H.A. Atwater, N.S. Lewis, Silicon microwire arrays for solar energy-conversion applications, J. Phys. Chem. C 118 (2014) pp.747–759.

6. M.D. Kelzenberg, S.W. Boettcher, J.A. Petykiewicz, D.B. Turner-Evans, M. C. Putnam, E.L. Warren, J.M. Spurgeon, R.M. Briggs, N.S. Lewis, H.A. Atwater, Enhanced absorption and carrier collection in Si wire arrays for photovoltaic applications, Nat. Mater. 9 (2010) pp.239–244.

7. F. Ahmad, E. Maqbool, N. Qurban, Z. Fatima, T. Ahmad, I. Zahid, A. Ali, S. Rana Rajpoot, M. W. Tasleem, Electrical Characterization of II-VI Thin Films for Solar Cells Application, ASEAN Journal of Science and Engineering 2(2) (2022) pp.199-208.

8. Y. Zhang, X. Xu, Yttrium barium copper oxide superconducting transition temperature modeling through gaussian process regression, Computational Materials Science 179 (2020) 109583.

9. Y. Zhang, X. Xu, Lattice Misfit Predictions via the Gaussian Process Regression for Ni-Based Single Crystal Superalloys, Metals and Materials International 27 (2021) pp.235–253.

10. L. Hafaifa, M. Maache, Z. Allam, A. Zebeir, Simulation and performance analysis of CdTe thin film solar cell using different Cd-free zinc chalcogenide-based buffer layers, Results in Optics 14 (2024) 100596.

11. S. Moujoud, B. Hartiti, S. Touhtouh, F. Belhora, A. Hajjaji, Optimizing Sb_2Se_3 thin-film solar cells: A comprehensive simulation study of multiple influential factors, Optik - International Journal for Light and Electron Optics 303 (2024) 171723.

12. S. R. Al Ahmed, M. Rahaman, A. Sunny, S. Rahman, Md. S. Islam, T. A. El-Mohaymen Taha, Z.A. Alrowaili, Md. S. Mian, Enhancing the efficiency of Cu_2Te thin-film solar cell with WS_2 buffer layer: A simulation study, Optics & Laser Technology 159 (2023) 108942.

13. E. Puente-Lopez, M. Pal, Numerical simulation and optimization of physical properties for high efficiency $CuSbS_2$ thin film solar cells, Optik - International Journal for Light and Electron Optics 272 (2023) 170233.

14. S. K. Biswas, M. K. Mim, Md. M. Ahmed, Design and Simulation of an Environment-Friendly ZrS_2/$CuInS_2$ Thin Film Solar Cell Using SCAPS 1D Software, Advances in Materials Science and Engineering, 8845555 (2023).

15. B. M. Sakunde, N. B. Chaure, S. Patole, S. R. Jadkar, H. M. Pathan, Numerical Modeling to Improve the Efficiency of Cadmium Sulfide/Copper Indium Sulfide Thin Film-based Solar Cells, ES Energy Environ.18 (2022) pp.111-121.

16. K. Vijayan, L. Thirumalaisamy, S. P. Vijayachamundeeswari, K. Sivaperuman, N. Ahsan, Y. Okada, A Novel Approach for Designing a Sub-Bandgap in $CuGa(S,Te)_2$ Thin Films Assisted with Numerical Simulation of Solar Cell Devices for Photovoltaic Application, ACS Omega 8 (2023) pp.22414−22427.

17. J.C. Zepeda Medina, E. R. Andres, C. M. Ruíz, E. C. Espinosa, L. T. Yarce, R. G. Isasmendi, R. R. Trujillo, G. G. Salgado, A. C. Solis, F. G. Nieto Caballero, A. C. Carranza Sanchez, Performance simulation of solar cell based on AZO/CdTe heterostructure by SCAPS 1D software, Heliyon 9 (2023) 14547.

18. M. Y. Ali, M. A. Abedin, M. S. Hossain, E. S. Hossain, Optimization of monoclinic Cu_2SnS_3 (CTS) thin film solar cell performances through numerical analysis, Chalcogenide Letters 17 (2) (2020) pp. 85 – 98.

19. H. Luo, Y. Zhang, H. Li, Effect of MoS_2 interlayer on performances of copper-barium-tin-sulfur thin film solar cells via theoretical simulation, Solar Energy 223 (2021) pp.384–397.

20. T. Pansuriya, R. Malani, V. Kheraj, Investigations on the effect of buffer layer on CMTS based thin film solar cell using SCAPS 1-D, Optical Materials 126 (2022) 112150.

21. M. Elbar, S. Tobbeche, Numerical simulation of CGS/CIGS single and tandem thin-film solar cells using the Silvaco-Atlas software, Energy Procedia 74 (2015) pp.1220 – 1227.

22. L.I. Nykyruy, R.S. Yavorskyi, Z.R. Zapukhlyak, G. Wisz, P. Potera, Evaluation of CdS/CdTe thin film solar cells: SCAPS thickness simulation and analysis of optical properties, Optical Materials 92 (2019) pp.319–329.

23. V. V. Kutwade, K. P. Gattu, M. E. Sonawane, D. A. Tonpe, I. M. S. Mohammed, R. Sharma, Theoretical modeling and optimization: Cd-free CTS/Zn(O,S)/ZnO thin film solar cell, Materials Today Communications 29 (2021) 102972.

24. W. Chen, X. Huang, Q. Cheng, C. Chen, D. Yun, F. Zhang, Simulation analysis of heterojunction ZnO/CdS/Cu(In,Ga)Se_2 thin-film solar cells using wxAMPS, Optik 127 (2016) pp.182–187.

25. H. Movla, E. Abdi, D. Salami, Simulation analysis of the CIGS based thin film solar cells, Optik 124 (2013) pp.5871–5873.

26. E. S. Hossain, P. Chelvanathan, S. A. Shahahmadi, K. Sopian, B. Bais, N. Amin, Performance assessment of Cu_2SnS_3 (CTS) based thin film solar cells by AMPS-1D, Current Applied Physics 18 (2018) pp.79-89.

27. D. Daksh, S. Mishra, B. S. Sengar, Simulation of antimony chalcogenide thin film solar cell with high efficiency, Materials Today: Proceedings 76 (2023) pp.336–340.

28. A. Paul, R. Mandal, Advances in nanostructure thin film materials for solar cell applications, Comprehensive Materials Processing (Second Edition), 4 (2024) pp.136-150.

29. J. Luo, X. Zhang, M. Liu, W. Ai, X. Zheng, S. Liu, L. Han, K. Huang, J. Wan, C. Luo, Rapid detection of viable Acinetobacter baumannii and antibiotic susceptibility testing based on a phage amplification-Taqman qPCR assay, Microchemical Journal 195 (2023) 109516.

30. S. Zinatloo-Ajabshir, H. Mahmoudi-Moghaddam, M. Amiri, H. A. Javar, A green and simple procedure to synthesize dysprosium cerate plate-like nanostructures and their application in the electrochemical sensing of mesalazine, J Mater Sci: Mater Electron 35 (500) (2024).

31. S. Zinatloo-Ajabshir, M. S. Morassaei, M. Salavati-Niasari, Eco-friendly synthesis of $Nd_2Sn_2O_7$–based nanostructure materials using grape juice as green fuel as photocatalyst for the degradation of erythrosine, Composites Part B 167 (2019) pp.643–653.

32. S. Zinatloo-Ajabshir, M. Salavati-Niasari, Facile route to synthesize zirconium dioxide (ZrO_2) nanostructures: Structural, optical and photocatalytic studies, Journal of Molecular Liquids 216 (2016) pp.545–551.

33. S. Zinatloo-Ajabshir, S. Mortazavi-Derazkola, M. Salavati-Niasari, Schiff-base hydrothermal synthesis and characterization of Nd_2O_3 nanostructures for effective

photocatalytic degradation of eriochrome black T dye as water contaminant, J Mater Sci: Mater Electron 28 (2017) pp.17849–17859.

34. S. Zinatloo-Ajabshir, M. S. Morassaei, O. Amiri, M. Salavati-Niasari, Green synthesis of dysprosium stannate nanoparticles using Ficus carica extract as photocatalyst for the degradation of organic pollutants under visible irradiation, Ceramics International 46 (2020) pp.6095–6107.

35. S. Zinatloo-Ajabshir, M. Ahmadi-Zeidabadi, M. Amiri, F. Sharifianjazi, Innovative sono-synthesis of cerium dioxide nanomaterials using mentha extract with efficient activity for cancer therapy application, Results in Engineering 23 (2024) 102720.

36. K. V. Gunavathya, K. Tamilarasana, C. Rangasamia, A. M. S. Arulanantham, Solution processed copper zinc tin sulfide thin films for thermoelectric device applications, Ceramics International 46 (18) (2020) pp.28342–28354.

37. T. S. Shyju, S. Anandhi, R. Suriakarthick, R. Gopalakrishnan, P. Kuppusami, Mechanosynthesis deposition and characterization of CZTS and CZTSe materials for solar cell applications, Journal of Solid State Chemistry 227 (2015) pp.165–177.

38. G. L. Agawane, S. A. Vanalakar, A. S. Kamble, A. V. Moholkar, J. H. Kim, Fabrication of $Cu_2(Zn_xMg_{1-x})SnS_4$ thin films by pulsed laser deposition technique for solar cell applications Materials Science in Semiconductor Processing 76 (2018) pp.50–54.

39. B. D. Chernomordik, A. E. Beland, N. D. Trejo, A. A.Gunawan, D. D. Deng, K. A. Mkhoyan, E. S. Aydil, Rapid facile synthesis of Cu_2ZnSnS_4 nanocrystals, Journal of Materials Chemistry A 27 (2014) 10389.

40. M. Shahiduzzaman, R. Yamada, T. Chikamatsu, T. Ono, Y. Tanaka, Y. Uesugi, M. Karakawa, T. Kuwabara, K. Takahashi, T. Ishijima, T. Taima, Thin film deposition method for ZnO nanosheets using low-temperature microwave-excited atmospheric pressure plasma jet, Thin Solid Films 674 (2019) pp.58–63.

41. M. A. Gaikwad, M. P. Suryawanshi, P. S. Maldar, T. D. Dongale, A. V. Moholkar, Nanostructured zinc oxide photoelectrodes by green routes M-SILAR and electrodeposition for dye sensitized solar cell, Optical Materials 78 (2018) pp.325–334.

42. S. B. Patil, A. K. Singh, Electrodeposited vertically aligned ZnO nanorods thin films on steel substrate for CdS quantum dots sensitized solar cell, Electrochimica Acta 56(16) (2011) pp.5693–5701.

43. S. Kushwaha, L. Bahadur, Studies of structural and morphological characteristics of flower-like ZnO thin film and its application as photovoltaic material, Optik 124 (22) (2013) pp.5696–5701.

44. M. Wang, J. Yi, S. Yang, Z. Cao, X, Huang, Y. Li, H. Li, J. Zhong, Electrodeposition of Mg doped ZnO thin film for the window layer of CIGS solar cell, Applied Surface Science 382 (2016) pp.217–224.

45. S. S. Kanmani, K. Ramachandran, Synthesis and characterization of TiO_2/ZnO core/shell nanomaterials for solar cell applications, Renewable Energy 43 (2012) pp.149–156.

46. A. A. Mohammed, A. S. S. Ahmad, W. A. Azeez, Fabrication of Dye Sensitized Solar Cell Based on Titanium Dioxide (TiO_2), Advances in Materials Physics and Chemistry 5(9) (2015) pp.361–367.

47. A. Afzal, A. Habib, I. Ulhasan, M. Shahid, A. Rehman, Antireflective Self-Cleaning TiO_2 Coatings for Solar Energy Harvesting Applications, Frontiers in Materials 8 (2021) 687059.

48. S. S. Shaikh, M. Shkir, E. U. Masumdar, Exploration of the spray deposited Cadmium Telluride thin films for optoelectronic devices, Physica B Condensed Matter 580 (2020) 411831.

49. A. Romeo, E. Artegiani, CdTe-Based Thin Film Solar Cells: Past, Present and Future, Energies 14(6) (2021) 1684.

50. R. A. Joshi, V. S. Taur, R. Sharma, Effect of annealing on conversion efficiency of nanostructured CdS/$CuInSe_2$ heterojunction thin film solar cell prepared by chemical ion exchange route at room temperature, Materials Research Bulletin 47(9) (2012) pp.2206–2211.

51. A. E. H. B Kashyout, E. Z. Ahmed, T. Meaz, M. Nabil, M. Amer, (One-step) electrochemical deposition and characterization of $CuInSe_2$ thin films, Alexandria Engineering Journal 53(3) (2014) pp.731–736.

52. A. S. Hassanien, A. A. Akl, Influence of composition on optical and dispersion parameters of thermally evaporated non-crystalline $Cd_{50}S_{50-x}Se_x$ thin films, Journal of Alloys & Compounds 648 (2015) pp.280-290.

53.Q.Fu, Radiation Transfer in the Atmosphere, Cloud- Radiation Processes, Encyclopedia of Atmospheric Sciences (Second Edition), 2015, pp.13-15, DOI: https://doi.org/10.1016/B978-0-12-382225-3.00338-8.

54. N. Nithya, S. R. Radhakrishnan, Effect of Thickness on the Properties of ZnO Thin Films, Advances in Applied Science Research, 3(6) (2012) pp.4041-4047.

55. M. I. Hossain, F. H. Alharbi, N. Tabet, Copper oxide as inorganic hole transport material for lead halide perovskite based solar cells solar energy 120 (2015) pp.370-380.

56. A. Tilemachou, M. Zervos, A. Othonos, T. Pavloudis, J. Kioseoglou, p-Type Iodine-Doping of Cu_3N and Its Conversion to γ-CuI for the Fabrication of γ-CuI/Cu_3N p-n Heterojunctions, Electron. Mater. 3(1) (2022) pp.15-26.

57. S. Tripathi, Sadanand, P. Lohia, D.K. Dwivedi, Contribution to sustainable and environmental friendly non-toxic CZTS solar cell with an innovative hybrid buffer layer, Solar Energy 204 (2020) pp.748-760.

58. N. A. Jayah, H. Yahaya, M. R. Mahmood, T. Terasako, K. Yasui, A. M. Hashim, High electron mobility and low carrier concentration of hydrothermally grown ZnO thin films on seeded α-plane sapphire at low temperature, Jayah et al. Nanoscale Research Letters 10:7 (2015).

59. W. k. Koh, A. Y. Koposov, J. T. Stewart, B. N. Pal, I. Robel, J. M. Pietryga, V. I. Klimov, Heavily doped n-type PbSe and PbS nanocrystals using ground-state charge transfer from cobaltocene, Scientific Reports 3 (2004) (2013).

60. J. Wróbel, G. A. Umana-Membreno, J. Boguski, D. Sztenkiel, P. P. Michałowski, Piotr Martyniuk, L. Faraone, J. Wróbel, A. Rogalski, Locally-Strain-Induced Heavy-Hole-Band Splitting Observed in Mobility Spectrum of p-Type InAs Grown on GaAs, Phys. Status Solidi RRL 14 (2020) 1900604.

61. S. Ganguly, K. Halder, N. A. Haque, S. Das, S. G Dastidar, A comparative study between electrical properties of bulk and synthesized nanomaterial of zinc sulphide, American Journal of Research Communication, 3(3) (2015) pp. 68-80.

62. H. Haug, S. W. Koch, Quantum Theory of the Optical and Electronic Properties of Semiconductors (3rd edition), World Scientific (1994), ISBN: 978-981-02-2002-0.

63. A. Richter, S. W. Glunz, F. Werner, J. Schmidt, A. Cuevas, Improved quantitative description of Auger recombination in crystalline silicon, Physical Review B. 86 (16) (2012)165202.

64. A. Cuevas, The recombination parameter J_0, Energy Procedia 55 (2014) pp.53-62.

65. P. Manjappa, H. K. Rajan, M. G. Mahesh, K. G. Sadananda, M. Channegowda, G. K. Shivashankar, N. B. Mutt, Effective Attenuation of Electromagnetic Waves by Synergetic Effect of α-Fe_2O_3 and MWCNT/Graphene in LDPE-Based Composites for EMI Applications, Materials 15 (24) (2022) 9006.

66. L. Bychto, M. Malinski, Influence of light intensity on the lifetime of carriers in silicon investigated by a photoacoustic method, Opto−Electronics Review 24(2) (2016) pp.58–61.

67. P. P. Altermatt, A. Schenk, F. Geelhaar, G. Heiser, Reassessment of the intrinsic carrier density in crystalline silicon in view of band-gap narrowing, J. Appl. Phys. 93 (3) (2003) pp.1598–1604.

68. Y. W. Chen, J. J. Horng, C. H. Chang, A. Kundu, Y. C. Peng, M. Chen, 18.7 A 0.7V, 2.35% 3σ-Accuracy Bandgap Reference in 12nm CMOS, IEEE International Solid-State Circuits Conference (ISSCC) (2019), DOI: 10.1109/ISSCC.2019.8662339.

69. V. Benda, Photovoltaics: The Basics, A Comprehensive Guide to Solar Energy Systems (2018), pp.151-179, DOI: https://doi.org/10.1016/B978-0-12-811479-7.00008-7.

70. M. M. Chowdhury, B. Debnath, Approximation of Carrier Generation Rate in Common Solar Cells and Studies for Optimization of $n^{+}p$ Silicon Solar Cell for AM1.5G and AM1.5D, 7th IEEE International Conference on Electrical and Computer Engineering, 2012.

71. H. A. S. Al-shamiri, M. O. Sid-Ahmed, M. O. Sid-Ahmed, F. A. Hezam, Simulation of Performance of Cadmium Telluride Solar Cell Using AMPS-1D Program, Journal of Photonic Materials and Technology, 2(2) (2016), DOI: 10.11648/j.jmpt.20160202.11.

72. D. Sahoo, R.V. Srikantiah, Solution growth of cadmium telluride, Bull. Mater. Sci., 19(3) (1996), pp. 483-493.

73. A. Abudulimu, S. Carter, A. B. Phillips, D. B. Li, S. Neupane, T. Brau, J. Friedl, E. Bastola, M. K. Jamarkattel, M. J. Heben, Y. Yan, R. J. Ellingson, Comprehensive Study of Carrier Recombination in High-Efficiency CdTe Solar Cells Using Transient Photovoltage, Sol. RRL 8 (2024) 2400131.

74. A.E. Delahoy, Z. Cheng, K.K. Chin, Carrier collection in thin-film CdTe Solar Cells: Theory and Experiment, 27th European Photovoltaic Solar Energy Conference and Exhibition, 2012.

75. U. Rössler, “Gallium arsenide (GaAs), intrinsic carrier concentration, electrical and thermal conductivity". Group IV Elements, IV-IV and III-V Compounds. Part b – Electronic, Transport, Optical and Other Properties. Landolt-Börnstein – GroupIII Condensed Matter (2002), pp. 1–8, DOI: https://doi.org/10.1007%2F10832182_196.

76. H. Fukui, Channel current limitations in GaAs MESFETS, Solid-State Electronics 22 (5) 1979, pp.507-515.

77. T. Kinsel, I. Kudman, Carrier recombination in gallium arsenide, Solid-State Electronics 8(10) (1965) pp.797-801.

77.(1). J.J. Loferski, Theoretical Considerations Governing the Choice of the Optimum Semiconductor for Photovoltaic Solar Energy, J. Appl. Phys. 27(1956) pp.777–784.

78. A. Paul, M. Ghosh, I. Dutta, R. Mandal, A novel method for fabricating semiconducting monocrystalline copper nitride nanowires for optoelectronic applications, Journal of Crystal Growth 617 (2023) 127307.

79. S. O. Kasap, P. Capper, Springer Handbook of Electronic & Photonic Materials, Springer (2007), ISBN 978-0-387-26059-4.

80. H. Ennaceri, A. Taleb, M. Boujuah, A. Khaldoun, J. Ebothe, A. Ennaoui, A. Benyoussef, Theoretical& experimental studies of Al doped ZnO thin films: optical & structural properties, Journal of Computational Electronics 20 (2021) pp. 1948-1958.

81. B. Weng, J. Qin, L. Zhao, C. Chang, Z. Shi, CdS/PbSe heterojunction for high temperature mid-infrared photovoltaic detector applications, Appl. Phys. Lett. 104 (121111) (2014).

82. H. Kroemer, The 6.1Å family (InAs, GaSb, AlSb) and its hetrostructures: a selective review, Physica E 20 (3-4) (2004) pp.196-203.

83. J. Vollbrecht, N. Tokmoldin, B. Sun, V. V. Brus, S. Shoaee, D. Neher, Determination of the charge carrier density in organic solar cells: A tutorial, J. Appl. Phys. 131(2022) 221101.

84. J. Vollbrecht, V. V. Brus, On Charge Carrier Density in Organic Solar Cells Obtained via Capacitance Spectroscopy, Adv. Electron. Mater. 6 (2020) 2000517.

85. F. Yu, G. Huang, W. Lin, C. Xu, W. Deng, X. Ma, J. Huang, Lumped-parameter equivalent circuit modeling of solar cells with S-shaped I-V characteristics, Solid State Electronics 156 (2019) pp.79–86.

86. S. Lun, C. Du, G. Yang, S. Wang, T. Guo, An explicit approximate I–V characteristic model of a solar cell based on Pade approximants, Solar Energy 92 (2013) pp.147–159.

87. S. Hubbard, Recombination, Photovoltaic Solar Energy: From Fundamentals to Applications, Wiley Publications (2016), DOI: https://doi.org/10.1002/9781118927496.ch5.

88. M. Asami, M. Hino, G. Li, K. Watanabe, Y. Nakano, M. Sugiyama, Comprehensive voltage-loss analysis and reduction of radiative recombination voltage loss in quantum-structured solar cells, Solar Energy Materials & Solar Cells 273 (2024) 112957.

89. Q. Yang, K. Bittkau, A. Eberst, U. Rau, K. Ding, The impact of interface recombination on the external quantum efficiency of silicon solar cells, Solar Energy Materials & Solar Cells 273 (2024) 112953.

90. R. B. Hall, J. D. Meakin, The design and fabrication of high efficiency thin film CdS/Cu_2S solar cells, Thin Solid Films 63 (1979) pp.203-211.

91. J. Hernandez-Borja, Y.V. Vorobiev, R. Ramirez-Bon, Thin film solar cells of CdS/PbS chemically deposited by an ammonia-free process, Solar Energy Materials & Solar Cells 95 (2011) pp.1882-1888.

92. I. E. Tinedert, F. Pezzimenti, M. L. Megherbi, A. Saadoune, Design and simulation of a high efficiency CdS/CdTe solar cell, Optik - International Journal for Light and Electron Optics 208 (2020) 164112.

93. Jae Yu Cho, SeongYeon Kim, Raju Nandi, Junsung Jang, Hee-Sun Yun, Enkhjargal Enkhbayar, Jin Hyeok Kim, Doh-Kwon Lee, Choong-Heui Chung, Jun Ho Kim, Jaeyeong Heo, Achieving over 4% efficiency for SnS/CdS thin-film solar cells by improving the heterojunction interface quality, J. Mater. Chem. A8 (2020) 20658.

94. Qi Cui, Changwen Liu, Fan Wu, Wenjin Yue, Zeliang Qiu, Hui Zhang, Feng Gao, Wei Shen, Mingtai Wang, Performance Improvement in Polymer/ZnO Nanoarray Hybrid Solar Cells by Formation of ZnO/CdS-Core/Shell Heterostructures, J.Phys. Chem. C 117(2013), pp.5626 −5 637.

Chapter 6

Summary, Discussion, and Conclusion

6.1 Summary and Discussion

The main goal of this present research work is to develop semiconducting-grade copper nitride (Cu_xN) nanostructure thin film for optoelectronics sensor and device applications. To achieve this goal, the author has adopted a simple and low-cost spray deposition technique for the fabrication and optimization of the Cu_xN film. It is perceivable from the discussions that are presented from Chapters 1-5 that copper nitride is a very promising semiconducting material for use in light-dependent resistor (LDR) and solar cell applications. This section provides a summary of the entire research work for this thesis, which is presented in Chapters 1-5, and the avenue of future research work in the context of this present work will also be presented in the next chapter of this thesis.

The aims and objectives of this research work have been presented in Chapter 1. Here a detailed literature review has been accomplished to cultivate various properties and different nanofabrication methods regarding various promising semiconducting materials used in optoelectronic sensors and devices applications. The usefulness of nanofabrication methods in optoelectronic devices has also been discussed in this section. The objectives of the entire thesis are presented here. The development of a nanostructured Cu_xN film by using a simple and low-cost fabrication technique to establish its applicability as a light-dependent resistor (LDR) as well as in solar cell applications has been discussed here.

Chapter 2 begins with a comprehensive review regarding properties and various nanofabrication methods of copper nitride (Cu_xN) semiconducting material. In this chapter, discussions are made about the entire work which is embedded in this thesis. The research gap and corresponding possible solutions have been illustrated here. It has been observed that copper nitride is a less thermally stable material, and it is very difficult to fabricate by high-temperature synthetic methods. Cu_xN film had mostly fabricated by physical deposition methods, but the suitable compositional ratio of the material is not always consistent for providing optimum semiconducting properties in optoelectronic applications. Thus, Cu_xN nanostructure has been developed by utilizing a simple and low-cost spray deposition technique, and optimization of the compositional ratio of the material has been performed here by varying the doping of the film. The photoresistor performances have been executed by determining LDR gain. The photoconductive studies of the optimally developed Cu_xN film have been accomplished by variation of film thickness, and optimum film thickness has been used for solar cell applications. Finally, the development of the solar cell device by using Cu_xN as absorber and window layers in combination with various inorganic semiconductors to investigate photovoltaic performances has been executed in this work. The best photovoltaic parameters and characteristics have been observed from here, and finally, a conclusion has been accomplished regarding the suitability of copper nitride material as an LDR and solar cell application.

The working principle of various physical as well as chemical deposition methods and different characterization processes, such as structural and optical, regarding thin film semiconductors has been discussed in Chapter 3. The collective details regarding fabrication

and characterization techniques provide a comprehensive idea to determine the appropriate possibility regarding this being applicable in the present research work.

The fabrication and optimization of semiconducting-grade copper nitride (Cu_xN) nanostructure for the application of photoresistor or LDR is presented in Chapter 4. In this chapter, the author has adopted a simple and low-cost spray deposition method that maintains a low-temperature arrangement to develop optimum Cu_xN film for use in optoelectronic applications. In the present method the Cu_xN nanowires have been fabricated using chemical spray deposition of thiourea and ammonium hydroxide over hot copper (Cu) foil substrate surface. The present process involves meager capital equipment and low recurring input. The optimization of the compositional ratio of the material has been performed by varying the molarity of the precursor solution. The molarity of the solution was varied as 0.2(M), 0.4(M), 0.6(M), 0.8(M) and 1.0(M) respectively. The structural and optical analyses have been performed to determine crystallinity, surface morphology, optical band gap, and compositional ratio of the as-prepared as well as annealed samples. The electrical analysis of the optimized Cu_xN film has been performed to establish its acceptability for light-dependent resistor (LDR) applications.

The structural analysis of the fabricated copper nitride film indicated the formation of monocrystalline cubic Cu_3N and post-deposition annealing has improved the crystallinity and structural parameters of the samples. Here, the 0.6(M) Cu_xN sample has shown the best crystallinity among all, and the best structural parameters have been observed for the 0.8(M) Cu_xN sample. The same trend has been observed also for the annealed samples. The SEM and EDX have been performed for both 0.6(M) and 0.8(M) Cu_xN as-prepared and annealed samples. The formation of Cu_xN nanowires has been confirmed from SEM micrographs. It has been inferred from the EDX analysis that the ratio of Cu and N varies from 0.8 to 1.35. The UV-VIS-NIR spectra of highest crystalline 0.6 (M) as-prepared and annealed samples have revealed that it has excellent absorption in the visible and NIR range and low absorption in the UV range. Thus, it is a promising material in the application as an optical sensor. The direct and indirect bandgaps of the 0.6(M) Cu_xN as-prepared sample were found to be 1.79 eV and 1.54 eV, respectively, whereas the 0.6(M) Cu_xN annealed samples were 1.75 eV and 1.5 eV, respectively. It has been observed that annealing has improved overall structural and optical parameters of the film. The electrical analysis of the optimized 0.6 (M) Cu_xN annealed sample revealed that it exhibited a negative temperature coefficient of resistance of -0.004/°C and thus inferred semiconducting behaviour. The suitable compositional ratio (Cu:N) of the optimally fabricated 0.6(M) Cu_xN annealed sample is 1.35, for which it has been used for optoelectronic applications. It was observed from the photo response curve of the same sample that its resistivity is decreasing exponentially with increasing input luminous intensity. This property is an essential parameter in using this material in fabricating opto-electronic devices and sensors. The light-dependent resistor (LDR) gain of 51% at 1000 watt/sq.m light intensity has been achieved in this work.

Chapter 5 represents a modern computational analysis to investigate the optoelectronic response of crystalline, nanostructured copper nitride (Cu_xN) semiconducting material fabricated by a simple, low-cost spray deposition technique. The optical spectroscopy data of

the fabricated thin film was provided as input to Oghma-Nano software (8.1.020) for carrying out numerical simulations. This technique of providing experimental data as input to simulation software has been believed to produce accurate computational output compatible with real-time data. The photoconductive and photovoltaic responses of the fabricated optimized 0.6(M) Cu_xN annealed film have been studied here. The variation in photoconductive response by tuning film thickness from 50μm to 50nm and 50Å at different light intensities was observed. Then the photovoltaic response of the Cu_xN film with optimized thickness has been noted for testing its feasibility for solar cell applications. Here photovoltaic performances have been studied by considering Cu_xN as absorber and window layers, respectively. At first, Cu_xN as an absorber layer and CdS and ZnO as window layers have been simulated, and photovoltaic performance has been noted. Then Cu_xN as a window layer and PbSe and InAs as absorber layers have been simulated, and photovoltaic performance has been cultivated. The best photovoltaic parameters have been evaluated from here for Cu_xN based solar cells. This technique can be adopted in places lagging adequate infrastructure for solar cell fabrication.

The photoconductive and photovoltaic responses have been studied by considering the characteristics such as total charge density vs. applied voltage, current vs. applied voltage, recombination prefactor vs. excess carrier concentration and charge carrier generation rate vs. Y-position. The best photoconductive performance was observed for the 50 nm film thickness with a total charge density of $3x10^{25}C.m^{-3}$, cut-in voltage of 1.25V, recombination prefactor of $1.2x10^{-23}m^{-6}.s^{-1}$ and carrier generation rate of $2.5x10^{36}m^{-3}.s^{-1}$ respectively. These values were compatible with those of conventional semiconductors like Si, GaAs and CdTe respectively. Then photovoltaic performances have been observed for the fabricated 0.6 (M) Cu_xN film with optimized thickness. At first, considering Cu_xN as an absorber layer of thickness 50 nm and CdS and ZnO of thickness 20 nm as window layers have been evaluated. Then Cu_xN as a window layer of thickness 20 nm and PbSe and InAs of thickness 50 nm as absorber layers have been studied. The best photovoltaic parameters have been obtained for the solar cell with CdS as the window layer and Cu_xN as the absorber layer. This CdS-Cu_xN solar cell exhibited a maximum current density of $15.753mA/cm^2$, a maximum power density of $8.932mW/cm^2$, a fill factor of 0.85, a photo-conversion efficiency of 8.93% etc. which are compatible with experimental results of other conventional CdS-based solar cells like CdS-Cu_2S, CdS-PbS, CdS-CdTe etc. It can be concluded from the study that Cu_xN absorber layer thickness in the nanometer range (50 nm) with CdS as its window layer is most suitable for functioning as a solar cell.

6.2 Concluding Remarks

This study investigates the fabrication of copper nitride (Cu_xN) nanostructure-based thin film for the application in optoelectronic sensors and devices. It aims to develop optimized Cu_xN film with a suitable compositional ratio by a simple and low-cost spray deposition process for optoelectronic applications. The optimization of the film has been achieved by tuning the doping of the film. The structural and optical analysis of the film has been performed to determine surface morphology, crystallinity, compositional ratio, and band gap. The electrical analysis of the optimally produced film has been executed to test its acceptability as a light-

dependent resistor (LDR) application. Then photoconductive and photovoltaic performances of the optimized film have been performed by a modern computational technique where experimental data of the optical spectroscopy has been given as input to the simulation software. The photoconductive study has been accomplished by tuning the film thickness, and an optimized film thickness has been used for solar cell applications. The photovoltaic performances of the film considering optimized thickness have been cultivated here by using Cu_xN as absorber and window layers in combination with various inorganic semiconductors. The best photovoltaic combination has been obtained from here, and results have been compared with the conventional solar cell materials. Therefore, given the above-mentioned contribution, the methods and results reported in this research work, that the fabricated optimized copper nitride material as a light-dependent resistor (LDR) and solar cell application, are satisfactory. The author hopes that this research work provides a direction and contribution in the field of optoelectronic sensors and devices applications.

The summary of the entire research work has been presented in Chapter 6. The summary has started from the aim and objectives of the work to the investigation on optoelectronic response of crystalline nanostructure copper nitride (Cu_xN) thin film semiconducting material.

Although significant work related to the fabrication and optimization of copper nitride semiconducting material for optoelectronic sensor and device applications is presented in the present thesis, still some aspects are not covered due to the stipulated time span of my PhD work. Thus, all these unsolved and uncovered parts of this present research work are presented in Chapter 7. It is expected that future researchers will look into these uncovered aspects and will deliver possible solutions for the successful exploration regarding this topic.

Chapter 7

Avenue of the future work

7.1 Future Scope

The application of nanostructure thin film material for the development of optoelectronic devices plays an important role due to its higher conductivity, mobility, mechanical strength and stability. Therefore, nanostructure material can increase device efficiency and thus reduce cost. In this present study, nanostructured copper nitride thin film has been developed for the application in optoelectronic sensors and devices. The copper nitride film had mainly been developed by the physical deposition methods, but the suitable chemical composition of the material is not always obtained for providing optimum optoelectronic properties for device applications. Therefore, in this present context, fabrication and optimization of the Cu_xN film have been performed by a simple and low-cost spray deposition method for the application in LDR and solar cell. There are several aspects regarding the fabrication and optimization of the film which are mentioned in this dissertation. There is a substantial portion of the work that is unfinished due to the measurable time span. It is discussed in the following section of this chapter. Future researchers can fill these gaps by introducing several deposition and optimization techniques of copper nitride based thin film for the suitable application in optoelectronic devices.

The development of the film has been executed by utilizing the spray deposition process, and optimization of the material has been performed here by varying the doping of the film. There is another alternative way by which the fabrication and optimization of the film can be performed. The combination of computational simulation and one of the physical deposition techniques, such as molecular beam epitaxy, can be implemented to conduct this work. At first, optimization of the compositional ratio of the material can be performed by computational simulation technique, and then the film can be deposited by molecular beam epitaxy process, considering the optimum chemical composition of the material. Then the photoresistor and solar cell performance can be evaluated by considering this optimally prepared film. The photoconductive and photovoltaic performances will be observed by simulation technique to determine its acceptability as a solar cell application. On the other hand, photovoltaic performances can also be cultivated by experimental processes considering optimum parameters of the material. Then a comparative study will be executed between simulation and practical outputs. In this present study, the experimental data was provided as input to Oghma-Nano software (8.1.020) for carrying out numerical simulations for obtaining photoconductive and photovoltaic responses of the fabricated 0.6(M) CuxN optimized annealed film. Oghma-nano can be used alongside machine learning tools for research in optoelectronics. An ML model can be trained on experimental data to predict more accurate initial parameters for Oghma Nano's fitting tool. In this present work, optimization of film thickness has been performed for a particular value in micrometer, nanometer and angstroms range. Here nanometer range thickness provides the best results among the all. Thus, optimization of thickness in the nanometer range for more precise results as an optoelectronic device application will be a future work. The optimization of material thickness in the nanometer range should improve photovoltaic performance, and it will give more precise results in device applications. This optimization can be applicable for both the window and absorber layers. At first, the variation in absorber layer thickness will be

performed by keeping the window layer's thickness constant. This variation of thickness will be cultivated by tuning the doping of the film. The doping can vary depending on the ratio of reactants, temperature, and rate of spraying during fabrication. Thus, the optimum thickness of the absorber layer will be determined. Thereafter the variation of window layer thickness will be performed by keeping the optimum thickness of the absorber layer, and it will be accomplished the same way mentioned for the absorber layer. These two sets of data can be provided as input in a machine learning model, and it will give optimum results in device application. Optimization of the thickness of the window as well as the absorber layer and good control of absorber layer thickness for optimum absorption can be accomplished using a machine learning model in great detail and will be future work. It has also been observed that post-deposition annealing of the as-prepared film has improved crystallinity as well as other structural parameters and thus enhanced stability as well as efficiency of the device. Therefore, optimization of post-deposition annealing temperature for more convenient outputs can be accomplished in further studies. It has been observed from the optical analysis that absorption of the fabricated copper nitride sample was found to be extremely high in the visible and NIR ranges, respectively. The absorption of light in the NIR range can provide information about various properties, such as chemical composition, moisture content, etc., of the sample. Thus, this as-deposited film can be used as an optical sensor in the NIR spectrum range for applications in the fields of medical imaging, industrial process monitoring, food and pharmaceuticals, etc., and future research work would be needed to fulfill these uncovered issues.

However, this thesis is required to be completed in a specific period of time. Therefore, a measurable amount of work could not be completed within this stipulated time span. It is expected that many researchers will have completed the remaining part of this research work.

Journal of Crystal Growth 617 (2023) 127307

Contents lists available at ScienceDirect

Journal of Crystal Growth

journal homepage: www.elsevier.com/locate/jcrysgro

A novel method for fabricating semiconducting monocrystalline copper nitride nanowires for optoelectronic applications

Avijit Paul, Mainak Ghosh, Indranil Dutta, Ratan Mandal *

School of Energy Studies, Jadavpur University, Kolkata, India

ARTICLE INFO

Communicated by Pierre Muller

Keywords:
B1. Copper nitride
A3. Spray pyrolysis
B1. Nanowires

ABSTRACT

Semiconducting grade copper nitride(Cu_3N) nanowires have been fabricated using a simple and low-cost method. The standard technique for fabricating Cu_3N nanowires is physical methods and this is costly due to the involvement of capital equipment and recurring input. In the present method the Cu_3N nanowires have been fabricated using chemical spray pyrolysis of thiourea and ammonium hydroxide over hot copper (Cu) foil substrate surface. The present process involves meager capital equipment and low recurring input. Studies on the quality of nanowires fabricated by the present method have been conducted using various molar concentration of spray solution and the ambient temperature of Cu substrates. The structural analysis indicated about the formation of cubic Cu_3N. The optical analysis indicated about the low absorption in UV range and enhanced absorption in visible and NIR ranges with variation of direct and indirect bandgap of nanowire ranging from 1.5 to 1.79 eV. The light dependent resistance of the fabricated nanowires was tested and indicated its applicability in usage as light sensing devices. The result obtained so far is similar with that of Cu_3N nanowires fabricated by physical deposition method. The present method for fabrication of Cu_3N nanowires is simple and can be adopted by industries for large scale fabrication of nanowires for various device applications. Detailed fabrication technique and various properties of the nanowires are discussed in the text of the paper.

1. Introduction

Exploration on the use of II-VI and III-V group compound semiconductors in device fabrication gained attention since 1954 due to their several advantages over the elemental semiconductors like Si and Ge. Transition metal nitrides are also attractive class of semiconducting materials for their several technological applications [1]. Copper nitride (Cu_3N) is one such compound semiconductor in this class because of its tremendous potential in applications such as recording and electronics sectors [2,3]. Copper nitride exhibits cubic anti- ReO_3 type crystal structure (a = 3.807 Å) having several interstitial sites. If appropriate atoms are made to occupy these interstitial sites then optical and electrical properties of Cu_3N could be enhanced [4]. Copper nitrides have relatively low thermal stability allowing these compounds to decompose into copper [5]. This encourages further research on copper nitrides in the field of electronics.

In earlier works the Cu_3N films had been deposited by atomic layer deposition (ALD) technique on Ru and SiO_2 substrates. The film was reduced to metallic Cu after annealing at 200 °C. The ALD Cu_3N as well as reduced Cu films were found to exhibit smooth surface and outstanding step coverage. The resistivity of the 4.2 nm thick film was obtained to be 30 μΩ-cm [6]. Previously Cu_3N films were developed by depositing copper from an electron gun in ambience of atomic nitrogen obtained from a RF plasma source upto thickness of 10 μm. It was observed that the N_2 adsorption on the Cu ⟨1 0 0⟩ surface at room temperature and also at 100 °C altered the Cu surface morphology drastically, probably due to presence of dislocations for relieving the stress caused due to difference in lattice parameters between Cu and Cu_3N [7]. The copper nitride films had been deposited in the past by pulsed laser ablation process by ablating a copper target at various pressures of nitrogen. The [N]/ [Cu] ratio i.e. x varied between 0 and 0.33 for a corresponding variation of N_2 pressure in the range of 9×10^{-2} to 1.3×10^{-1} torr. It was feasible to obtain sub, over as well as stoichiometric films by simply controlling N_2 pressure. The lattice constants was 3.85 Å for x = 0.25 and found to vary between 3.81 Å to 3.83 Å for x = 0.33. The electrical resistivity of the film with x = 0.25 was found to be lower than that of x = 0.33 [8]. In the past Cu_3N films were developed by DC magnetron sputtering of Cu target in ambience of nitrogen. Cu_3N

* Corresponding author.
E-mail address: ratan_mandal99@yahoo.co.in (R. Mandal).

https://doi.org/10.1016/j.jcrysgro.2023.127307
Received 23 February 2023; Received in revised form 13 May 2023; Accepted 1 June 2023
Available online 3 June 2023

J Mater Sci: Mater Electron (2025) 36:87

Investigation on optoelectronic response of crystalline copper nitride (Cu_xN) thin film semiconducting material

Avijit Paul[1], Mainak Ghosh[1], Tanay Chattopadhyay[2], and Ratan Mandal[1,*]

[1] *School of Energy Studies, Jadavpur University, Kolkata, West Bengal 700032, India*
[2] *Solar Division, Bidyut Unnayan Bhaban, WBPDCL, Kolkata 700106, India*

Received: 27 September 2024
Accepted: 8 December 2024
Published online: 5 January 2025

ABSTRACT

The present study represents a modern computational analysis of optoelectronic response of crystalline, nanostructured copper nitride (Cu_xN) semiconducting material fabricated by a simple, low-cost spray pyrolysis technique that can be adopted in places lagging high-grade fabrication infrastructure. The optical spectroscopy data of the fabricated thin film was provided as input to Oghma-Nano software for carrying out numerical simulations. The variation in photoconductive response by tuning film thickness from 50 µm to 50 nm and 50 Å at different light intensities was observed. The best photoconductive performance was observed for 50 nm film with total charge density of 3×10^{25} C m^{-3}, cut-in voltage of 1.4 V, recombination prefactor of 1.2×10^{-24} m^{-6} s^{-1} and carrier generation rate of 2.5×10^{36} m^{-3} s^{-1}, respectively. These values were compatible with those of conventional semiconductors like Si, GaAs and CdTe, respectively. The feasibility of 50 nm Cu_xN film in photovoltaic applications was probed by modelling a device by using it as absorber and window layers in combination with various inorganic semiconductors as mentioned in the text of this paper. The best photovoltaic characteristics and parameters were noted for the solar cell with Cu_xN as absorber layer and CdS as window layer. This CdS–Cu_xN solar cell exhibited maximum current density of 9.98 A m^{-2}, maximum power density of 89.32 W m^{-2}, fill factor of 0.85, photoconversion efficiency of 8.93% etc. which are compatible with experimental results of other conventional CdS-based solar cells like CdS–Cu_2S, CdS–PbS, CdS–CdTe. Optoelectronic performance analysis for various device applications using present technique is simple and can be adopted in places lagging high-grade fabrication and characterization infrastructure.

Address correspondence to E-mail: ratan_mandal99@yahoo.co.in

https://doi.org/10.1007/s10854-024-14065-3

Invertis Journal of Renewable Energy, Vol. 7, No. 2, 2017 ; pp. 106-112 DOI No. : 10.5958/2454-7611.2017.00015.7

Scope and possibilities of copper based semiconducting materials in optoelectronic applications - A review

AVIJIT PAUL[1]* and RATAN MANDAL[2]
[1]*Department of Electronics & Communication Engineering, Mallabhum Institute of Technology, Bankura, West Bengal, India*
[2]*School of Energy Studies, Jadavpur University, Kolkata-700032*
**E-mail:* avijit.paul06@gmail.com

Abstract

In the present work we cultivate various scope and opportunities of Copper (Cu) based semiconducting materials by analysis of 84 different research papers. The objectives of the present work are: Introduce of different Copper (Cu) based semiconducting materials and their merits & de-merits, Different fabrication method regarding different materials according to different authors, Applications and future work based on different materials. From this review paper, beginners who are working on copper (Cu) based materials will gain a lots. Researchers will acknowledge various types of Cu based materials & their different fabrication processes. Apart from this they will also be aware of advantages and disadvantages of various materials & the possible defined problems which will carry out in future work. So beginners who are working on this, will find a convenient path to find a problem regarding future research work on Copper (Cu) based semiconducting material.

Key words : Cu based semiconducting materials, Different fabrication processes Applications & Future work.

1. Introduction

The demand of energy will increase day to day with increase of population and advancement of technology. There are different renewable energy sources like solar energy; wind energy, oceanic energy, and bio-energy etc are available to solve this energy crisis. Here we reviewed different Copper (Cu) based semiconducting material & their fabrication process for the application in solar cell or other optoelectronic devices. We reviewed here 84 different research papers and from there we analysis 32 different Copper (Cu) based materials. The following analysis shows the name of 32 materials and their merits & demerits.

Copper-indium-gallium-diselenide (CIGS)-has high absorption coefficient, wide absorption spectrum and high stability and it exibit lower conversion efficiency. The optical band gap of $CuBO_2$ is higher than compared to Cu based delafossite compounds. But it was observed that the film have shown lower conductivity. Cuprous oxide (Cu_2O) is one of the promising materials for solar cell applications due to its acceptable solar efficiency, low cost preparation technique, abundance of copper in the earth's crust and its non-toxic nature and the formation of phase-pure Cu_2O films is difficult. Cu_xS (Copper sulphide) has good absorption in the visible region and high natural abundance in earth and it was observed that Cu_xS thin film shown the low resistivity as well as decreasing bandgap. Efficiency of the CTGSe solar cells was dramatically improved to over 3%with the incorporation of Ge in the Cu_2SnSe_3(CTSe) film and the carrier concentration of the CTGSe sample was decreased to the level of 10^{17} cm^{-3} found in Co-evaporation method analysis.

ScienceDirect

Comprehensive Materials Processing (Second Edition)

Volume 4, 2024, Pages 136-150

4.09 - Advances in nanostructure thin film materials for solar cell applications

Avijit Paul, Ratan Mandal ✉

Show more

https://doi.org/10.1016/B978-0-323-96020-5.00162-X ↗

Get rights and content ↗

Abstract

In the present study, 10 different semiconducting nanostructured materials, namely Copper Sulfide ($Cu_{2-x}S$), Copper Nitride (Cu_3N), Tin Sulfide (SnS), Copper Zinc Tin Sulfide (CZTS), Copper Oxide (CuO), Zinc Oxide (ZnO), Titanium dioxide (TiO_2), Cadmium Sulfide (CdS), Cadmium telluride (CdTe) and Copper indium diselenide (CISe) along with different fabrication techniques, have been mentioned for photovoltaic applications. Nanostructure formation can improve the overall stability of the device. Carrier conduction and device efficiency have also shown an increase in nanostructured based solar cells. So, various fabrication methods for the formation of nanostructures using the mentioned semiconducting materials have been discussed in detail in his chapter. The usefulness of these nanomaterials for application in solar cells has also been presented here. Hence, beginners working on PV cells will find a convenient path to perform nanofabrication of these semiconducting materials in future research work.

References (0)

ScienceDirect

Comprehensive Materials Processing (Second Edition)

Volume 4, 2024, Pages 547-564

4.33 - Electroless nickel coating on magnesium substrates: Fabrication method and applications

Ratan Mandal ✉, Mainak Ghosh, Avijit Paul

Show more

Share Cite

https://doi.org/10.1016/B978-0-323-96020-5.00203-X ↗

Abstract

In the present chapter, a comprehensive study of electroless nickel (Ni) deposition on magnesium (Mg) substrates has been made. Magnesium and its alloys are used in electronics, aerospace and automobile industries, but their applicability is often compromised due to their high susceptibility to corrosion. Electroless Ni deposition results in formation of a very hard coating which provides corrosion protection to the magnesium substrate. Here, 23 most convenient Ni based coatings have been identified and their detailed fabrication methods with applications have been studied. Aspirants working on electroless Ni deposition will find a convenient pathway for carrying out extensive research in future.

References (0)

Cited by (0)

ScienceDirect

Comprehensive Materials Processing (Second Edition)

Volume 4, 2024, Pages 39-60

4.03 - Thin film fabrication for wearable electronics: Journey so far

Mainak Ghosh, Avijit Paul, Ratan Mandal ✉

Show more

Share Cite

https://doi.org/10.1016/B978-0-323-96020-5.00267-3 ↗

Get rights and content ↗

Abstract

In the present chapter, a comprehensive study on thin film fabrication for wearable electronics has been performed. Thin film based microelectronic devices being less expensive and highly efficient are conducive for wearable electronic applications in biomedical, electrochemical, electrical sectors, etc. Here 38 most promising thin film materials have been selected and their detailed fabrication techniques along with corresponding applications have been elucidated. This study provides an overall insight into thin film fabrication for wearable electronic devices to aspiring researchers for carrying out extensive future research work in this field.

References (0)

Cited by (1)

CHAPTER 2

Synthesis Methods, Fabrication and Performance Evaluation Techniques of Electrode Materials

RATAN MANDAL*, MAINAK GHOSH AND AVIJIT PAUL

School of Energy Studies, Jadavpur University, Kolkata, India
*E-mail: ratan_mandal99@yahoo.co.in

2.1 Introduction

Energy availability has transformed humanity over the last few centuries. In the twentieth century, electricity was overwhelmingly generated by the combustion of conventional fossil fuels. Less fuel was incinerated when power demand was low and more when the demand for electricity was high.[1] Another convenient source of energy generation that has been available for several years is hydroelectric power. Large hydropower stations have been a reliable source of electricity almost for a few centuries.[2] Nuclear power is the third conventional source of energy. Nuclear power uses nuclear reactions, *i.e.*, nuclear fission of radioactive elements like uranium, plutonium and thorium for electricity generation. The global installed capacity of nuclear power has increased to 390 GW (by 2022) generating almost 2586 TW h of electricity (in 2019), tantamount to almost 10% of worldwide electricity generation.[3] Factors relating to air pollution, global warming, and energy

Optical, Electronic and Magnetic Materials No. 3
Supercapacitors: Fundamentals, Advances and Future Applications
Edited by Dakeshwar Kumar Verma and Jeenat Aslam

Published by the Royal Society of Chemistry, www.rsc.org

IEEE
Advancing Technology for Humanity

INTERNATIONAL CONFERENCE ON

21ST CENTURY ENERGY NEEDS – MATERIALS, SYSTEMS AND APPLICATIONS

School of Energy Science & Engineering
Indian Institute of Technology Kharagpur, India

Certificate of Participation

Certified that Dr./Ms./Mr Avijit Paul

Participated in ***International Conference on 21st Century Energy Needs - Materials, Systems and Applications 2016*** *and presented a paper titled*

Some Studies on The Contact Properties of Cd1-Xznxte Thin Film For Application In Optoelectronic Devices

(S K Srivastava)
Chair

(J N Roy)
Convenor

ICREST-2024

International Conference
on
Renewable Energy and Sustainable Technologies

CERTIFICATE OF PARTICIPATION

This is to certify that Prof./Dr./Mr./Ms. Avijit Paul

has participated and presented (Oral/Poster) a paper entitled Analytical Study of the Efficiency of CdS/CuxS Based Thin Film Solar Cells Using MATLAB Platform

in the International Conference on Renewable Energy and Sustainable Technologies (ICREST-2024), organized by Department of Applied Sciences & Humanities, Faculty of Engineering & Technology, Jamia Millia Islamia, New Delhi, India on July 04-06, 2024.

Prof. Zishan Husain Khan
Organizing Chair

Dr. Faheem Ahmed
Organizing Secretary

Dr. Navaid Zafar Rizvi
Organizing Secretary

PLAGIARISM CHECK RESULTS:

Some Studies on the Fabrication and Optimization of CuxN based Optoelectronic Sensors and Devices

ORIGINALITY REPORT

7%
SIMILARITY INDEX

PRIMARY SOURCES

1	coek.info Internet	126 words — < 1%
2	www.science.gov Internet	101 words — < 1%
3	www.licn.phys.soton.ac.uk Internet	98 words — < 1%
4	repository.tudelft.nl Internet	65 words — < 1%
5	Zhixiong Cai, Feiming Li, Mingcong Rong, Liping Lin, Qiuhong Yao, Yipeng Huang, Xi Chen, Xiaoru Wang. "Introduction", Elsevier BV, 2019 Crossref	54 words — < 1%
6	lib.buet.ac.bd:8080 Internet	50 words — < 1%
7	c.coek.info Internet	40 words — < 1%
8	L. Derbali, F. Bo... A. Derbali, B.M. Soucase. "Enhanced ZnO ... and nanostructured interface modif... improved perovskite solar cells efficiency", Opti... s, 2023 Crossref	38 words — < 1%

Avijit Paul

Mr. Avijit Paul